Preliminary Report of the Hakuho-Maru Cruise KH92-1

January 21 - March 4, 1992

Tokyo - Guam - Cebu - Tokyo

Geophysical and Geological Investigations of the Mariana Region and the Ayu Trough

[WESTPAC and IGBP]

1993

Ocean Research Institute

The University of Tokyo

Preliminary Report of the Hakuho-Maru Cruise KH92-1

January 21 - March 4, 1992

Tokyo - Guam - Cebu - Tokyo

Geophysical and Geological Investigations of the Mariana Region and the Ayu Trough

[WESTPAC and IGBP]

1993

Ocean Research Institute

The University of Tokyo

Preliminary Report of the Hakuho-Maru Cruise KH92-1

January 21 - March 4, 1992

Tokyo - Guam - Cebu - Tokyo

Geophysical and Geological Investigations of the Mariana Region and the Ayu Trough

[WESTPAC and IGBP]

by
The Scientific Members of the Cruise
Edited by
Jiro SEGAWA

Frontispiece 1 (Confer Section 6.3)

The SeaBeam bathymetric contour map of the Mariana Trough. The data were processed using the UNIRAS graphic software package. A 3-kilomerter interpolation search radius was employed. Contour interval is 100 meters. Legends of the colors are also shown in the right of the figure. Color scale interval is 200 meters. The overlapping spreading center of the Mariana Trough centered at the latitude of 18°N is clearly seen in this figure. In this area very intensive geophysical measurements such as seismic reflection/refraction survey, gravity and magnetics were conducted.

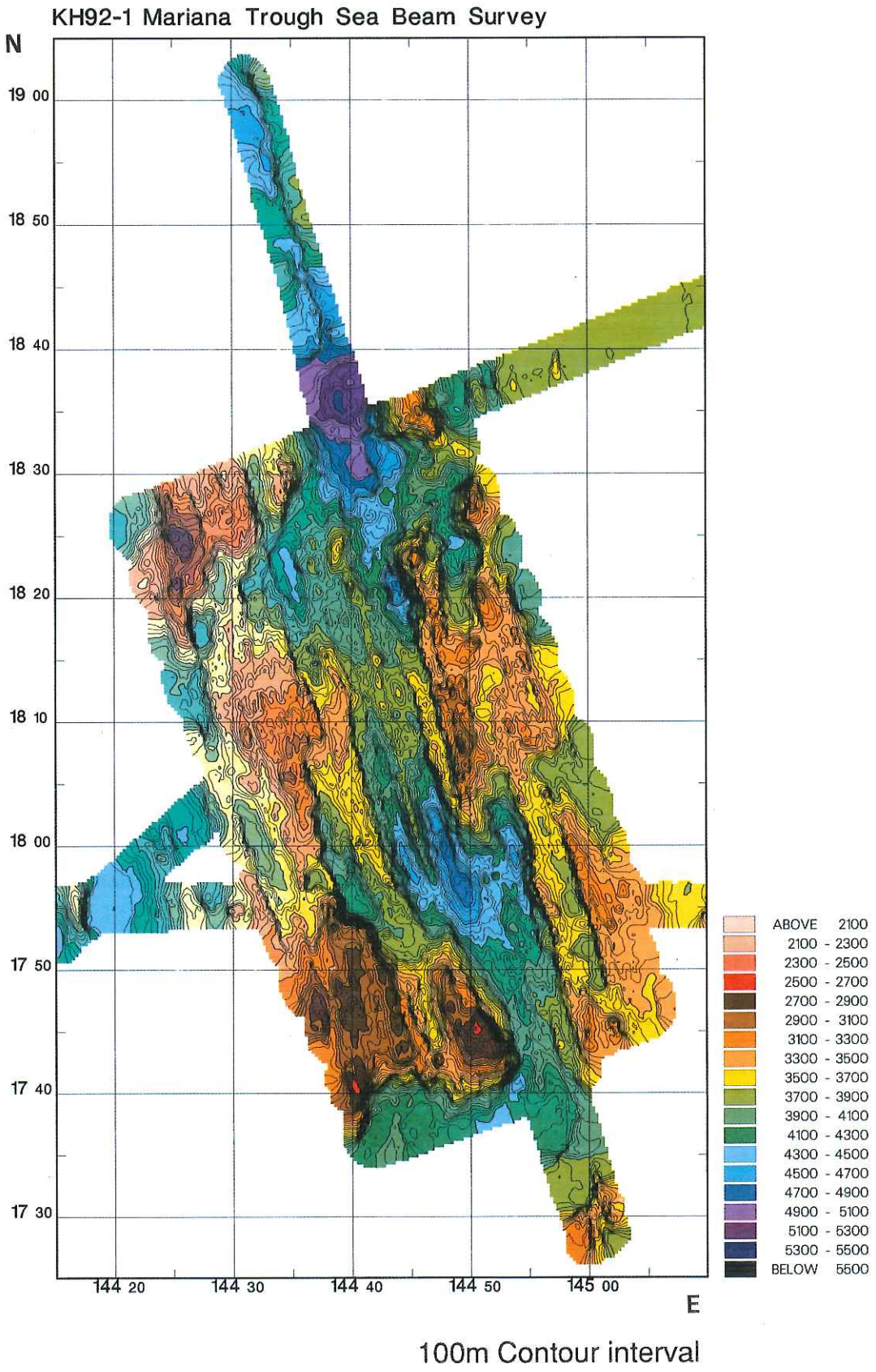
KH92-1 Mariana Trough Sea Beam Survey
N
19 00
18 50
18 40
18 30
18 20
18 10
18 00
17 50
17 40
17 30
144 20
144 30
144 40
144 50
145 00
E
ABOVE 2100
2100 - 2300
2300 - 2500
2500 - 2700
2700 - 2900
2900 - 3100
3100 - 3300
3300 - 3500
3500 - 3700
3700 - 3900
3900 - 4100
4100 - 4300
4300 - 4500
4500 - 4700
4700 - 4900
4900 - 5100
5100 - 5300
5300 - 5500
BELOW 5500
100m Contour interval

Frontispiece 2 (Fig. 6.4.2)

The SeaBeam bathymetric contour map of the Ayu Trough. The data were processed using the UNIRAS graphic software package. A 3-kilomerter interpolation search radius was employed. Contour interval is 100 meters. Colors indicate depth from 500 (red) to 7,000 meters (dark blue). Color scale interval is 300 meters. The axis of the Ayu Trough is marked by a 5-6 kilometer-deep valley in the southern part of the map, and the axis of the Palau trench is marked by a 6-7 kilometer-deep valley in the north-eastern part of the map. The bathymetric map shows that there are many similarities between the bathymetry of the Ayu Trough and that of the mid-ocean ridges which separate at a slow spreading rate. This fact suggests that the oceanic plates separate at a slow spreading rate at the Ayu Trough. The topography is symmetrical about the trough axis. The periodic topographic highs and lows appear, which show axial symmetry. The trough axis deep is a V-shaped valley. Sediment is thin at the trough axis valley. A gradual increase of sediment as the distance from the trough axis is identified by the existence of flat basin . The basement subsides symmetrically about the trough axis and is gradually deepened as the distance from the trough axis, following empirical root age law.

KH92-1 Ayu Trough Sea Beam Survey

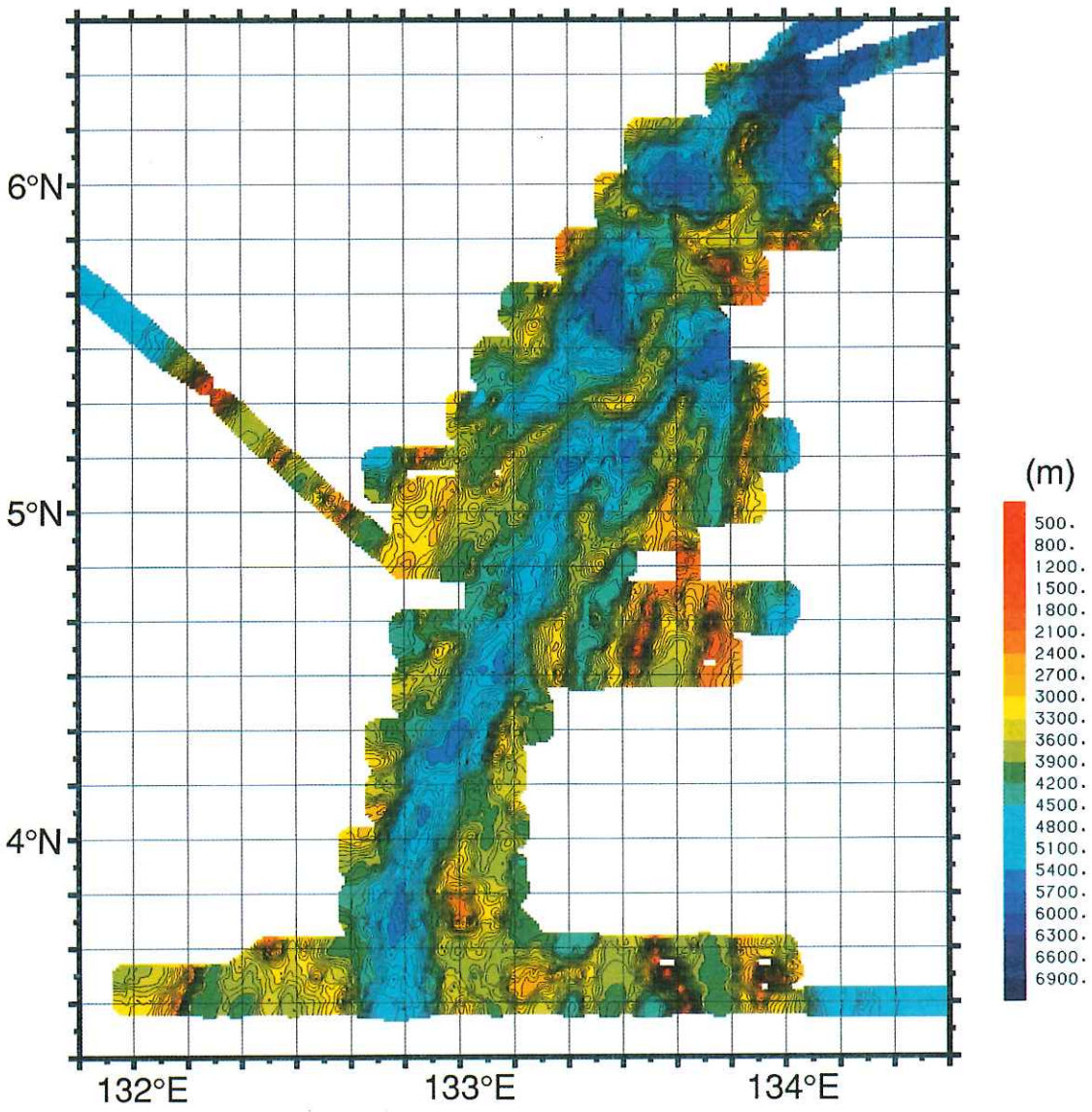

100m Contour interval

Preface

The HAKUHO-MARU Cruise KH92-1 was planned to make a detailed investigation of geophysical and geological features of the north-western part of the Pacific Ocean. In this cruise emphases were laid on the Mariana Ridge area and the Ayu Trough area north of the Equator and west of 150°E. These investigations include two objectives: The first is to understand the crustal structures and the tectonic settings of the areas and to grasp consistent images on their relationship with the global plate motions. The second is for the sake of the Paleoenvironmental study, for which oceanic sediments were sampled from the basins shallower than 4000m to make comparative studies between the current living plankton and the plankton fossils involved in the sediments. This cruise was devoted partly to the International Co-operative Programs "WESTPAC" and "IGBP" sponsored by UNESCO.

The R/V HAKUHO-MARU left Tokyo for the next port of call Guam on 21 January 1992 (Leg 1). After making surveys in the Mariana Ridge and the Mariana Trough between 18°N and 19°N, she paid a visit to the port of Guam on 8 February, and on 11 February she left Guam for the 2nd port of call Cebu, Philippine (Leg 2). The survey of the Ayu Trough which is located at about 5°N was made twice; its first half was made during Leg 1 and the second half during Leg 2. From Cebu where she stayed from 22 to 27 February, Leg 3 of the cruise began. Since there was little time left, this leg was used mostly for cruising back to Tokyo, except for one important work, i.e., a bathymetric survey of the Hakuho Seamount located at about 28°N and 137°30'E on the Kinan Seamount Chain using the Sea Beam System.

It is noteworthy that in this cruise very high density surveys were successfully carried out in two important spots, Mariana and Ayu, and we were able to obtain valuable data on bathymetry, gravity, magnetics, sedimentary layer, heat flow and crustal structures. The only thing regrettable is that the deep-towed TV system was not available in this cruise because of an electronical trouble that happened just before the cruise.

Before closing my words I would like to appreciate cooperation of all the persons and organizations concerned, particularly those of Captain and crew of the Hakuho-Maru, and to congratulate the privileged cruise with good weather, good results and no accidents.

Jiro SEGAWA
Chief Scientist

List of Participants on board R/V Hakuho-Maru during KH92-1 Cruise

SEGAWA, Jiro Leg 1 Chief Scientist	Ocean Research Institute, the University of Tokyo 1-15-1, Minamidai, Nakano-ku, Tokyo 164 JAPAN
FUJIMOTO, Hiromi Leg 1 Co-chief Scientist	Ocean Research Institute, the University of Tokyo 1-15-1, Minamidai, Nakano-ku, Tokyo 164 JAPAN
FUJIWARA, Toshiya Leg 1,2 and 3	Ocean Research Institute, the University of Tokyo 1-15-1, Minamidai, Nakano-ku, Tokyo 164 JAPAN
IGARASHI, Chiaki Leg 1,2 and 3	Ocean Research Institute, the University of Tokyo 1-15-1, Minamidai, Nakano-ku, Tokyo 164 JAPAN
ISHII, Teruaki Leg 1,2 and 3	Ocean Research Institute, the University of Tokyo 1-15-1, Minamidai, Nakano-ku, Tokyo 164 JAPAN
KASAHARA, Junzo Leg 1	Earthquake Research Institute, the University of Tokyo 1-1-1, Yayoi, Bunkyo-ku, Tokyo 113 JAPAN
KIDO, Motoyuki Leg 2 and 3	Earthquake Research Institute, the University of Tokyo 1-1-1, Yayoi, Bunkyo-ku, Tokyo 113 JAPAN
KINOSHITA, Hajimu Leg 2	Earthquake Research Institute, the University of Tokyo 1-1-1, Yayoi, Bunkyo-ku, Tokyo 113 JAPAN
KOBAYASHI, Kazuo Leg 2 and 3	Ocean Research Institute, the University of Tokyo 1-15-1, Minamidai, Nakano-ku, Tokyo 164 JAPAN
KOIZUMI, Kin-ichiro Leg 1,2 and 3	Ocean Research Institute, the University of Tokyo 1-15-1, Minamidai, Nakano-ku, Tokyo 164 JAPAN
KONG, Laura Leg 1	Pacific Tsunami Warning Center 91-207 Fort Weaver RD. Ewa Beach, HI 96706 U.S.A.
KORESAWA, Sadayuki Leg 1	Earthquake Research Institute, the University of Tokyo 1-1-1, Yayoi, Bunkyo-ku, Tokyo 113 JAPAN

LU, Rui Feng Leg 1	Department of Earth Sciences, Faculty of Science, Chiba University 1-33, Yayoi-cho, Inage-ku, Chiba 263 JAPAN
MATSUOKA, Hiromi Leg 1,2 and 3	Department of Geology, Faculty of Science, Kochi University 2-5-1, Akebono-cho, Kochi 780 JAPAN
MORITA, Sumito Leg 1,2 and 3	Ocean Research Institute, the University of Tokyo 1-15-1, Minamidai, Nakano-ku, Tokyo 164 JAPAN
MURAYAMA, Masafumi Leg 1, 2 and 3	Ocean Research Institute, the University of Tokyo 1-15-1, Minamidai, Nakano-ku, Tokyo 164 JAPAN
OBA, Tadamichi Leg 2 and 3	Department of Geology, College of Liberal Arts, Kanazawa University 1-1, Marunouchi, Kanazawa 920 JAPAN
OKAMOTO, Takanori Leg 1,2 and 3	Department of Geology, Faculty of Science, Kochi University 2-5-1, Akebono-cho, Kochi 780 JAPAN
SEAMA, Nobukazu Leg 1	Ocean Research Institute, the University of Tokyo 1-15-1, Minamidai, Nakano-ku, Tokyo 164 JAPAN
SENO, Tetsuzo Leg 2 and 3	Earthquake Research Institute, the University of Tokyo 1-1-1, Yayoi, Bunkyo-ku, Tokyo 113 JAPAN
SUZUKI, Masaya Leg 1	Department of Earth Sciences, Faculty of Science, Chiba University 1-33, Yayoi-cho, Inage-ku, Chiba 263 JAPAN
SUZUKI, Takehiko Leg 1	Department of Geography, Tokyo Metropolitan University 2-1-1, Fukazawa, Setagaya-ku, Tokyo 158 JAPAN
TAKEMURA, Osamu Leg 1,2 and 3	Department of Earth Science, Faculty of Science, Kobe University 1-1, Rokkodai, Nada-ku, Kobe 657 JAPAN
TAMAKI, Kensaku Leg 2	Ocean Research Institute, the University of Tokyo 1-15-1, Minamidai, Nakano-ku, Tokyo 164 JAPAN

TANJI, Tatsuo
Leg 1,2 and 3
Department of Computer Science and Systems Engineering, Faculty of Engineering, Muroran Institute of Technology
27-1, Mizumoto-cho, Muroran 050 JAPAN

TOH, Hiroaki
Leg 2 and 3
Ocean Research Institute, the University of Tokyo
1-15-1, Minamidai, Nakano-ku, Tokyo 164 JAPAN

TSUKAWAKI, Shinji
Leg 2 and 3
Institute of Geology and Paleontology, Tohoku University
Aramaki-aza-Aoba, Aoba-ku, Sendai 980 JAPAN

YAMAGUCHI, Takashi
Leg 1
Department of Earth Sciences, Faculty of Science, Chiba University
1-33, Yayoi-cho, Inage-ku, Chiba 263 JAPAN

YANG, Chul Soo
Leg 1
Ocean Research Institute, the University of Tokyo
1-15-1, Minamidai, Nakano-ku, Tokyo 164 JAPAN

Shorebase Scientists

MAEKAWA, Hirokazu
Earth Science, Kobe University
1-2-1, Turukou, Nada-ku, Kobe 657 JAPAN

OHARA,Yasuhiro
Geologieal Institute, the University of Tokyo
7-3-1, Hongo, Bunkyo-ku, Tokyo 113 JAPAN

Contents

1. Outline of Research Conducted in R/V Hakuho-Maru Cruise KH92-1 (21 January - 4 March, 1992) from Leg 1 through Leg 3

J. Segawa and K. Kobayashi

The objectives of research by this cruise are: 1) Detailed geophysical and geological study of the Mariana Ridge, Mariana Trough and Ayu Trough. 2) Study of long wavelength variation of gravity and magnetic field. 3) International co-operative study under the programs 'IGBP' and 'WESTPAC'.

The R/V Hakuho-Maru set sail from the Harumi Pier, Tokyo, on 21 January 1992 and arrived at Guam on 8 February. This is Leg 1 of the cruise. The main area of survey in this leg is the Mariana Ridge and the Mariana Trough in the west-to-east zone between 18°N and 19°N. Before coming to this area the ship cruised to the south along the outer edge of the Izu-Bonin and Mariana Ridge, where several seamounts characteristic of extrusion of mantle diaper are distributed. These seamounts are believed to be composed of low density anomalies, unlike the usual seamounts. The gravity anomalies measured in this cruise actually showed such tendency.

In the Mariana Survey area we took a long-span gravity line which was extended in about 900km west-to-east. The zone along 18°N was once interpreted through gravity anomalies and expected to be associated with an unusually low-density body underneath the basin between the Mariana Trough and the Mariana Ridge. The present gravity survey was conducted to make the previous results more convincing. In this area the surveys of detailed bathymetry, sedimentary layer and crustal structures were made using the SeaBeam system, Air-gun system and the ocean bottom seismometers.

In the last part of Leg 1 the ship cruised for the Ayu Trough zone to make a bathymetric grid survey. About half of the survey scheduled was conducted in this period. Another work conducted in Leg 1 was the operation of the piston corer and the dredger. By the piston corer which is 11m long were sampled sediments from the bottom shallower than CCD (Carbonate Compensation Depth). The fossils of plankton involved in the sediments are compared with the living fauna to find the difference of marine environments between the past and the present. Dredging was performed twice in this leg, but it was successful only once. By the dredging some ultramafic rocks were sampled at the inner slope of the Mariana Trench located at about 11°40'N with the depth of 7000m.

On the way to Guam the Hakuho-Maru happened to cross the Challenger Deep of the Mariana Trench. Since there is still a debate about whether or not the Challenger Deep exceeds 11,000m in depth, we tried to make a bathymetric

survey of the deep for confirmation using the seabeam. The measurement resulted that it showed the depth 10,933m, which is in harmony with the result obtained by the Japan Hydrographic Department.

After two-day port-of-call at Guam the R/V Hakuho-Maru began her Leg 2 cruise having two major objectives and other associated tasks in the West Caroline Basin and surrounding regions. The first of them is comprehensive survey of the Ayu Trough located south of the Palau Trench. The second is the sampling and onboard investigation of bottom sediments collected by piston corers and box corers at two sites shallower than the CCD depth. Plankton was also collected at a site east of the Ayu Trough in order to fix isotope ratios of the living faunas.

In addition to these two themes underway, geophysical measurements including SeaBeam bathymetry, gravity, geomagnetic total force and three-component measurement, 3.5kHz subbottom survey were made while cruising at 16 knots. Areas investigated are the Sorol Trough, the crest of Eauripik Rise, the west Caroline Basin, southern portion of the Sorol Trough and Philippine Trench. The ship took zigzag courses to find regional morphology of these deeps.

In Leg 3 after four days of port-of call at Cebu, Philippine the ship took a heading toward Tokyo. Considering restriction of time left and predicted bad weather in the northern regions, we had no plan of station works in this leg. Nevertheless, her track from Cebu to Tokyo is invaluable for geophysicists, since it transects the whole west Philippine Basin and Shikoku Basin in addition to crossing over several elongated bottom features such as the Philippine Trench, the Central Basin Fault, the Oki-Daito and Daito Ridges and the Kyushu-Palau Ridge.

Because we have not surveyed the Hakuho Seamount in the Shikoku Basin since the Hakuho-Maru installed the SeaBeam multi-narrow beam echo sounder, a grid survey of bathymetry was proposed. It was fortunate to gain several hours of cruising time until the ship reached the site owing to good weather and current conditions so that a reasonable size of polygon was set to survey its topography. Data of S/V Takuyo offered from Hydrographic Department, MSA, Japan was helpful to plan the grid. It was proved that our former results based upon old wide-beam bathymetry is essentially correct, although much additional information on detailed morphology was obtained by the present measurement.

Owing to very clear weather and calm sea the Hakuho-Maru sailed smoothly and station works were conducted without any difficulty.

2. Ship's Tracks during the Cruise

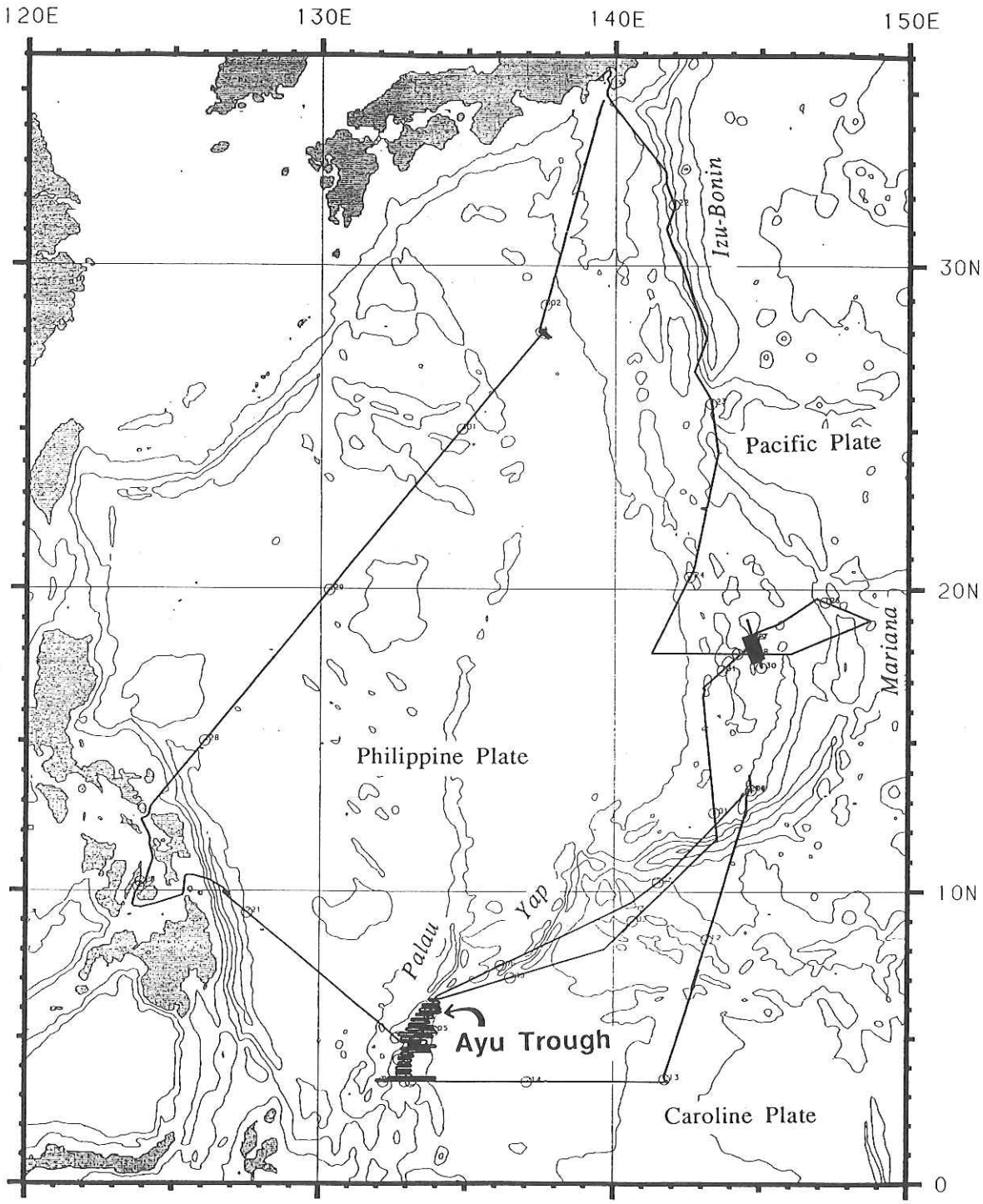

Fig. 2.1 Ship's track during KH92-1 cruise

3. Items of Routine Observations

C. Igarashi

The following observations were carried out throughout the cruise as a routine. Some of the results will be reported in the other articles.

3.1 Meteorological and Oceanographical Data

The following data were measured and recorded every minute all through the cruise.

Date and Time	GMT	Air temperature	°C
Ship position		Dew point	°C
(Lat and Lon)	deg	Water temperature	°C
System heading	deg	System speed	kt
Gyro heading	deg	Rain strength	mm/h
Log speed	kt	Air pressure	mb
Water depth		Wind speed	m/s
(Seabeam or PDR)	m	Short wave radiation	kw/m^2
Relative humidity	%	All wave radiation	kw/m^2
Salinity		All radiation temperature	°C
Wind direction	deg	Conductivity	mmho

Infrared radiation temperature °C
Water temperature for conductivity sensor °C

3.2 3.5kHz Subbottom Profiler Survey (SBP)

The survey system is composed of an acoustic transducer and tranceiver system installed in the bow sonar dome, and a signal processor and recorder in the laboratory No.3. This system has twelve transducers (3*4 TR109), and the laboratory equipments consist of a correlation echo sounder processor (CESP III) , a tranceiver (PTR-105B), and a graphic recorder (LSR-1807) manufactured by Raytheon Co.Ltd. It is possible to feed the ship cruising data through the onboard LAN system.

The subbottom profiling was made at 1000m range, scanning interval of 1.33 sec/scan, with the paper speed 200 lines/inch, and transducer output power of -6 db.

4. Articles

4.1 Seafloor Spreading in the Mariana Trough

L. S. L. Kong

Abstract

The Mariana Arc in the western Pacific is a typical intraoceanic convergent margin. Located in the region are the Challenger Deep, which boasts the deepest seafloor depths on Earth, the well-developed volcanic Mariana Island arc, and the actively-spreading Mariana Trough within the back-arc basin. In early 1992, the R/V Hakuho Maru conducted a series of experiments aimed at increasing our knowledge of plate subduction, seamount construction, and back-arc spreading, and gaining a better understanding how these processes affect global energy and material fluxes within and between the oceans and the Earth's interior. An areally-dense geophysical data set was collected about the Mariana Trough ridge axis near 18°N to establish it as a well-characterized geophysical and geological natural seafloor laboratory for future detailed studies. The data set is comparable in data type, density, and extent to those recently collected along the slowly-spreading Mid-Atlantic Ridge, allowing for the first time the comparison of equivalent data sets from two different tectonic settings that spread at similar spreading rates.

4.1.1 Introduction

Global plate tectonics has provided a theory in which material is created at mid-ocean ridges, evolves and moves as a rigid plate away from the spreading center, and finally is consumed at oceanic trenches or convergent margins. As the slab subducts, sufficient heat is generated for magma production, thereby giving rise to active volcanism and the formation of island arcs. Marginal or back-arc basins, some of which are actively spreading, are ubiquitous features behind many western Pacific subduction zones (Figure 4.1.1).

In order to further understand the character of plate spreading at convergent margins, an international team of scientists carried out detailed geophysical surveys of the actively-spreading Mariana and Ayu Troughs during January-February, 1992 (Figure 4.1.2). The multi-disciplinary cruise aboard the Japanese R/V Hakuho Maru (KH92-1) also included rock dredging, sediment piston and box coring, biological sampling, and atmospheric aerosol experiments within the Mariana Arc region. Peridotities dredged from the southern Mariana Trench

inner slope will help to constrain forearc origin and evolution [Ishii et al., this volume], and information on the paleoceanographic and biogeographic environments of the Philippine Sea and western equatorial Pacific Ocean can be obtained from sediment and plankton samples collected in the Mariana Arc [Oba et al., this volume; Murayama, this volume]. Results from the Ayu Trough, located near the Philippine plate's pole of rotation and whose northward extent intersects the Palau Trench, are presented in companion chapters of this Preliminary Report. This article presents an overview of the Mariana Arc region, with emphasis on the Mariana Trough and the rationale for its choice as the primary study area; preliminary KH92-1 results from the Mariana Trough are presented in greater detail in other chapters of this volume.

4.1.2 Overview of the Mariana Arc Region

The Mariana Arc is an intraoceanic, arc-trench, convergent margin system. It is a typical Pacific-type island-arc margin, and is characterized, from east to west, by the deep Mariana Trench, a simple inner trench slope, a well-developed frontal arc which includes the Mariana Island arc volcanoes, and a marginal basin consisting of the actively-spreading Mariana Trough and the West Mariana Ridge remnant arc (Figure 4.1.2). The Mariana Trench, a 2550-km long feature averaging 70 km in width [*Gross*, 1977], is a narrow, steep-side trough boasting the deepest ocean floor depth on Earth [Challenger Deep, 10,933 m, *Fujimoto et al.*, this volume].

The formation of the Mariana back-arc (island arc and marginal basin) appears to be related to ocean-ocean lithospheric subduction. The crescent-shaped island arc has been volcanically active over the last 5 Ma [10-15 km^3/km/Ma, *Sample and Karig*, 1982]. Mariana back-arc rocks show compositions closer to ocean basalt, presumably because ascending magma must necessarily pass through oceanic-type crust on its way to the surface [*Hawkins and Melchior,* 1985; *Hawkins et al.*, 1990]. *Ringwood* [1977] has argued that the observed arc volcanic rock compositions are consistent with primary magma formation from hydrous tholeiitic basalts or peridotites near the Benioff zone (80-100 km depth). The mode of buoyant rise is not well known, possibly occurring as propagating cracks and/or as distinct bodies. Based on the width of the volcanic arc and configuration of the Benioff zone from earthquake seismicity, magmatic sources are thought to be associated with processes within a low velocity zone above the Benioff zone.

Several hypotheses for the causes of back-arc spreading have been discussed in the literature. In general, spreading is thought to result from global plate interactions in which tensional stresses within the upper plate are created by the

oceanward migration of the trench system during subduction [*Karig*, 1971; *Packham and Falvey*, 1971; *Sleep and Toksoz*, 1971; *Uyeda and Kanamori*, 1979], or alternatively, when landward velocities of the upper plate are greater (due, for example, to a second subduction system) than those of the subducting slab anchored to the slower-moving mantle [*Karig*, 1971; *Uyeda and Kanamori*, 1979].

Using data for the 10 largest earthquakes between 1904 and 1976, *Uyeda and Kanamori* [1979] showed that 90% of the seismic energy was released by events occurring in subduction zones without active back-arc basins, such as beneath the Peru-Chile Trench. They attribute this to differences in the extent of mechanical coupling between the upper and lower portions of the subducting plate. For the Mariana Arc, which does contain an active island arc and marginal basin, they postulate that the weak resistive forces encountered by the subducting plate promotes plate decoupling, and that it is this decoupling that is responsible for a simple upward slope from the trench axis, the steeply-dipping Benioff zone [down to 700 km with westward, near-90° slope below 200 km depth, *Katsumata and Sykes*, 1969], and active back-arc spreading. The flattening of the Benioff zone above 200 km may be a manifestation of trench migration [*Karig*, 1971], and the poorly-developed outer gravity high and topographic rise oceanward of the trench suggests little horizontal compression during subduction [*Uyeda and Kanamori*, 1979]. Local models for rift initiation include mantle diapirism [*Karig*, 1971] and convection within the upper plate due to slab subduction [*Sleep and Toksoz*, 1971]; both models, however, cannot entirely explain the observed temporal and spatial distributions of basins, volcanism, and spreading centers.

Historically, two end-member scenarios have been proposed to describe the accretion process, one in which spreading is similar to mid-ocean ridge (MOR) seafloor spreading with ridge segments offset by transform faults [e.g., *Packham and Falvey*, 1971; *Sclater et al.*, 1972], and the other proposing a diffuse spreading model in which volcanism occurs contemporaneously throughout the basin [*Sclater et al.*, 1972, *Lawver and Hawkins*, 1978]. Previous studies of both active and inactive back-arc spreading centers in the western Pacific have documented general similarities in ocean floor depth and topography, seafloor spreading rate and magnetic lineations, heat flow, petrology and geochemistry, and seismic crustal structure with those characterizing the mid-ocean ridge environment, in spite of their very different tectonic settings [*Packham and Falvey*, 1971; *Bibee et al.*, 1980; *Lee et al.*, 1980; *Weissel*, 1981; *Taylor and Karner*, 1983].

4.1.3 Mariana Trough Back-arc Spreading Center

The Mariana Trough is a 1300-km long arcuate-shaped feature bounded by the active Mariana volcanic arc 90 km to the east and West Mariana Ridge remnant arc [inactive for the last 9 MA, *Scott et al.*, 1980] 180 km to the west. Its narrowness in the north near the Bonin arc, broadness and lack of frontal arc in the south, and general curvilinear shape suggests that Mariana Trough formation was accomplished by progressive opening from south to north, rather than a simple rigid-body plate rotation about a single pole [*Karig et al.*, 1978; *Smoot*, 1990]. The spreading process is focused within a well-defined rift valley (this volume), and in a direction that parallels the vector motion (east-west) of the subducting Pacific plate. Bottom sampling and visual age correlation using manganese encrustations on basalts and sediment thicknesses suggested an extrusion zone width of less than 20 km [*Hart et al.*, 1972; *Meijer*, 1976]. 12-kHz and 3.5-kHz echo sounding and single-channel seismic profiling data collected near 18N in 1976 [*Bibee et al.*, 1980] show thick arc-derived volcanoclastic sediments (up to 2 km) abutting crestal ridges in the eastern part of the basin; these sediments are generally undeformed suggesting no extension is taking place east of the axial trough. Especially-thick sequences are found in the Pagan fracture zone, which have provided a channel for turbidity current sediment transport from the volcanic arc.

Most previous geophysical surveys (Figure 4.1.2) investigating the area near 18°N have shown that a coherent and definable spreading axis exists. *Bibee et al.* [1980] and *Hussong and Uyeda* [1981] reported a 7-8 Ma age for the basin, but because of the area's nearness to the magnetic equator, east-west spreading direction, and rough topography, magnetic anomaly evidence for MOR-like seafloor spreading are not convincing. For example, earlier studies observed no coherent magnetic anomaly pattern [*Karig*, 1971; *Anderson*, 1975], leading *Lawver and Hawkins* [1978] to propose the diffuse spreading model. *Bibee et al.* [1980] calculated 1.5 cm/yr for the last 3 Ma by forward modeling the low-amplitude anomalies collected during the 1976 cruise, and *Fryer and Hussong* [1981] reported 1.65 cm/yr based on correlations with basal sediment ages determined from Deep Sea Drilling Project Leg 60 data. Seismic refraction studies carried out both inside and outside the rift valley indicate the oceanic crust to be similar to young (< 5 Ma) Mid-Atlantic Ridge crust with a thickness of 5-7 km [e.g., *Bibee et al.*, 1980; *LaTraille and Hussong*, 1980; *Fryer and Hussong*, 1981; *Ambos and Hussong*, 1982]. At 17°35'N, the ridge intersects the Pagan Fracture Zone, which consists of a series of short *en echelon*, small-offset spreading segments and a 7-km left offset, and to the south, the ridge axis continues as several longer *en echelon* rift valley ridge segments [*Lonsdale*, unpublished manuscript]. This complexity has led *Bibee et al.* [1980] to speculate

that frequent 'ridge jumps' had occurred in response to locally-complex stress patterns associated with the arc-trench tectonic environment.

Near-bottom surveys using the Scripps Institution's Deep Tow system, and ALVIN submersible dives along an Axial Ridge at 18°N, have documented little sediment, fresh basalts, and active hydrothermal venting atop the ridge [*Hawkins et al.*, 1990, *Lonsdale*, unpublished manuscript]. The presence of hydrothermal venting results in a large variation in the observed heat flow [0.26-8.45 HFU; *Anderson*, 1975; *Watanabe et al.*, 1977]. Dredged and ALVIN-collected basalts are similar chemically and mineralogically to normal MOR basalts [*Hawkins and Melchoir*, 1985]. Most observed rock types can be explained by fractional crystallization and magma mixing at low pressures (< 1.5 GPa), with variations due to volatile differences probably related to previous mantle melt histories and the effects of metasomatism on the source. Isotope data suggest a heterogeneous source comprised of both a MORB and an arc source.

4.1.4 KH92-1 Mariana Trough Survey

The high-quality, dense geophysical coverage obtained during KH92-1 about the Mariana Trough spreading center near 18°N, along with previous detailed median valley near-bottom surveys [e.g., *Hawkins and Melchior*, 1985; *Hawkins et al.*, 1990; *Lonsdale*, unpublished data] and off-axis regional experiments [e.g., *Anderson*, 1975; *Bibee et al.*, 1980; *Fryer and Hussong*, 1981; *Hussong and Uyeda*, 1981; *Ambos and Hussong*, 1982], establishes this region as a well-characterized natural geological and geophysical seafloor observatory. Conducted under the auspices of the Japanese InterRIDGE (International Ridge Inter-Disciplinary Global Experiments) program and RIDGE scientific objectives [*Ridge Science Plan*, 1992], KH92-1 cruise data provides the first comprehensive and comparable data set (in data type, density, and areal coverage) of an active back-arc spreading center that can be directly contrasted to the mid-ocean ridge environment.

During the KH92-1 cruise, multi-narrow beam Sea Beam bathymetric, shipboard 3-component and ship-towed total force magnetometer, ocean bottom seismometer refraction and reflection, and gravimeter data were collected along a 100-km long section of the slowly-spreading [~1.5 mm/yr half-spreading rate, *Seama et al.*, this volume] Mariana Trough spreading axis northward of the Pagan Fracture Zone (Figures 4.1.2 and 4.1.3). Results from this cruise should provide a better understanding of the morphology, tectonics, crustal, thermal, and mechanical structure at this back-arc spreading center, and enable a comparison with the crustal accretion process, as it pertains to tectonic setting, spreading rate,

and magma supply, at mid-ocean ridge spreading segments. It is toward these goals that the following preliminary results and discussions are presented.

The near-complete bathymetric data coverage (80%, > 4200 km^2) revealed the existence of a segmented spreading center with a clearly-delineated spreading axis and well-defined median valley (Figure 4.1.3). Three morphologically-distinct spreading segments, each offset 5-8 km by a non-transform discontinuity, were mapped. Simultaneously-collected magnetic data correlated well with the segmentation morphology. A 63-km long, 840-m high axial constructional volcanic ridge, centered at 18°12'N within the 10-14 km wide median valley, represented the dominant spreading segment feature in the study area. Magnetization minima near the axial ridge segment midpoint [*Seama et al.*, this volume], suggesting the existence of sub-seafloor high-temperature anomalies or extensive hydrothermal alteration of the magnetic minerals, were consistent with the presence of the documented ridge crest high- and low-temperature hydrothermal activity [*Hawkins et al.*, 1990]. Numerous small seamounts (20-220 m high, 200-2125 m mean radius) were observed within the median valley. Regularly-spaced and similarly-shaped rift mountain topography (8-11 km in across-axis direction, 35-40 km along-axis shoaling towards ridge midpoint) suggest a temporal and spatial variation in the processes that control crustal accretion.

4.1.5 Crustal Accretion at Slow Spreading Centers

The median valley and rift mountain segmentation, volcanic morphology, and magnetic signature describing the Mariana Trough back-arc spreading center compare similarly with well-studied areas of the Mid-Atlantic Ridge. No evidence for a steady-state magma chamber has been documented at either setting, but both are actively spreading at slow spreading rates (~1.5 mm/yr half-spreading rate). In contrast, seismic data indicates the presence of a thin magma lens beneath the fast-spreading (5 mm/yr) East Pacific Rise [*Detrick et al.*, 1987], and the ridge axis morphology (lacking a median valley) at fast spreading centers differs greatly with that describing the slow spreading centers [e.g., *Macdonald*, 1982]. The remarkable similarities between the Mariana Trough and Mid-Atlantic Ridge indicate that spreading rate is the primary variable, with tectonic setting being only a minor factor, controlling crustal accretionary styles at spreading centers [*Kong et al.*, this volume].

A preliminary comparison shows that both environments (back-arc and mid-ocean ridge) possess a segmented ridge system in which linear constructional volcanic ridges and small seamounts are common identifiable features within a well-defined median valley of comparable width and depth. Previous seismic

studies of the Mariana Trough region document an oceanic crustal structure similar to that found for young Mid-Atlantic Ridge crust [*Bibee et al.*, 1980; *Ambos and Hussong*, 1982; *Purdy and Detrick*, 1986]. Along-axis variations in crustal magnetization, with minima observed near the segment midpoints where the shallowest seafloor depths are found, are observed; the along-ridge topographic variation suggests a spatial variation in the amounts of constructed topography or magma availability. Hydrothermal activity, indicating the presence of elevated crustal temperatures which can reduce magnetization, has also been documented at both settings, but to date, no evidence has been found for a continuous or steady-state magma chamber at slow-spreading centers. High-resolution bathymetry shows the median valley walls to be composed of several hundred meter-high, inward-facing faults spatially offset by several kilometer-wide terraces, and near-bottom surveys document a pervasively-fissured seafloor and extensive mass-wasting of fault scarp faces. The mapping of regularly-spaced off-axis ridges suggest a spatial or temporal variation in the processes that control ridge construction, either by constructional volcanism or through tectonic faulting.

4.1.6 Conclusion

The collection of an extensive geophysical data set from the Mariana Trough back-arc spreading center has, for the first time, permitted a detailed comparison of the crustal accretionary styles at two spreading centers spreading at similar rates, but in response to different tectonic forces (simple plate divergence at a mid-ocean ridge versus extension behind a subducting plate in a marginal basin). Preliminary comparisons show similar styles of crustal accretion, suggesting that the processes responsible for construction of the crust and evolution of seafloor topography may be similar. Results from this geophysical survey, along with other careful geological studies, have made the Mariana Trough near 18°N a regionally well-characterized natural seafloor laboratory. More detailed experiments can now be carried out to better constrain the nature of energy transfer and flux within the Earth's global rift system.

Acknowledgments

This cruise would not have been a success without the efforts of the captain and crew of the R/V Hakuho-Maru. L.S.L.K.'s cruise participation was supported through a Japan Society for the Promotion of Science Postdoctoral Fellowship, and the Japan InterRIDGE program.

References

Ambos, E. L., and D. M. Hussong, Crustal structure of the Mariana Trough, *J. Geophys. Res., 87*, 4003-4018, 1982.

Anderson, R. N., Heat flow in the Mariana marginal basin, *J. Geophys. Res., 80*, 4043-4048, 1975.

Bibee, L. D., G. G. Shor, and R. S. Lu, Inter-arc spreading in the Mariana Trough, *Mar. Geol., 35*, 183-197, 1980.

Detrick, R. S., P. Buhl, E. Vera, J. Mutter, J. Orcutt, J. Madsen, and T. Brocher, Multichannel seismic imaging of a crustal magma chamber along the East Pacific Rise, *Nature*, 326, 35-41, 1987.

Fryer, P., and D. M. Hussong, Seafloor spreading in the Mariana Trough: Results of leg 60 drill site selection surveys, *Initial Rep. Deep Sea Drill. Proj., 60*, 45-55, 1981.

Gross, M.G., *Oceanography - A View of the Earth*, Prentice Hall, Inc., Englewood, N.J., 1977.

Hart, S. R., W. E. Glassley, and D. E. Karig, Basalts and sea floor spreading behind Mariana Island arc, *Earth Planet. Sci. Lett., 15*, 12-18, 1972.

Hawkins, J. W., and J. T. Melchior, Petrology of Mariana Trough and Lau Basin basalts, *J. Geophys. Res.*, 90, 11431-11468, 1985.

Hawkins, J. W., P. F. Lonsdale, J. D. Macdougall, and A. M. Volpe, Petrology of the axial ridge of the Mariana Trough backarc spreading center, *Earth Planet. Sci. Lett., 100*, 226-250, 1990.

Hussong, D. M., and S. Uyeda, Tectonic processes and the history of the Mariana Arc: A synthesis of the results of Deep Sea Drilling Project leg 60, *Initial Rep. Deep Sea Drill. Proj., 60*, 909-929, 1981.

Karig, D. E., Structural history of the Mariana Island arc system, Geol. Sci. Am. Bull., 82, 323-344, 1971.

Karig, D. E., R. N. Anderson, and L. D. Bibee, Characteristics of back arc spreading in the Mariana Trough, *J. Geophys. Res., 83*, 1213-1226, 1978.

Katsumata, M., and L. R. Sykes, Seismicity and tectonics of the western Pacific: Izu-Mariana-Caroline and Ryukyu-Taiwan regions, *J. Geophys. Res.*, 74, 5923-5948, 1969.

LaTraille, S. L., and D. M. Hussong, Crustal structure across the Mariana Island arc, in *The Tectonic and Geologic Evolution of Southeast Asian Seas and Islands, Geophys. Monogr. Ser.*, vol. 23, ed. by D. E. Hayes, pp. 209-222, AGU, Washington, D. C., 1980.

Lawver, L. A., and J. W. Hawkins, Diffuse magnetic anomalies in marginal basin: Their possible tectonic and petrologic significance, *Tectonophysics, 45*, 323-339, 1978.

Lee, C. S., G. G. Shor, L. D. Bibee, R. S. Lu, and T.W. C. Hilde, Okinawa Trough: Origin of a back-arc basin, *Mar. Geol., 35,* 219-241, 1980.

Macdonald, K. C., Mid-ocean ridges: Fine scale tectonic, volcanic, and hydrothermal processes within the plate boundary zone, *Ann. Rev. Earth Planet. Sci., 10,* 155-190, 1982.

Meijer, A., Pb and Sr isotopic data bearing on the origin of volcanic rocks from the Mariana island arc system, *Geol. Sci. Am. Bull., 87,* 1358-1369, 1976.

Packham, G. H., and D. A. Falvey, An hypothesis for the formation of marginal basins in the western Pacific, *Tectonophysics, 11,* 79-110, 1971.

Purdy, G. M. , and R. S. Detrick, The crustal structure of the Mid-Atlantic Ridge at 23°N from seismic refraction studies, *J. Geophys. Res.,* 91, 3739-3762, 1986.

RIDGE Science Plan, 1993-1997, RIDGE Office, Woods Hole Oceanographic Institution, Woods Hole, MA, 101 pgs, 1992.

Ringwood, A. E., Petrogenesis in island arc systems, in *The Earth's Crust and Upper Mantle,* ed. by P. J. Hart, *Geophys. Monogr. 13,* AGU, Washington, D. C., 1977.

Sample, J. C., and D. E. Karig, A volcanic production rate for the Mariana island arc, *J. Volcanol. Geotherm. Res., 13,* 73-82, 1982.

Sclater, J. G., J. W. Hawkins, J. Mammerickx, and C. B. Chase, Crustal extension between the Tonga and Lau ridges: Petrologic and geophysical evidence, *Geol. Soc. Amer. Bull., 83,* 505-518, 1972.

Scott, R. B., L. Kroenke, G. Zakariadze, and A. Sharaskin, Evolution of the south Philippine Sea: Deep Sea Drilling Project leg 59, *Initial Rep. Deep Sea Drill. Proj., 59,* 803-816, 1980.

Sleep, N. H., and M. N. Toksoz, Evolution of marginal basins, *Nature, 33,* 548-550, 1971.

Smoot, N. C., Mariana Trough by multi-beam sonar, *Geo-Mar. Lett.,* 10, 137-144, 1990.

Taylor, B., and G. D. Karner, On the evolution of marginal basins, *Rev. Geophys. Space Phys., 21,* 1727-1741, 1983.

Uyeda, S., and H. Kanamori, Back-arc opening and the mode of subduction, *J. Geophys. Res.,* 84, 1049-1061, 1979.

Watanabe, T., M. G. Kangseth, and R. N. Anderson, Heat floor in back-arc basins of the western Pacific, in *Island Arcs, Deep Sea Trenches and Back-Arc Basins, Maurice Ewing Ser.,* vol. 1, ed. by M. Talwani and W. C. Pitman III, pp. 137-161, AGU, Washington, D.C., 1977.

Weissel, J. K., Magnetic lineations in marginal basins of the west Pacific, *Philos. Trans. R. Soc. London Ser. A, 300,* 223-247, 1981.

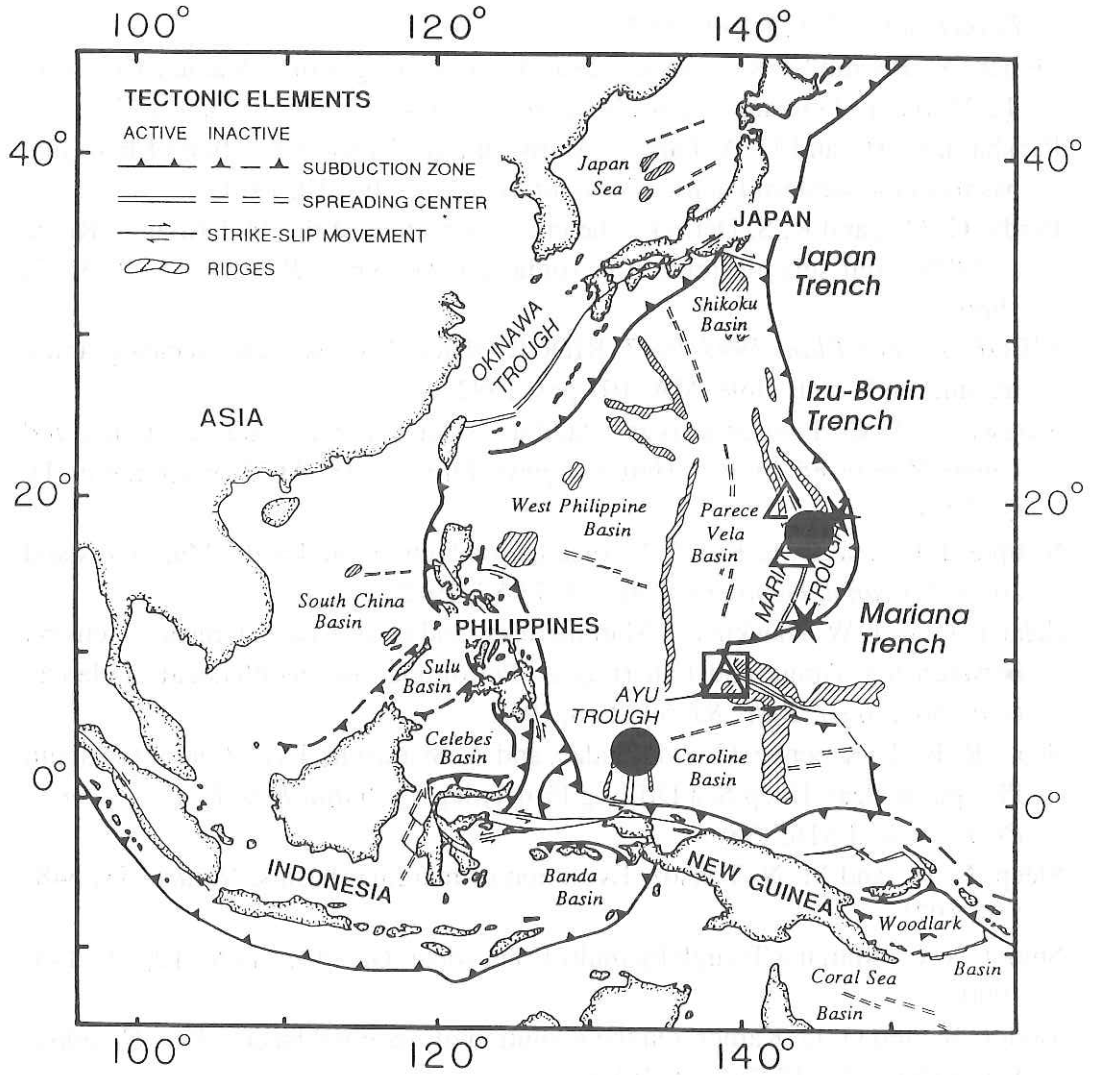

Fig.4.1.1 Distribution of marginal basins and trenches in the western Pacific Ocean. Solid circles indicate locations of the KH92-1 geophysical surveys, stars the locations of petrologic sampling, open triangles the locations of sediment cores, and an open square the location of biological sampling.

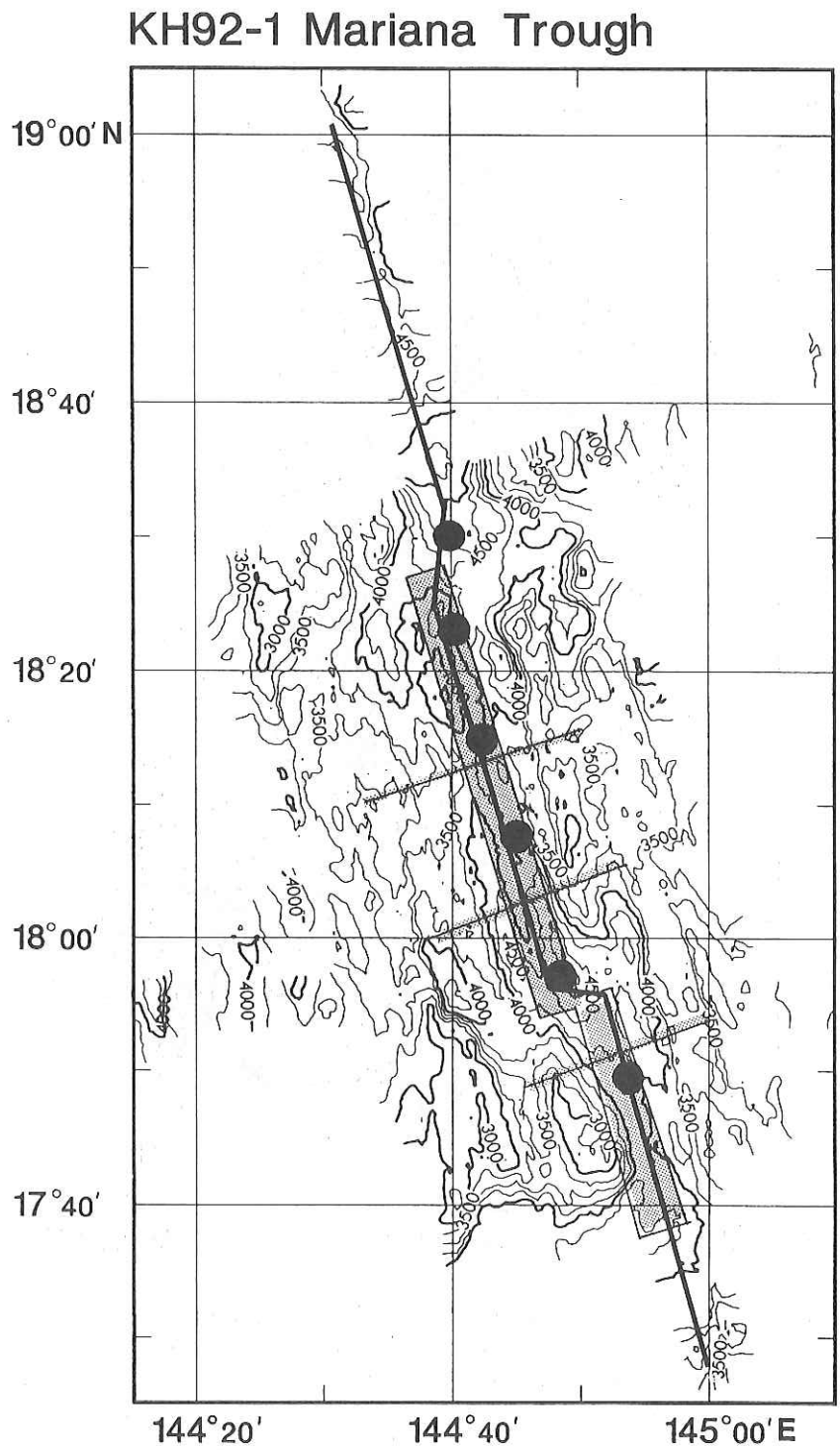

Fig. 4.1.2 KH92-1 Sea Beam bathymetric map of the Mariana Trough area. Along-axis seismic refraction/reflection line is shown as a solid line and ocean bottom seismometer locations as solid circles. Stippled areas show the locations of detailed ALVIN and near-bottom surveys [*Hawkins et al.*, 1990; *Lonsdale*, unpublished data].

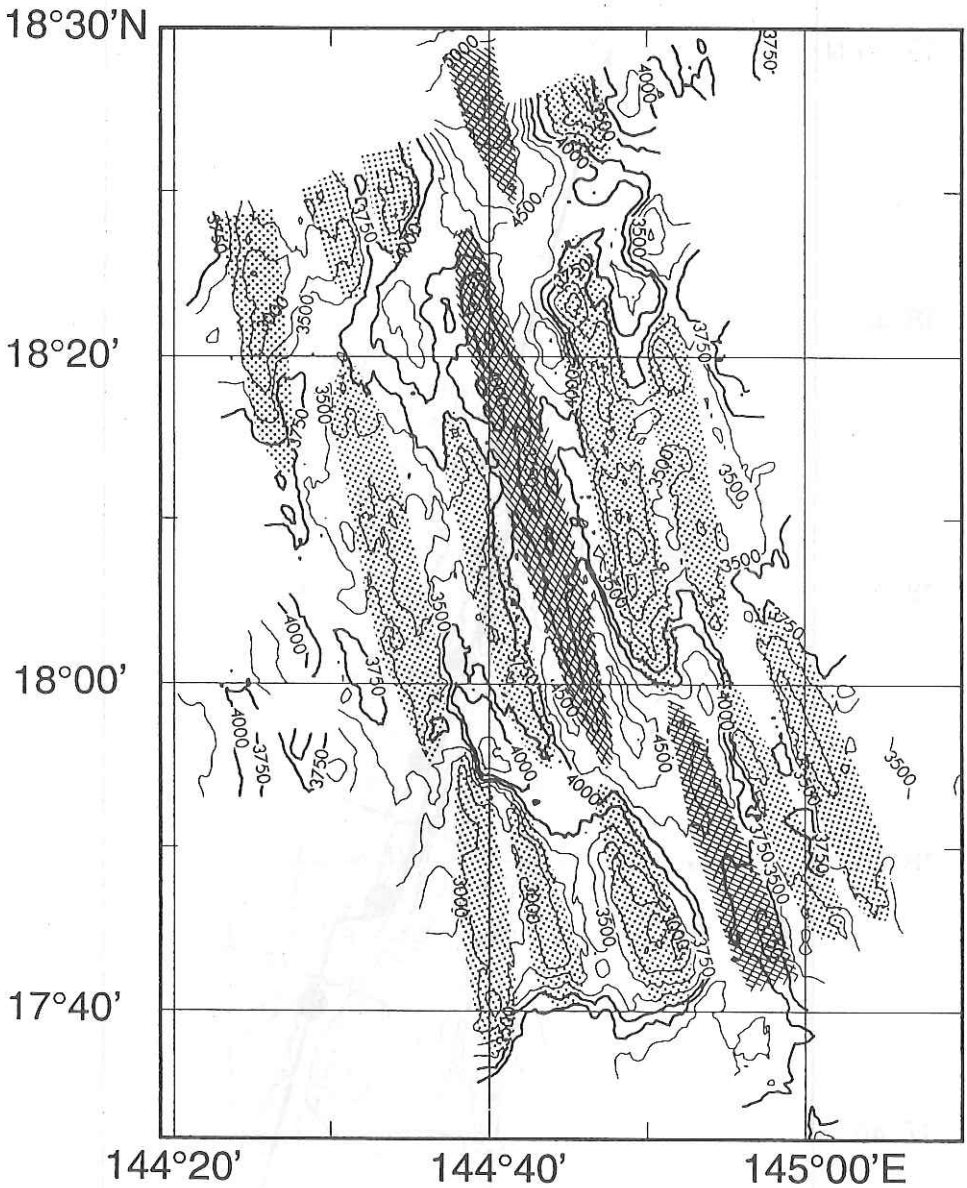

Fig. 4.1.3 Morphotectonic map of the Mariana Trough spreading center near 8°N. Three ridge-axis segments (cross-hatched areas) can be identified within the median valley (stippled areas), with the most prominent characterized by an axial ridge centered at 18°12'N. The ridge is shallowest near its midpoint, and deepens and narrows in width towards its distal ends. The *en echelon* segments are separated by 5-8 km long non-transform discontinuities. Regularly-spaced, similarly-shaped off-axis topographic features are also prominent (stippled areas).

4.2 Significance of the Ayu Trough in the Global Tectonics

T. Seno and K.Tamaki

The Ayu trough is located south of the Palau Trench, forming a divergent boundary between the Philippine Sea and Caroline plates (Fig. 4.2.1, Weissel and Anderson, 1978). This divergence shows a marked contrast with the other convergent boundaries surrounding the Philippine Sea plate (denoted by 'ph' hereafter). This contrast provides a significance of this trough in the global as well as local tectonics. The junction between the Ayu Trough and the Palau Trench forms a scissors-shape junction (Fig. 4.2.2, Wilson, 1963). The above junction is a unique example of this type of junction in the world. We intended to know how this type of transition from convergence to divergence occur by investigating topography and crust/lithosphere structure. The Seabeam survey and other conventional geophysical surveys were conducted in the junction area to clarify the features of the area, though the surveys were not enough because of paucity of ship time. There were found peculiar circular- shape depressions in the area, which might represent the shift of the junction during the geological past.

For the purpose of determining the motion of ph, the only data available are earthquake slip vectors. This makes the determination very difficult (See Seno et al., 1992). Ranken et al. (1984), using the fact that ph is juxtaposed to the Caroline plate (hereafter denoted by 'cr'), showed that the spreading at the Ayu Trough can be used as a constraint to determine the ph motion. That is, they used the rotation vector of Weissel and Anderson between ph and cr (Fig. 4.2.1), and added this vector to the rotation vector of the Pacific plate (pa) and ph, and produced the pa-cr vector. After then, they examined whether the velocities calculated from this vector along the pa-cr boundaries conform to the spreading/strike-slip motion along the Sorol Trough or convergence along the Mussau Trench. This produced a unique solution for the ph-pa or ph and the Eurasian plate (eu) motion. However, because they used the cr-pa rotation vector of Weissel and Anderson, which has a 2.2 deg/My rotation rate, their solution gave a very small convergence at the Sagami Trough and did not satisfy the observed slip vectors along the northernmost Bonin Trench and the Sagami Trough (Seno et al., 1992). Seno et al. (1992) perturbed the ph-cr vector, and obtained the result that the rotation rate of 7.0 deg/My or less harmonizes with the slip vector data around ph. Fig. 4.2.3 shows the relative velocities around the boundaries of ph calculated by their optimal solution. This give a small spreading rate, a few to several mm/yr, along the Ayu Trough. Their possible

solutions, however, permit a smaller spreading rate along the trough. This result implies that if we can determine the spreading rate along the trough, we can constrain the ph motion better. Thus, the determination of the spreading rate at the trough was one of our important objectives in this cruise.

As stated above the plate kinematic consideration suggests that the spreading rate along the Ayu Trough could be very small. We can address a number of questions on this slow accretion process. The magma production rate might be small, so we expect that the axial valley could become deep. This was actually observed (See section 6.4). How is the magma chamber distribution for such slow spreading? Is it segmented like the mid-Atlantic ridge? What kind of geomorphological features are seen in the axial valley and the abbysal hills? Can the crustal thickness anomalies be detected by the residual gravity data? Can the three components magnetic measurements identify the anomaly stripes in the E-W spreading in the equatorial area? In summary, the survey of the trough might be helpful to reveal these general problems related to the accretion processes occurring at the very slow spreading ridges.

References

Ranken, B., Cardwell, R. K., Karig, D. E., Kinematics of the Philippine Sea Plate, Tectonics, 3, 555-575, 1984.

Seno, T., S. Stein, and A. Gripp, A model for the motion of the Philippine Sea plate consistent with NUVEL-1, submitted, 1992.

Weissel, J. K., and R. N. Anderson, Is there Caroline Plate?, Earth Planet. Sci. Letters ,41,143-158, 1978.

Wilson, J. T.,A new class of faults and their bearing on continental drift, Nature, 207, 343-347, 1965.

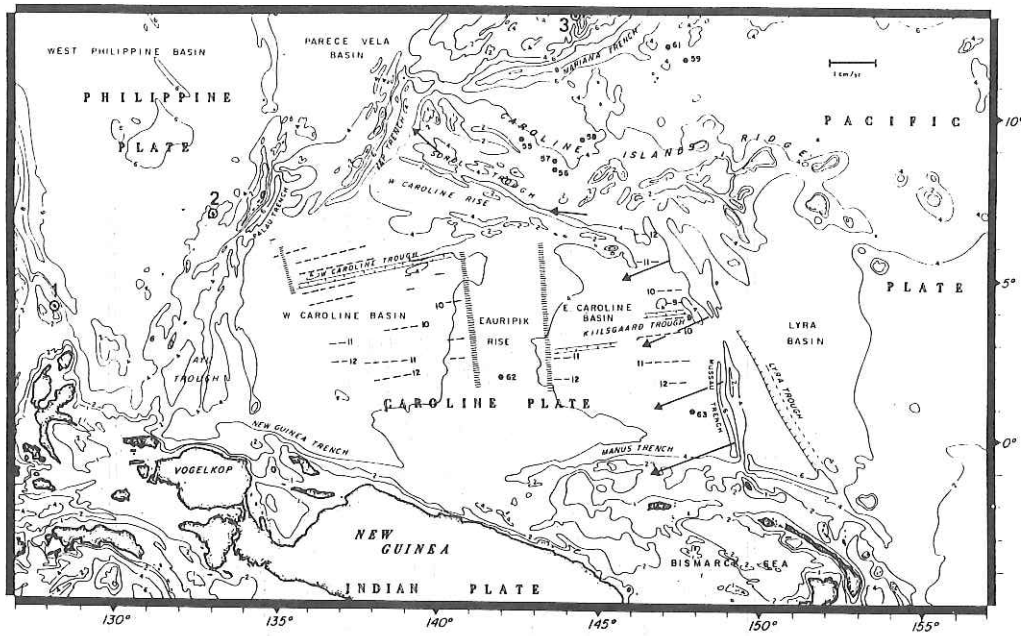

Fig. 4.2.1 Tectonic setting of the Caroline-Philippine Sea plates (Weissel and Anderson, 1978). The motion of the Pacific relative to the Caroline plate calculated by Weissel and Anderson is shown by the arrows. Bathymetric contours are in kilometers.

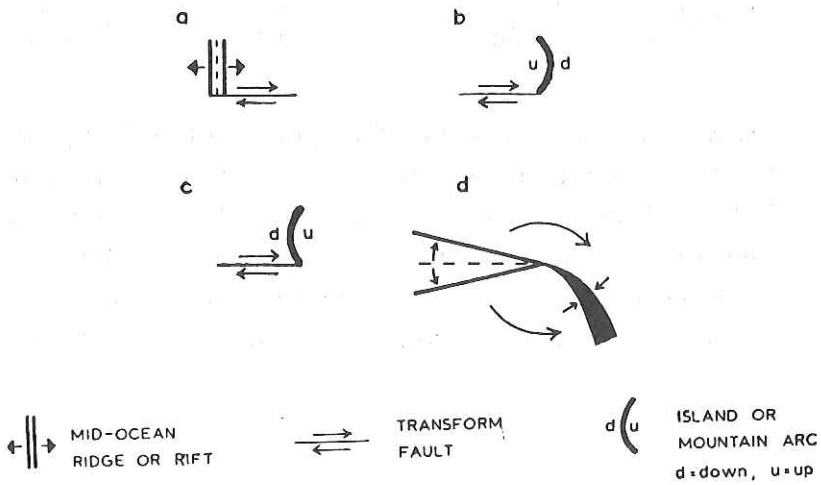

Fig. 4.2.2 Diagram illustrating the four possible right-hand transforms: a, ridge to dextral half-shear: b, dextral half-shear to concave arc; c, dextral half-shear to convex arc; d, ridge to right-hand arc (Wilson, 1965). Type d corresponds to the Ayu Trough - Palau Trench junction.

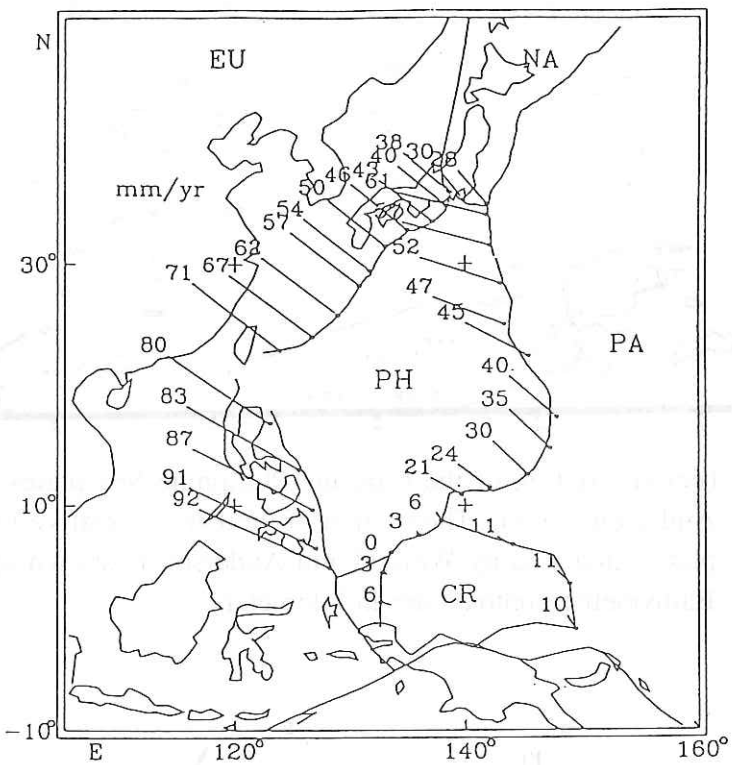

Fig. 4.2.3 Relative velocities around the Philippine and Caroline plates (Seno et al., 1992). Azimuths are indicated by the bars directed from the circles and rates are shown in mm/yr. Along the eu-ph and na-ph boundaries, ph motion with respect to eu or na is shown. Along the pa-ph and pa-cr boundaries, pa motion with respect to ph or cr is shown. Along the cr-ph boundary, cr motion with respect to ph is shown.

5. Navigation and Data Logging

H. Fujimoto and S. Hayashikawa*

*Second Officer of Hakuho-Maru

The navigation and data logging system on board the Hakuho-maru is shown in Fig. 5.1. Hybrid navigation data based on Calman filtering is obtained by use of an integrated navigation system Magnavox Series 5000. The ship is operated with the "Total Navigator" based on the navigation data given by the Series 5000.

The Series 5000 utilizes the optical data network JCX8200 for data logging and real-time data distribution. Various observed data gathered through the local area network as well as navigation data are logged on magnetic tapes. Because the data Format is rather complicated, a special software is installed on awork station YHP835 in Laboratory No. 8 (see the section 6.1) for off-line processings of the data recorded on the magnetic tapes. Principal part of navigation data are distributed every 1 second through a channel of the local area network to each laboratory of the vessel. Various observed data and detailed information of navigation data are also distributed every 5 seconds through the same channel. Raw data of a GPS (Global Positioning System) receiver is distributed on another channel. The network is based on RS-232C or RS-422, and is easy of access from a personal computer.

Ship's positioning was not so accurate during this cruise, because accuracy of GPS (Global Positioning System) navigation has been degraded since the middle of November 1991, when the Department of Defense, U.S.A., started the operation of selective availability (SA) of GPS. The accuracy of GPS positioning by use of CA code was in general 20-30 m, but it is said that SA will degrade the accuracy to be about 100m.

Two other systems as well as the Magnavox Series 5000 were used for logging the data on hard disks of work stations. One is the "real-time mapping system", which was used for mapping and logging Sea Beam and geophysical data. The other is the "navigation development" work station, which was used for logging every 1 minute data distributed through the network JCX8200. The recorded data on each of the hard disks are easy of real-time access through the Ethernet network.

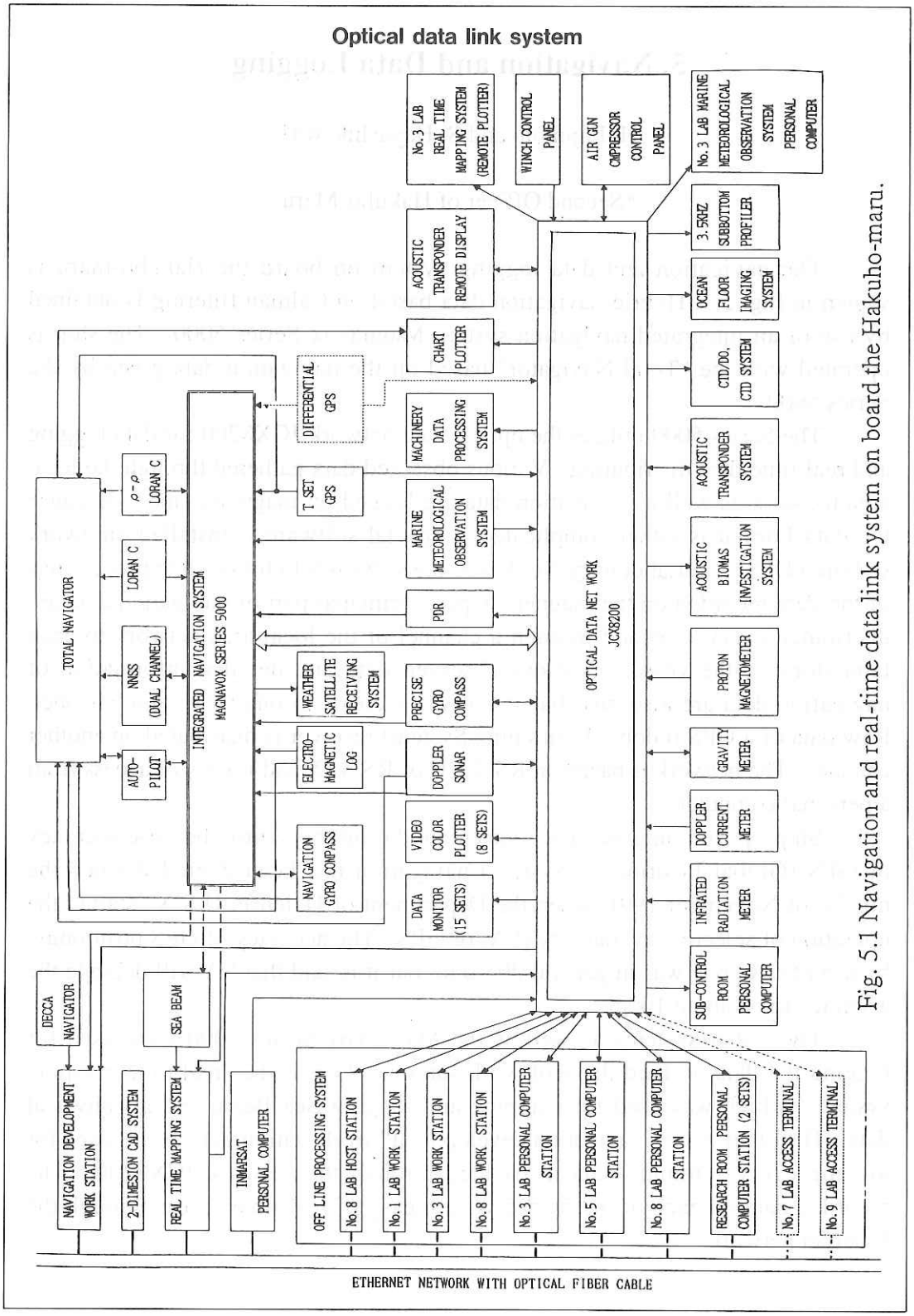

Fig. 5.1 Navigation and real-time data link system on board the Hakuho-maru.

6. Bathymetric Mapping using the Sea Beam System

6.1 Sea Beam System

H. Fujimoto, K. Tamaki and K. Kobayashi

Swath bathymetric survey was carried out throughout the cruise using a system of multi-narrow beam echo sounder "Sea Beam". Block diagram of the signal processing of the Sea Beam system on board the Hakuho-maru is shown in Fig. 6.1.1 The system has an option to utilize a precision gyro compass Tokyo Keiki SGC-I as a backup gyro. "Hippy" is a standard gyro system for the Sea Beam and was used during the cruise.

A real-time mapping system shown in Fig. 6.1.2 was used for bathymetric mapping with navigation data. An A0-size flat-bed plotter is used for detailed bathymetric contouring, and a colour graphic display shows the outline of seafloor topography.

The system is used also for the logging of geophysical data as well as Sea Beam data. The data are stored in a 300MB hard disk to be easy of realtime access from any of several work stations on board the ship through an optical Ethernet LAN (Local Area Network). During this cruise, however, the work station for the real-time mapping system had some problem with the network; a cassette tape was used to transfer the data to a 2GB hard disk of the main work station YHP835.

Off-line processing of the observed data was carried out mainly by use of the YHP835 system with a color electrostatic plotter. A few kinds of mapping software developed by Dr. K. Tamaki and his colleagues by use of subroutines of UNIRAS have helped us produce nice topographic maps.

SEA BEAM SIGNAL PROCESSING

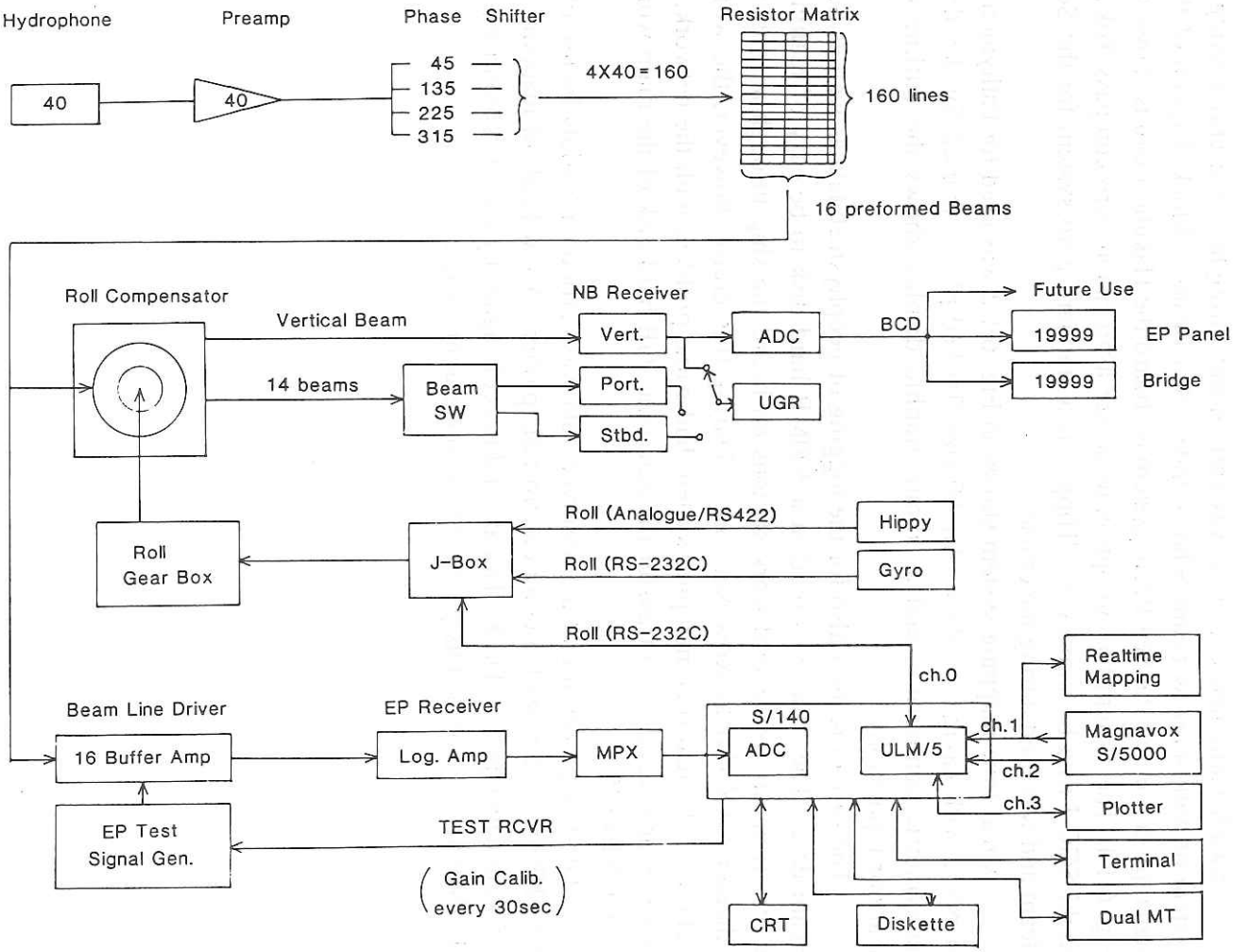

Fig. 6.1.1 Block diagram of the signal processing of the Sea Beam system on board the Hakuho-maru.

Real-time Mapping System

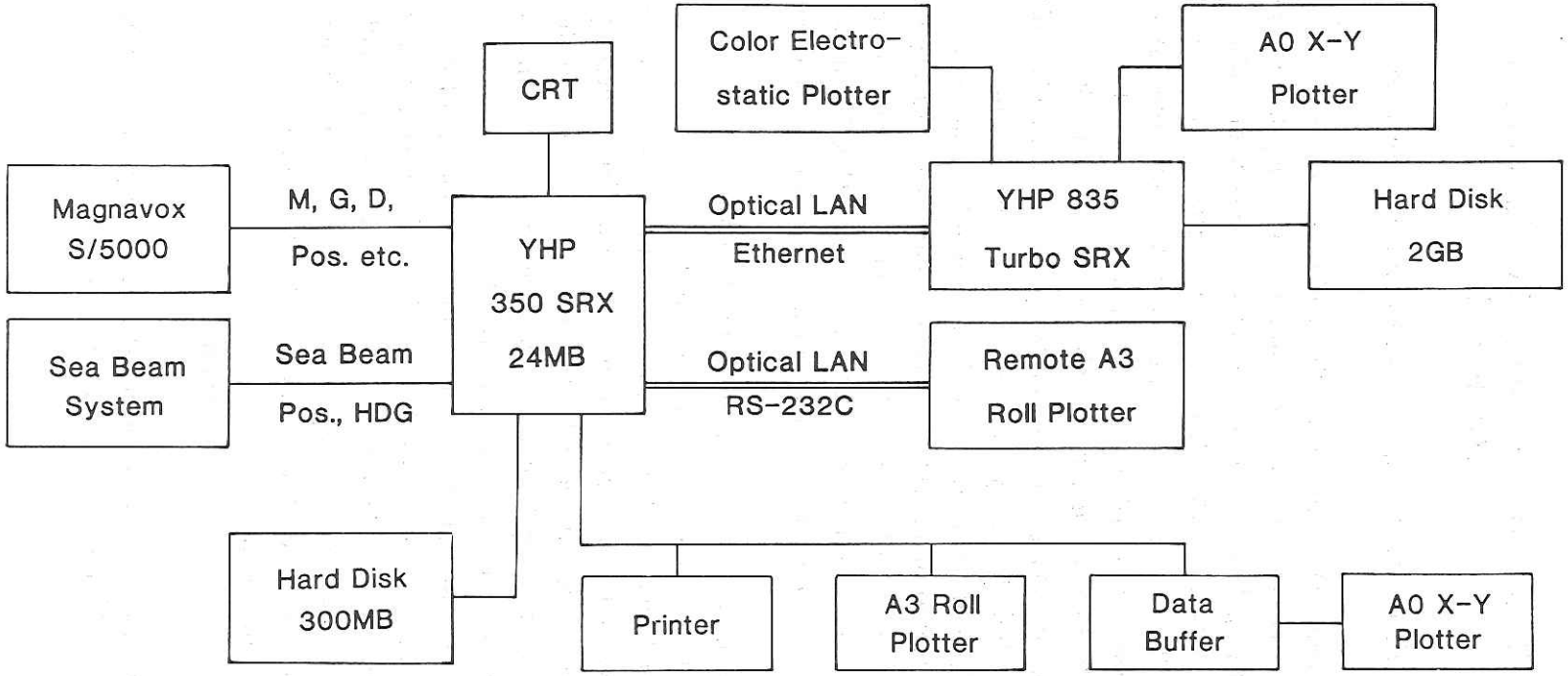

Fig. 6.1.2 Reai-time mapping system on board the Hakuho-maru.

6.2 Sea Beam Survey over the Challenger Deep Revisited

H. Fujimoto, T. Fujiwara, L. Kong and C. Igarashi

The Challenger Deep in the southern Mariana Trench is known as the deepest place in the world. The maximum water depth ever recorded is 11,034m(R/V Vityaz, 1957). The Hydrographic Department, Maritime Safety Agency, Japan, carried out Sea Beam survey in 1984 around the Challenger Deep by using the survey vessel Takuyo and found several deep holes (Hydrographic Department, 1984). The maximum water depth was recorded at 11° 22.4' N, 142° 35.5' E, and the depth was 10,924m +/- 10m. This water depth was obtained by using a velocity profile given by in situ CTD observation.

The deepest hole found by the Hydrographic Department was revisited on February 7, 1992, on the way from the Ayu Trough to Guam in the final stage of Leg 1 of the Hakuho-maru KH-92-1 cruise. Bathymetric survey by using the Sea Beam system and 3.5 kHz sub-bottom profiler was carried out. Figure 6.2.1 shows the on-line record of the Sea Beam survey. The Hakuho-maru passed just over the deepest hole at a cruising speed of about 16 knots; good navigation is noticeable.

The maximum water depth obtained by the on-line system was 10,550m. The on-line output from the Sea Beam system is based on a sound velocity of 1500 m/s. Although in situ CTD or XBT measurement is necessary to obtain an accurate sound velocity, we can estimate the value fairly well by using the Carter's correction table for the echo sounding. According to the table, the correction value for the depth sounding is 383m, so that the maximum water depth observed during our survey is about 10,933 m.

It is noteworthy that much the same value was obtained from the two Sea Beam surveys. These results show the reliability of bathymetric survey by the Sea Beam system, and also the reliability of the survey of the Challenger Deep by the Hydrographic Department. Revisiting the deepest hole during this cruise was realized owing to a good coordination by the chief scientist Prof. J. Segawa and the captain S. Shimamune.

Reference

Hydrographic Department, Japan Maritime Safety Agency, Mariana Trench Survey by the "Takuyo", 351-352, International Hydrographic Bulletin, 1984.

05/59/44
046° 20 M

06/11/27
046° 20 M

KH-92-1 Leg 1
7th Feb. 1992

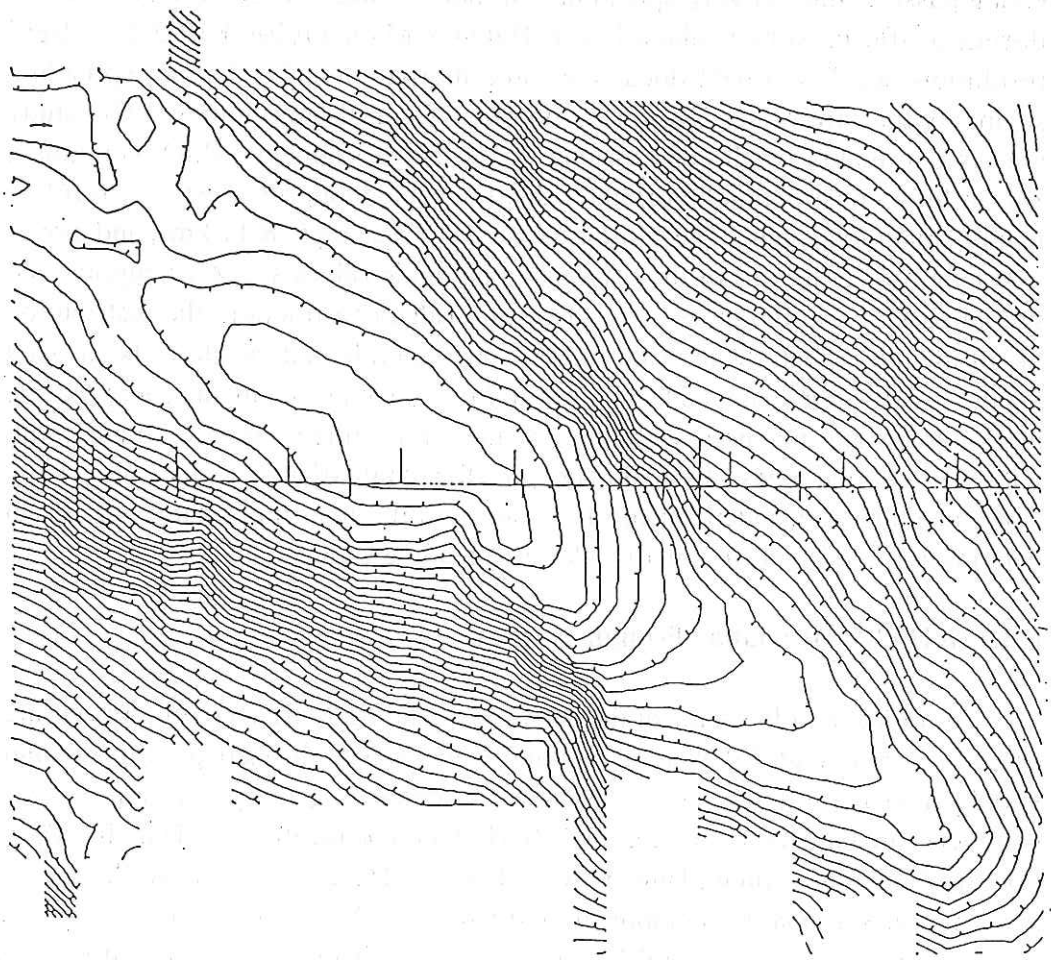

Fig. 6.2.1 On-line record of the Sea Beam survey over the Challenger Deep.

10220 10400 10540 10540 10360 10200 10040

6.3 Segmentation of the Mariana Trough Backarc Spreading Center at 18°N

L. Kong, J. Kasahara, H. Fujimoto, T. Fujiwara, C. Igarashi and N. Seama

Abstract

Near-complete geophysical coverage of a 50 km by 100 km area encompassing the actively-spreading Mariana Trough at 18°N was obtained during a 100-hr survey aboard R/V Hakuho Maru cruise KH92-1. High-resolution Sea Beam data document three morphologically-distinct spreading segments that are offset 5-8 km by non-transform discontinuities. The study area is dominated by the 63-km long Axial Ridge segment, which contains a 840-m high constructional volcanic ridge traceable along its crest as a N165°E line of small volcanoes. The constant across-axis spacings (8-11 km), and along-axis lengths (35-40 km) of the off-axis topographic ridges suggest temporal and spatial variation in the processes that control ridge construction; the distribution of rift mountain features indicates that segmentation boundaries have been fixed for the last 1.5 Ma. The median valley and rift mountain segmentation, volcanic morphology, and magnetic signature [Seama et al., this volume] compare well with well-studied areas of the slowly-spreading Mid-Atlantic Ridge, suggesting that spreading rate, independent of tectonic setting, is an important variable in determining crustal accretionary styles at spreading centers.

6.3.1 KH92-1 Mariana Trough Survey

In order to help establish the actively-spreading Mariana Trough back-arc spreading center at 18°N as a regionally well-characterized geological and geophysical natural seafloor observatory, a detailed geophysical survey was conducted in January-February, 1992 (KH92-1), aboard the R/V Hakuho Maru (Ocean Research Institute, University of Tokyo). Multi-narrow beam Sea Beam bathymetry, shipboard 3-component and ship-towed total force magnetometer, ocean bottom seismometer (OBS) refraction and seismic reflection, and gravity data were collected along a 100-km long region centered about the spreading axis and extending northward from the Pagan Fracture Zone (Figures 6.3.1 and 2 and see also the frontispiece 1 facing front cover); the 100-hr Mariana Trough survey was part of a 19-day multi-disciplinary cruise that included Mariana forearc and Ayu Trough studies [*Segawa and Kobayashi*, this volume]. A 500-km long west-east geophysical profile (Parece Vela Basin to Mariana Trench) was also carried out to investigate the density structure of the subducting Pacific

plate, and to characterize the deployment region for an ocean-floor geophysical station that will reuse the TPC-1 Japan-Guam telephone cable for scientific data collection scientifically [*IRIS Steering Committee for Scientific Use of Submarine Cables*, 1992].

The high-resolution Sea Beam data were essential for selecting and successfully deploying the OBSs, and for accurately locating the seismic shooting line along the Axial Ridge, suggested by *Hawkins et al.* [1990] as the most likely along-axis locale for an active magma chamber from petrologic data and ALVIN observations of hydrothermal vent deposits and fauna. The depth data were also critical for determining accurate topographic corrections to the seismic, gravity, and magnetic data; the existence of three-dimensional bathymetric coverage of the seafloor is especially important in slow spreading environments where the topography is characteristically rugged.

This paper documents the along-axis variations in median valley morphology, rift-axis segmentation, and rift mountain topography that were mapped at the active Mariana Trough slow-spreading center. The near-complete geophysical coverage collected along a 100-km length of the Mariana Trough then allowed a comparison of its characteristics with those of well-studied ridge segments on the slow-spreading Mid-Atlantic Ridge. Preliminary results show a number of similarities indicating that crustal accretion at this back-arc spreading center is indistinguishable morphologically and magnetically from that characterizing the mid-ocean ridge.

6.3.2 Sea Beam Data

Altogether, over 1700 km of General Instrument Corporation Sea Beam data were collected during the 46-hour bathymetric survey and the ensuing seismic experiment (Figure 6.3.1). The bathymetric survey encompassed a 50 by 100 km area centered about the ridge axis; four lines nearest the Pagan Fracture Zone were shortened to 47 km in order to keep to the cruise time schedule. About 80% areal coverage (> 4200 km^2 of data) was obtained using a 4-km track spacing and average ship speed of 16 kts (nominal Sea Beam data sampling of 8 s, or 125 m). Watch standing by members of the shipboard scientific party from the Earthquake Research and Ocean Research Institute of the University of Tokyo, and Chiba University ensured the integrity of the Sea Beam data collection process.

A Magnavox Series 5000 navigation system utilizing Kalman filtering derived the best possible estimate of ship location and speed using a number of navigational sensors; in the study area, Global Positioning System data were generally available 24-hours a day. Sea Beam track crossings, especially in

areas of steep topography, were visually examined to estimate the accuracy of the ship's navigation. The good correlation found indicated that errors were in general minimal (< 50-100 m), thus allowing the seismic survey team to confidently select desirable deployment locations for the OBSs, and then to use the character of the bathymetry to successfully deploy the OBSs (e.g., a change from a steep slope to flat plateau where the OBS was to be dropped). The small navigation errors also allowed the merging of Sea Beam data sets from different volumes without compromising the validity of a particular day's data.

Real time interpretations were made possible through real time color displays on a computer workstation, 4-color pen plotter, and roll chart recorder. Data were collected on both 9-track magnetic tape and through the computer workstation. Volume changing of the magnetic tape and further processing of the Sea Beam data were performed daily, enabling the merging and color-plotting of a gridded data set on the shipboard Hewlett Packard computer; UNIRAS software was used to grid, contour, and color shade the data for plotting on a Calcomp color electrostatic plotter. In addition, color copies of the computer workstation screen were possible using a A3-size thermal wax printer. Typical times for making Sea Beam bathymetric maps ranged from 20 minutes for black-and-white contour line plots to more than 2 hours for color-shaded plots of the entire 50,000-sample data set (20 Mb of disk space for the plot file only).

6.3.3 Results

6.3.3.1 Median Valley Segmentation

Three morphologically-distinct, ridge-axis spreading segments with clearly delineated neovolcanic zones were found within the median valley from 17°40'N to 18°35'N (Figure 6.3.2). The median valley (taken as the 3750 m depth contour) narrows and widens along axis, being narrowest adjacent to the Pagan Fracture Zone and at the Axial Ridge Segment center (9 km), and widest at the segment boundaries (20-25 km). Magnetic structural boundaries, or magnetically-defined segments [*Seama et al.*, this volume], are well-correlated with the locations of the morphologically-defined segments. The ridge axis segmentation is consistent with earlier interpretations based on less-comprehensive U.S. Naval Oceanographic Office bathymetry data [*Hawkins et al.*, 1990; *Lonsdale*, unpublished manuscript].

The segments each have uniquely different morphologic characters that presumably reflect variations in the amounts and vigor of tectonism and magmatism. The segment boundaries, small (5-8 km) non-transform

discontinuities, are also recognizable in the magnetic structure as an abrupt change in magnetic boundary strike at 18°25'N, 144°41'E, and as an offset in the magnetic strikes at 17°52'N, 144°44'E [*Seama et al.*, this volume]. Numerous circular-to-elliptical contours interpreted as small volcanic cones can be identified within the median valley (Figure 6.3.3). A compilation of 40 of these features for the Mariana Trough reveals an average diameter of 1.1±0.7 km, elongation (ratio of basal length to width) of 1.8±1.3, and height / mean radius ratio of 0.13±0.07.

The 100-km long study region is dominated by an axial ridge (Figure 6.3.2, 4000 m depth contour) traceable as a N164°E-trending line of volcanic cones (Figure 6.3.3). The seamounts are spaced about 3 km apart, and have heights and basal diameters up to 220 m (70 m average) and 4 km, respectively. The ridge crest from 18°10'-18°14'N, where ALVIN dives have discovered high- and low-temperature hydrothermal venting [*Hawkins et al.*, 1990], exists as a 2-km wide plateau topped by several volcanoes (<3750 m deep, Figure 6.3.3). The vertical magnetic field strength varies significantly along the ridge, being high in the north and south and markedly subdued from 18°05'-18°12'N near the segment middle [*Seama et al.*, this volume]. To the north and south, the ridge tapers and deepens until it disappears into the deepest regions (> 4400 m) along the valley floor. The ridge can be traced along-axis for 63 km, and in some places rises more than 800 m above the surrounding seafloor.

Southward toward the Pagan Fracture Zone and offset 8 km to the east of the Axial Ridge segment, the Sea Beam bathymetry and magnetic data [*Seama et al.*, this volume] define the Southern Mariana Trough segment located near the eastern median valley wall (Figure 6.3.2). The segments are separated by a morphological deep (> 4900 m), coincident with a noticeable decrease in the vertical component magnetic field strength and an offset to the east in the location of the central magnetic anomaly. This segment is characterized again by a N164°E trending line of circular contours, or volcanic cones, averaging 65 m in height and 1.1 km in basal diameter. The Southern segment (4250 m depth contour) can first be identified by volcanic cones at 17°57'N, 144°51.5'E (just to east of 4500 m depth contour), and in contrast to the linear Axial Ridge segment, has instead a sinuous character that suggests a more dispersed volcanic construction process. The southern terminus of the segment can traced as a 100-m high ridge into the Pagan Fracture Zone trough.

The third segment (Northern Mariana Trough segment) north of the Axial Ridge segment is less well-documented because of the limited amount of Sea Beam and magnetic data. The trough axis of this segment is offset about 5 km to the east from the Axial Ridge segment, and dominated by a morphologic deep (5400 m at 18°36'N, 144°39'E) at its southern terminus (Figure 6.3.2, 4500 m

depth contour). Although a few circular cones can be identified, it is not known whether this is characteristic of the segment, nor whether the KH92-1 Sea Beam ship track steamed over the axis of the ridge segment; the limited data suggest that the ship track may have been shifted toward the eastern median valley wall and away from the segment axis.

6.3.3.2 Rift Mountain Segmentation

Mapping of the rift mountain topography reveals several interesting features. To both the east and west of the Axial Ridge segment, two sets of 30-45 km long, axis-parallel, linear-trending topographic highs can be identified (Figure 6.3.2, thick dashed lines). Across-axis spacing between the features, which have similar elevations and shapes (several 100-m high with a tapering and deepening toward the distal ends), is remarkably constant (8-11 km), suggesting a temporal variation in the processes that control ridge construction (either by magmatism and/or tectonic faulting). Assuming an average half-spreading rate of 15 mm/yr based on the observed width of the zone of normal magnetization, this corresponds to a 0.5-0.7 Ma variation. Similarly-spaced rift mountain features are also present to the north and south of the segment boundaries (Figure 6.3.2).

The along-axis lengths of the rift mountain topographic highs also appear to be relatively constant (35-40 km) and shallowest toward the segment midpoint, suggesting a spatial variation in the amounts of the constructed topography or availability of magma. Furthermore, comparison of the locations of the ridge segments within the median valley with those inferred off-axis (rift mountains) suggests that the segmentation boundaries have been fixed for the last 1.5 Ma.

6.3.4 Discussion - Mariana Trough versus Mid-Atlantic Ridge

The collection of near-equivalent geophysical data sets (in type and coverage) has, for the first time, allowed the examination of crustal accretion at two spreading centers that are forming in response to different tectonic forces (back-arc spreading center and slow-spreading mid-ocean ridge). Preliminary comparison reveals no significant differences in their morphologic and magnetic characters, suggesting that the slow spreading rate may be an important variable controlling crustal accretionary styles at spreading centers.

Both the Mid-Atlantic Ridge [e.g., *Kong et al.*, 1988; *Sempere et al.*, 1990; *Grindlay et al.*, 1992] and Mariana Trough possess a segmented ridge system. In the MARK area (Mid-Atlantic Ridge at 23°N), two morphologically-

distinct *en echelon* ridge segments were identified along a 100-km length of ridge south of the Kane Fracture Zone [Figure 6.3.4, *Kong et al.*, 1988]; of the two, the 50-km long northern spreading cell was considered magmatically-active and dominated by a 500-m high constructional volcanic ridge and high-temperature hydrothermal activity [*Detrick et al.*, 1986]. Similarly, four ridge segments were documented along a 227-km long region from 25°S to 27°30'S, with the southernmost segment showing an median volcanic ridge [*Grindlay et al.*, 1992]. Topographic reliefs characterizing the Mariana Trough segments (63-km long Axial Ridge - 840 m, 34-km long Southern Segment - 330 m) are also consistent with linear correlations of ridge segment length versus ridge elevation found along the Mid-Atlantic Ridge from 24°-30°N [*Lin et al.*, 1990], and 25°-27°S [*Grindlay et al.*, 1992].

The Mariana Trough Axial Ridge morphologic character compares similarly with the axial ridge found in the MARK area [Figure 6.3.4, *Kong et al.*, 1988]. Along-axis magnetization minima [near the Axial Ridge segment midpoint, *Seama et al.*, this volume], consistent with elevated temperatures or extensive hydrothermal alteration of the magnetic minerals, has also been observed associated with hydrothermal activity on the Mid-Atlantic Ridge in the MARK area [*Schultz et al.*, 1988] and the TAG area [Mid-Atlantic Ridge at 26°N, *McGregor et al.*, 1977; *Wooldridge et al.*, 1992]. Finally, regularly-spaced rift mountain topography coincident with the latitudes of inferred ridge segments appear to also be characteristic of the slow-spreading Mid-Atlantic Ridge [e.g., Figure 6.3.4, MARK area, *Kong et al.*, 1988]. The presence of a median valley linear volcanic ridge with hydrothermal activity at the shallowest points along the ridge, as well as similarly-shaped, regularly-spaced rift mountain topography in both areas, suggests that linear volcanic ridge formation may be a dominant form of topographic construction during voluminous periods of magmatism, and that the preferred magmatic source locations for segment formation appear to be spatially-variable, but persistent for several magmatic episodes, along the ridge axis.

Circular-shaped volcanic edifices appear to be common features at both this back-arc spreading center and on the Mid-Atlantic Ridge. Volcano statistics (mean radius 0.55±0.35 km, height/mean radius ratio 0.13±0.07) for the Mariana Trough are very similar to those found for 65 MARK area volcanoes on the Mid-Atlantic Ridge [1.2±0.5 and 0.14±0.05, respectively; *Kong and Cann*, unpublished manuscript], suggesting that the processes responsible for volcanic cone formation are the same at a back-arc spreading center as at a mid-ocean ridge. Recent high-resolution bathymetric data of the MAR reveal that seamounts are ubiquitous features along the mid-ocean ridge system; *Smith and*

Cann [1990] report that more than 480 median valley volcanoes (50-600 m high) were mapped over an 800 km long length the ridge from 24°-30°N.

6.3.5 Summary

Over 4200 km^2 of Sea Beam data, with 80% areal coverage, were collected over a 50 by 100 km area of the Mariana Trough spreading center extending northward from the Pagan Fracture Zone during the cruise leg KH92-1. Real time data display and processing made possible real-time morphologic and tectonic analysis of the bathymetric data during the survey. Results document a segmented ridge axis dominated by a 63-km long medial axial ridge; segments to the north and south are offset 5-8 km to east. The linear Axial Ridge segment is topped by a line of circular to elongated volcanic cones. Examination of rift mountain topography reveals that the segmentation observed within the median valley persists off axis (35-50 km length scale), with a time scale of about 0.6 Ma. Comparison with the Mid-Atlantic Ridge suggests that Mariana Trough crustal accretion is morphologically and magnetically indistinguishable from the slow-spreading mid-ocean ridge.

Acknowledgments

We gratefully recognize the efforts of the shipboard scientific party, and the captain and crew of the R/V Hakuho-Maru for the collection of an excellent data set. L.S.L.K. acknowledges the support of the Japanese Education Ministry, and in particular the Japan InterRIDGE program, for funds toward her participation on this cruise.

References

Detrick, R. S., J. Honnorez, and Leg 106 Scientific Party, Drilling the Snake Pit hydrothermal sulfide deposit on the Mid-Atlantic Ridge, lat. 23°22'N, *Geology, 14*, 1004-1007, 1986.

Grindlay, N. R., P. J. Fox, and P. R. Vogt, Morphology and tectonics of the Mid-Atlantic Ridge (25°-27°30'S) from Sea Beam and magnetic data, *J. Geophys. Res., 97*, 6983-7010, 1992.

Hawkins, J. W., P. F. Lonsdale, J. D. Macdougall, and A. M. Volpe, Petrology of the axial ridge of the Mariana Trough backarc spreading center, *Earth Planet. Sci. Lett., 100*, 226-250, 1990.

IRIS Steering Committee for Scientific Use of Submarine Cables, Scientific use of submarine telecommunications cables, *EOS, 73*, 97, 1992.

Kong, L. S. L., R. S. Detrick, P. J. Fox, L. A. Mayer, and W. B. F. Ryan, The morphology and tectonics of the MARK area from Sea Beam and Sea MARC I observations (Mid-Atlantic Ridge 23°N), *Mar. Geophys. Res.*, *10*, 59-90, 1988.

Lin, J., G. M. Purdy, H. Schouten, J.-C. Sempere, and C. Zervas, Evidence from gravity data for focused magmatic accretion along the Mid-Atlantic Ridge, *Nature*, *344*, 627-632, 1990.

McGregor, B. A., C. G. A. Harrison, J. W. Lavelle, and P. A. Rona, Magnetic anomaly pattern on the Mid-Atlantic Ridge crest at 26°N, *J. Geophys. Res.*, *82*, 231-238, 1977.

Schultz, N. J., R. S. Detrick, and S. P. Miller, Two and three-dimensional inversions of magnetic anomalies in the MARK area (Mid-Atlantic Ridge 23°N), *Mar. Geophys. Res.*, *10*, 41-47, 1988.

Sempere, J.-C., G. M. Purdy, and H. Schouten, Segmentation of the Mid-Atlantic Ridge between 24°N and 30°40'N, *Nature*, *344*, 427-431, 1990.

Smith, D. K., and J. R. Cann, Hundreds of small volcanoes on the median valley floor of the Mid-Atlantic Ridge at 24-30°N, *Nature*, 348, 152-155, 1990.

Wooldridge, A. L., C. G. A. Harrison, M. A. Tivey, M. A., P. A. Rona, and H. Schouten, magnetic modeling near selected areas of hydrothermal activity on the Mid-Atlantic and Gorda Ridges, *J. Geophys. Res.*, *97*, 10911-10926, 1992.

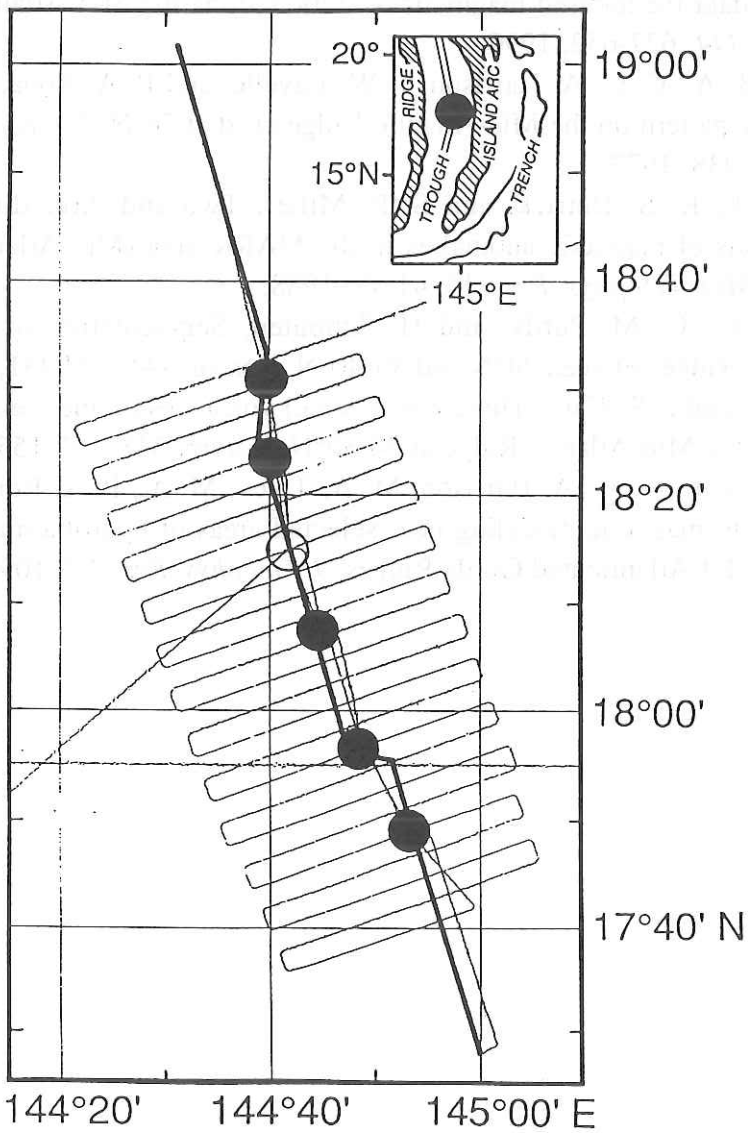

Fig. 6.3.1 Mariana Trough KH92-1 Sea Beam ship track (thin line), seismic line (thick line), and OBS locations (circles, open circle denotes unrecovered OBS).

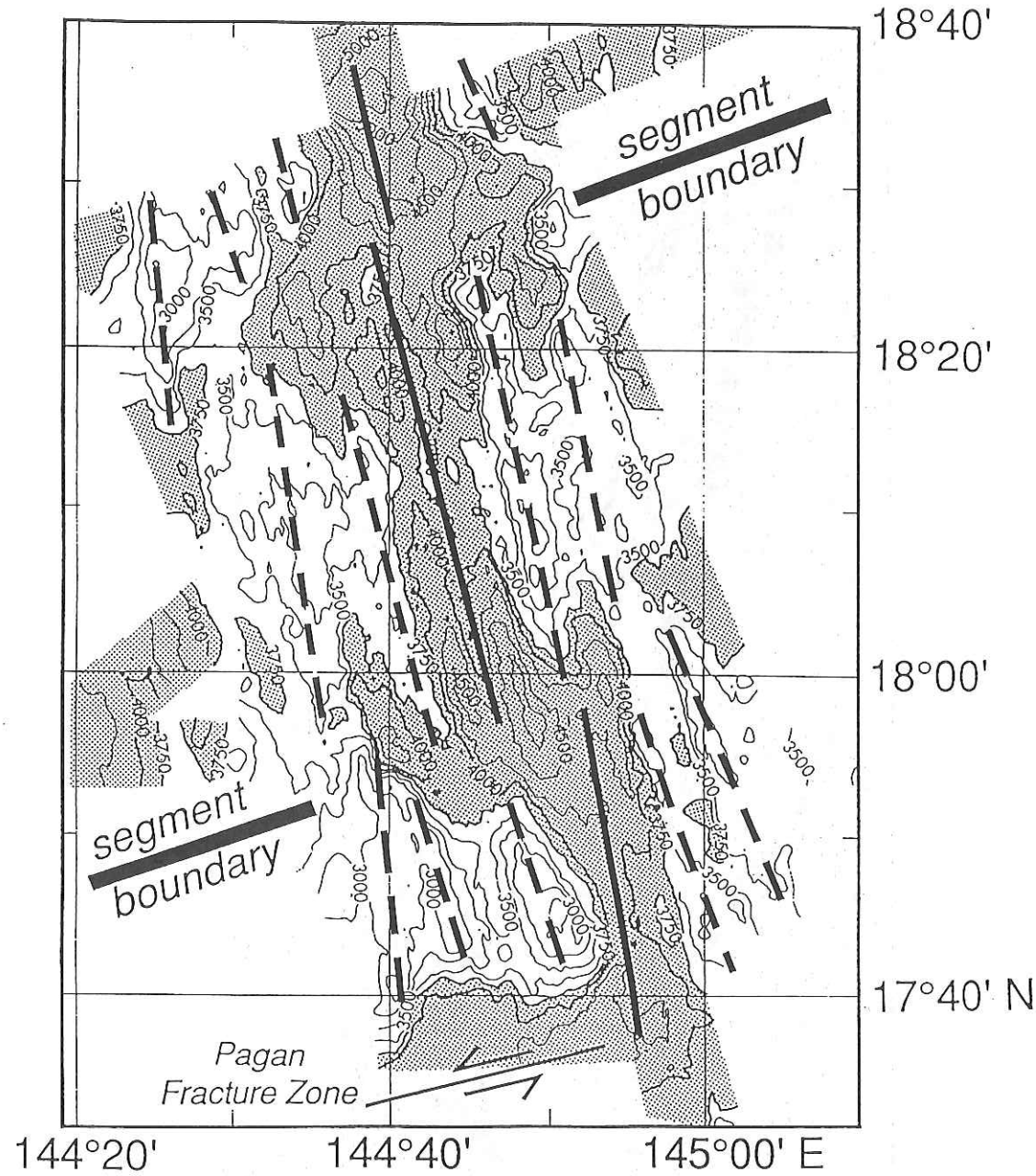

Fig. 6.3.2 Sea Beam bathymetry (250 m contour interval) and tectonic interpretation. The 3750 m contour line and shaded area delineate the median valley, and the 4000 m contour line outlines the Axial Ridge Segment centered at 18°12'N. Three morphologically-defined ridge segments (thick solid line denotes neovolcanic zone) can be identified within the median valley. Regularly-spaced, similarly-shaped ridges (thick dashed lines) are prominent off-axis.

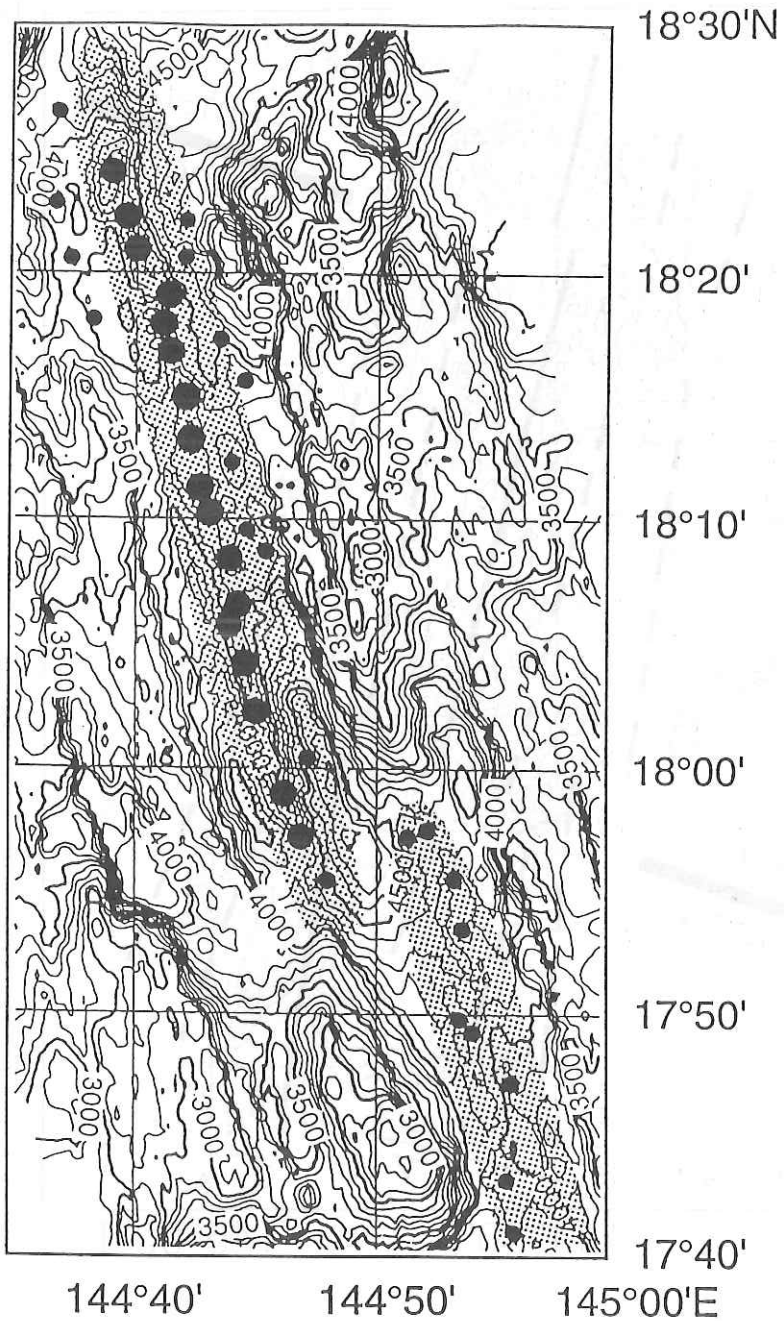

Fig. 6.3.3 Distribution of volcanic cones (circles) and spreading segments (shaded areas) within the median valley. Large circles show volcanoes associated with the Axial Ridge Segment, which appears morphologically similar to that found in the Mid-Atlantic Ridge MARK area (Figure 4). Sea Beam bathymetry contoured at 100 m intervals.

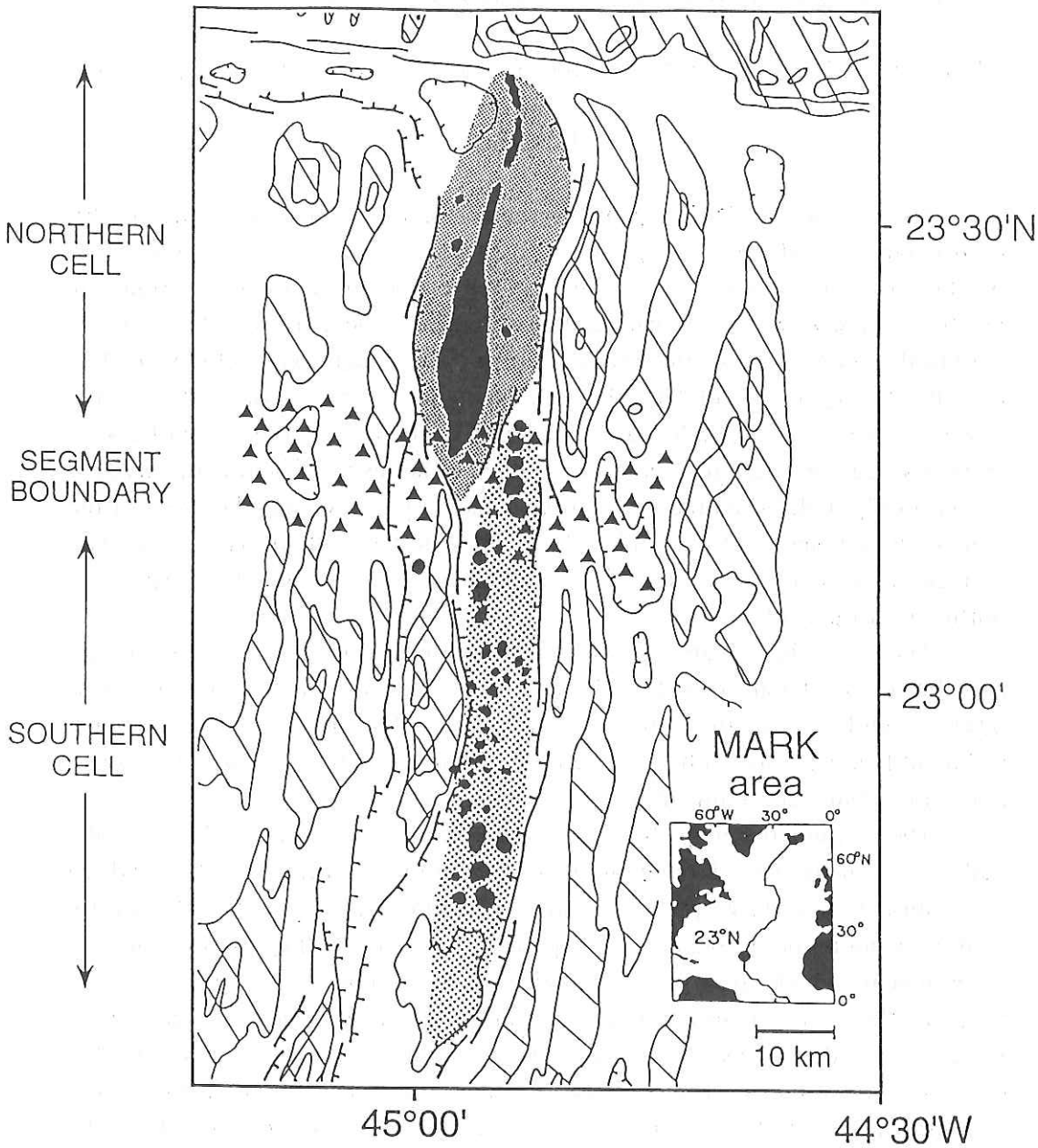

Fig. 6.3.4 MARK area (Mid-Atlantic Ridge, 23°N) morphotectonic elements [*Kong et al.*, 1988]. The median valley (10-17 km in width and delineated by a network of opposing fault scarps), is composed of two spreading segments (stippled areas), which overlap in a discordant zone (triangles) lacking a well-developed rift valley or neovolcanic zone. The Northern cell is dominated by a 500 m-high, hydrothermally-active, constructional volcanic ridge (black area), and the Southern cell is characterized by a band of 50-200 m high conical volcanoes. Regularly-spaced, similarly-shaped ridges (cross-hatched and diagonally-lined areas) are observed off-axis.

6.4 Sea Beam Bathymetric Mapping of the Ayu Trough

T. Fujiwara, H. Fujimoto, K. Tamaki, H. Toh, C. Igarashi, T. Seno, M. Kido
and
K. Kobayashi

As part of a geophysical measurement of the Ayu Trough, the multi-narrow beam "SeaBeam" bathymetric survey was carried out. The survey track is shown in Fig. 6.4.1. The survey lines extend southward from the junction of the Ayu Trough and the Palau Trench. The survey area covers a 350km distance north to south centered about the trough axis and designed so that the spacing is 5 nautical miles (9.25km) and the survey lines were in the east-west direction perpendicular to the strike of the trough axis. About a 40% areal coverage of swath mapping was attained. The result of SeaBeam survey is shown in Fig. 6.4.2 (See the frontispiece 2 facing front cover). The axis of the Ayu Trough is marked by a 5-6 km-deep valley in the southern part of the map, and the axis of the Palau Trench is marked by a 6-7 km-deep valley in the north-eastern part of the map.

There are sharp distinctions between the topography of the Ayu Trough and that of the Palau Trench. The depth of the trough axis is about 5,000-6,000m, while that of the trench axis is about 6,000-7,000m. There are thick sediment layers identified by the existence of flat basin topography in the trench axis valley, but little sediment in the trough axis valley.

The bathymetric map shows that there are many similarities between the bathymetry of the Ayu Trough and that of the mid-ocean ridges both of which have spread at a slow spreading rate. The topography shows bathymetric symmetry about the trough axis. The periodically spaced topographic highs and lows appear, which show axial symmetry. The trough axis deep forms a V-shaped valley. Sediment is thin at the trough axis valley. However, a gradual increase of sediment as the distance from the trough axis is identified by the existence of flat basin. The basement subsides symmetrically about the trough axis gradually, and the subsidence becomes significant as the distance from the trough axis. This subsidence follows the empirical $\sqrt{t}$ law. These facts suggest that the oceanic plates separate at a slow spreading rate at the Ayu Trough.

This map also shows that there are some differences between the bathymetry of the Ayu Trough and that of the mid-ocean ridges. The depth of the trough axis valley is about 5,000m and the depth of the basement near the trough center is about 3,000m, which is too deep compared with that of typical mid-ocean ridges, considering that the ocean floor of the trough center is zero

in age. This fact is appealing evidence that the Ayu Trough is not an active ocean ridge.

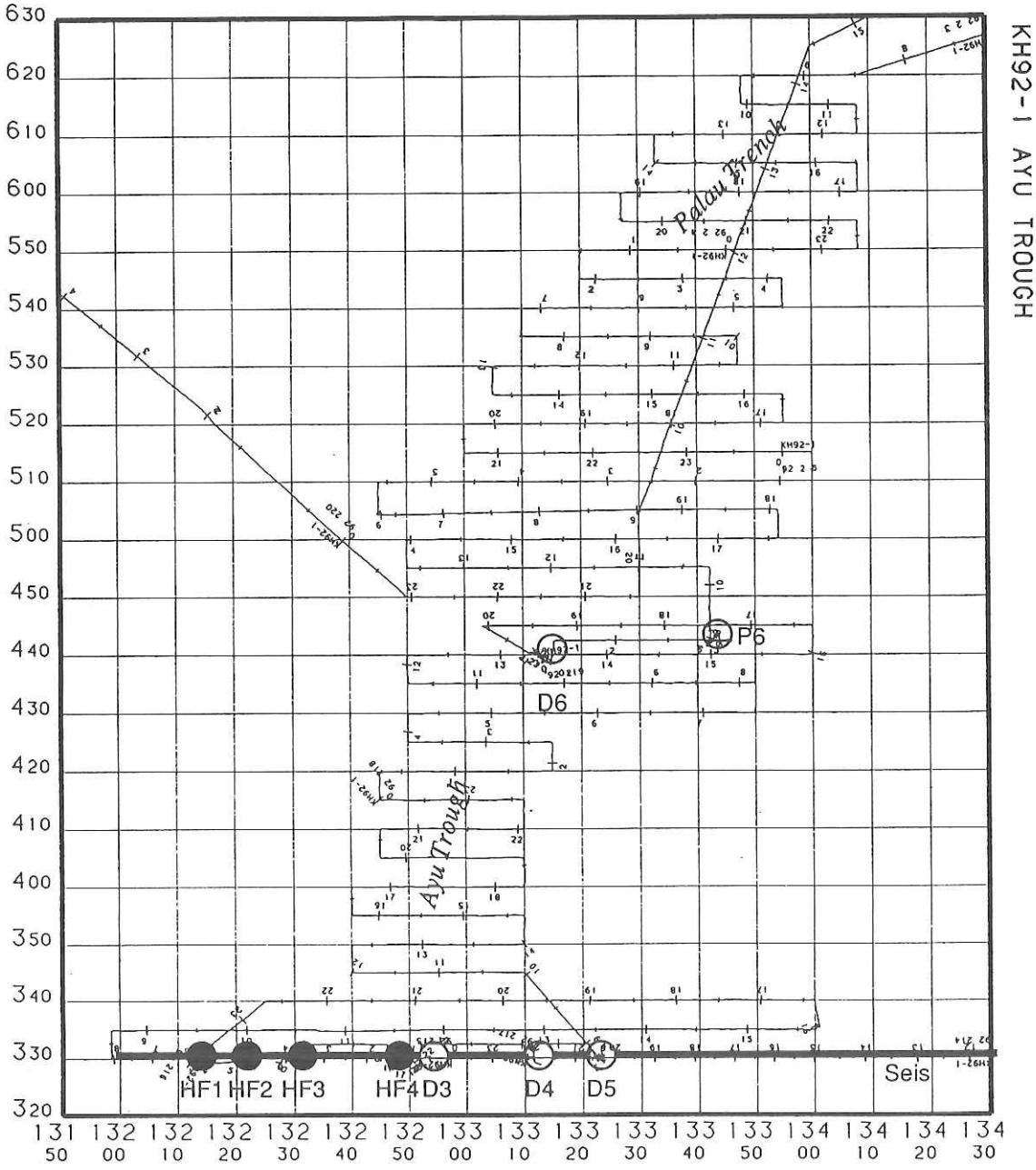

Fig. 6.4.1 The ship tracks of the Ayu Trough survey.

7. 3.5 kHz Subbottom Profiling of the Ayu Trough

C. Igarashi, K. Tamaki, M. Kido, T. Fujiwara, H. Toh and T. Seno

3.5 kHz subbottom profiling survey was conducted all through the survey of the Ayu Trough zone using the Raytheon Subbottom Profiling System whose transducer is attached to the ship's bow. Conditions of the surveys are summarized as follows.

Ship speed: 8-16 knots
Real time processing: Raytheon CESPIII
Graphic recorder: Raytheon LSR
Graphic recorder scan speed: 1.33 sec (1000m by two-way)
Time/Depth annotation: every 15 minuets by IMI annotation generator

Quality of the record was sufficiently good for the identification of the surface sedimentary structure. The 3.5 kHz subbottom profiling records were critically used for the precise allocation of heat flow measurement site and piston coring site.

Maximum acoustic penetration observed is 110 m at the eastern margin of the Ayu Trough zone along 3°30'N (Figure 7.1). Except for the eastern and western margins of the Ayu Trough zone, the acoustic penetration is generally less than 50 m (Figure 7.2).

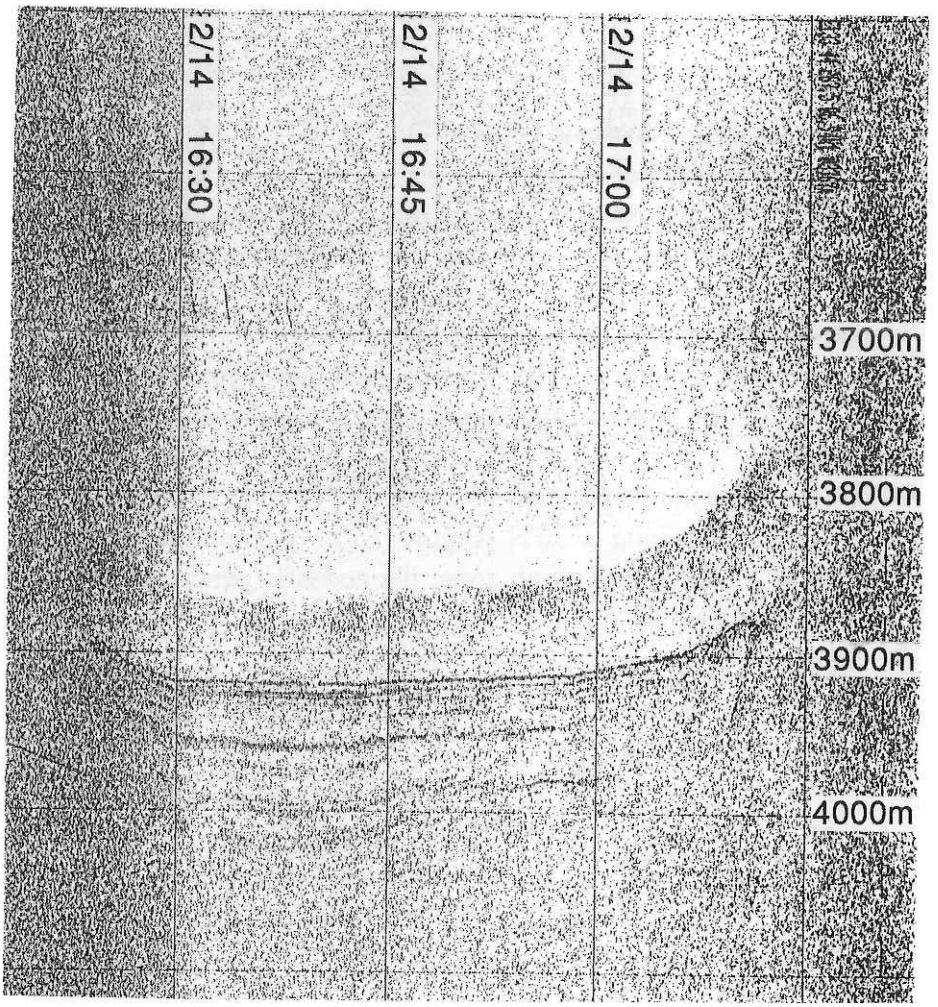

Fig. 7.1 A typical record showing maximum acoustic penetration.

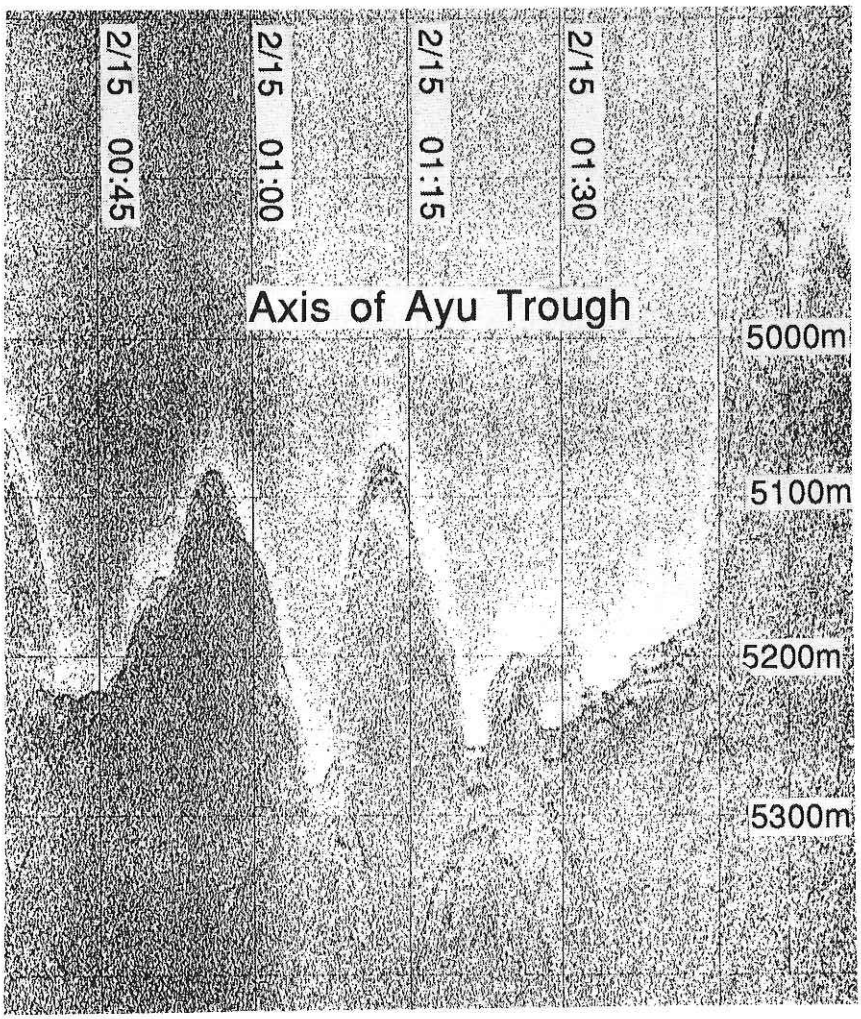

Fig. 7.2 A record showing thin deposition in the bottom of the axial rift of the Ayu Trough.

8. Seismic Reflection Surveys

8.1 Seismic Reflection Survey of the Mariana Trough

C. Igarashi, T. Yamaguchi, M. Suzuki and R. Feng. Lu

8.1.1 Introduction

The Mariana Trough is located west of the Mariana island chain. There are several active volcanoes along the Mariana islands. The Trough extends from 22°N to 13°N. The shape of the Trough is crescent. The median valley axis is not easily identified except at 18°N. Even at 18°N, it is difficult to locate the exact position of the Trough axis without detailed bathymetry map. This is what is quite different from the mid oceanic ridge axes. To study the differences between oceanic ridge, the Mariana Trough and the other back arc basins, OBS-airgun refraction survey was done near the 18°N region over the Mariana Trough axis. Sea Beam survey was done prior to the airgun refraction/reflection survey, by which the shooting line was determined. The shooting line was approximately on the center of the Mariana Trough axis between 18°10'N and 18°28'N. Other shooting locations in addition to the above region were selected across the valley to the east or west of the expected trough axis.

The shooting was made along the OBS array with nearly 15 km spacings between adjacent OBS's, parallel to the Mariana Trough axis. The objective of this study was to obtain the crustal structure in the Mariana Median valley region and to collect reflection records along the shooting line. The total length of shooting line is approximately 185 km. The ship track during airgun shooting is shown in Fig. 8.1.1.

More detailed description of geophysical setting in the survey area can be referred to the OBS-Airgun refraction section in this report.

8.1.2 Field Experiment

Two 12 liters airgun were used. Towing two airguns at the same time was the first attempt since the new Hakuho Maru was used. The firing time for two airguns were adjusted using Auto sync I-Wg. The pressure of each airgun was kept at 100 atoms. Shooting interval was precisely kept at 30 seconds. The total shooting period was approximately 19 hours. The overall airgun control system is shown in Fig. 8.1.2. To get the above pressure and shooting intervals, two LMF 200E-D-Vgd2310W17 compressors were used. The exhaust volume

of these compressors is 20 cubic meter/min. and the highest pressure is 150 atoms. Two Bolt 1500C airguns were used. The size of chambers was 12 liters for both airguns. To detect shot instances and reflection signals from the subbottom, a Teledyne single channel hydrophone(50 sensor units) streamer was used. The analog signal from the hydrophone streamer was digitized by a 12 bit A/D convertor and digital signale outputs were saved in MO disk of personal computers.

Two airguns were towed from the fantail of the ship. The distance between two guns were approximately 7m. The guns were apart from the fantail by 30 m. The hydrophone streamer was towed from the left side of the ship fantail. Towing speed was kept at 5kt during shooting in order to keep airguns 2m deep in water. Navigation of the ship was monitored by Magnabox 5000 hybrid system. The water depth beneath shot positions was obtained by both airgun reflection record and Sea Beam data.

Unfortunately, during the shooting from shot #1200 to #1594, one of the airguns failed to shoot for approximately 2.5 hours due to the damages of pressure hose and pressure packing. After fixing the damaged spot, normal two airguns shooting was recovered.

An example of reflection records obtained by the shipboard analog monitor is shown in Fig. 8.1.3. The monitor record shows very little sediment over the shooting line. Considerable sediment filled depressions are seen around shot #500 and shot #2000-2100. The former ponding corresponds to the location of northern deep valley where MT-6 OBS was deployed. The latter corresponds to so called "Pagan Fracture Zone" crossing the Trough axis at 17°39'N. The Pagan Fracture Zone is covered by turbidite flow from volcanic islands located east of the Trough axis. The thickness of sediments is nearly 1 second for both regions. This corresponds to 750-1000m thickness of sediments. The inclined structure of the sediment fill may be attributed to the activity of Pagan Fracture Zone . Around the Pagan Fracture Zone a thin layer of sediment covers the acoustic basement from shot #2100 to #2250. By this Pagan Fracture Zone, the ridge axis is offset approximately 25 km to the west. This offset of the Trough axis ,however,was not clear by our Sea Beam data due to poor coverage of this region. The other areas are nearly no sediment area,suggesting very young age of basement rock. The dredged rock samples by Hawkins et al. (1990) shows that the rocks are basalt forming a bare rock base.

Acknowledgements

We thank Prof. J. Segawa for his nice coordination of research during the KH92-1 cruise. We also thank officers and the crew of Hakuho-Maru for their

professionality during airgun shooting.

Reference

Hawkins, J. W., P. F. Londsdale, J. D. Macdougall and A. M. Volpe, Petrology of the axial ridge of the Mariana Trough backarc spreading center, Earth and Planet. Sci. Lett. 100, 226-250, 1990.

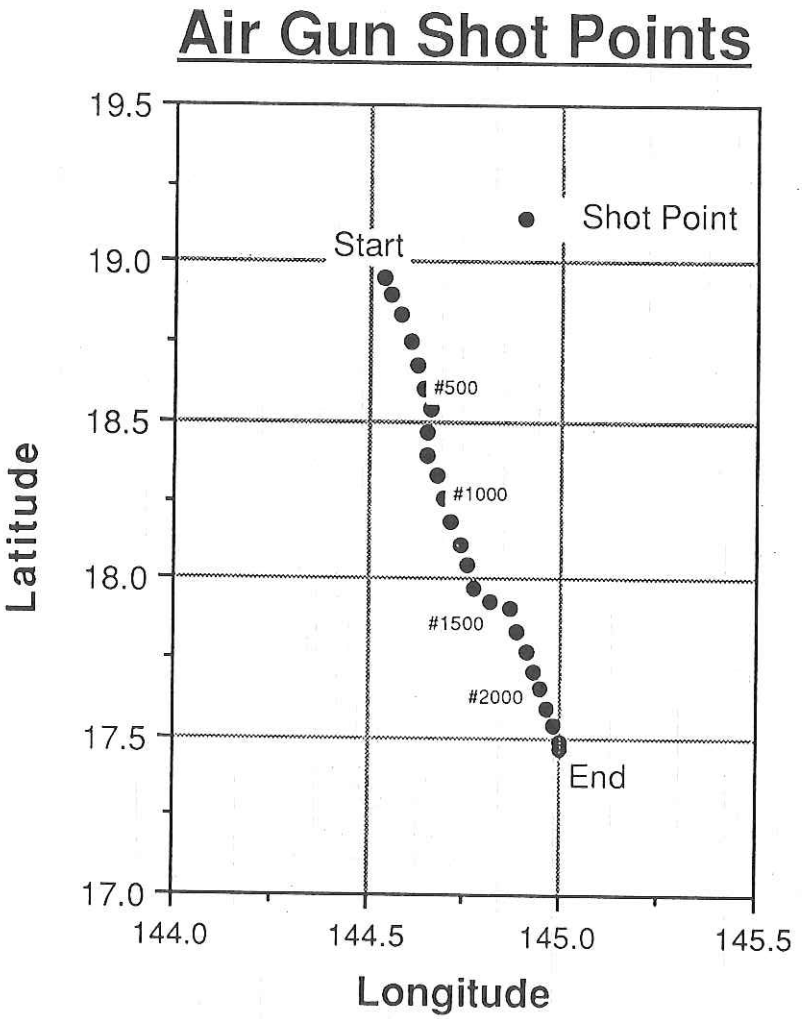

Fig. 8.1.1 Map of Air Gun Shot Points.

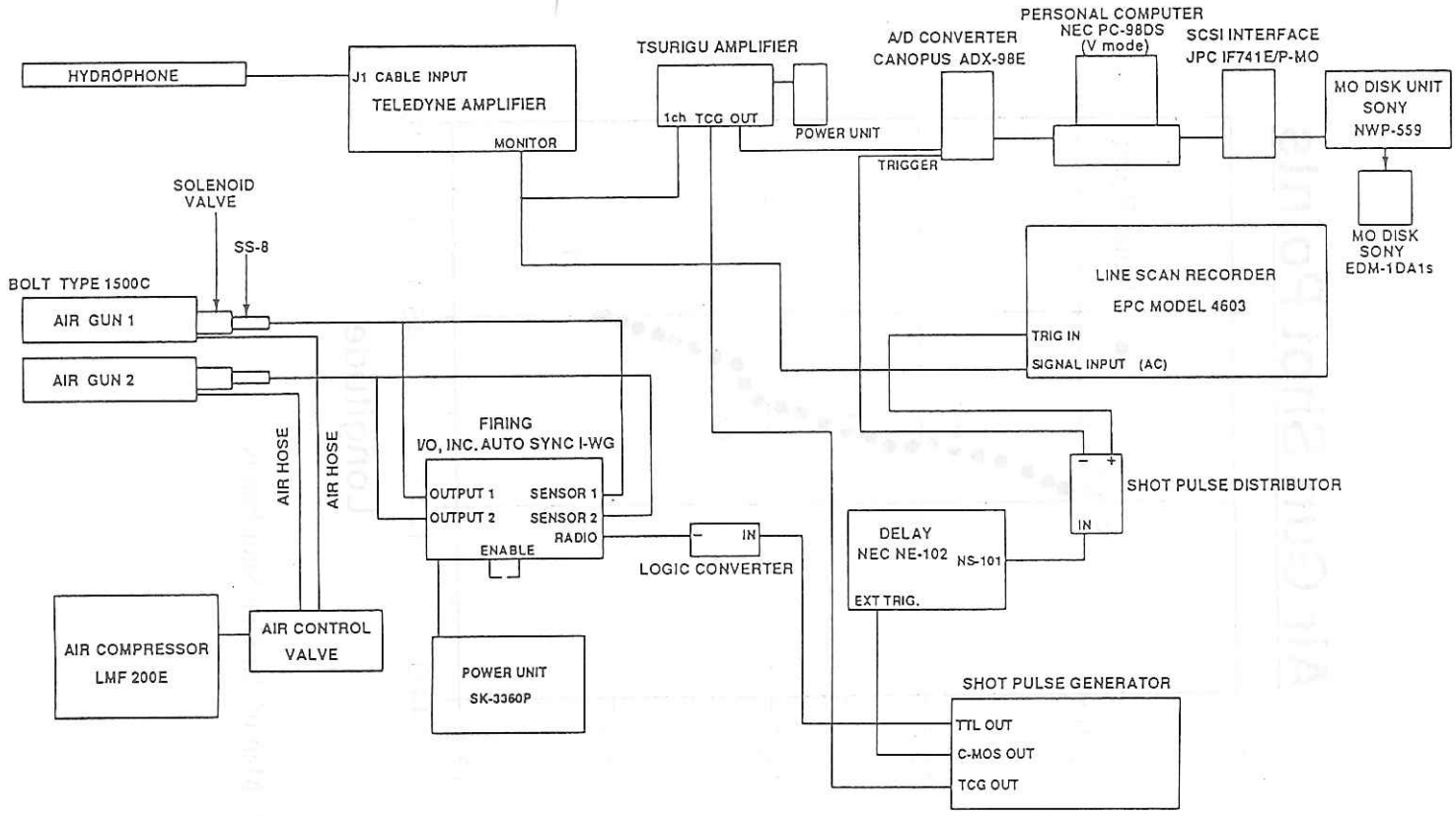

Fig. 8.1.2 Schematic block diagram of Single Channel Seismic Survey System

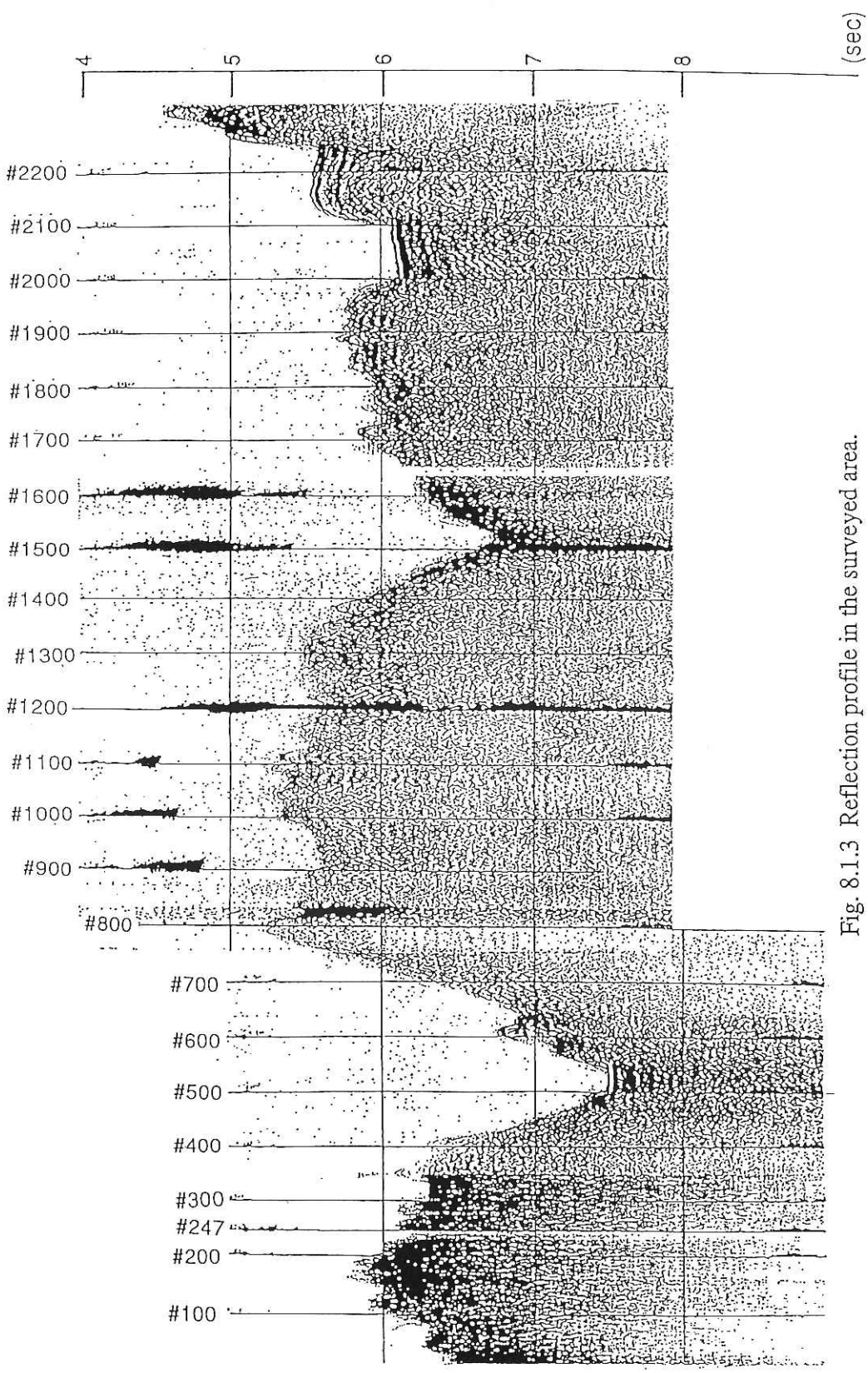

Fig. 8.1.3 Reflection profile in the surveyed area.

8.2 Seismic Reflection Survey of the Ayu Trough

K. Tamaki, C. Igarashi, T. Seno, T. Fujiwara, H. Toh, M. Kido
and
H. Kinoshita

An east-west track line of seismic reflection profiling survey was done along 3°30'N, from 135°30'E to 132°00'E. Survey condition and instrumentation are summarized as follows.

Sound source: A Bolt 1900C Airgun
Chamber volume: A 120 cubic inches chamber
Air pressure: 120 km/cm^2 (1700 psi)
Shot interval: 10 seconds
Ship speed: 8 knots (partly by 10 knots)
Streamer: Teledyne(50 elements)
Amplifier: Teledyne Model 300LF Low Frequency Amplifier
Filter: 30-125Hz or 40-160Hz
Graphic Recorder: EPC Model 4603
Graphic recorder sweep speed: 4 seconds per scan
Digital recording: 12 bit A/D converter/MO disk storage.

Ship speed was originally planned to be 10 knots. However, the data quality with a ship speed of 10 knots was not sufficient for interpretation of the geological structure. So it was lowered to 8 knots after the ship entered the Ayu Trough area (west of 134°00'E).

Figure 8.2.1 shows a brief track line of the seismic profiling survey. Figure 8.2.2 shows a typical example of the seismic record. The data quality is sufficient to identify full sediment thickness and sedimentary structure. The thickest sediments observed are 0.95 second at the eastern and western margin of the Ayu Trough zone. The sediment thickness is thinner in the central area of the Ayu Trough zone. Several tilted blocks of the basement are observed as typically shown in Figure 8.2.2. Tilted blocks have steep slopes toward the inner side (toward the axis) and gentle slopes toward the outer side. The sediment thickness in the Caroline Basin is uniform with a thickness of 0.4 second. All the observed sediments are acoustically transparent.

The reflection record was digitally stored, so that further processing will be made to get clearer structural information of the Ayu Trough.

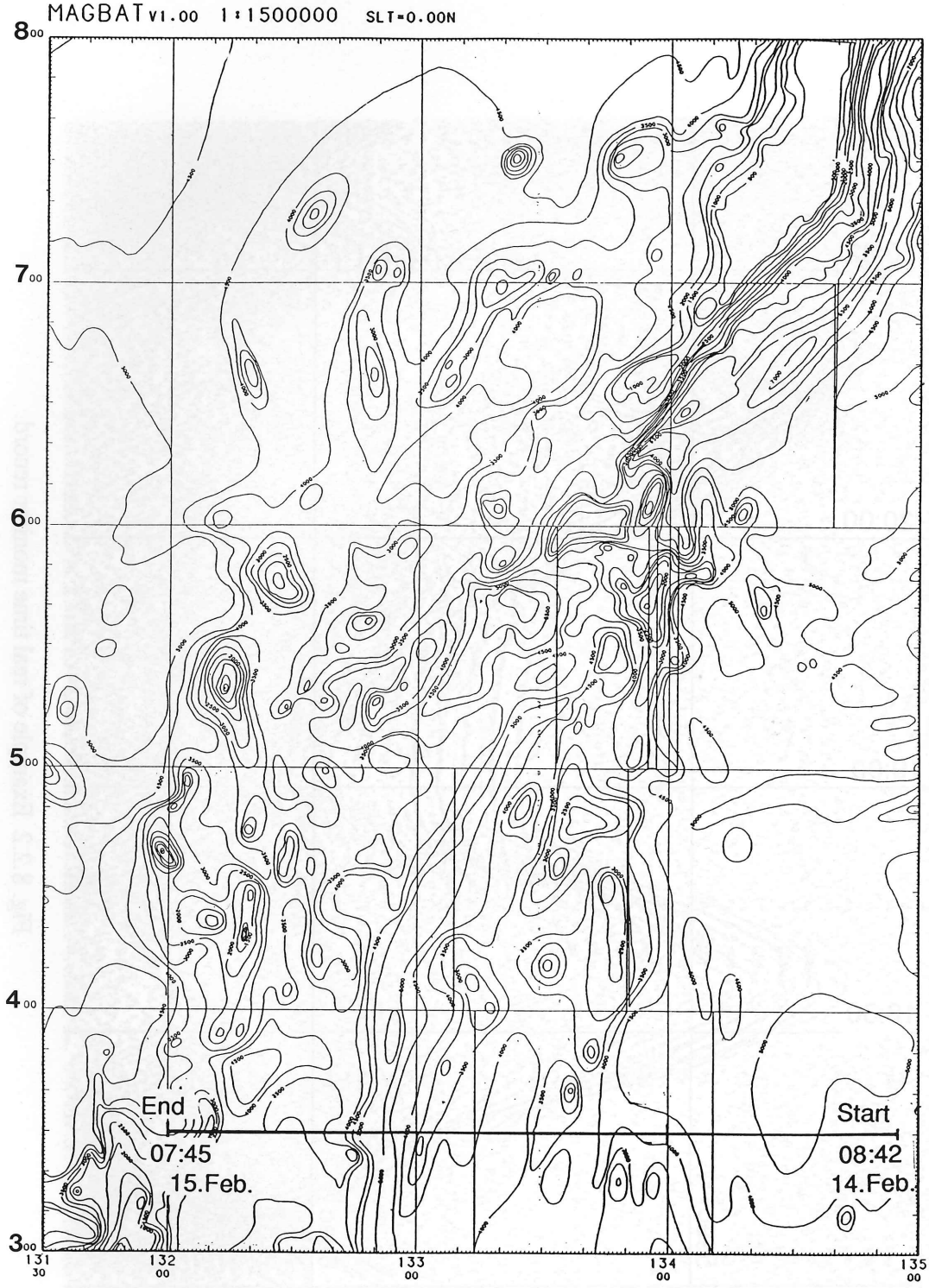

Fig. 8.2.1 Survey track of the seismic profiling.

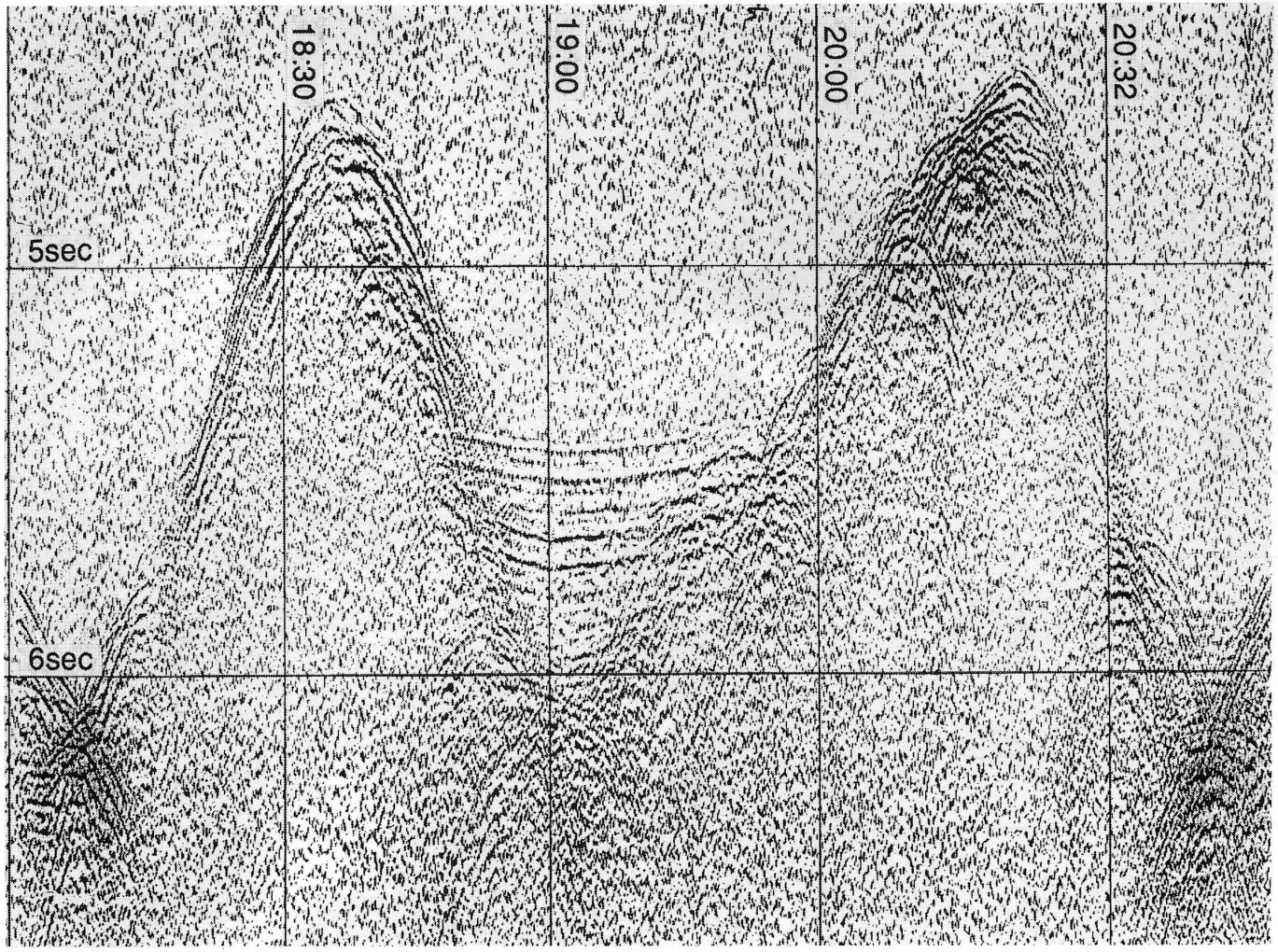

Fig. 8.2.2 Example of real time monitor record.

9. Gravity Surveys

J. Segawa, K. Koizumi, T. Fujiwara, C. S. Yang and H. Toh

9.1 Instrument

A surface ship gravimeter NIPR-ORI Model 2 was used. This gravimeter was built in 1989 but its sensor was replaced later because of a relatively large drift of the former sensor. This cruise is 44 days long and the gravity varies by 1520 mgal between the ports of call. We intended, by taking advantage of this cruise, to determine the exact scale factor of the new sensor, but it was difficult to do because the drift of the new sensor was still large. The data obtained from NIPR-ORI were compared with the measurements by use of LaCoste-Romberg G-124 at ports of call. The results are as follows:

Location	Date	L & R	NIPR-ORI	NIP-LR
Tokyo	21/JAN/92 04:27 GMT	979774.8	979774.0 mgal	-0.8 mgal
Guam-A	08/FEB/92 01:35 GMT	978529.2	978566.5 mgal	+37.3 mgal
Guam-D	11/FEB/92 03:30 GMT	978529.2	978575.1 mgal	+45.9 mgal
Cebu-A	22/FEB/92 02:30 GMT	978254.1	978320.7 mgal	+66.6 mgal
Cebu-D	271FEB/92 01:33 GMT	978254.1	978326.9 mgal	+72.8 mgal
Tokyo-A	04/MAR/92 01:50 GMT	979774.8	979879.7 mgal	+104.9 mgal

In this table L & R and NIP-LR denote LaCoste -Romberg gravimeter and NIPR-ORI minus LaCoste, respectively. The notations such as Guam-A or Guam-D mean arrival and departure, respectively. The differences in gravity at the ports of call are caused by either gravimeter drift or improper scale factor, or both. If the drift of NIPR-ORI only occurred during the measurements it is +2.08 mgal/day on an average. The room temperature was controlled within ±1.5 degrees centigrade in this case.

In Leg 1 the interface circuit for automatic input of Log data (ship's course and speed) which are necessary to control gyro did not work, so that they had to be input manually. This interface was replaced by a different one which fits to

this gravimeter (it had been wrongly inserted before). However, another problem happened in Leg 2. As the interfacing board for Log input includes the function of gyro control, particularly the function of determining the feedback time constant, the gyro erection became improper. In Legs 2 and 3 the gyro platform was not properly controlled, so that gravity measurements showed unreasonable variations with the amplitude ±8 mgal and period of 5 to 10 min. These noises are clealy identified in the record of Leg.2.

9.2 Gravity Anomalies at the Seamount Chain along the Eastern Flank of the Izu-Bonin Ridge

Figure 9.1 shows the ship's track in Leg 1 from Tokyo to Guam via the Ayu Trough. On the way southwards we crossed several seamounts running along the eastern flank of the Izu Bonin Ridge, which runs parallel to the Izu-Bonin Trench. These seamounts are geologically considered as mantle diapirs which are mostly composed of fractured serpentinite. The mantle diapir is the indication of the activity of plate subduction and interesting from geological point of view. The exact locations of the seamounts are shown in Figures 9.2 and 9.3. We surveyed 10 seamounts from A to J. These seamounts stand from the depth of 6000 to 7000 m with the height of 1500 to 2000 m.

The bathymetry and the Free Air Gravity Anomaly are shown in Figure 9.4. Although it is difficult to make any definite remark as to the relationship of gravity with topography, the effect of seamounts on gravity anomalies appears weak in general. This may be because of low density of the material (fractured serpentinite) which composes the seamounts.

9.3 Gravity Anomaly across the Mariana Arc

As seen from Figure 9.1, a long profile of gravity was obtained across the Mariana Arc on a parallel of about 18 degrees North (Point G2 to G1). This section covers the Parece Vela Basin, West Mariana Ridge, Mariana Trough,East Mariana Ridge and the Mariana Trench. On this section the gravity anomaly was interpreted by Yang et al(Tectonophysics Vol.206, 325-339, 1992). The interpretation was made along the west-to-east profile at 18 degrees North. This area is known as the zone where there is an abnormally low density upper mantle. The location is beneath the Mariana Trough. Since the gravity data used by Yang et al were not complete because there are some important places where gravity is lacking, the present data will be useful to make their result more convincing. For reference the Free Air Gravity Anomaly used by Yang et al is reproduced in

Figure 9.6. The gravity anomaly and bathymetry measured by the present work are shown in Figure 9.5.

Comparing Figure 9.5 and 9.6 we see a good coincidence between the two measurements. The anomaly at the Mariana Trough changes from about 30 mgal to 70 mgal west to east. In the western part of the Mariana Trough the bathymetry is almost the same, but in the eastern part there is some variation. From these results it seems very probable that the ultralow density material does exist beneath the Mariana Trough.

9.4 Gravity Anomaly in the Ayu Trough

As mentioned before the gyro platform did not work properly in Legs. 2 and 3. This affected the measurements in the Ayu Trough considerably. Figure 9.7 shows Free Air Gravity Anomaly and Bathymetry along a long west-to-east profile across the Ayu Trough. This line is from 3°30'N,132°00'E to 3°30'N, 134°30'E. Bathymetry is rather rough, showing variations from 1000m to 5000m. The gravity anomaly is largely positive, but this may not be true. These data must be corrected for the meter's drift with the magnitude of about 45mgal. The data also shows unnatural modulation with the amplitude of 5 to 8 mgal and period of 5 to 10 min. As mentioned before this is due to malfunctioning of gyro.

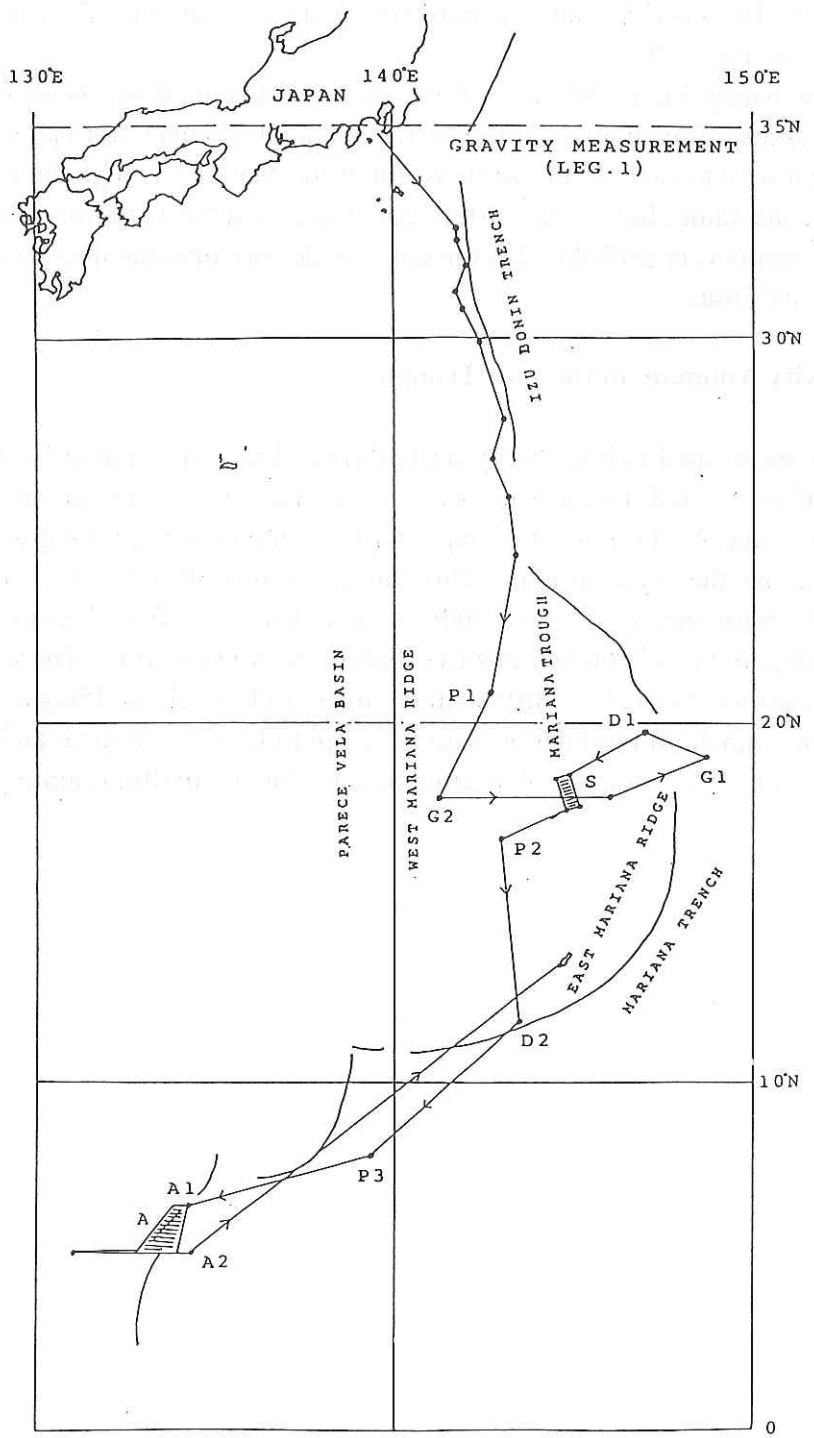

Fig. 9.1 Ship's tracks in Leg.1 from Tokyo to Guam via the Ayu Trough.

Fig. 9.2 Locations of Seamounts A to F which are supposed to be mantle diapirs.

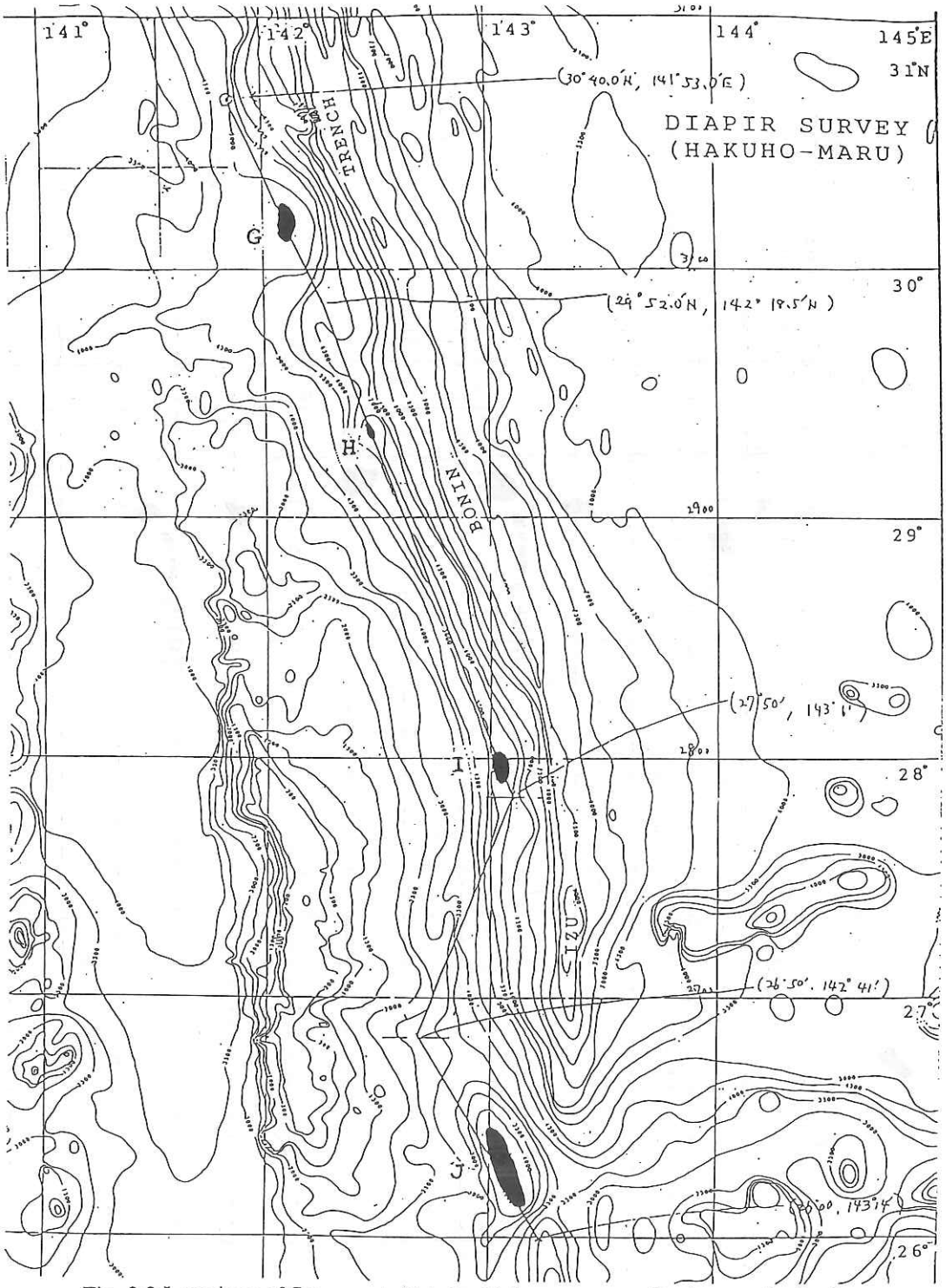

Fig. 9.3 Locations of Seamounts G to J which are supposed to be mantle diapirs.

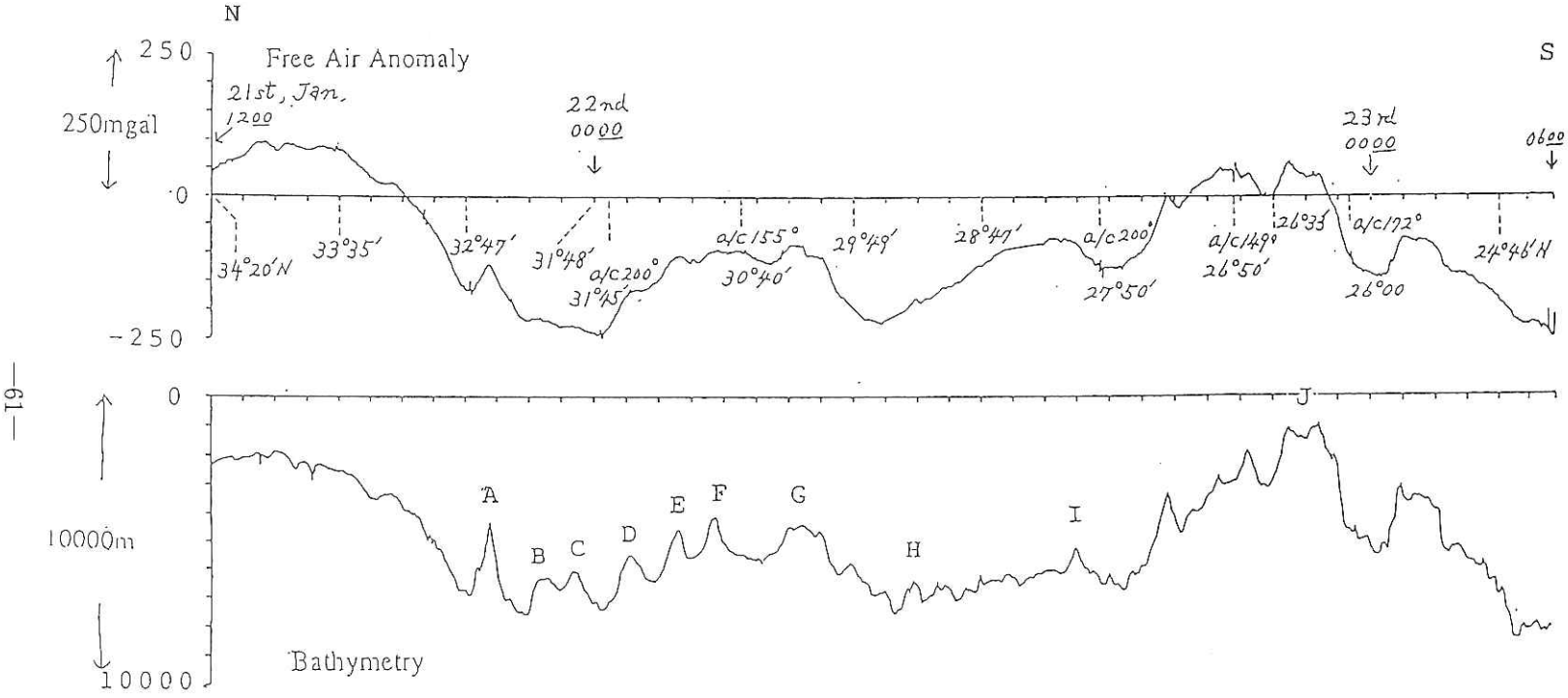

Fig. 9.4 Bathymetry and Free air gravity anomaly on the track along the diapiric seamounts.

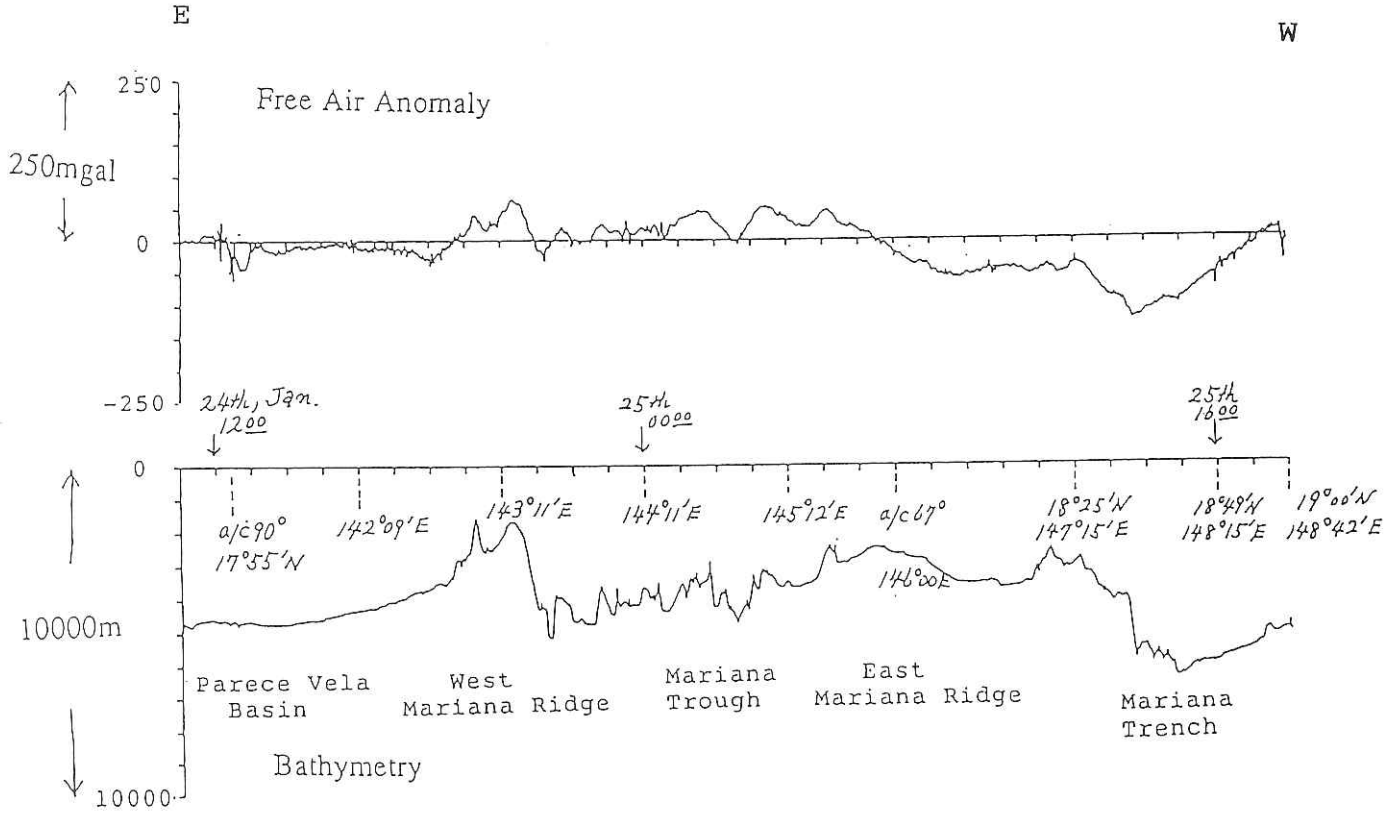

Fig. 9.5 Bathymetry and Free air gravity anomaly along the long west-to-east track (G2 to G1 in Fig. 9.1) across the Mariana Arc.

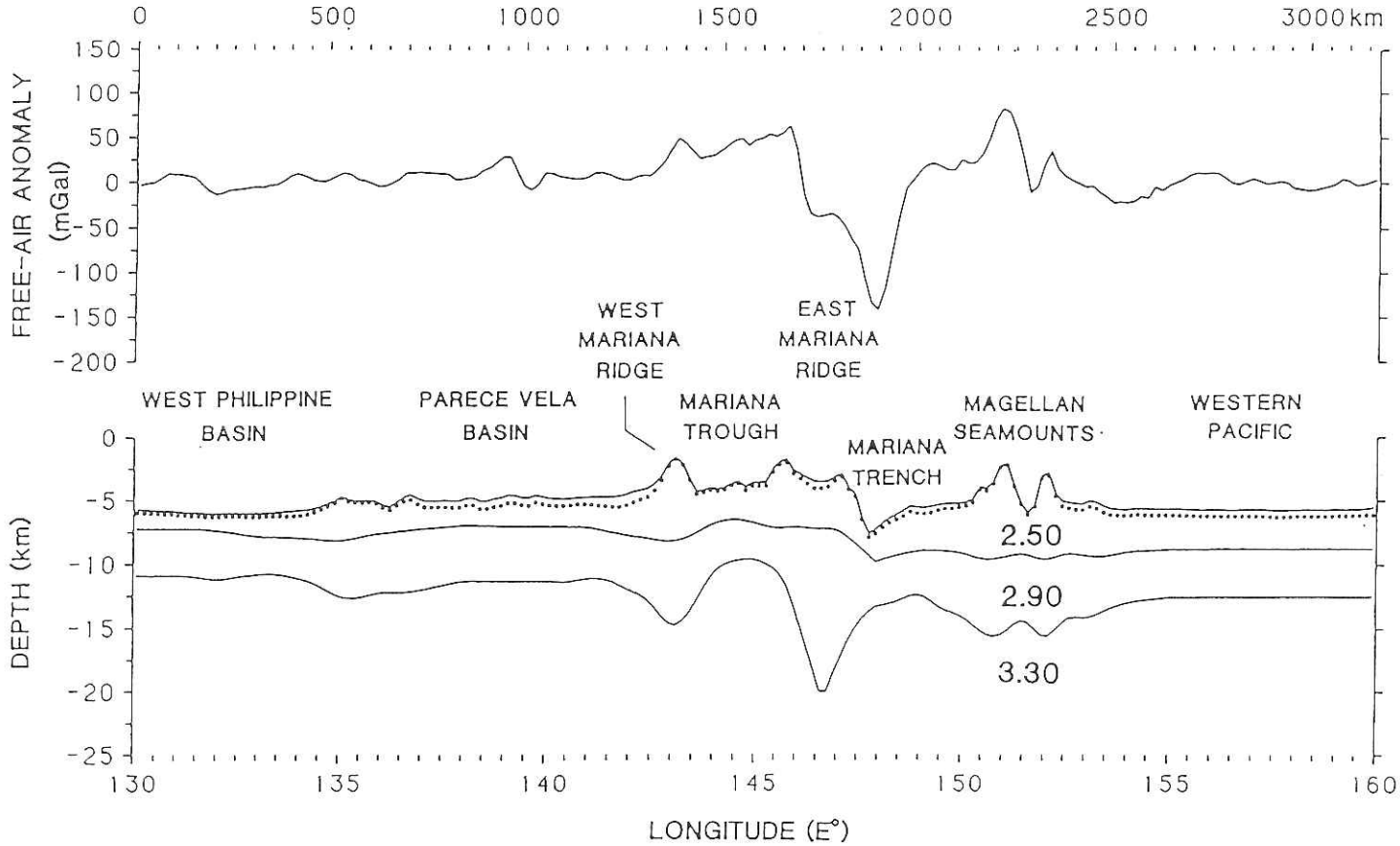

Fig. 9.6 Free air gravity anomaly and density structure of the crustal layers along latitude 18°05'N. The dotted lines denote sediment isopach. The density of the sedimentary layer is assumed to be 2.20g/cm^3. (reproduced from Yang et al, 1992).

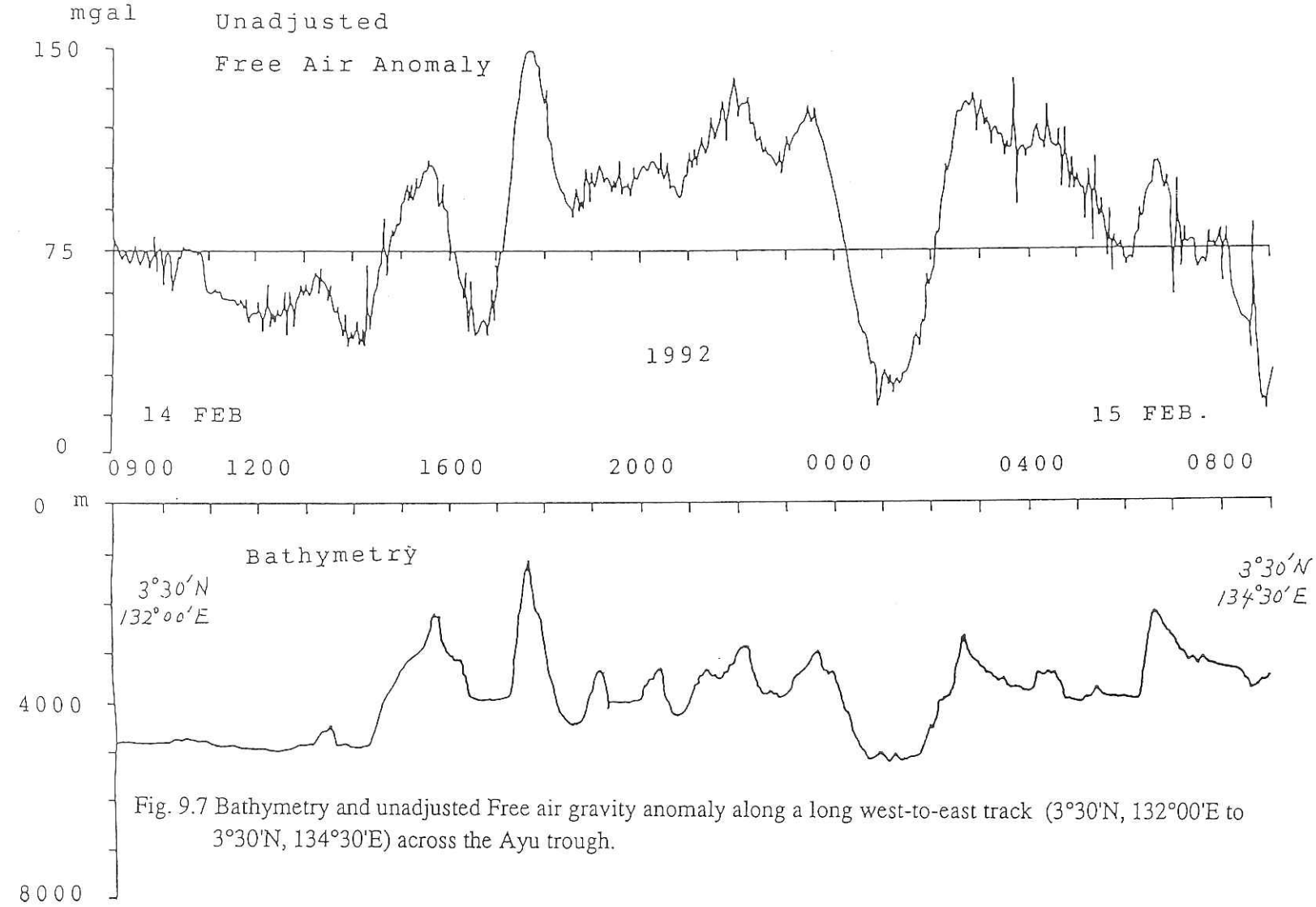

Fig. 9.7 Bathymetry and unadjusted Free air gravity anomaly along a long west-to-east track (3°30'N, 132°00'E to 3°30'N, 134°30'E) across the Ayu trough.

10. Geomagnetic Measurements in the Mariana Arc and the Ayu Trough

10.1 Measurement of Vector and Total Intensity Geomagnetic Field

N. Seama, T. Fujiwara, H. Fujimoto and J. Segawa

10.1.1 Vector Geomagnetic Field Measurement

We used a shipboard three component magnetometer (STCM; Isezaki, 1986) with some improvements (Seama et al., in prep.) for the vector geomagnetic field measurements. Principle of STCM system is as the following. During the cruise, we obtained vector magnetic data, $\overrightarrow{H_{ob}}$ using three flux gate magnetometers mounted on the ship's deck and gyrocompass data to provide ship roll ($\tilde{R}$), pitch ($\tilde{P}$) and yaw ($\tilde{Y}$). Then, the ambient geomagnetic field vector, $\vec{F}$, is given by

$$\overrightarrow{H_{ob}} = \tilde{A}\cdot\tilde{R}\cdot\tilde{P}\cdot\tilde{Y}\cdot\vec{F} + \overrightarrow{H_p} , \qquad (1)$$

where $\tilde{A}$ is a constant matrix including the sensors' location and the ship's magnetic susceptibility distribution, and $\overrightarrow{H_p}$ is the magnetic field produced by the ship's permanent magnetic moment (Isezaki, 1986). We used the following equation instead of using eq.(1),

$$\tilde{B}\cdot\overrightarrow{H_{ob}} + \overrightarrow{H_{pb}} = \tilde{R}\cdot\tilde{P}\cdot\tilde{Y}\cdot\vec{F} , \qquad (2)$$

where $\tilde{B}$ and $\overrightarrow{H_{pb}}$ are constant. This eq.(2) is easily derived from eq.(1). The reason for using eq.(2) is that we can calculate the magnetic field vector, $\vec{F}$ more easily than using eq.(1). Furthermore, we can understand eq.(2) better, because the left terms of eq.(2) show corrections for the ship's magnetic effect and the right terms show the transformation from the ship fixed coordinate system to the earth coordinate system (Seama et al., in prep.). $\tilde{B}$ and $\overrightarrow{H_{pb}}$ are what we call 12 constants and are determined using data obtained at six different places during the cruise while the ship steers in figure eight motion(Table 10.1.1 and 2).

The measurement system of the Hakuho-maru STCM is shown as a block diagram in Figure 10.1.1. A micro-computer in Lab.No.1 controls all the system and collects three types of data; (1) three component magnetic field data, (2) ship movement (yaw, roll and pitch angle) data, and (3) general information

(time (G.M.T.), location, water depth, gravity and atmospheric temperature). Three component magnetic field was measured by three fluxgate magnetometers mounted on the ship's deck. The data were converted from analog signal to digital signal and were transmitted to the micro-computer through a PIO. The ship movement was measured by a precise gyrocompass (SGC-1) in Lab.No.9. The data were sent to Lab.No.1 through the Hakuho-maru LAN (Local Area Network) and were transmitted to the micro-computer using RS232C. These two types of data (magnetic data and ship movement data) were sampled at the same time every 1 second synchronized with the precise gyro compass time. The general information was supplied from the Magnavox Series 5000 of the Hakuho-maru though LAN. The sampling interval of these data is 1 minute. All the data were saved at the hard disk of the micro-computer. The one second interval data are converted to binary code for saving the memory space of the hard disk. The unit value of magnetic data is 3 nT while the unit value of angles is 0.01 degrees. A file was made every 6 hours with its volume of about 0.29 Mbytes; one 2HD floppy disk is good for whole one day data (four files).

Real time display is available on the CRT of the micro-computer. 8 hour profiles of each geomagnetic field component, yaw angle, and water depth are displayed, which provides not only the condition of sampling data but also geomagnetic information on the ocean floor in real time.

Data were collected when the ship ran under very good conditions. There are some lack of data until 25th of January because of too many tasks on the micro-computer in a very limited time. After 25 of January few data lack occurred because the sampling software was changed on 25th of January.

10.1.2 Total Intensity Geomagnetic Field Measurement

We used a proton precession magnetometer for the total geomagnetic field measurements. This measurement system is shown as a block diagram in Figure 10.1.2. The system is composed of a microcomputer, a main magnetometer unit, a condenser box, an oscilloscope, a pen recorder and a sensor with a cable 250m,long.

Total intensity geomagnetic data were collected using this system in 30 second intervals as the following. The main magnetometer unit in Lab.No.3 sends an exciting current to the sensor towed by the ship 200m apart and counts the frequency of proton's precessional motion in the geomagnetic field. The microcomputer receives the frequency data to calculate the total intensity geomagnetic field, saves the geomagnetic data in a floppy disk, and prints out every one minute. The general information i.e. time (G.M.T.; the data

processing system is controlled by this time), location, water depth, and ship speed and direction against the seafloor) was also collected.

Reference

Isezaki, N., A new shipboard three component magnetometer, Geophysics, **51**, 1992-1998, 1986.

Table 1 List of 'figure eight steering'

No.	DATE	TIME	LOCATION	
1.	January 21, 1992,	11:30-11:50,	34°20.7'N	140°12.1'E
2.	January 23, 1992,	05:42-06:03,	24°20.0'N	143°30.0'E
3.	January 24, 1992,	12:06-12:26,	17°55.8'N	141°15.4'E
4.	February 1, 1992,	03:29-03:50,	11°42.9'N	143°29.6'E
5.	February 5, 1992,	05:57-06:07,	5°04.5'N	132°45.2'E
6.	February15, 1992,	15:42-16:04,	3°35.5'N	134°00.4'E

Table 2 List of '12 constants'

$$\tilde{B} = \begin{pmatrix} 0.7905 & 0.6809 & 0.0752 \\ -0.7379 & 0.8849 & -0.0823 \\ 0.0880 & -0.0063 & 0.9517 \end{pmatrix}, \quad \overrightarrow{H_{pb}} = \begin{pmatrix} 310 \\ -1378 \\ -9321 \end{pmatrix}$$

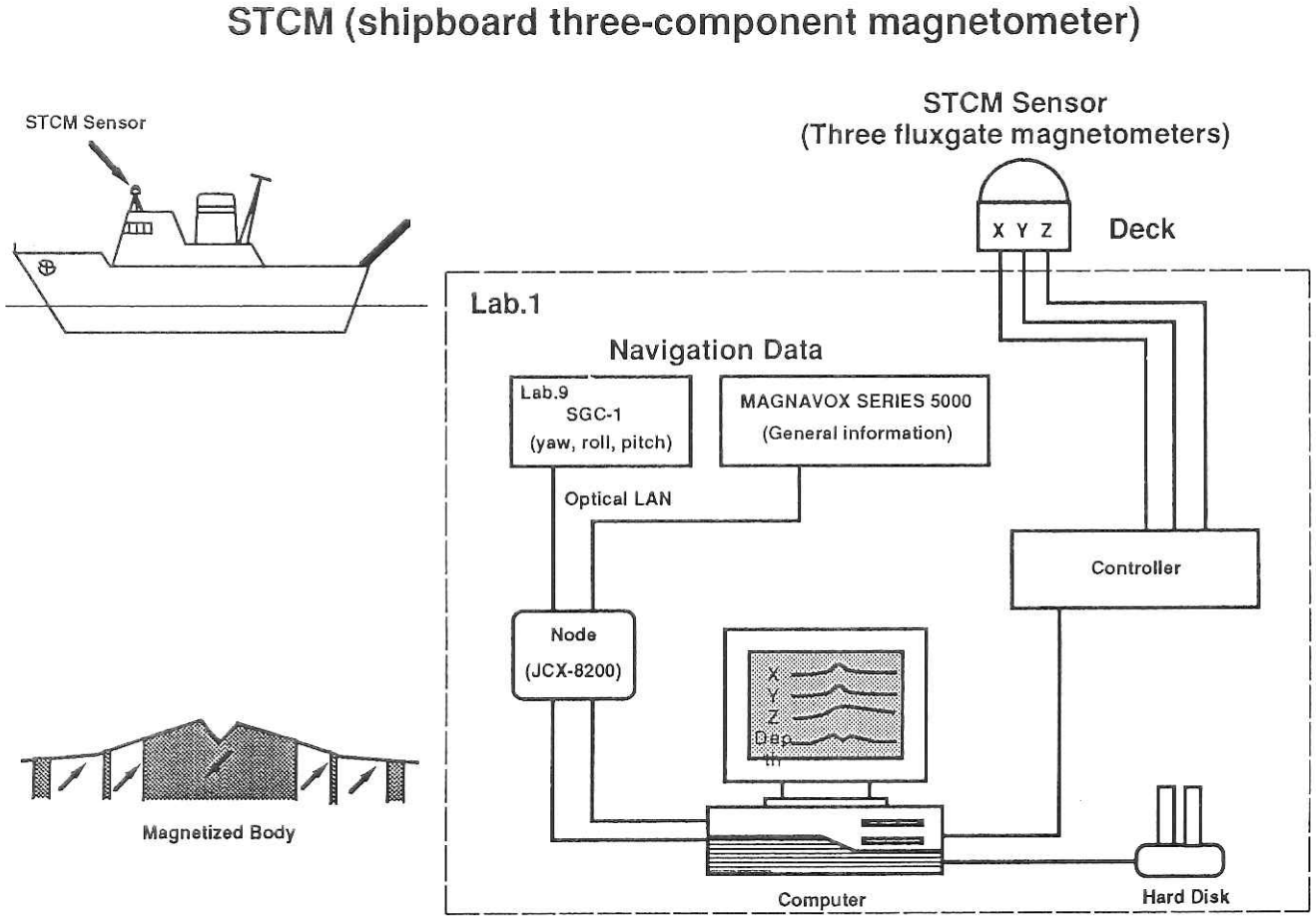

Fig. 10.1.1 Block diagram of the vector geomanetic field measurement system.

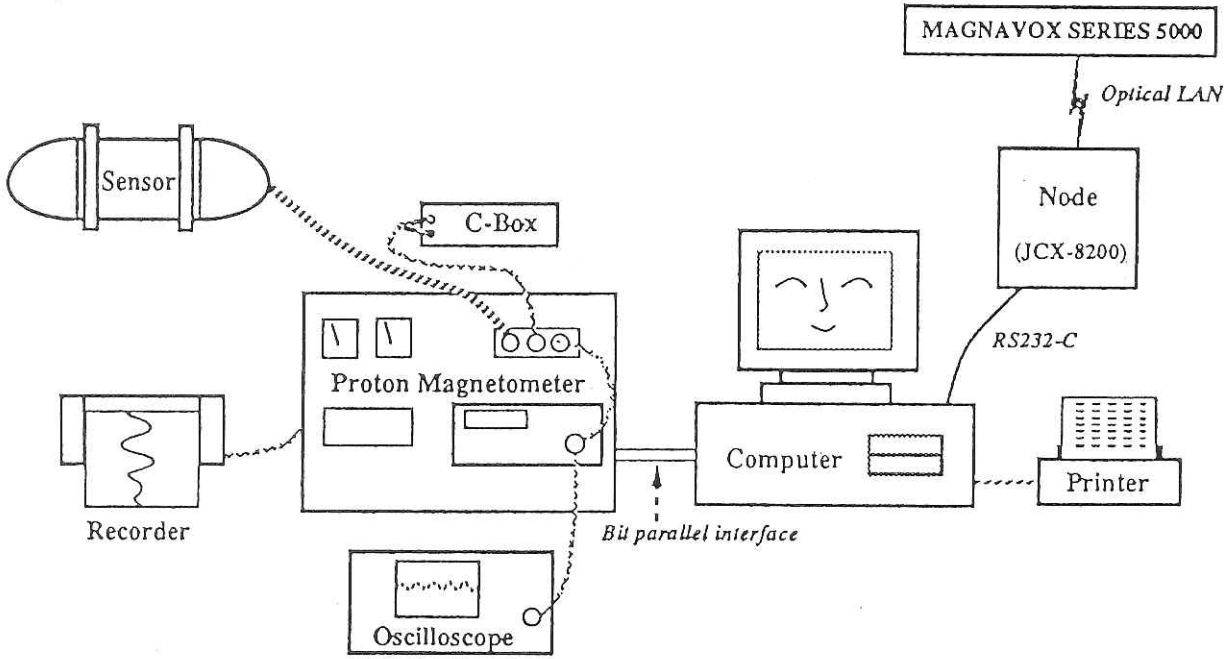

Fig.10.1.2 Block diagram of the total intensity geomagnetic field measurement system.

10.2 Geomagnetic Anomalies in the Mariana Trough, 18°N

N. Seama and T. Fujiwara

Vector and total intensity geomagnetic field data were collected using the STCM and the proton precession magnetometer of the R/V Hakuho-Maru (Seama et al., in this volume) in the 50 by 100 km area centered about the Mariana Trough axis at 18°N. The objective is to clarify the actively-spreading Mariana Trough.

Vector magnetic anomaly field was calculated using IGRF90 (IAGA Division V Working Group 8) after the correction for the ship's magnetic effect using l-second sampled data, which was then filtered and resampled at 1 minute intervals to remove short wavelength anomalies. Total intensity anomaly field was also calculated using IGRF90, and were used as the component anomaly field parallel to IGRF90 to compare with the vector magnetic anomaly data (Seama et al., in prep.). The geomagnetic anomaly profiles along the ship tracks are shown in Figure 10.2.1.

The amplitudes of the east and downward component of the geomagnetic anomaly field reach 600 nT and that of the north component is around 200 nT; These are much larger than that of the total intensity anomaly field (200 nT). This may be because the amplitudes of total intensity anomalies are much reduced depending on the direction of magnetization, direction of regional field, and strike of lineation, whereas vector anomalies are not affected by such parameters.

Positions, strikes and characters (two-dimensional or three-dimensional magnetic sources) of magnetic boundaries were obtained by the newly-developed method (Seama et al., 1992) using the vector geomagnetic anomaly field data. Our results are summarized in a magnetic boundary strike diagram (MBSD; Figure 10.2.2). The MBSD shows the position, strike and character of magnetic boundaries as crosses in map view.

Results

Vector geomagnetic anomalies (Figure 10.2.1) and magnetic strike boundary diagram (MBSD; Figure 10.2.2) show four main results.

(1) Existence of magnetic anomaly lineations suggests the seafloor spreading of the Mariana Trough.
(2) Half-spreading rate is 13 - 17 mm/yr during the Brunhes epoch (slow spreading).

(3) Ridge segmentation agrees with the morphologically-defined segmentation (Kong et al. in this volume).
(4) Variation in the magnetized source layer along the axis (thinner magnetized layer and/or lower magnetization intensity in the middle of segments compared to the segment edges) suggests the variation in the thermal condition beneath the spreading axis.

References

IAGA Division V Working Group 8 (R. A. Langel, Chairman), International geomagnetic reference field, 1991 revision, J. Geomag. Geoelectr., **43**, 1007-1012, 1991.

Isezaki, N., A new shipboard three component magnetometer, Geophysics, **51**, 1992-1998, 1986.

Seama, N., Y. Nogi, and N. Isezaki, A new method for precise determination of the position and strike of magnetic boundaries using vector data of the geomagnetic anomaly field, Geophys. J. Int., (accepted), 1992.

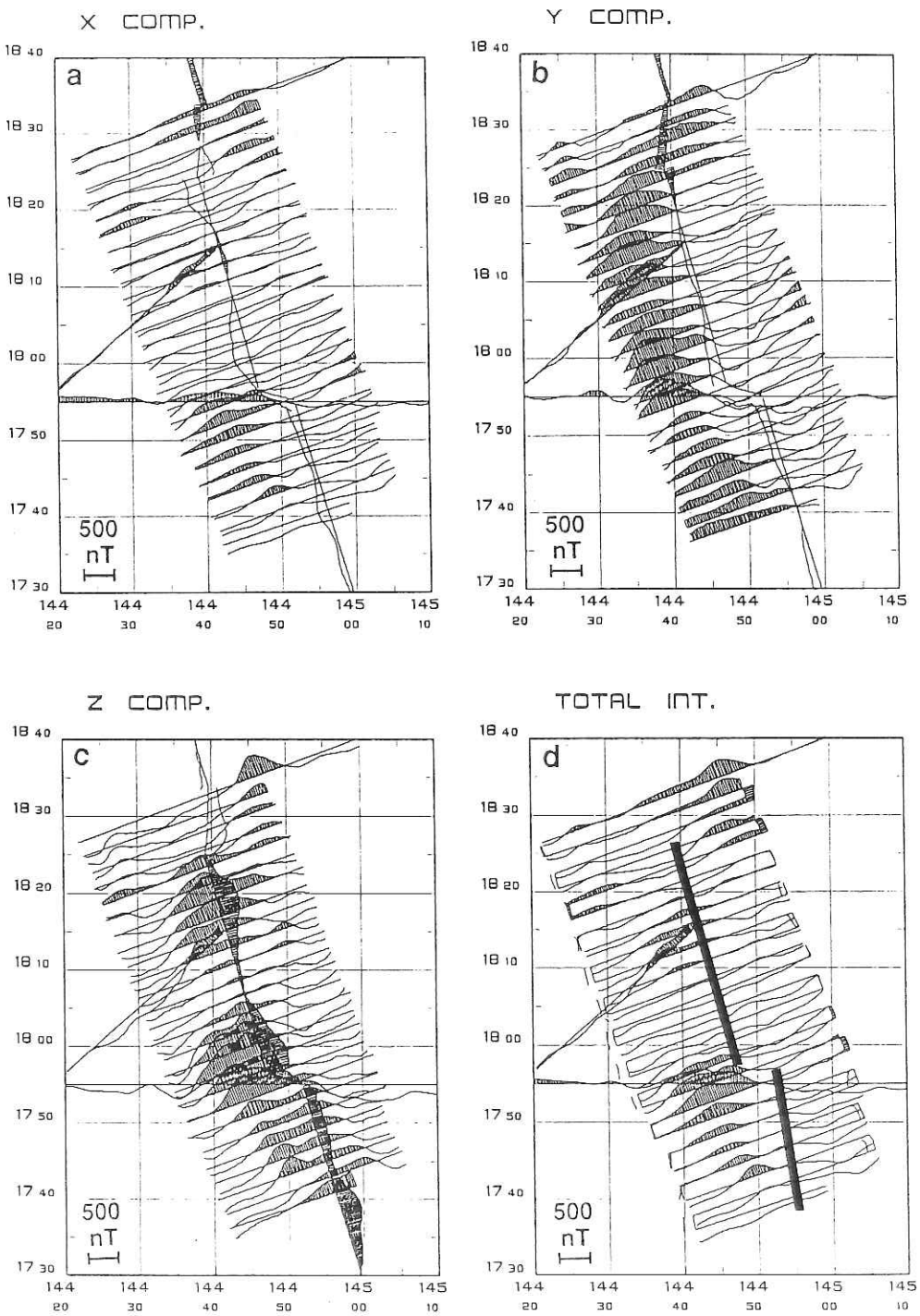

Fig. 10.2.1 Vector (a - north, b - east, c - downward) and total intensity (d) geomagnetic anomaly field profiles along the ship's track (which is plotted as the zero value datum for the anomaly). Positive values are shaded. Thick solid lines in (d) show spreading axes inferred from the morphological structure in this area.

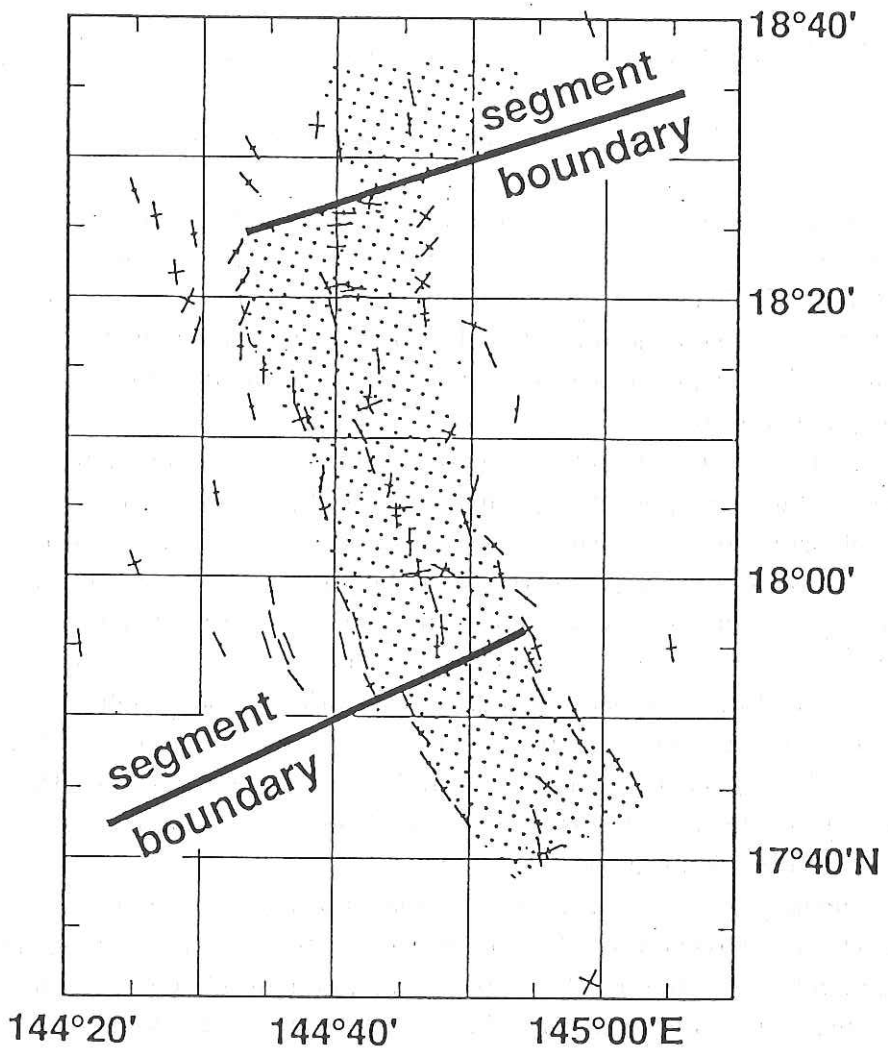

Fig. 10.2.2 Magnetic boundary strike diagram (MBSD; Seama et al., 1992). Positions (crosses) and strikes (long lines) of magnetic boundaries are shown. The length of the longer line is proportional to the cosine of the boundary inclination. The shorter line of the cross corresponds to twice the standard deviation in the strike. Hence, a perfectly two-dimensional boundary results in a single long line with no cross bar, whereas three-dimensional magnetic boundaries cause the longer line to shorten and the shorter line to lengthen. A boundary with zero inclination and 26.6° standard deviation will plot as an equilateral cross. Since positions, strikes and character of magnetic boundaries are displayed in the MBSD, the magnetic structures can be clearly seen. Diagonally hatched areas show regions of normal magnetization (the Brunhes epoch).

10.3 Geomagnetic Anomalies in the Ayu Trough

T. Fujiwara, H. Toh, N. Seama and K.Tamaki

As part of a geophysical measurement of the Ayu Trough, geomagnetic measurement was carried out. Objective of geomagnetic measurement is to make sure whether ocean floor spreading ocurs at the Ayu Trough or not. If lineation of geomagnetic anomaly is found, we can conclude that the ocean floor spreading did occur and can determine the age and the spreading rate from geomagnetic lineation.

In this cruise, vector magnetic survey was carried out by using a shipboard three component magnetometer (STCM; Isezaki, 1986) in addition to total intensity survey by using a proton magnetometer. This is a very powerful tool because vector geomagnetic anomalies are not affected by the ambient geomagnetic field. Previous studies using total intensity anomalies have never reported on recognizable geomagnetic lineations in this area. The reasons are probably due to geomagnetic latitude and the strike of the trough. The trough is located near the geomagnetic equator. The geomagnetic field has little downward component (Z-component) in the geomagnetic equator. The strike of the trough is almost in the N-S direction. Under these conditions, it is hard to detect geomagnetic lineations.

Geomagnetic anomalies were calculated using the reference field of IGRF 1990 (IAGA, Division Working Group 1, 1990). Total intensity, northward component (X-component), eastward component (Y-component) and Z-component anomaly profiles are shown in Figure 10.3.1. Vector geomagnetic anomalies are biased due to change in ship's permanent magnetization.

Total intensity anomalies and X-component anomalies resemble closely each other. We believe that ambient geomagnetic field is mostly X-component. The amplitudes of these geomagnetic anomalies in the trough area are smaller than those in the West Philippine Basin and the West Caroline Basin. This fact is probably due to the strike of the trough. These geomagnetic anomalies are reduced by ambient geomagnetic field. Y and Z-component anomalies show the axially symmetric pattern of geomagnetic lineations. We can easily find them around 4°N. It is possible to think that these are geomagnetic lineations. We calculated the magnetic boundaries following the method of Seama et al. (1993). As the result, axially symmetric magnetic boundaries were calculated as shown in Figure 10.3.2. Although we have to inspect that the cause of magnetic boundaries are due to change in magnetization or topographic effect, we can get geomagnetic lineations.

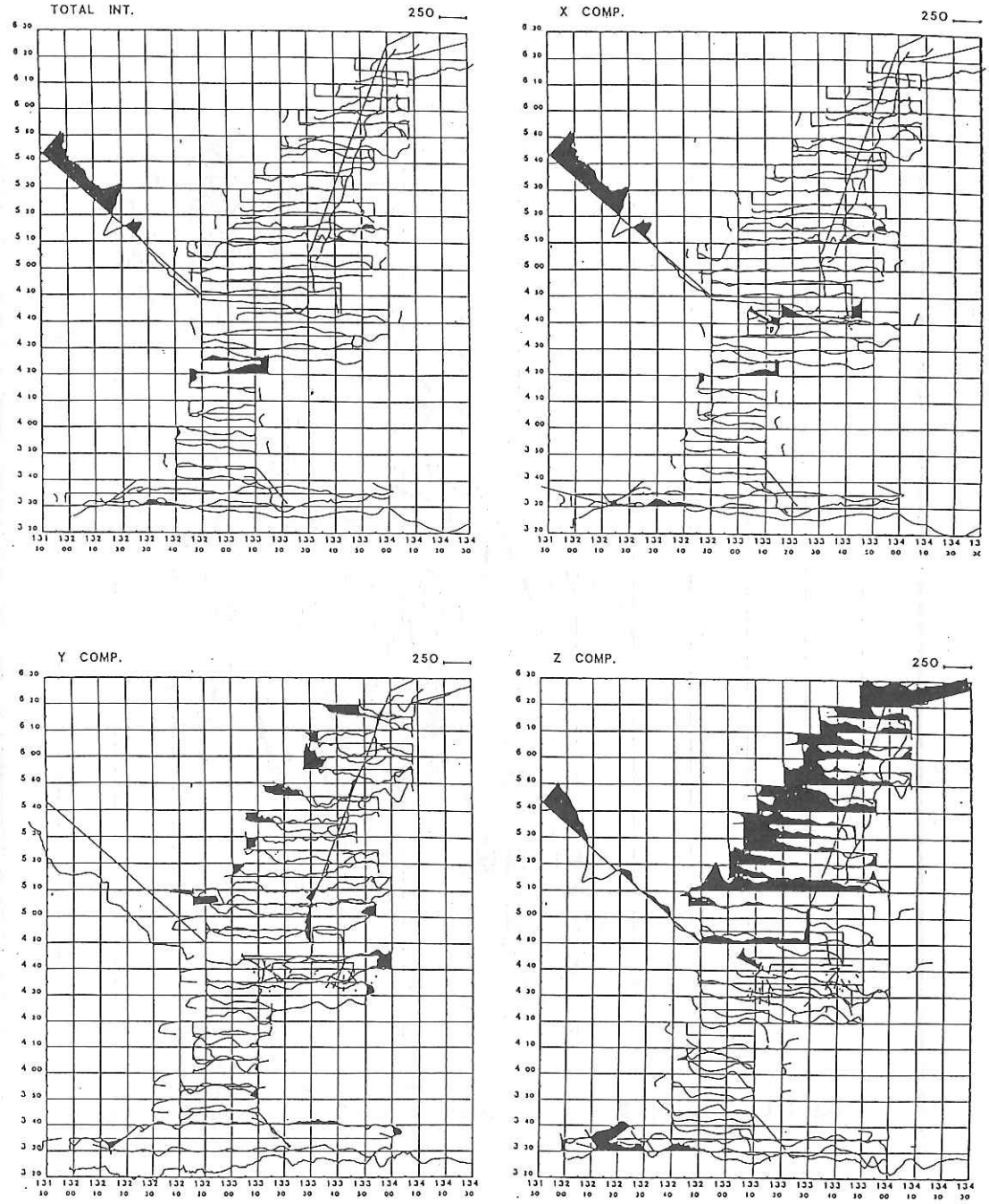

Fig. 10.3.1 Total intensity, X-component, Y-component and Z-component anomalies profiles along ship tracks.

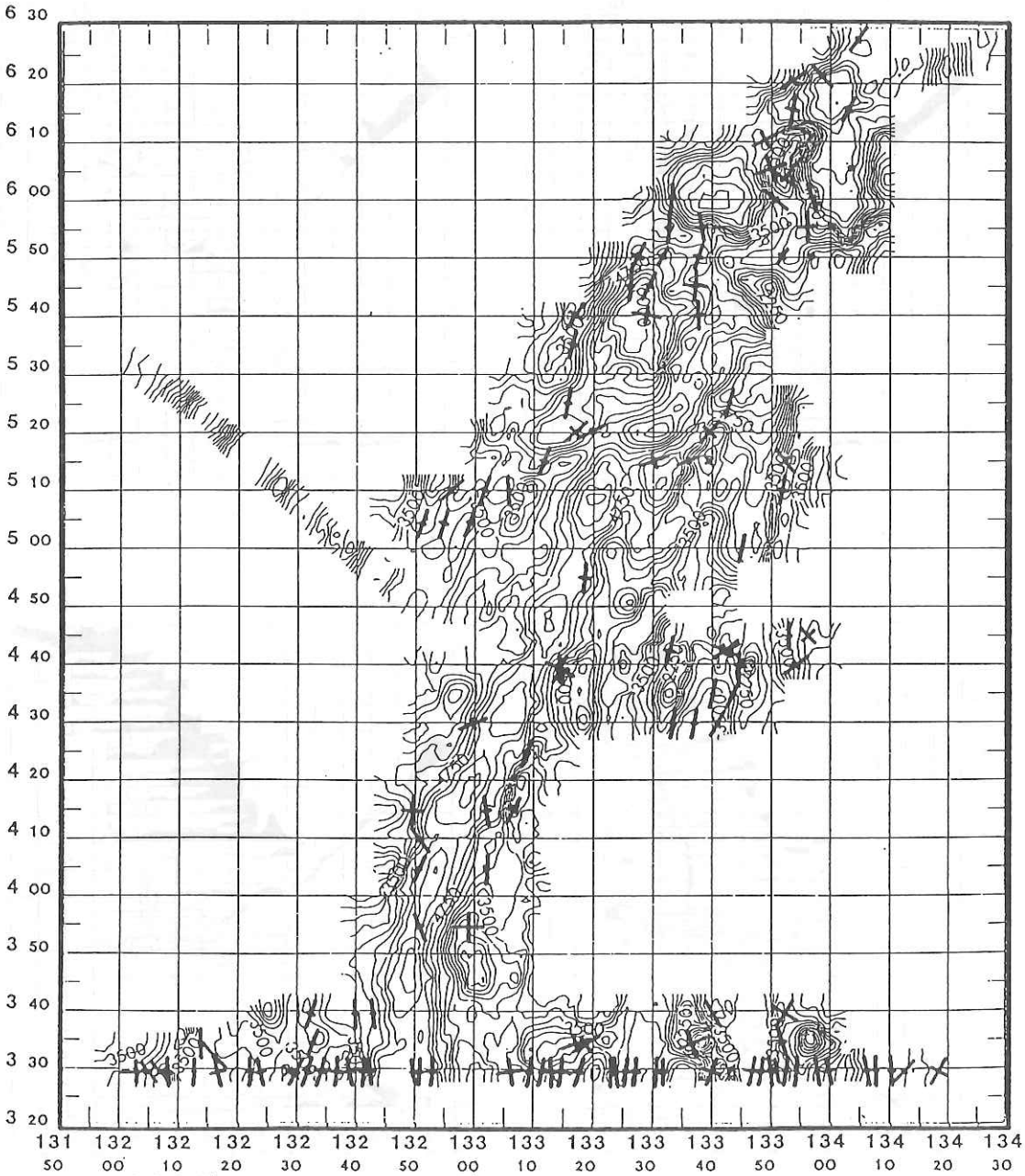

Fig. 10.3.2 The calculated magnetic boundaries. The positions of crosses show the positions of magnetic boundaries. The longer line of the crosses shows the strike of magnetic boundary and the shorter line shows an error bar.

11. Seismic Observation at the Mariana Trough at 18°N and Its Relation to the Detailed Bathymetry

J. Kasahara, L. Kong, S. Koresawa, C. Igarashi,T. Yamaguchi, M. Suzuki
and
R. Feng.Lu

11.1 Objectives and Geophysical Setting

In the last several years, we have been investigating seismic structures of the back arc basins near Japan such as the Yamato Basin, Japan Sea and Okinawa Trough. The main objectives of studies of these back arc basin are to understand the rifting process and to determine the crustal structure of the back arc basin. Results from these studies indicate that they are of the typical oceanic structure in the eastern part of the Japan Sea (Kasahara et al., 1991; Kong et al., 1991) and approximately 15 km of crustal thickness for the Yamato Basin (Katao, 1988) and the Okinawa Trough (unpublished). It is thought that the Okinawa Trough is in an immature rifting stage. We did not find the oceanic velocity structure in these areas which is similar to that found in the Mid-Atlantic Ridge or the East Pacific Rise.

The TPC-1 submarine cable runs from Ninomiya,Japan to Guam, USA. In 1990, the cable was donated from private cable companies to the scientific community (University of Tokyo and IRIS in US) for scientific reuse. To utilize this cable, we have proposed construction of two seismic stations and one geophysical station that will be attached to the cable. This project's name is GeO-TOC (Geophysical and Oceanographical Trans Ocean Cable) Project (e.g., Kasahara et al., 1990). In the Mariana region, the cable runs through the Mariana Trough region. At 18°N, the cable lies approximately 80 km to the west of the Mariana Trough Axis (Fig. 11.1). Since one of the most probable site for GeOTOC geophysical station is located near 18°N in the Mariana Trough, in order to define the site of station deployment it is necessary to collect detailed geophysical data in this region. For the above purpose, we conducted a detailed Sea Beam survey and seismic refraction study in this region during KH92-1 cruise (Fig. 11.2).

The Mariana Trough is a back-arc basin in the Mariana Island Arc system. The Trough is a crescent-shaped back-arc basin lying to the east of the Mariana island chain, extending from 13°N to 22°N. The Trough axis is the clearest at 18°N, and obscured in the other locations. Turbidite flows of volcanic ash and tuff of the Mariana Islands are likely to cause the indistinct character of the trough. Karig (1971) proposed a rifting process similar to that occurring in the

Lau Basin and at mid-oceanic ridges. In this context, the Mariana Trough constitutes one of most geophysically-interesting regions where active spreading or rifting in a tectonically unique area can be studied.

The Mariana Trough region at 18°N has been geologically and geophysically investigated by numbers of authors. In 1979, DSDP drilled several holes at different longitudes along the 18°N latitude. Hole 454 and Hole 456, in particular, among them are located to the east and west of the median valley (Hussong and Uyeda, 1981). Although the age of Mariana Trough is not certain, DSDP data suggest that it is younger than several Ma. In 1987, deep sea submersible "Alvin" dived in the median valley axis,and discovered 285 oC water temperature, chimney structures, and hydrothermal type biological colonies (Craig et al., 1987). They also found 1-2 m high hydrothermal mound approximately 50 km west of the axis, suggesting active hydrothermal circulation (Leinen et al., 1987, 1990, Becker et al., 1990).

There have been only a few seismic experiments in this area. Bibee et al. (1980) reported seismic and geophysical results from a two-ship refraction study using explosives near the Pagan Fracture Zone at 18°N. Although the number of data points are not large, their results show existence of oceanic type structure beneath the Trough axis. They used the classical layer models. However, although LaTrailee and Hussong (1981) used sonobuoys in a refraction survey along the latitude of 18°N they did not find oceanic structure across the Trough Axis. Using ocean bottom seismometers, Ambos and Hussong (1982) obtained a P wave velocity of 7.7 km for the Moho and 6 km for the crustal thickness at 18°N. Sinton and Hussong (1982) studied the crustal structure along the Pagan Fracture Zone at 17°35'N and obtained 7.5 -8.0 km/s for the upper mantle velocity. They also found an oceanic-like seismic structure for N-S line nearly on the Trough axis, but the velocities for lower crust and upper mantle were highly variable from place to place.

A Deep-tow geophysical survey and dredge samples collected during the Alvin dive program (Hawkins et al., 1990) document a topography resembling the FAMOUS area in Mid-Atlantic ridge, suggesting that the Mariana Trough may be an another typical example of slow-spreading ridges.

Because of the importance of geophysical character at a possible TPC-1 cable remote station , we thought it important to carry out a comprehensive, high-resolution bathymetric and seismic study of the active rifting center in the Mariana region. The results from this study, together with those from the KH92-1 magnetometer and gravity data sets (Seama et al., in this volume) and the existing geological and petrological studies, will define the Mariana Trough at 18oN as regionally well-characterized natural geological and geophysical observatory.

11.2 Field Experiments

In total, seven OBSs were deployed in the KH92-1 seismic refraction study: four analog OBSs and two digital OBSs from Earthquake Research Institute, University of Tokyo and one analog OBS from Chiba University. OBS positions are shown in Table 11.1 and Fig. 11.3. The analog OBSs of both institutions have four channels: one vertical seismometer, one horizontal seismometer,hydrophone and one time code channel. 2 Hz seismometers were used. Two magneto-optical disk OBSs, called MOOBS (MagnetoOptical OBS) (Kasahara and Matsubara, 1991) were used. The MOOBS can record data up to 320 Mb on one side of the MO disk. Four channel, one 2 Hz vertical seismometer with 20 dB and 40 dB, and two 2 Hz horizontal seismometers with 20 dB are used. The seismometers are installed in external pressure case outside the recording unit glass sphere in order to suppress MO drive noise during recording. After amplification of the analog signals, the signals were digitized by a 16-bit A/D converter enabling 96 dB dynamic range to be obtained. Time information for each record is saved in the header record. Event-triggering algorithm was employed to record seismic signals. To minimize the loss of time during recording, pre-trigger length and post-trigger length of each 180 seconds were used. 100 Hz sampling rate was used.

Prior to the refraction survey, a two-day Sea Beam survey covering 50 km x 100 km area was conducted. The bathymetric map obtained by Sea Beam is shown in Fig. 11.4 with 50 m contour intervals.

Based on the results of Sea Beam survey, three stations (MT3,4 and 5) on or besides axial highs which are several hundred-meter-wide flat tops were chosen. Precise navigation using SeaBeam bathymetry map enabled us to drop the OBSs at the selected location by observing the depth recorder when the ship passed from a steep seafloor slope to a flat bottom. It is important to recognize the necessity of obtaining a detailed bathymetry map prior to deployment because, without such a map, successful OBS deployment would not be possible. The last OBS was dropped near the deepest survey area at 18°N. Among OBSs, MT2 and MT-5 are MOOBS stations and MT-2' is Chiba analog OBS station.

Because of the extremely rough topography, careful acoustic measurements of slant range between ship and OBS were made during deployment. Comparison of the depths between the Sea Beam data and OBS estimation indicates that the difference was within 10 meters. Fig. 11.5 shows the airgun shooting lines. 19-hour shooting using two 12-liter Bolt airguns was carried out along the neovolcanic zone of the median valley and the axial high. Total length of the line is 185 km. The distance from southern end OBS point

(MT-1) and northern end OBS point (MT-6) is approximately 75 km. The airgun pressure was kept as 100 atoms and firing interval was 30 seconds. The shot times were calibrated by a shipboard reference clock synchronized with that used for OBS deployments.

After the shooting, 6 OBSs were retrieved, but one (MT-4) unfortunately lost. Although several release commands were sent, MT-4 did not appear to be released from the seafloor since the distance between ship and OBS did not change.

Examination of the data recorded by the digital OBS show 114 files were recorded on MT-2 and 169 files were recorded on MT-5. The 114 files correspond to 15.2 hours and the 169 files correspond to 22 hours. The records are mixture of natural earthquakes, airgun records and some unknown noises.

11.3 Linear Faults System Obtained by SeaBeam Map

Fig. 11.6 shows a tectonic interpretation of SeaBeam map shown in Fig. 11.4 (Kasahara et al., 1992). The trough axis shows zig-zag shape which defines segment boundaries. There are three segment boundaries: Pagan Fracture zone around 17°30'N, one unknown around 17°50'N and one around 18°30'N. The length of the segment boundary of the middle one is shorter than the others. As clearly seen in 50 m interval bathymetry map (Fig. 11.4), there are many faults nearly parallel to the trough axis. These fault system is not evident in the previous bathymetry map of 150 m contour interval. The fault system obtained by the present authors is similar to that obtained by Hawkins et al. (1990), but if examined in detail there are some differences. These faults form hors-graben structures. Most of faults are interpreted as normal faults. Spacings between faults are 3 to 10 km. The maximum length of the faults is about 40 km. The other shorter faults are about a few km long. The cross-sections corresponding to the lines nearly perpendicular to the trough axis are shown in Fig. 11.7. In the middle of the surveyed area, the profiles 6-16 have central highs in the axial area. However, in the north and the south of the surveyed area (profiles 2-3 and 20-25), central high is not clearly seen. Since in north and south region, the seabottom of the trough axis is covered by sediment, the central highs may be buried in sediment. Fig. 11.8 shows comparison of topographies across the ridge axes among various spreading centers. The profiles 6-16 in Fig. 11.7 is very similar to the topography seen in the slow spreading ridges such as Mid-Atlantic ridge shown in Fig. 11.8. Both area show central highs in the axial region and very rugged topography. The resemblance between the two suggests the strong possibility of slow spreading of the oceanic crust in the Mariana Trough region at 18°N. This is the same conclusion as that of Hawkins et al.

(1990). They discussed this by the topography obtained using deep tow sonar.

11.4 Seismic Activity Observed by OBS's in the Mariana Trough

Although the OBSs were deployed for the sake of refraction survey (Fig. 11.9), so the observation period was only 1.5 days (Table 11.1), many natural earthquakes were observed. Most events were local earthquakes. The S-P times of local events show 3 seconds to several seconds suggesting seismic sources near the OBSs. The number of events which have shorter S-P time than 3 seconds are listed in Table 11.2. ST-6 near the north segment boundary recorded 30 events and ST-1 near Pagan Fracture zone in the south recorded 32 events. This is as high as or higher than the seismicity level near Japan Trench or Izu-Bonin Trench. On the other hand, ST-3 in the middle of the OBS sites observed only 4 events. Although ST-5 and ST-2 used digital triggering algorithm they picked up 7 nearby events. Some examples of seismic records for nearby earthquakes are shown in Fig. 11.10. From the above observations, seismic activity along the north segment and the south segment (Pagan FZ) boundaries were extremely active during the observation period. On the other hand, the seismic activity in the middle is weaker than those in the north and south. The ST-3 is located near the hydrothermal vent found by Alvin dive shown by the cross in Fig. 11.9. The low seismicity on this station can be explained by complimentary nature with seismicity and thermal activity. Many events observed by OBS have T-phase which suggests very shallow source depth. The hypocenters corresponding to the observed events can not be determined because the seismic network is nearly a line shape.

Open circles in Fig. 11.11 show ISC hypocenters which have magnitude greater than 3 since 1964. The hypocenters are concentrated near Pagan FZ (shaded zone in the south part of this map) and it shows rather weak activity in the north. Hussong and Sinton (1982) observed extremely strong activity along the Pagan FZ. However, the present observation indicate the similar seismic activity level between north region and south region around the Mariana Trough around 18°N, and the seismicity level in this region is as high as that in Japan or Izu Bonin Trenches. These are new evidence concerning the seismicity.

The present results and ISC hypocenters seem to correspond to the segment boundaries, not to that the normal fault region. This might indicate normal fault system was mostly born in the axial region through non-seismic process such as slow deformation. On the other hand, movement at the segment boundaries is more frictional than at the axial region. However, the magnitude of earthquakes are not large, so this might be explained by small scale slipping fault such as mesh-like shear zone. If there is meshlike shear zones, each fault

length should be very short, but the total displacement will be large.

The seismic noise level over the frequency range of 10 mHz to 30 Hz is also analyzed using records obtained by ST-2 and ST5 (Mochizuki et al., 1992). Noise spectrum of ST-5 is similar to that obtained by OBSs deployed at Boso region in which the spectrum has a peak around 3 seconds and a trough at 10 mHz -0.1Hz, but the absolute noise level of ST-2 is extremely low compared to other OBS records in Boso area and Sagami Bay.

11.5 Airgun Records

The airgun records obtained by OBSs show very fsst attenuation of refraction arrivals over the distance of 5 km on both stations ST-2 and ST-5. It is thought that this is due to either very high attenuation in the upper part of the crust at high temperature or the weak OBS-bottom coupling due to bare-rock ocean basement. Both cases are very possible. If the temperature in the axial high area is very high as suggested by Alvin dives, the seismic attenuation might be very large. And the bottom topography near the OBS stations are extremely rough and the bottom seems no sediment cover. This might cause weak coupling and low level of signals.

OBS records obtained by the analog OBSs will be analyzed later.

Acknowledgements

We greatly thank Prof. J. Segawa (Chief Scientist of KH92-1) for his assistance in collecting the Sea Beam and air gun-OBS survey data. We also commend the professionalism of the officers and crews of the R/V Hakuho-Maru during the study. The Sea Beam survey was done in cooperation with Dr. Fujimoto and Mr. N. Seama. The interpretation of SeaBeam bathymetric map was conducted as cooperative works with Dr. T. Sato.

References

Ambos, E. L., and D. Hussong, Crustal structure of the Mariana Trough, J. Geophys. Res., 87, 4003-4018, 1982.

Becker, K., M. Leine, R. McDuff, K. Dadey, M. Hamano and N. Fujii, Eos Trans. AGU, 71, 1568, 1990.

Bibee, L. D., Shor, G. G. Jr. and Lu, R. S., Inter-arc spreading in the Mariana Trough, Marine Geology, 35, 183-197, 1980.

Craig et al., Hydrothermal vents in the Mariana Trough; results of the first ALVIN dives, Eos Trans. AGU, 68, 1531, 1987.

Hawkins, J. W., P. F. Lonsdale, J. D. Macdougall and A. M. Vople, Earth Planet. Sci. Lett., 100, 226-258, 1990.

Hussong, D. M. and Sinton, J. B., Seismicity associated with back arc crustal spreading in the central Mariana Trough, in "Tectonic and geological evolution of southeast Asia seas and islands, Part 2, ed. D. E. Hays, 217-235, 1982.

Hussong, D. M. and S. Uyeda, Initial reports of the Deep Sea Drilling Project, Leg 60, U.S. Government Printing Office, Washington, D. C., 1981.

Karig, D. E., Structural history of the Mariana island arc system, Geol. Soc. Am. Bull., 83, 323-344, 1971.

Kasahara, J., Y. Hamano and T. Yukutake, Geoscientific study using trans ocean cable, Kaiyo Monthly, 22, 447-451, 1990.

Kasahara et al., Air-gun OBS study in the Japan Sea, Seismol. Soc. Jpn., Fall Meeting Abstract, 1991.

Kasahara, J. and Matsubara, Development of MOOBS (Magneto Optical Ocean Bottom Seismometer), Seismol. Soc. Jpn., Fall Meeting Abstract, 1991.

Kasahara, J., L. Kong, T. Sato, S. Koresawa and N. Seama, Seismicity and tectonics of the Mariana Trough, Seismol. Soc. Japn., Fall Meeting Abstract, 37, 1992.

Katao, H., Bull. Earthq. Res. Inst., University of Tokyo, 1988.

Kong et al., Explosion-OBS refraction study in the Japan Sea, Seismol. Soc. Jpn., Fall Annual Meeting Abstract, 1991.

LaTraille, S. L. and D. M. Hussong, Crustal structure across the Mariana Island arc, in "The Tectonic and Geological Evolution of Southeast Asian Seas and Islands", Geophys. Monogr. Ser., 23, ed. D.B.Hayes, 209-222, AGU, Washington, D. C., 1981.

Leinen, M. et al., Off-axis hydrothermal activity in the Mariana Mounds field, Eos Trans. AGU, 68, 1531, 1987.

Leinen, M. et al., A model for the formation of off-axis hydrothermal features in the Marina Trough, Eos Trans. AGU, 71, 1568, 1990.

Mochizuki, K., Sato, T., J. Kasahara and S. Koresawa, Wide band microseism spectrum obtained by digital OBS (MOOBS), Abstract of Japan Seismol. Soc. Fall Meeting, 105, 1992.

Sinton, J. B. and D. M. Hussong, Crustal structure of a short length transform fault in the central Mariana Trough, in "Tectonic and geological evolution of southeast Asia seas and islands, Part 2, ed. D. E. Hays, 236-254, 1982.

Yamano, M., Long term temperature observation for hydrothermal system, Kaiyo Monthly, 23(5), 244-249, 1991.

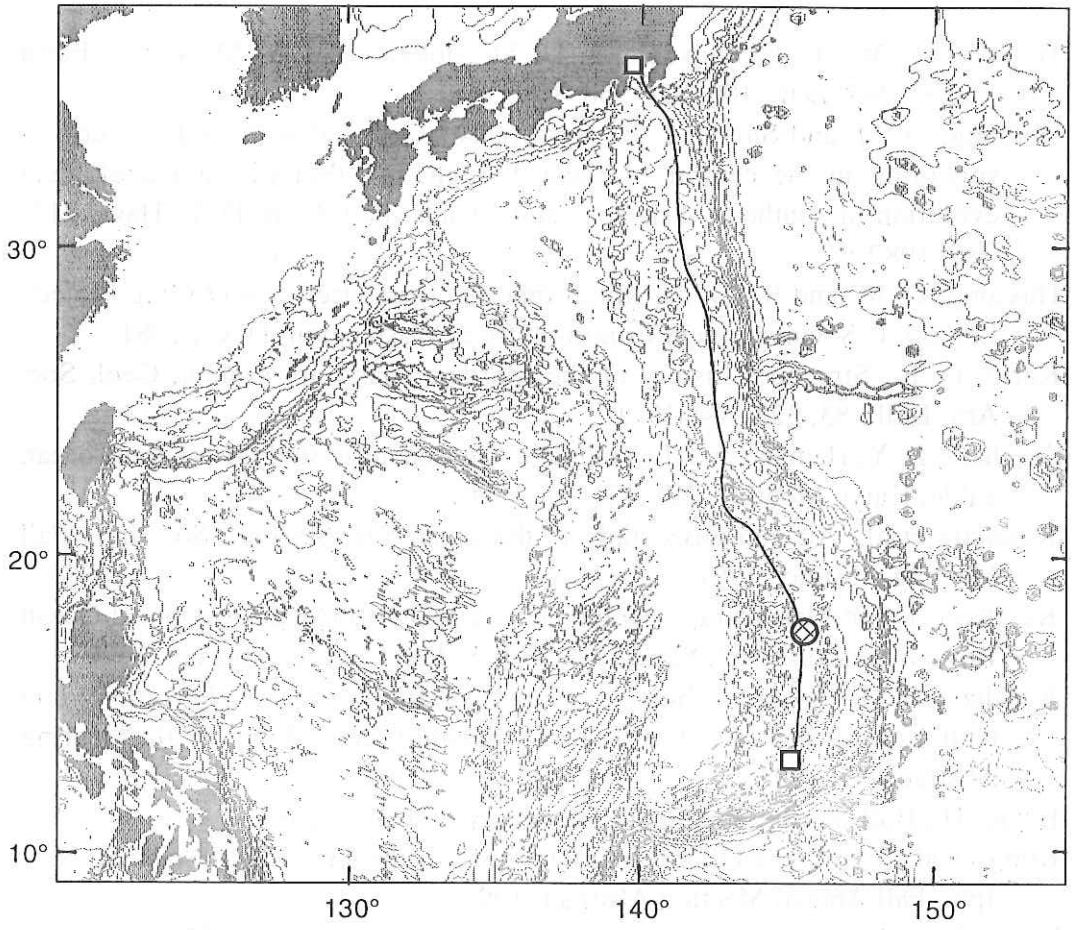

(a)

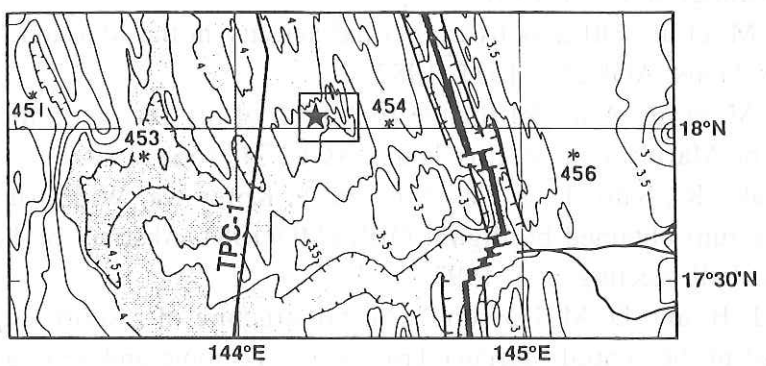

(b)

Fig. 11.1 (a) Possible location of geophysical station along the TPC-1 cable proposed by GeO-TOC project, (b) TPC-1 cable and axis of Mariana Trough around 18°N (after Yamano, 1991).

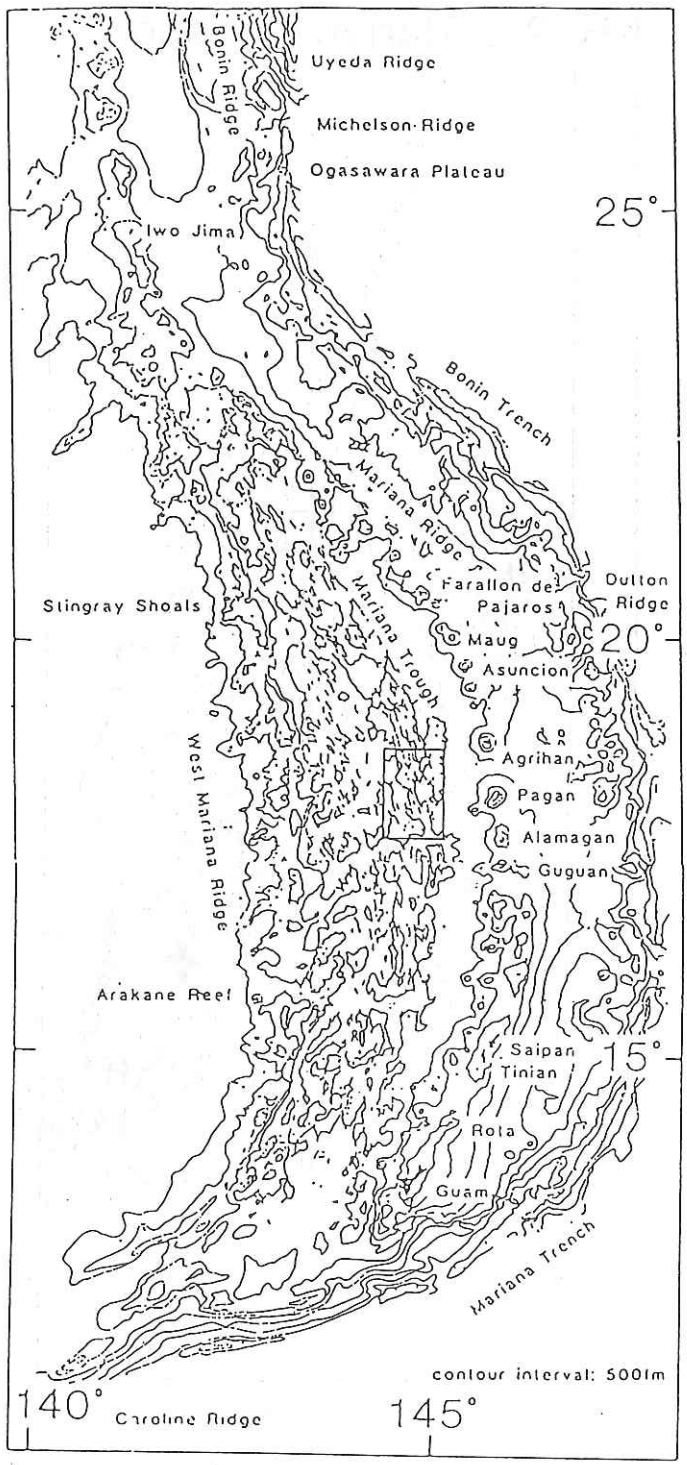

Fig. 11.2 Location of Mariana region and survey area shown by box(modified from Smoot, 1988).

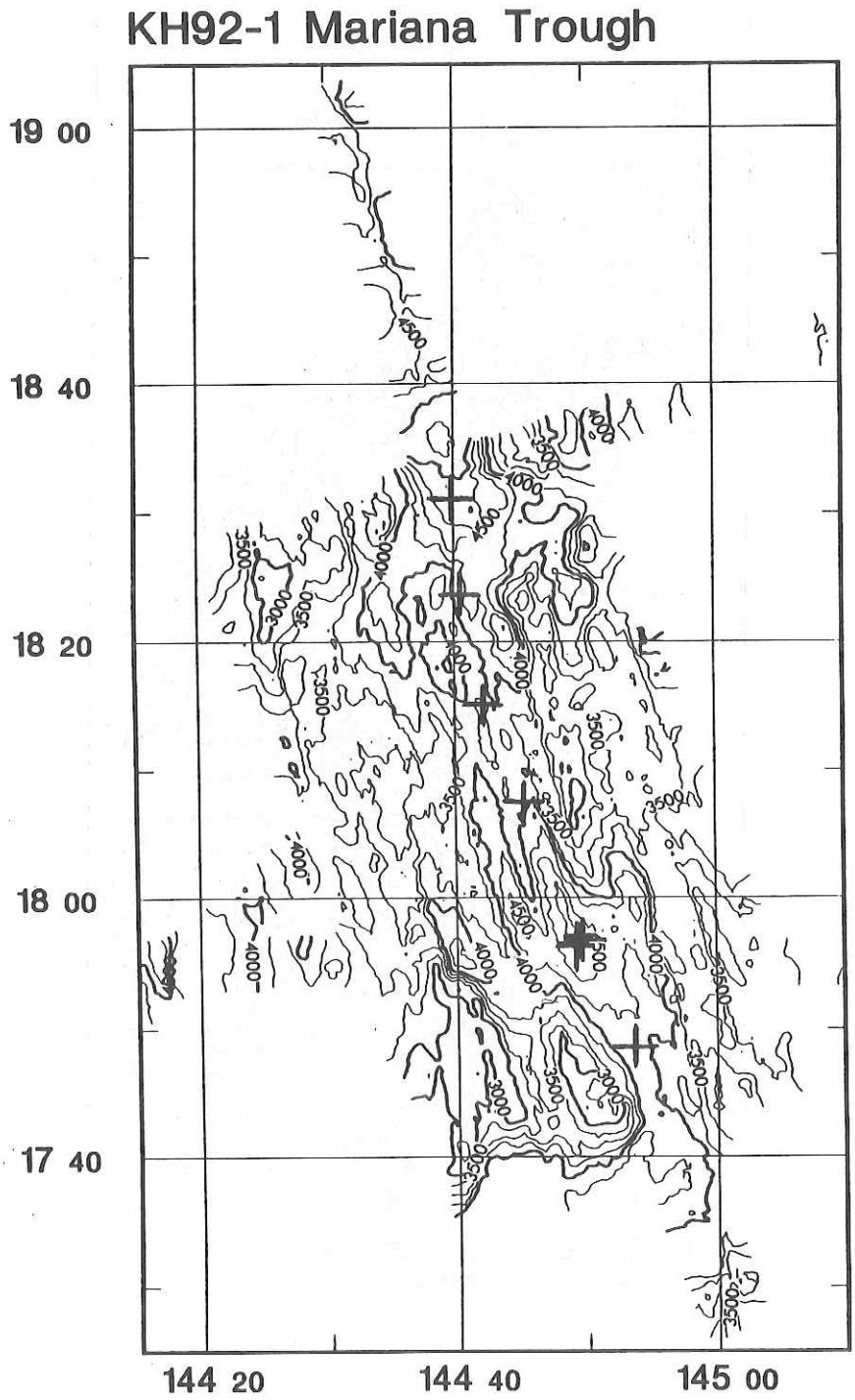

Fig. 11.3 Location of OBS shown by plus marks.

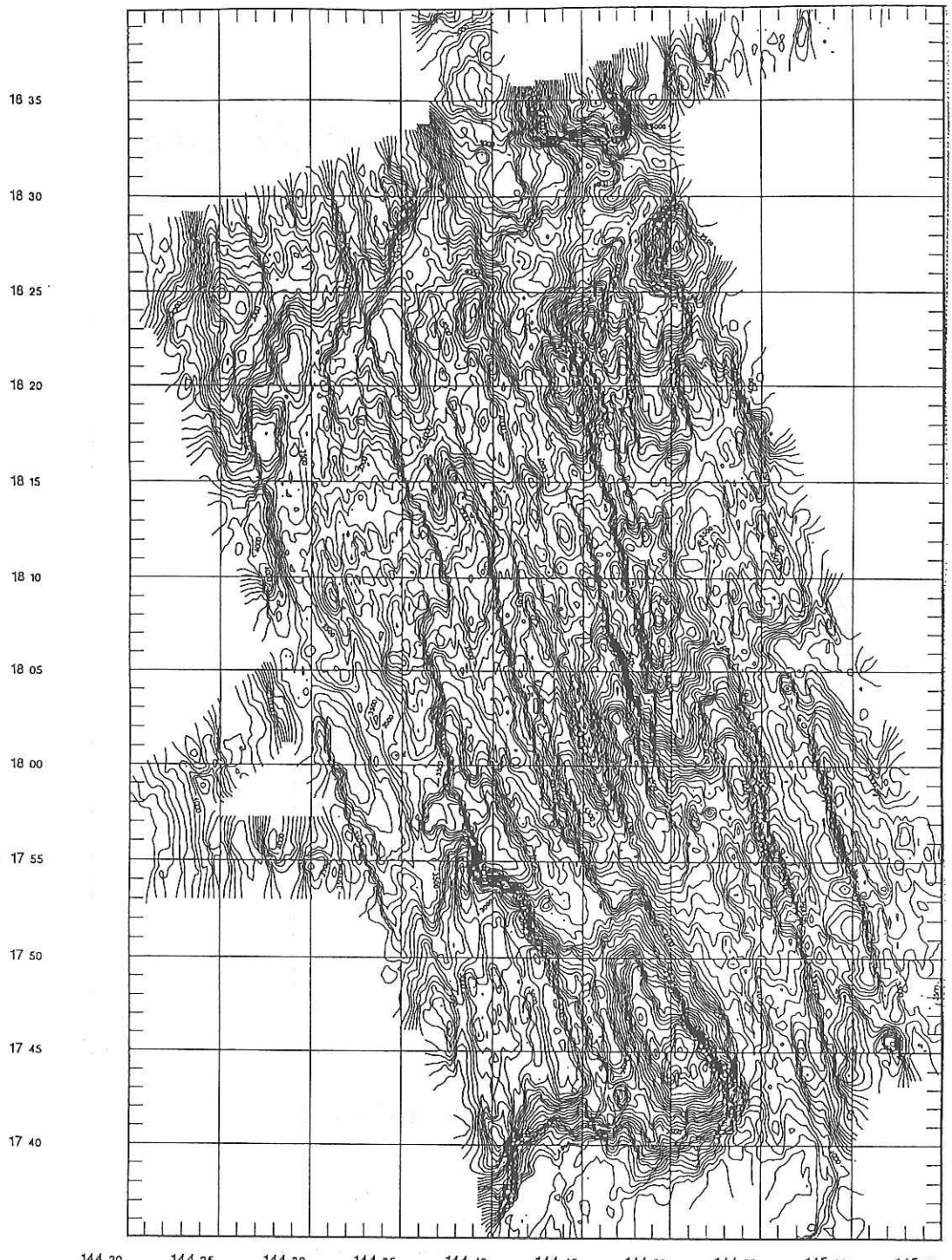

Fig. 11.4 Bathymetric map obtained by SeaBeam Survey. Contour interval is 50 m. Normal faults are clearly seen in this figure as steep change of depth contours.

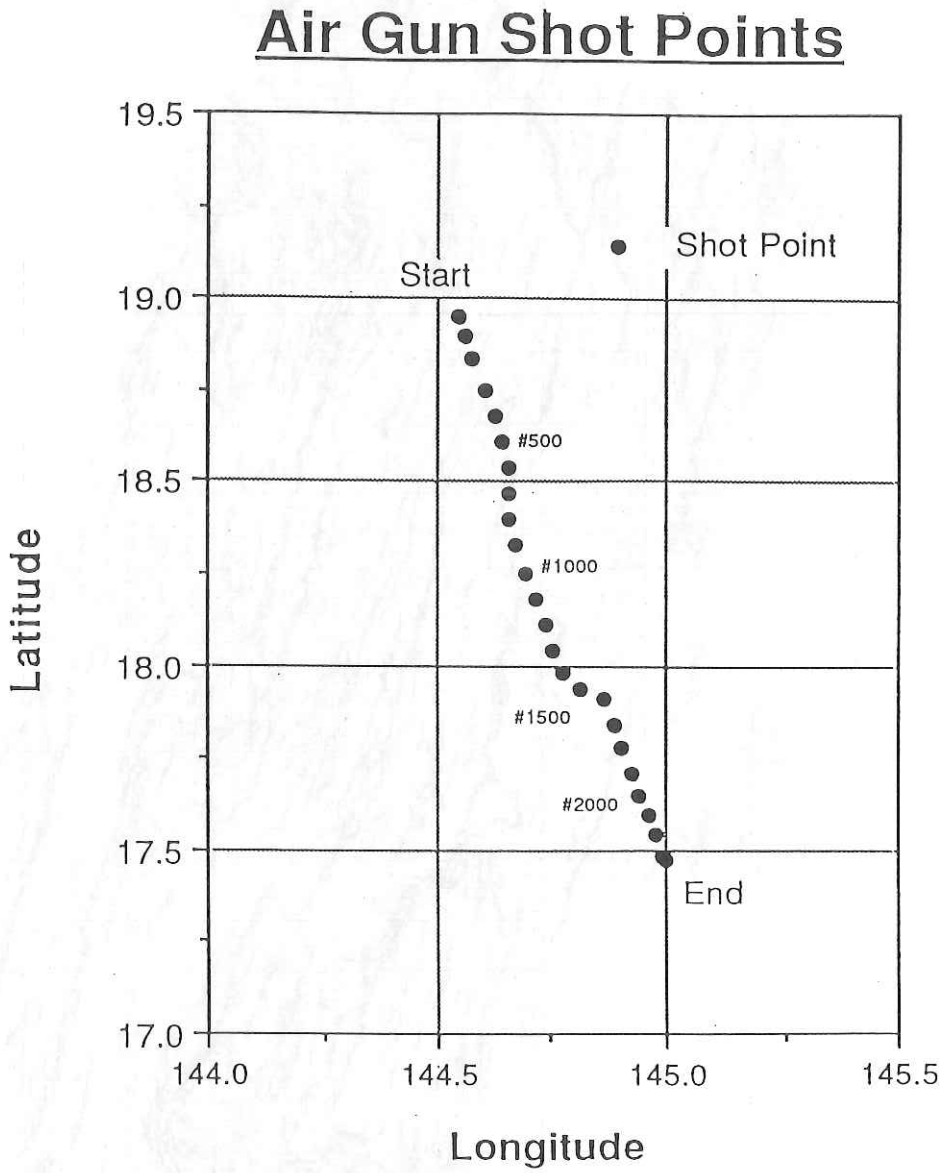

Fig. 11.5 Air gun shooting line shown by dots.

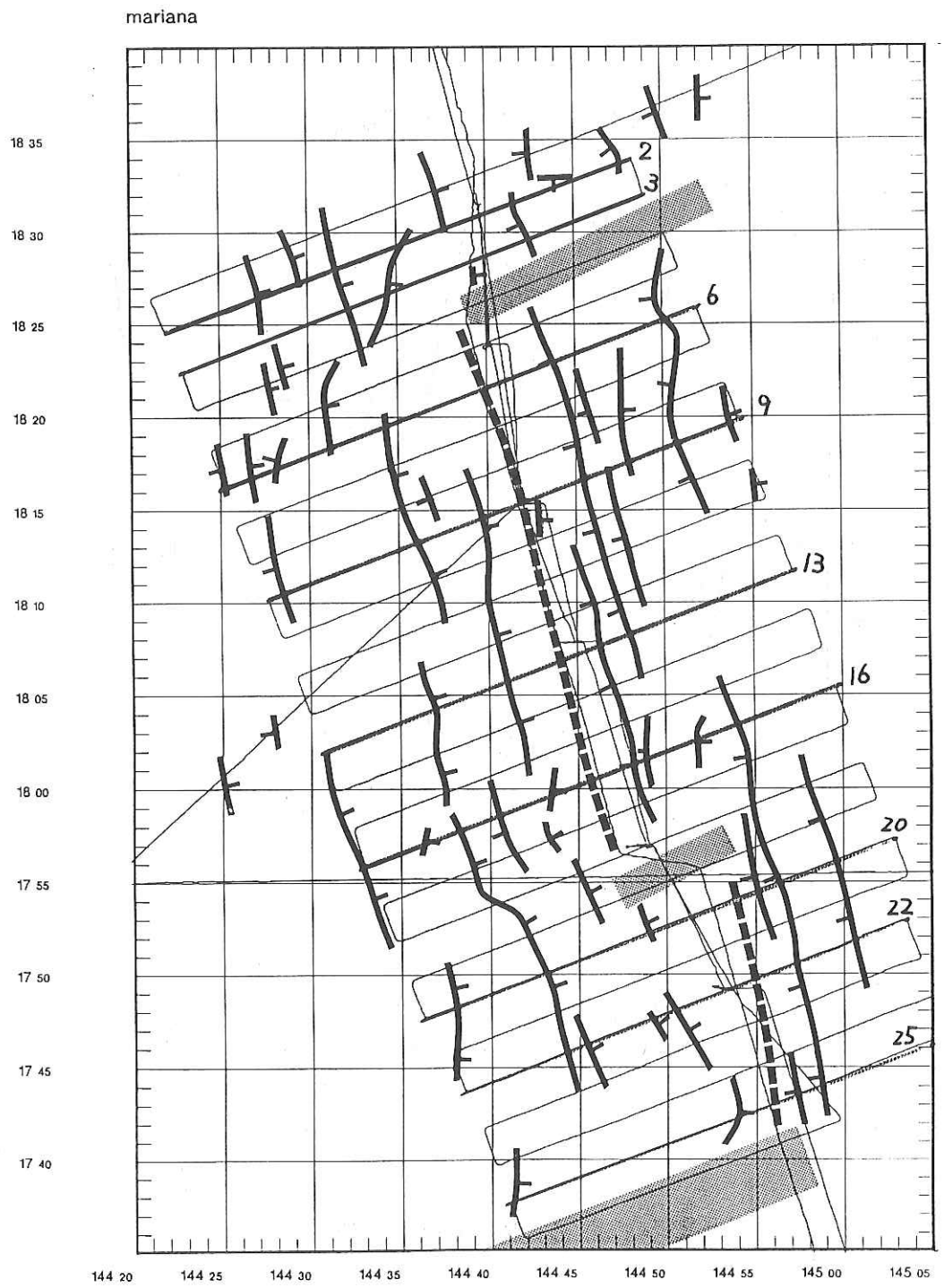

Fig. 11.6 Interpretation of faults system (heavy solid lines)(Kasahara et al., 1992). All faults are interpreted as normal faults. Tic marks with faults indicate dip direction of faults.Shaded zones show segment boundaries. Heavy dotted lines show axial region of the Marina Trough. Light solid lines show SeaBeam survey lines. Numbers correspond to profiles shown in Fig. 11.7.

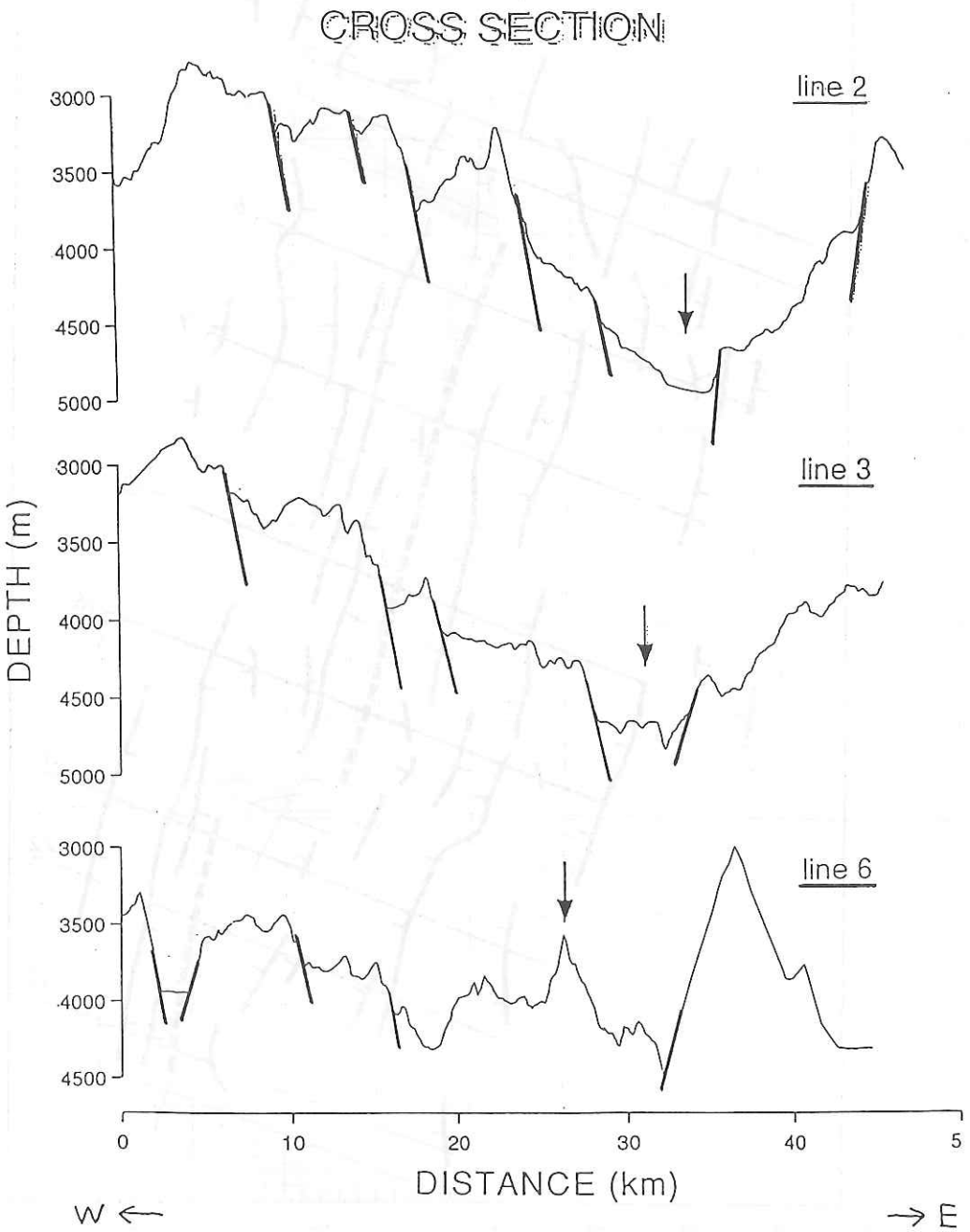
CROSS SECTION
line 2
line 3
line 6
3000
3500
4000
4500
5000
DEPTH (m)
0
10
20
30
40
5
DISTANCE (km)
W ←
→ E

(a)

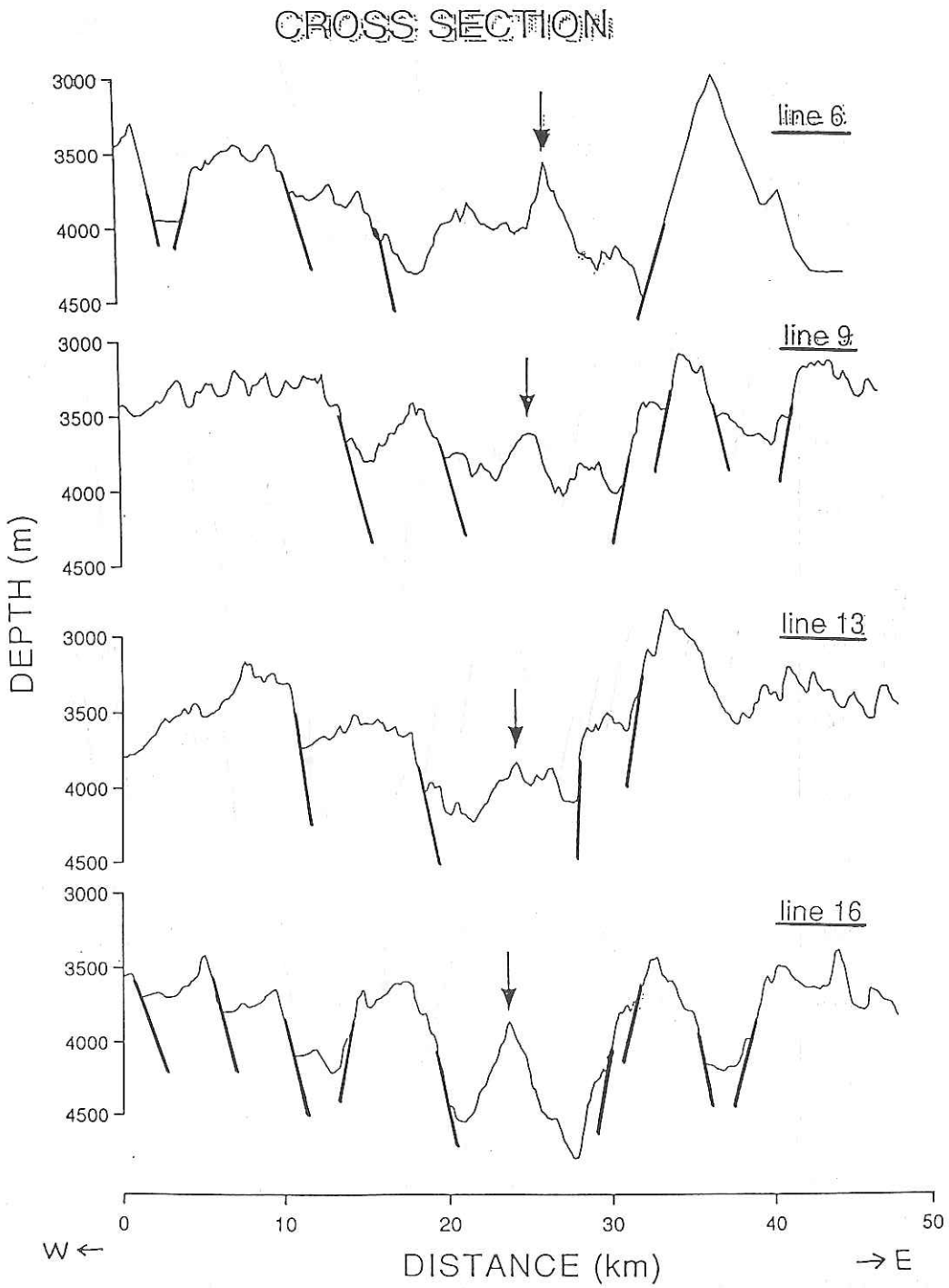
CROSS SECTION
line 6
line 9
line 13
line 16
3000
3500
4000
4500
DEPTH (m)
0
10
20
30
40
50
W ←
DISTANCE (km)
→ E

(b)

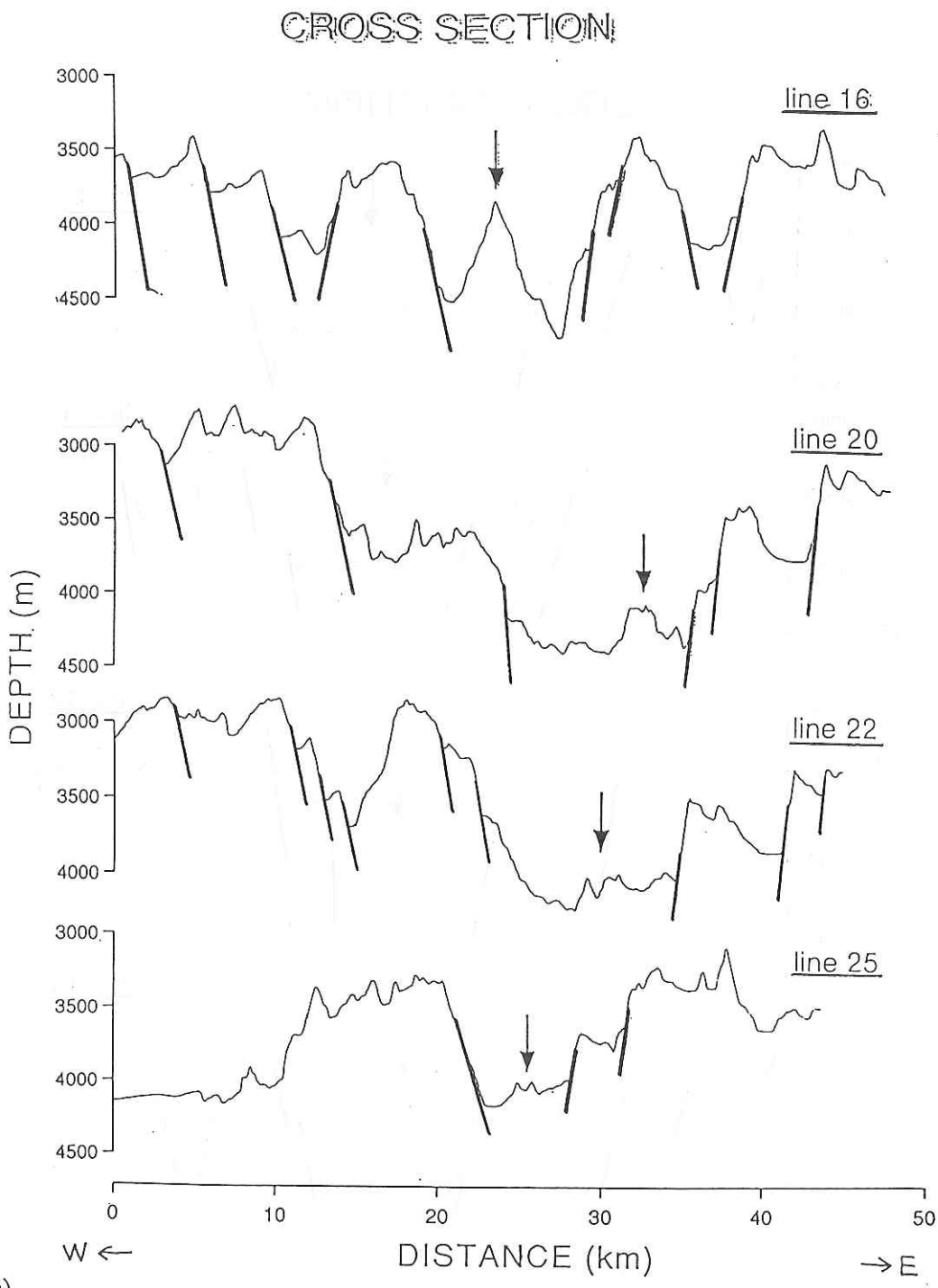

(c)

Fig. 11.7 (a) - (c) Depth profiles along survey lines shown in Fig. 11.6 (Kasahara et al., 1992). Arrows show central axis. Heavy solid lines show faults. Note central highs seen in Lines 6-16.

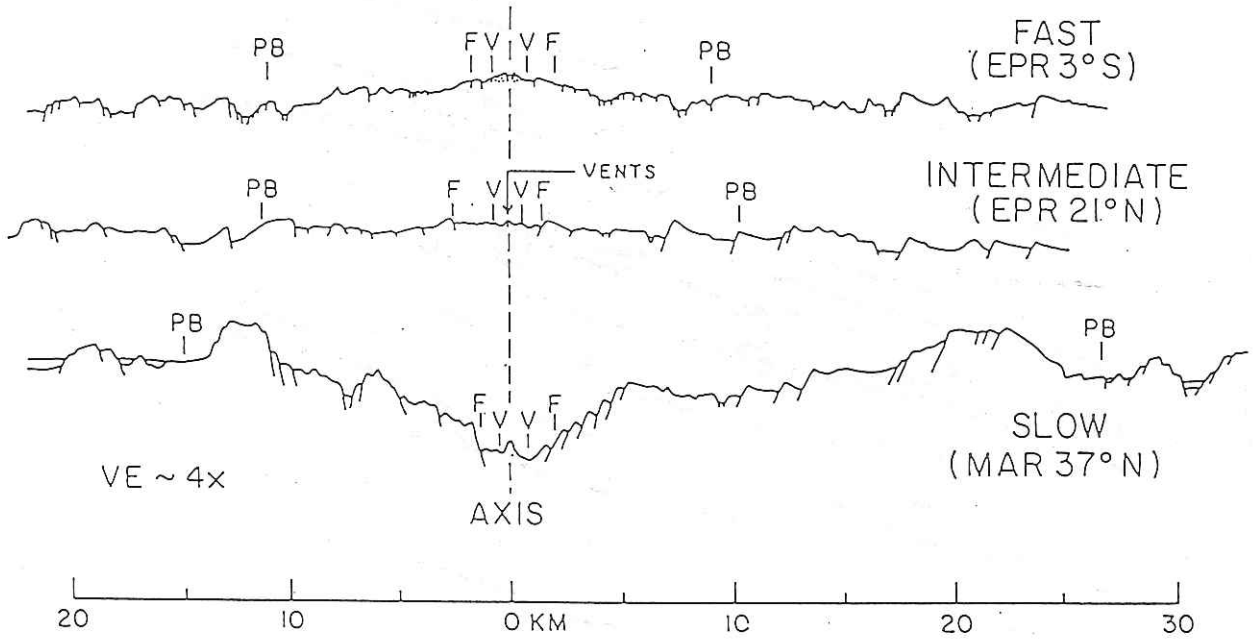

Fig. 11.8 Comparison of cross section traversing three different spreading axes (after Hawkins et al., 1990).

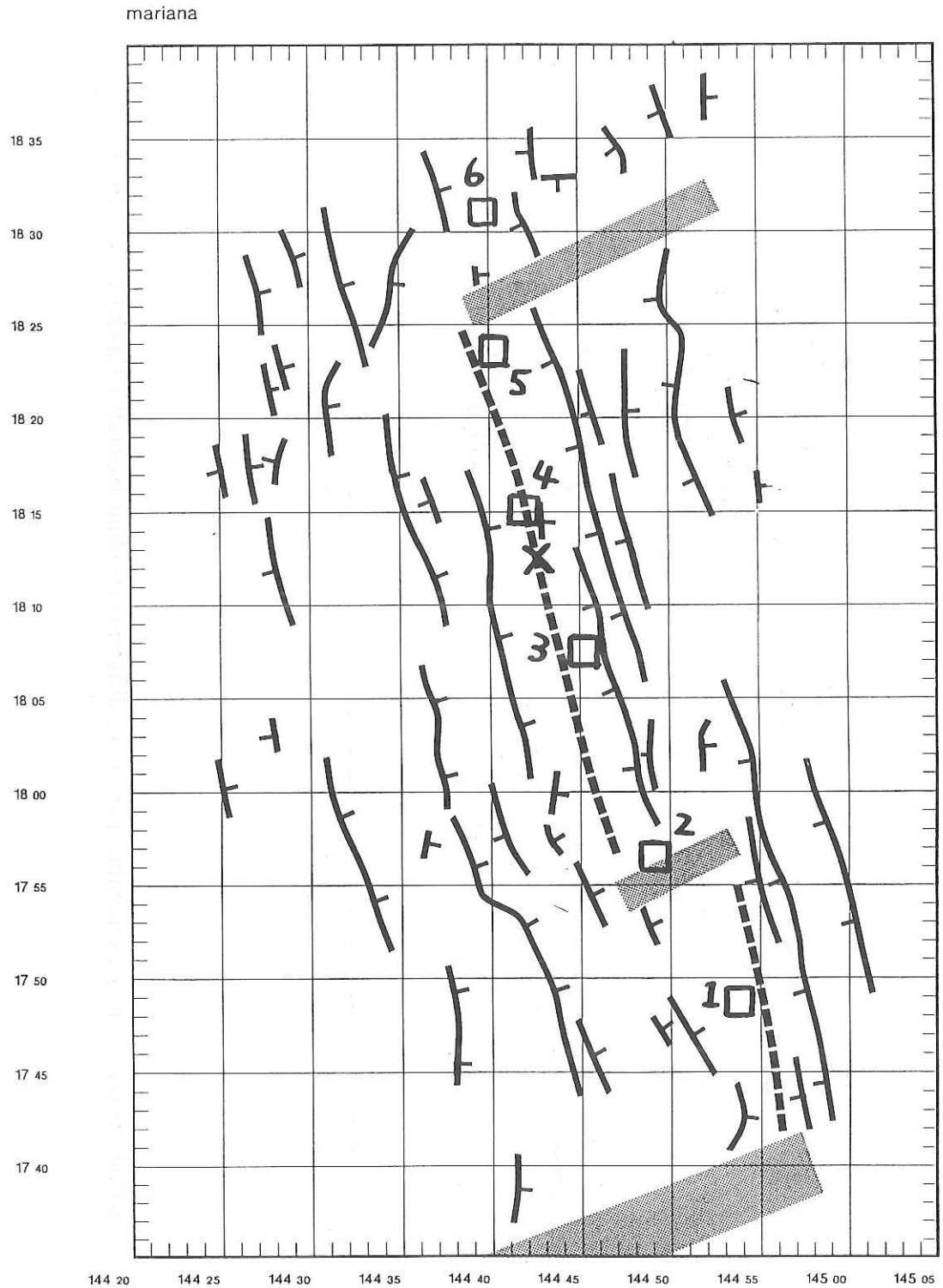

Fig. 11.9 Fault system and location of OBSs(squares).Number shows OBS station number. Cross mark:location of vent found by Alvin dive. ST-3 is close to vent region.

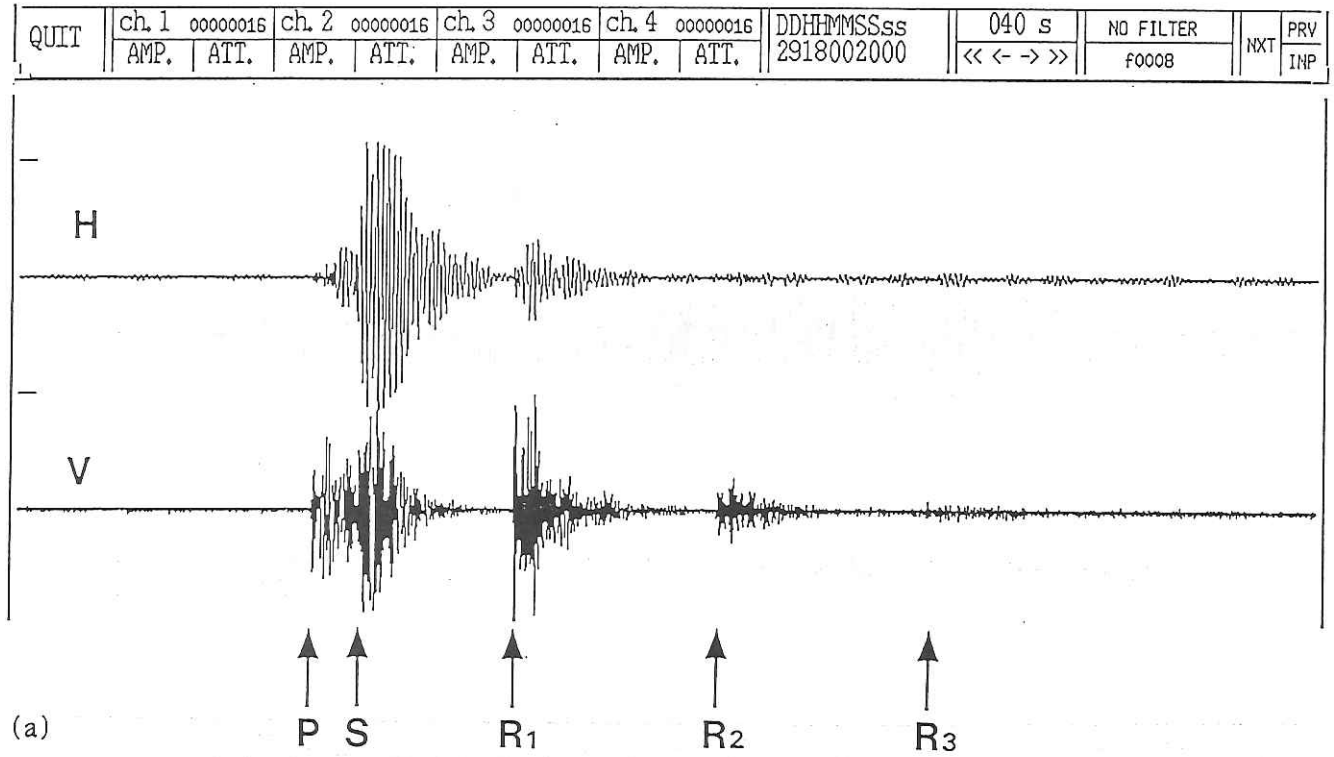

Fig. 11.10 Examples of natural earthquakes observed by digital OBS (MOOBS) at ST-2(a) and at ST-5(b).

ST 5

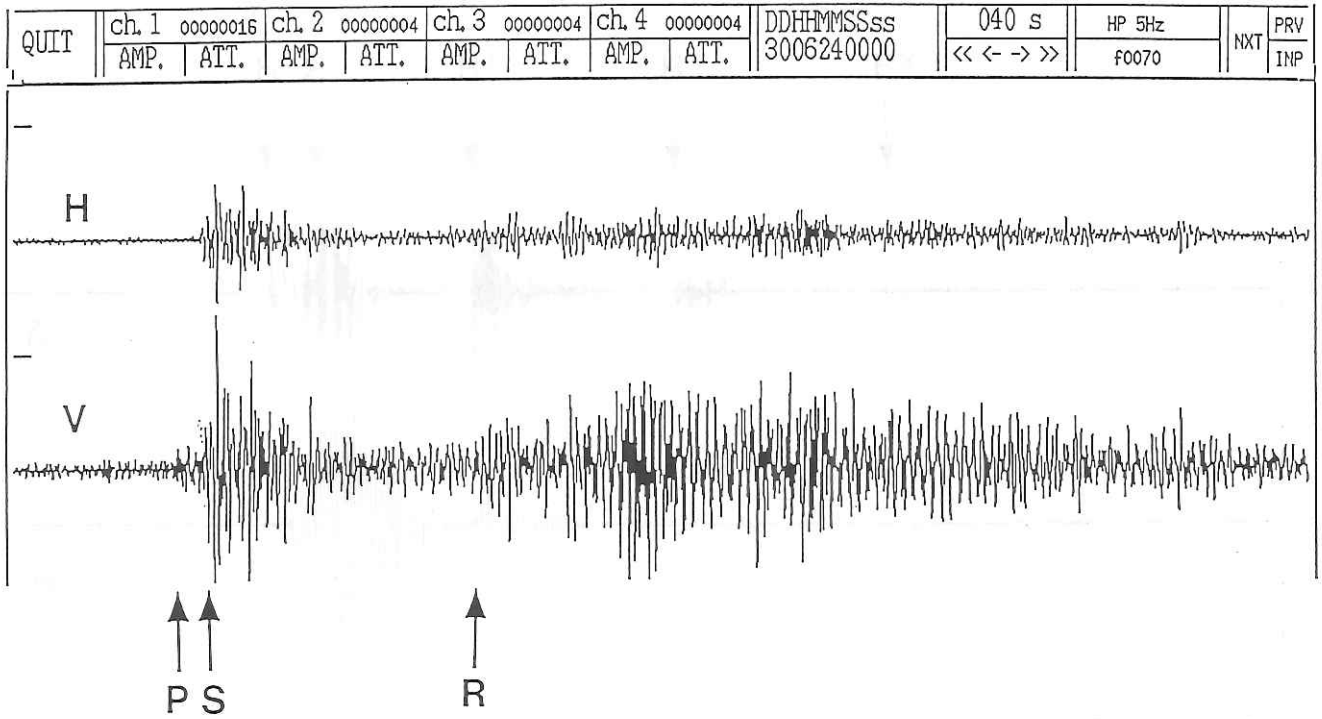
QUIT
ch. 1 00000016
AMP. ATT.
ch. 2 00000004
AMP. ATT.
ch. 3 00000004
AMP. ATT.
ch. 4 00000004
AMP. ATT.
DDHHMMSSss
3006240000
040 s
<< <- -> >>
HP 5Hz
f0070
NXT
PRV
INP
H
V
P S
R

(b)

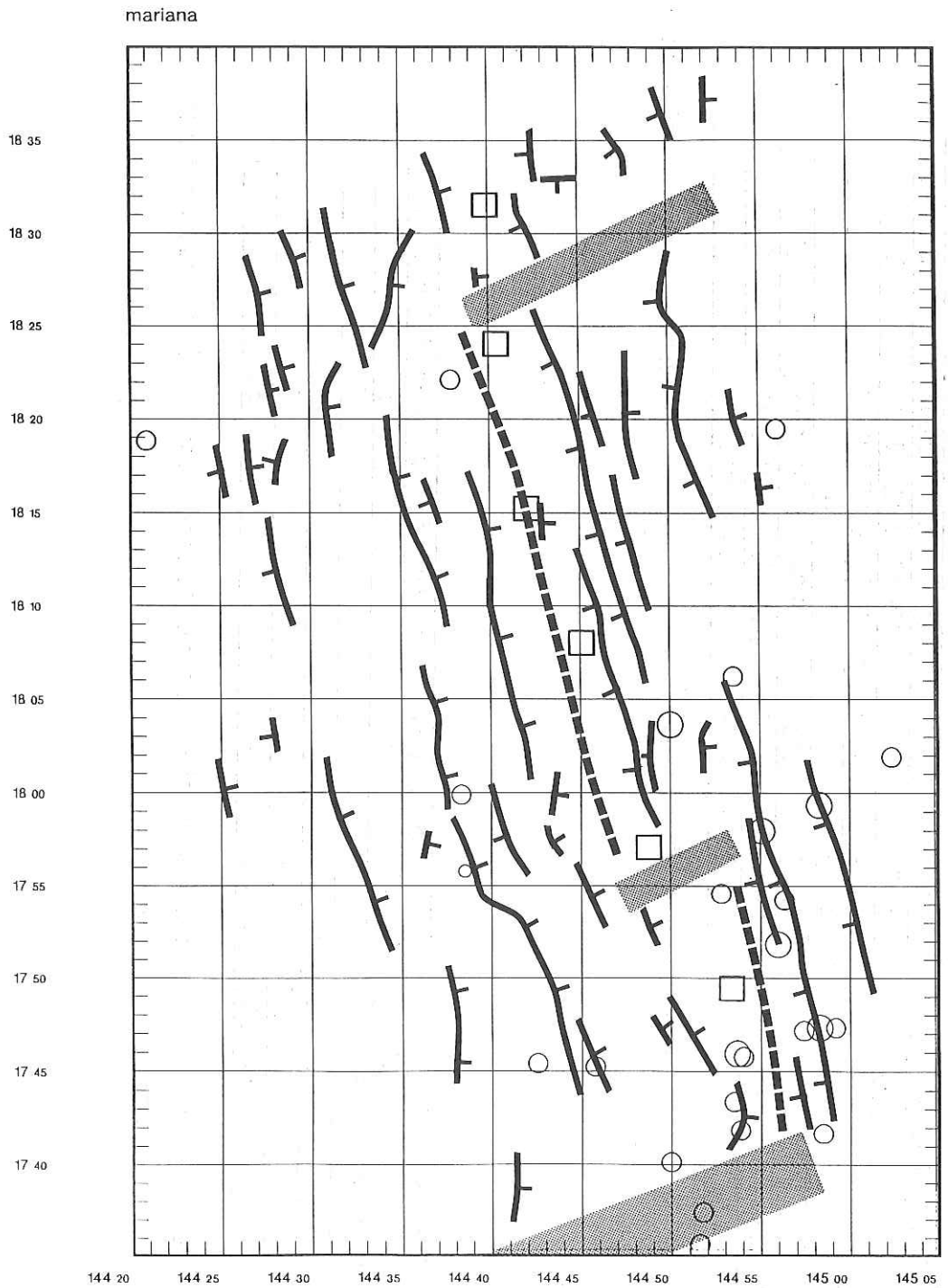

Fig. 11.11 Open circles: ISC hypocenters since 1964. Rectangular: OBS positions. Note hypocenters obtained by world-wide network are concentrated on the north of Pagan Fracture zone in the lowest segment boundary in this figure.

OBS No.	Latitude (N)	Longitude (E)	Depth (m)	Observation Period	No. of Earthquakes
ST-6 (A)	18°31.04	144°39.74	4918	1/29 10:32-1/30 23:41	38
ST-5 (D)	18°23.53	144°40.29	4051	1/29 08:00-1/30 20:52	15
ST-4 (A)	18°15.04	144°41.99	3632	-----	---
ST-3 (A)	18°07.53	144°45.17	3850	1/29 04:21-1/30 16:38	21
ST-2 (D)	17°56.56	144°49.07	4792	1/29 06:00-1/30 13:41	8
ST-1 (A)	17°48.86	144°53.53	4229	1/29 01:48-1/30 10:41	46

Table 11.1 OBS No,latitude, longtitude, depth of OBSs, observation period in 1992 and number of local events obtained by these OBSs.

OBS No.	Recording Format	No. of Earthquakes	No. of Earthquakes (S-P time < 3s)
ST-6	Analog,Continuous	38	30
ST-5	Digital,Trigger	15	7
ST-3	Analog,Continuous	21	4
ST-2	Digital,Trigger	8	7
ST-1	Analog,Continuous	45	32

Table 11.2 OBS No, recording method, total number of events during January 29 and 30,1992 and number of events with shorter S-P times than 3 seconds.

12. Heat Flow Measurements in the Ayu Trough

M. Kido, H. Kinoshita and T. Seno

12.1 Introduction

During leg 2 of KH92-1 cruise, heat flow measurements were made at four sites in the western side of the Ayu Trough. All of the sites were located on the survey line along latitude of 3°30'N, where other geophysical and geological surveys, e.g., sea beam surveys, geomagnetic measurements, seismic reflection and dredging etc. were also conducted.

Realtively low heat flow values, which might be affected by hydrothermal activities, were obtained at most of the sites. But at one of the sites, where there thought to be no hydrothermal activities, we got a value which might constrain the seafloor age.

12.2 Site Locations

In this cruise the heat flow measurements were carried out at four sites which are located at the sedimentary basins between the tilted blocks on western side of the trough axis. All sites were aligned on the latitude of 3°30'N, nearly perpendicular to the trough axis.

The sites are denoted by HF4-HF1 in order of distance increase from the trough axis. At the sites of HF1 and HF3, heat flow was measured twice and they are very close each other. Notation of site names as -A or -B corresponds to these sites. Locations of the sites are illustrated in Fig. 12.1 and listed in Table 12.1.

12.3 Measurements of Heat Flow

The heat flow measuring tool used in this cruise consists of an about 3 m-long spear in which seven thermistors are installed at an interval of 40 cm, and a cylinder-shaped pressure-tight vessel which contains measuring and data recording devices. It weighs about 50 kg in air, and we put some additional weight of 100 kg. The electrical resistance of each thermistor and tilt of the instrument are recorded every 30 seconds in an IC memory (RAM). These data are also telemetered by means of transponder system of 12 kHz acoustic pulses to the ship for real-time monitoring. The bottom thermistor is equipped with a heating wire for in-situ measurement of the thermal conductivity.

Geothermal gradient measurements endure for 8 minutes after penetration. The temperatures are extrapolated up to equiliblium state using T(t)=A/t (T: temperature, A: constant, t: time) appoximation.

12.4 Thermal Conductivity

A heat flow value is defined as the product of thermal gradient and thermal conductivity. Thermal conductivity was determined by in-situ heat pulse measurement.

We used an analytic approximation for the decay of temperature after the pulsive heating. A heating time was 12 seconds which generated 510 Joule total heat. To evaluate the thermal conductivity, measurements were kept for another 8 minute interval after the geothermal gradient measurements. The decay patterns of the temperature of the thermistor after pulsive heating is fit to a series of Bessel functions. A convenient method to determine the thermal conductivity is to plot the temperature data on a graph or "nomogram" (Hyndman et al.,1979) with curved time grid lines whose curvature is considered above function.

In situ heat conductivity was measured at every heat flow site, but the thermistor which was equipped with the heating wire malfunctioned with the exception at the site HF1B. Therefore, the thermal conductivity at the other sites were assumed to be the same as the value at HF1B (variations of the value for each sites might be less than several per cent). The thermal conductivity at HF1B determined graphically by the nomogram was 0.86 [W/km].

12.5 Results

Although, for all heat flow measurements of this cruise, the spear completely penetrated into the sediments, three thermistors out of seven did not work. So the thermal gradients were calculated by only four temperature data. As illustrated in Fig. 12.2, linearity is good enough and two data in the same location (-A and -B) are similar. Relative depth of each sites in Fig. 12.2 were corrected by tilt data. Thermal gradients and heat flow values for each sites calculated using thermal conductivity 0.86 [W/km] at HF1B are listed in Table 12.1. They are 101 [mW/m^2] at the site HF1A, 103 at HF1B, 16 at HF2, 17 at HF3A, 17 at HF3B and 47 at HF4. Sediment thickness estimated by seismic reflection profile at each sites are also listed in Table 12.1.

Fig. 12.3 shows heat flow values and depth profile along line 3°30'N across the Ayu Trough axis obtained by sea beam surveys.

12.6 Discussion

Sites with anomalously low heat flow value are located in the places with thin sediments. At the sites of HF2, HF3 and HF4, sediments are about 100-250 m in thickness. In these areas, hydrothermal activity may occur. The above low values might be caused by this effect.

At the site HF1 which is by 66 km distant from the trough axis, the sediment thickness amounts to 510 m, so that the hydrothermal activity might have ceased and the heat flow values are probably real. The values of 101 and 103 [mW/m^2] are typical with 22 Ma old seafloor. This age is consistent with the age inferred from the basement depth slope obtained by sea beam and seismic reflection profile of this cruise.

If the Ayu Trough is active now, heat flow values near the axis are expected to be highly variable. But at the site HF4 which is very close to the axis, we got only one measurement. So it can not be concluded from the heat flow data whether this trough is actively spreading or not at present.

References

Hyndman, R. D., E. E. Davis and J. A. Wright, The measurement of marine geothermal heat frow by a multipenetration probe with digital acoustic telemetry and insitu thermal conductivity, Marine Geophys. Res., 4, 181-205, 1979.

Parsons, B. and J. G. Sclater, An analysis of the variation of ocean floor bathymetry and heat flow with age, J. Geophys. Res., 82, 803-827, 1977.

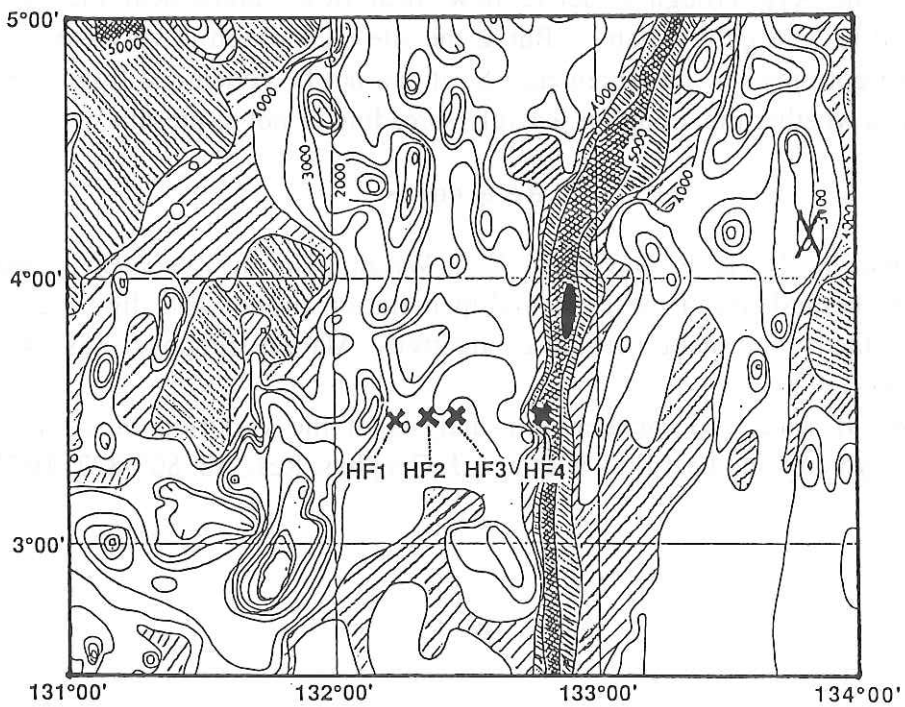

Fig. 12.1 Bathymetry of central part of the Ayu Trough reproduced from the GEBCO map series. The hatched area is deeper than 4000 m. The heat flow sites of this cruise are shown by cross.

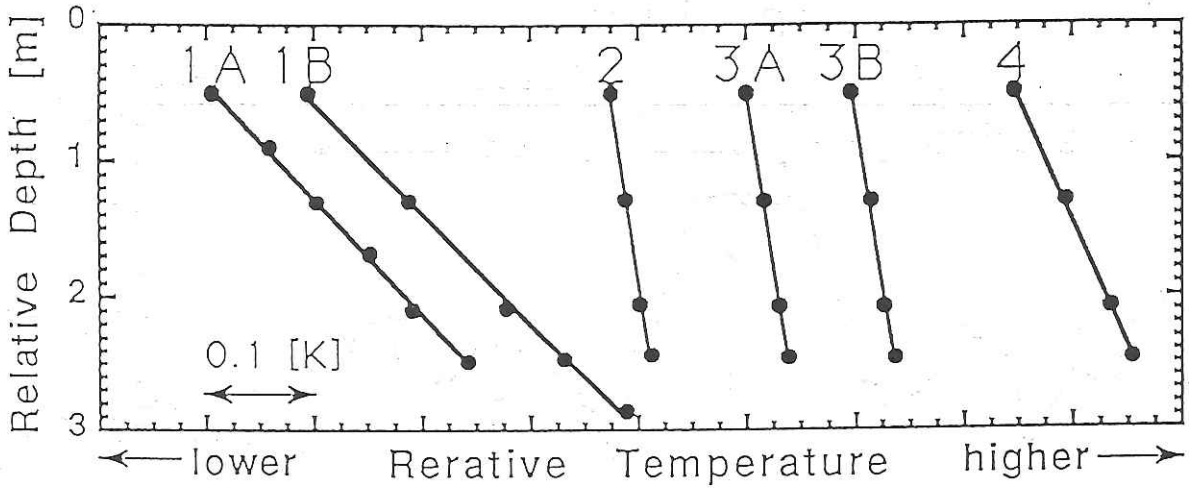

Fig. 12.2 Thermal gradients for each sites. Relative depth are corrected by tilt data. Bottom thermister equipped heater wire is only available at the site HF1B.

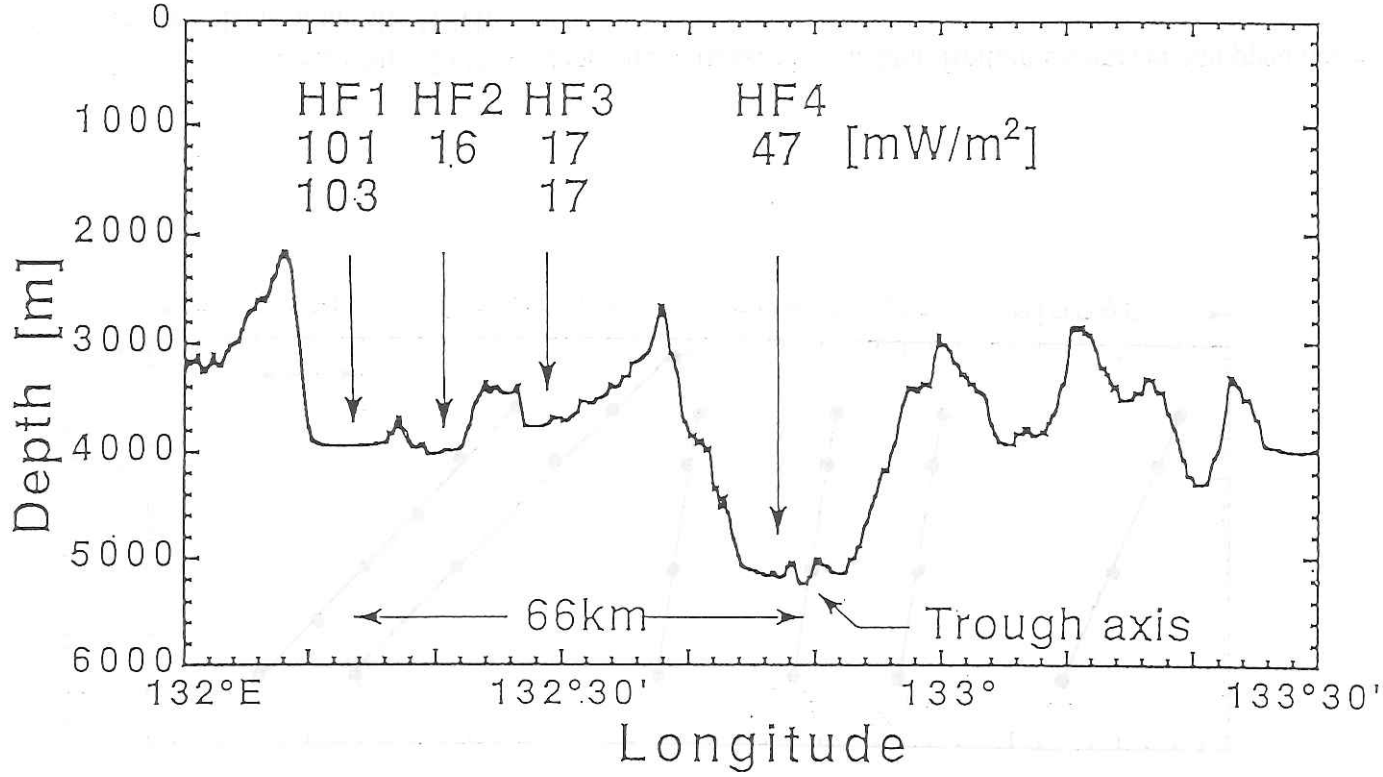

Fig. 12.3 Heat flow data and depth profile along the 3°30'N survey line from sea beam data. Dashed lines denote the basements obtained by seismic reflection data.

Site	Lat.	Lon.	Depth [m]	S [m]	Tilt [deg.]	G [mK/m]	K [W/K/m]	Q [mW/m^2]
HF1A	3°29.7'	132°13.3'	3941	510	8.9	117.9	0.86	101.4
HF1B	3°29.4'	132°13.6'	3941	510	12.0	119.5	0.86	102.8
HF2	3°29.2'	132°20.6'	4039	250	16.1	19.0	0.86	16.3
HF3A	3°29.8'	132°28.7'	3765	200	13.3	19.8	0.86	17.0
HF3B	3°29.8'	132°28.8'	3763	200	12.7	20.2	0.86	17.2
HF4	3°30.3'	132°46.4'	5172	100?	10.7	54.4	0.86	46.8

S: sediment thickness, G: thermal gradient, K: conductivity, Q: heat flow

Table 12.1 Results of heat flow measurement in this cruise. Sediment thickness are obtained by seismic reflection data.Values of thermal conductivity for all sites are assumed to be the same as the value measured in situ at site HF1B

13 Results of Bottom Rock Samples

13.1 Operation Logs of the Dredge Hauls

Date 1992.01.26 Ship Hakuho-maru Cruise KH92-1 Station No.D1
Location Mariana forearc (30km ENE from Conical seamount)
Weather Fine Wind 102°, 8.2m/s Sea caim,small swell
Bottom Topgraphy slope (west wall of graven with triangie shape)
Type of Dredge Nalwalk chain-bag with a bucket Add.Wt. 100kg+chain
Fuse wire 8mm,1m Life wire 10mm,7m Pinger position 700m above
Time lowered 10h 16m Uncorr.Water Depth 5876m
Initial Time on Bottom 11h 54m Uncorr.Water Depth 5879m
Wire Length 5855m Wire Angle 20°
Ship Position Lat. 19°40.57'N Long. 146°57.31'E
Direction of Haul 277° Ship Speed 1.5kt. (till 14h 00m)
Speed Wire-in 0.5m/min (from 14h 00m) Winch No.1
Final Time on Bottom 14h 33m Uncorr. Water Depth 5005m
Wire Length 4500m Wire Angle 25°
Ship Position Lat. 19°42.01'N Long . 149°54.52'E
Time Surfaced 15h 46m
Dredged Materials and comments Soft sediments (red silt, 1g)

Date 1992.02.01 Ship Hakuho-maru Cruise KH92-1 Station No.D2
Location Southern Mareana forearc (220km SW from Guam)
Weather Fine Wind 88° Sea calm (small swell)
Bottom Topgraphy slope of Mariana Trench inner wall
Type of Dredge Nalwalk chaon-bag with a bucket Add.Wt. 300kg+chain
Fuse wire 8mm,1m Life wire 10mm,7m Pinger position 700m abave
Time lowered 13h 11m Uncorr.Water Depth 7502m
Initial Time on Bottom 15h 00m Uncorr.Water Depth 7431m
Wire Length 7630m Wire Angle 20°
Ship Position Lat. 11°14.16'N Long. 143°29.62'E
Direction of Haul 300° Ship Speed 1.2kt. (till 17h 00m)
Speed Wire-in 0.5m/min (from 17h 00m) Winch No.1
Final Time on Bottom 17h 23m Uncorr. Water Depth 6594m
Wire Length 7783m Wire Angle 20°
Ship Position Lat. 11°42.92'N Long . 143°27.64'E
Time Surfaced 19h 04m
Dredged Materials and comments About 500 ophiolitic rocks (ultramafic and mafic rocks) Swell conpensator was out of order

Date 1992.02.17 Ship Hakuho-maru Cruise KH92-1 Station No.D3
Location Ayu Trough (east wall of trough axis)
Weather fine Current Wind 27 °, 5.9m Sea calm,small swell
Bottom Topgraphy steep slope forward crest
Type of Dredge Nalwalk chain-bag with a bucket Add.Wt. 300kg+chain
Fuse wire 8mm,1m Life wire 10mm,7m Pinger position 500m above
Time lowered 02h 01m Uncorr.Water Depth 5203m
Initial Time on Bottom 03h 32m Uncorr.Water Depth 5312m
Wire Length 5340m Wire Angle 20°
Ship Position Lat. 03° 29.05'N Long. 132° 49.28'E
Direction of Haul 50° Ship Speed 1.0kt. (till 5h 00m)
Speed Wire-in 0.5m/min (from 5h 00m) Winch No.1
Final Time on Bottom 05h 31m Uncorr. Water Depth 5062m
Wire Length 5300m Wire Angle 20°
Ship Position Lat. 03° 30.11'N Long . 132° 50.67'E
Time Surfaced 05h 41m
Dredged Materials and comments silt (3000 cc) and siltstone (2 pieces)

Date 1992,02.17 Ship Hakuho-maru Cruise KH92-1 Station No.D4
Location Ayu Trough (40km east from trough axis)
Weather fine Current Wind 27 °, 5.9m Sea calm,small swell
Bottom Topgraphy steep slope forward crest
Type of Dredge Nalwalk chain-bag with a bucket Add.Wt. 300kg+chain
Fuse wire 8mm,1m Life wire 10mm,7m Pinger position 500m above
Time lowered 08h 18m Uncorr.Water Depth 3211m
Initial Time on Bottom 09h 26m Uncorr.Water Depth 2924m
Wire Length 3100m Wire Angle 15°
Ship Position Lat. 03° 30.03'N Long. 133° 10.30'E
Direction of Haul 45° Ship Speed 1.0kt (till 10h 04m)
Speed Wire-in 0.4m/min (from 10h 03m) Winch No.1
Final Time on Bottom 10h 33m Uncorr. Water Depth 2866m
Wire Length 2986m Wire Angle 15°
Ship Position Lat. 03° 30.12'N Long . 133° 10.86'E
Time Surfaced 11h 23m
Dredged Materials and comments pale yellow silts (0.5g),Ship was drifted before bottomed

Date 1992,02.17 Ship Hakuho-maru Cruise KH92-1 Station No.D5
Location Ayu Trough (61km east from trough axis)
Weather fine Current Wind 67°, 5.4m/s Sea calm
Bottom Topgraphy slope
Type of Dredge Nalwalk chain-bag with a bucket Add.Wt. 300kg+chain
Fuse wire 8mm,1m Life wire 16mm,7m Pinger position 500m above
Time lowered 12h 36m Uncorr.Water Depth 4305m
Initial Time on Bottom 13h 36m Uncorr.Water Depth 4086m
Wire Length 4100m Wire Angle 25°
Ship Position Lat. 03° 29.98'N Long. 133° 21.69'E
Direction of Haul 65° Ship Speed 1.0kt (till 15h 30m)
Speed Wire-in 0.5m/min (from 15h 30m) Winch No.1
Final Time on Bottom 16h 49m Uncorr. Water Depth 3601m
Wire Length 3650m Wire Angle 25°
Ship Position Lat. 03° 30.13'N Long. 133° 22.51'E
Time Surfaced 17h 39m
Dredged Materials and comments about 100 pieces (5kg weight) of andesites(?), siltstone, conglomerates and Mn-crusts

Date 1992,02.19 Ship Hakuho-maru Cruise KH92-1 Station No.D6
Location Ayu Trough (---km east from trough axis)
Weather fine Current 110-150fl, 1.4kt Wind 45°, 5.5m/s Sea calm
Bottom Topgraphy slope
Type of Dredge Nalwaik chain-bag with a bucket Add.Wt. 300kg+chain
Fuse wire 10mm,1m Life wire 10mm,7m Pinger position 500m above
Time lowered 05h 53m Uncorr.Water Depth 4956m
Initial Time on Bottom 07h 49m Uncorr.Water Depth 4000m
Wire Length 4700m Wire Angle 20°
Ship Position Lat. 04° 40.17'N Long. 133° 12.69'E
Direction of Haul 120° Ship Speed 1.0kt (till 0.8h 35m)
Speed Wire-in 0.25m/min (from 08h 35m) Winch No.1
Final Time on Bottom 09h 03m Uncorr. Water Depth 3776m
Wire Length m Wire Angle 20°
Ship Position Lat. 04° 39.37'N Long. 133° 14.03'E
Time Surfaced 10h 04m
Dredged Materials and comments about 200 pieces (12kg weight) of pillow basalts(BABB?), Mn-crust and pumices

13.2 Description of Dredged Samples from Mariana Forearc during the First Leg (Tokyo to Guam) of KH92-1 Cruise

T. Ishii, O. Takemura, C. Igarashi, Y. Ohara and J.Segawa

More than five hundred rocks (about 300 kg weight in total) were dredged during the first leg (Tokyo to Guam) of KH92-1 cruise. Two sites (Stations KH92-1-D1 and D2) were selected to investigate the origin and evolution of the Mariana forearc terrain. Precise positions, depth of each station and relevant infomation are given at the operation logs of dredge hauls (11-1. this volume), and position of each station is shown in Figs. 13.2.1 and 13.2.2.

Improved Nalwalk chain-bag dredges with backet (Isii et al.,1985) were used to collect boulder to granule rock samples as well as psammitic to pelitic soft sediments. The Benthos pinger was installed on the winch wire at 700 and 500 meters above the dredge in dredge hauls at D1 and D2, respectively, to confirm the dredge hitting the sea bottom.

Because most of the dredged rock-samples were more or less covered with soft sediments and/or Mn-coating, these rocks were first separated from the sediments by washing. They were cut by a diamond saw into two or more pieces for observation and description of visual features inside the samples. Washed samples were classified into several groups according to their lithologic characteristics. After numbering the samples (in the order of size), diameter (L, M and S), roundness, weight and thickness of Mn-coating, lithology and remarks of each samples were observed on board and described in Table 13.2.1, where roundness is expressed after the Powers' system (Powers, 1953), that is, 0.10 = very angular, 0.20 = angular, 0.30 = sub-angular, 0.40 = sub-rounded, 0.60 = rounded and 0.85 = well-rounded. Some thin sections of rock were made for microscopic observations.

Graven in the Outer Mariana Forearc

Detailed bathymetric maps have enabled one to recognize several topograhic depressions in the forearc regions along the Mariana Trenches within 40 to 100 km of the axis. Dredge Station KH92-1-D1 was selected to investigate geological section of forearc terrain in the western lower slope of huge graven with about 6000 m bottom depth (Fig. 13.2.1) located about 50 km west of the trench axis (19°40'N). This dredge haul was, however, unfortunately not successful.

Ophiolitic Rocks from the Mariana Trench Inner Slope

Many topographic highs are recognized along the Izu-Ogasawara-Mariana forearc region from the detailed bathymetric charts. Ophiolitic rocks were dredged from some of these seamounts by several investigaters (Bloomer 1983, Ishii 1985, Sakai et al.,1990), who concluded that these seamounts have originated from serpentinite diapirs derived from the upper parts of the mantle wedge.

Ophiolitic rocks were also reported from lower part of trench inner slope along the Southern Mariana Trench (Bloomer and Hawkins, 1983) and they assumed that the origin of these ophiolitic rocks are the same as those from forearc seamount. On the other hand, Ishii et al. (1992) suggested the different origins for these ophiolites, on the basis of the petrological difference of peridotite between them. The assemblages of peridotites from the serpentinite seamounts and those from the lower part of the Southern Mariana Trench inner slope are harzburgite + dunite and harzburgite + dunite + lherzolite, respectively.

Dredge Station KH92-1-D2 was selected for the petrological studies and to investigate the origin of peridotites located in the lower part of the Southern Mariana Trench inner slope (Fig. 13.2.2). More than 500 ophiolitic rocks (with about 300 kg in total weight) including serpentinized peridotites (harzburgite, dunite), pyroxinite, metamorphosed basic rocks (gabbroes, dolerites and basalts) and there derivatives were collected by dredge haul at the station (Fig.13.2.3).

Generally speaking, olivine crystals commonly have very few cleavages. On the other hand, cleavable olivines (= cleavage-rich olivines) are very commonly observed among the harzburgites as well as dunites in up to 50 % of dredged samples from this site, as shown in Table 13.2.1. It is assumed that these cleavable olivines were induced by reheating the mantle peridotites by multiple igneous activities. The investigations on the origin of the cleavable olivine are now under progress. As far as megascopic observation, no lherzolite has been identified, so accurate microscopic observation, no lherzolite has been identified,so accurate microscopic obswrvations on many rock-thin-sections of peridotite are required to confirm existance of lherzolite.

Dredged metamorphic rocks from the station are described in more detail by Takemura et al. in this volume (Chapter 13.3).

References

Bloomer, S.H.:Distribution and origin of igneous rocks from the landward slopes of the Mariana Trench: Implications for its structure and evolution. J. Geophys. Res., 88, 7411-7428, 1983.

Bloomer, S.H. and Hawkins, J.W.:Gabbroic and ultramafic rocks from the Mariana Trench: An island arc ophiolite, in Hayes, D.E., ed., The tectonic and geologic evolution of Southeast Asian seas and islands, Part II: Washington D.C., American Geophigical Union, p.294-317.

Ishii, T.: Dredged samples from the Ogasawara fore-arc seamount or "Ogasawara Paleoland"-"fore-arc ophiolite". In Formation of Active Ocean Margins (eds. Nasu, N., Kushiro. I., et al.), Terr Scientific Publishing Company, Tokyo, 307- 342, 1985.

Ishii, T., Kobayashi, K., Shibata, T., Naka, J., Jonson, K., Ikehara, K., Iguchi, M., Konishi, K., Wakita, H., Zang, F., Nakamura, Y. and Kayane, H.: Description of samples from Ogasawara fore-arc, Ogasawara Plateau and Mariana Trough, during KH84-1 Cruise. In Preliminary Report of the Hakuho-Maru Cruise KH84-1 (Ocean Reserch Institute, University of Tokyo), 105-165, 1985.

Ishii, T., Robinson, P. T., Maekawa, H., and Fiske R.: Petrological studies of peridotites from diapiric serpentinite seamounts in the Izu-Ogasawara-Mariana forearc, Leg 125. Proceedings of the Ocean Drilling Program, Scientific Results, 125; Ocean Drilling Progrm, College Staion, TX, (in press).

Johnson, L, E., Fryer, P., Taylor, B., Silk, M., Jones, D, L., Sliter, W, V., Itaya, T., and Ishii, T.: New evidence for crustal accretion in the outer Mariana forearc: Cretaceous radiolarian cherts and mid-ocean ridge basalt-like lavas. Geology, 19, 811-814, 1991.

Sakai, R., Kusakabe, M., Noto, M., and Ishii, T.: Origin of waters responsible for serpentinization of the Izu-Ogasawara-Mariana forearc seamounts in view of hydrogen and oxigen isotope. Earth Planet. Sci. Lett., 100, 291-303,1990.

Powers, M.C.: A new roundness scale for sedimentary particles.J. Sed. Pet., 23, 117-119, 1953.

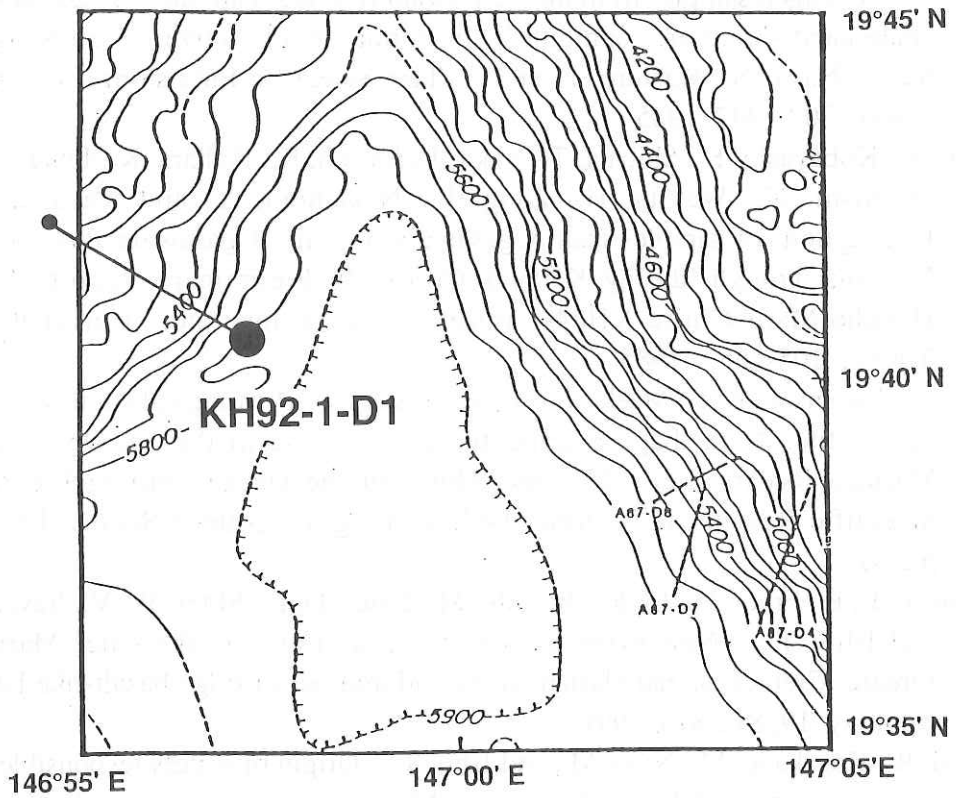

Fig. 13-2-1 Location of dredge hauls (Station KH92-1-D1) in the Mariana forearc graven (Johnson et al., 1991) during KH92-1. Large and small circles indicate ship positions at the initial and final time on bottom of dredge, respectivly.

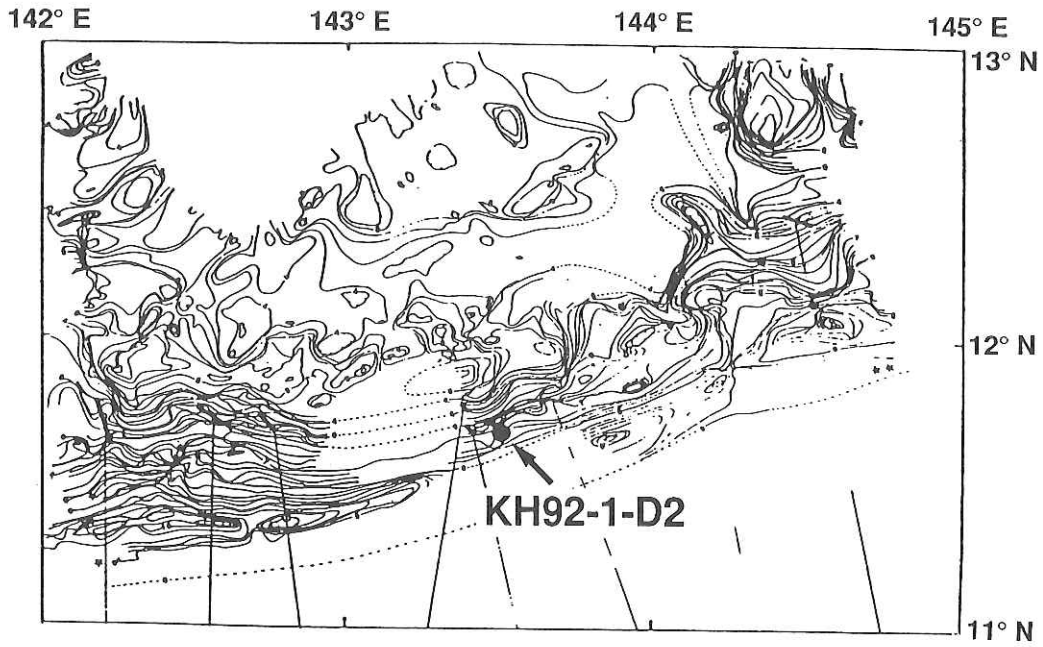

Fig. 13-2-2 Location of dredge hauls (Station KH92-1-D2) in the lower part of the Southern Mariana Trench inner slope (Bloomer and Hawkins, 1983) during KH92-1.

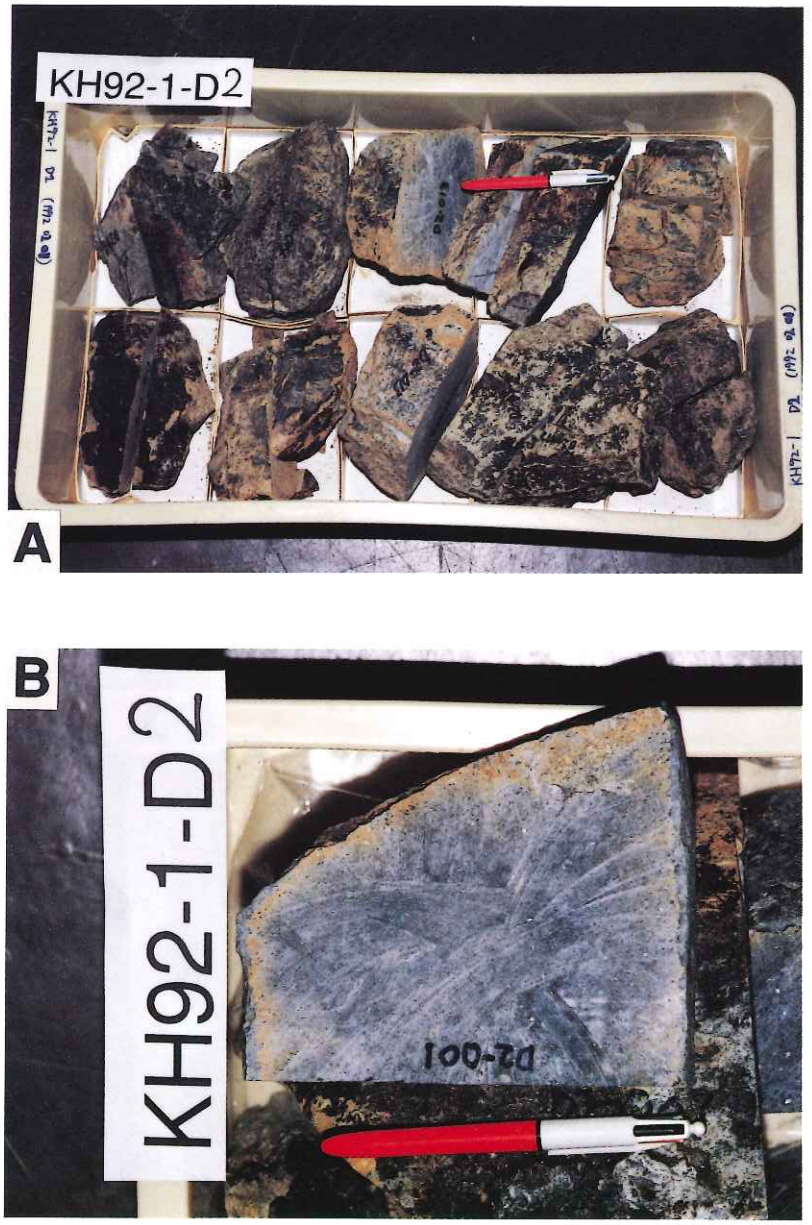

Fig. 13.2.3 Photographs of dredged rocks at Station KH92-1-D2. (A) Thinly Mncoated boulders of serpentinized harzburgite and dunite with very-angular (0.1 in Powers' number) to sub-angular (0.3) shape. (B) Typical example of serpentinized harzburgite with abundant cleavable olivines (KH92-1-D2-001).

Table 13-2-1 List of materials dredged during the first leg (Tkyo to Guam) of KH92-1 cruise.

Sample No.	Diameter (mm) L	M	S	Round-ness	Wt. (g)	Mn-coating (mm)	Lithology & Remarks
D2-001	410	330	165	0.1	32000	f	Harzburgite (with clevable olivine)
002	440	230	150	0.1	24000	f	Dunite
003	230	150	140	0.3	9450	p	Harzburgite
004	360	160	140	0.2	9000	p	"
005	190	170	140	0.35	7050	0.5	"
006	170	150	130	0.3	4200	p0.5	"
007	200	130	120	0.35	4700	pf	Harzburgite (with clevable olivine)
008	200	130	120	0.15	3650	pf	" "
009	180	110	110	0.3	2300	pf	Dunite
010	150	130	110	0.35	2500	pf	Harzburgite
011	210	110	110	0.25	3600	pf	" (with clevable olivine)
012	220	170	100	0.2	7400	pf	" "
013	180	170	120	0.45	6900	pf	" "
014	190	130	95	0.5	2900	pf	Dunite (with clevable olivine)
015	170	140	80	0.15	2070	pf	"
016	180	150	80	0.15	2450	0.5	Harzburgite
017	170	110	52	0.4	1800	0.5	"
018	180	165	90	0.3	3530	pf	Dunite (with clevable olivine)
019	110	78	75	0.3	980	pf	Metabasalt
020	130	90	80	0.45	1290	pf	Dunite (with clevable olivine)
021	190	115	65	0.5	3600	pf	Harzburgite "
022	110	110	80	0.7	1125	pf	Dunite "
023	190	85	85	0.4	2200	0.5pf	Harzburgite "
024	170	135	65	0.35	1650	0.5	"
025	235	85	75	0.15	1770	pf	Dunite (with clevable olivine)
026	120	90	38	0.25	510	f	Harzburgite "
027	110	75	53	0.2	535	-	Dunite
028	120	90	65	0.35	750	f	Harzburgite (with clevable olivine)
029	100	80	65	0.35	480	-	" "
030	180	105	60	0.2	515	pf	Harzburgite
031	130	90	50	0.4	705	pf	Dunite
032	125	90	85	0.35	1380	pf	Harzburgite (with clevable olivine)
033	145	110	50	0.35	450	-	" "
034	140	65	65	0.2	880	f	Dunite
035	115	110	80	0.3	1100	pf	"
036	90	70	70	0.2	690	-	Harzburgite
037	110	90	50	0.25	650	pf	Dunite
038	120	105	70	0.4	815	f	"
039	140	130	80	0.1	1285	-	"
040	75	65	60	0.1	1375	f	"
041	140	140	85	0.4	405	pf	Harzburgite (with clevable olivine)
042	125	110	60	0.2	1000	f	" "
043	110	80	35	0.2	465	-	Harzburgite
044	95	80	65	0.35	610	pf	" (with clevable olivine)
045	90	95	80	0.2	730	-	" "
046	115	90	70	0.3	745	pf	Dunite "

Sample No.	Diameter (mm) L	M	S	Round-ness	Wt. (g)	Mn-coating (mm)	Lithology & Remarks
D2-047	65	57	55	0.3	385	-	Harzburgite (with clevable olivine)
048	95	65	60	0.3	480	f	" "
049	150	65	50	0.1	660	pf	" "
050	140	125	75	0.3	1520	-	" "
051	145	100	80	0.4	1930	-	"
052	130	130	80	0.2	1830	pf	" (with clevable olivine)
053	175	130	60	0.4	1900	-	" "
054	170	120	90	0.3	2370	pf	" "
055	155	100	100	0.15	2000	f	" "
056	140	80	55	0.15	875	1	" "
057	150	85	70	0.2	835	pf	"
058	185	90	50	0.1	1360	1	" (with clevable olivine)
059	110	85	65	0.35	735	-	" "
060	70	60	35	0.1	180	0.5	Serpentinite
061	50	45	45	0.3	215	pf	Pyroxenite
062	100	85	70	0.3	780	0.2p	Dunite
063	100	60	35	0.1	450	0.1	"
064	120	90	50	0.1	605	f	Dunite (with clevable olivine)
065	160	90	80	0.3	1125	0.2	Harzburgite
066	150	110	60	0.2	1090	3	" (with clevable olivine)
067	130	80	55	0.25	805	f	" "
068	110	70	65	0.1	520	pf	Dunite
069	90	75	47	0.3	575	-	Harzburgite
070	135	50	70	0.3	665	3~4	"
071	65	55	40	0.2	210	p4	" (with clevable olivine)
072	155	90	55	0.05	580	-	" "
073	95	70	55	0.2	480	0.05	Dunite "
074	85	60	40	0.3	200	f	"
075	75	60	55	0.2	310	-	Harzburgite
076	80	80	40	0.15	430	1	Dunite
077	115	110	75	0.05	725	-	"
078	95	90	65	0.4	820	pf	"
079	140	85	60	0.2	860	pf	Harzburgite
080	130	75	60	0.2	810	f	"
081	140	110	60	0.3	290	-	"
082	140	130	60	0.4	1350	pf	"
083	90	60	55	0.2	1310	-	"
084	130	90	80	0.1	1405	1	Dunite
085	120	53	35	0.15	250	0.5	Harzburgite (with clevable olivine)
086	55	50	40	0.4	235	0.5	"
087	90	65	42	0.2	360	p2	" (with clevable olivine)
088	90	60	42	0.3	475	-	Dunite
089	120	80	70	0.1	1400	p3	Harzburgite (with clevable olivine)
090	70	53	40	0.3	290	pf	Dunite "
091	75	75	35	0.4	550	pf	" "
092	75	55	30	0.3	150	-	"

Sample No.	Diameter (mm) L	M	S	Round-ness	Wt. (g)	Mn-coating (mm)	Lithology & Remarks
D2-093	80	60	35	0.6	230	p1	Harzburgite
094	50	45	40	0.3	175	p1	" (with clevable olivine)
095	100	60	55	0.2	395	pf	Dunite
096	80	50	45	0.1	315	pf	Harzburgite (with clevable olivine)
097	85	70	50	0.2	375	pf	Dunite
098	111	95	40	0.3	455	pf	"
099	90	55	40	0.1	200	pf	Harzburgite (with clevable olivine)
100	80	50	50	0.2	212	pf	"
101	150	115	50	0.2	1170	1	Pyroxenite
102	111	65	55	0.4	600	0.5	Harzburgite (with clevable olivine)
103	80	75	60	0.3	600	0.3	Dunite
104	90	90	45	0.5	410	pf	"
105	120	90	60	0.6	1700	pf	Harzburgite (with clevable olivine)
106	120	75	65	0.3	875	1	" "
107	100	78	34	0.3	250	f	Dunite "
108	750	65	55	0.35	365	f	Harzburgite "
109	90	60	40	0.1	200	1	" "
110	85	60	50	0.4	310	p0.2	" "
111	85	65	50	0.15	290	pf	Harzburgite
112	110	80	50	0.2	365	pf	Dunite
113	110	70	65	0.2	800	f	Harzburgite
114	100	75	35	0.3	300	f	" (with clevable olivine)
115	140	70	50	0.2	710	0.5	Pyroxenite
116	70	55	23	0.3	105	pf	Dunite
117	50	50	40	0.4	175	pf	Harzburgite (with clevable olivine)
118	115	80	70	0.2	710	pf	" "
119	110	85	35	0.35	350	0.5	Dunite
120	90	60	40	0.25	260	-	"
121	75	45	30	0.3	160	1	Harzburgite
122	95	70	45	0.4	295	-	"
123	75	50	50	0.35	230	1	Harzburgite (with clevable olivine)
124	90	70	55	0.35	360	-	Dunite
125	120	90	23	0.1	270	pf	"
126	105	80	30	0.5	285	pf	Harzburgite
127	60	40	40	0.2	70	pf	Dunite
128	105	50	30	0.1	190	pf	" (with clevable olivine)
129	90	80	35	0.3	285	pf	"
130	90	55	30	0.3	250	pf	" (with clevable olivine)
131	85	57	50	0.2	270	1	Harzburgite
132	90	48	35	0.3	250	pf	" (with clevable olivine)
133	85	55	45	0.3	260	-	"
134	100	60	45	0.25	340	pf	"
135	90	60	35	0.3	2290	0.2	Dunite
136	110	70	40	0.3	505	-	Harzburgite
137	80	80	40	0.4	310	pf	"
138	85	65	45	0.3	340	pf	"

Sample No.	Diameter (mm) L	M	S	Round-ness	Wt. (g)	Mn-coating (mm)	Lithology & Remarks
D2-139	70	65	40	0.4	205	f	Dunite
143	85	60	55	0.4	470	-	Dunite (with clevable olivine)
144	70	65	35	0.4	270	pf	" "
145	90	70	50	0.25	320	0.4	Harzburgite
146	90	50	30	0.3	230	pf	Dunite
147	90	70	60	0.3	505	pf	Harzburgite
148	105	40	35	0.1	265	pf	" (with clevable olivine)
149	125	80	35	0.3	205	pf	" "
150	120	65	50	0.1	185	pf	"
151	80	75	40	0.4	335	pf	" (with clevable olivine)
152	70	50	35	0.3	195	pf	" "
153	95	60	55	0.1	420	pf	Dunite "
154	80	65	35	0.4	255	-	" "
155	120	90	40	0.1	675	pf	Harzburgite "
156	120	60	45	0.1	600	-	" "
157	85	65	23	0.2	260	-	"
158	90	70	45	0.3	330	f	"
159	85	70	50	0.4	330	pf	"
160	90	50	35	0.4	220	0.3	Dunite
161	80	50	35	0.7	165	p0.3	"
162	85	60	40	0.1	255	-	Harzburgite (with clevable olivine)
163	95	60	55	0.4	315	1	Dunite
164	90	90	30	0.3	265	pf	Harzburgite (with clevable olivine)
165	92	75	35	0.15	315	pf	Dunite "
166	90	50	30	0.3	200	pf	" "
167	90	80	35	0.1	310	pf	" "
168	90	60	40	0.1	305	pf	Harzburgite "
169	85	70	45	0.35	300	pf	Dunite
170	70	60	45	0.1	205	pf	"
171	75	50	35	0.1	210	pf	Harzburgite (with clevable olivine)
172	90	60	35	0.15	265	pf	" "
173	90	85	40	0.2	410	pf	" "
174	85	50	30	0.3	180	pf	" "
175	85	60	30	0.1	170	-	Harzburgite
176	75	55	35	0.3	150	-	"
177	70	60	35	0.25	170	f	Dunite (with clevable olivine)
178	70	50	45	0.7	150	pf	Harzburgite "
179	70	45	40	0.2	170	p1	"
180	65	50	35	0.25	145	pf	"
181	80	55	40	0.25	210	pf	Dunite (with clevable olivine)
182	70	50	42	0.4	230	pf	" "
183	80	55	40	0.4	210	p1	Harzburgite "
184	80	60	30	0.35	195	pf	"
185	80	60	45	0.35	255	pf	"
186	65	45	40	0.5	185	-	Dunite

Sample No.	Diameter (mm) L	M	S	Round-ness	Wt. (g)	Mn-coating (mm)	Lithology & Remarks
D2-187	80	60	30	0.2	190	pf	Harzburgite (with clevable olivine)
188	80	50	30	0.1	165	pf	" "
189	65	55	43	0.8	165	-	Dunite
190	95	62	40	0.1	300	pf	"
191	75	55	40	0.6	200	1	Harzburgite (with clevable olivine)
192	85	60	40	0.1	190	pf	Dunite "
193	50	43	43	0.3	145	-	"
194	65	40	40	0.2	120	pf	"
195	70	60	35	0.3	145	pf	Harzburgite
196	70	43	35	0.3	125	0.6	Dunite
197	65	50	30	0.6	120	pf	" (with clevable olivine)
198	80	60	30	0.3	140	-	"
199	70	48	35	0.2	145	-	" (with clevable olivine)
200	50	35	30	0.15	95	pf	" "
201	80	45	32	0.1	115	f	Harzburgite
202	70	40	27	0.4	100	-	" (with clevable olivine)
203	60	55	30	0.4	100	pf	Dunite
204	60	50	30	0.3	140	pf	Harzburgite (with clevable olivine)
205	70	50	40	0.1	120	pf	Dunite
206	60	50	40	0.1	145	-	"
207	80	45	30	0.3	175	0.4	Harzburgite
208	55	43	35	0.2	145	pf	"
209	75	45	40	0.1	120	pf	" (with clevable olivine)
210	70	45	40	0.25	100	-	Dunite "
211	60	40	35	0.1	110	pf	"
212	70	40	37	0.1	120	pf	Harzburgite
213	80	50	32	0.1	100	-	Dunite
214	80	50	30	0.1	100	-	Harzburgite (with clevable olivine)
215	70	40	40	0.1	120	0.3	"
216	55	50	22	0.3	100	p0.3	Dunite
217	85	75	23	0.15	135	p0.5	Harzburgite (with clevable olivine)
218	75	50	40	0.1	115	p0.5	"
219	80	65	25	0.1	115	0.5	Dunite
220	90	40	23	0.1	100	-	Harzburgite (with clevable olivine)
221	75	45	30	0.1	105	-	Dunite "
222	50	45	35	0.3	105	pf	Harzburgite
223	90	50	40	0.4	170	f	"
224	85	50	40	0.3	185	-	Dunite
225	75	45	30	0.15	120	pf	"
226	70	45	35	0.3	100	-	Harzburgite (with clevable olivine)
227	80	55	40	0.1	170	pf	"
228	75	35	27	0.3	100	pf	Dunite (with clevable olivine)
229	60	55	30	0.4	125	-	Harzburgite "
230	60	50	35	0.3	115	f	Dunite "
231	65	45	27	0.3	100	pf	Harzburgite "
232	60	55	35	0.3	130	p0.3	" "

Sample No.	Diameter (mm) L	M	S	Round-ness	Wt. (g)	Mn-coating (mm)	Lithology & Remarks
D2-233	60	50	42	0.5	150	pf	Harzburgite
234	77	42	25	0.1	95	f	"
235	60	60	30	0.1	115	pf	Dunite
236	90	60	30	0.3	105	-	Harzburgite (with clevable olivine)
237	60	40	35	0.5	85	pf	"
238	60	40	35	0.4	165	pf	" (with clevable olivine)
239	50	45	30	0.2	75	-	Dunite "
240	70	45	45	0.3	165	pf	" "
241	55	55	30	0.3	110	pf	Harzburgite
242	60	45	35	0.2	115	-	"
243	60	34	34	0.1	110	pf	"
244	60	50	35	0.1	75	pf	Dunite
245	60	40	25	0.2	100	0.5	Harzburgite
246	55	38	33	0.1	105	1	"
247	55	50	36	0.4	120	pf	Harzburgite (with clevable olivine)
248	65	30	27	0.4	90	-	"
249	60	60	40	0.3	105	pf	"
250	67	40	30	0.1	100	1	" (with clevable olivine)
251	65	40	40	0.3	110	f	"
252	73	60	20	0.2	120	pf	" (with clevable olivine)
253	60	50	35	0.35	120	pf	Dunite
254	65	45	30	0.3	125	-	Harzburgite (with clevable olivine)
255	65	50	30	0.3	120	pf	" "
256	63	52	35	0.1	100	pf	" "
257	80	45	40	0.2	150	pf	Dunite "
258	65	45	30	0.1	90	pf	Harzburgite
259	50	40	40	0.15	95	f	" (with clevable olivine)
260	60	40	25	0.3	90	pf	Dunite
261	50	45	40	0.4	95	1	" (with clevable olivine)
262	65	40	30	0.1	95	f	Harzburgite "
263	80	30	30	0.1	105	pf	"
264	60	50	30	0.5	85	-	"
265	80	40	20	0.1	70	pf	" (with clevable olivine)
266	70	50	23	0.3	70	pf	" "
267	60	35	30	0.1	75	pf	"
268	75	40	30	0.1	70	pf	Dunite (with clevable olivine)
269	50	50	40	0.4	100	-	"
270	75	40	32	0.1	120	pf	Harzburgite (with clevable olivine)
271	70	50	20	0.3	70	1	Dunite
272	65	40	30	0.1	100	pf	Harzburgite
273	55	50	20	0.5	60	-	Dunite
274	55	50	40	0.3	80	0.3	Harzburgite (with clevable olivine)
275	50	35	30	0.2	90	f	" "
276	50	30	30	0.5	65	f	"
277	60	40	30	0.3	95	f	" (with clevable olivine)
278	65	50	30	0.5	105	pf	" "

Sample No.	Diameter (mm) L	M	S	Round-ness	Wt. (g)	Mn-coating (mm)	Lithology & Remarks
D2-279	60	40	25	0.35	90	pf	Harzburgite (with clevable olivine)
280	40	30	20	0.3	60	0.5	Dunite
281	40	30	25	0.3	40	0.3	Harzburgite
282	70	50	20	0.3	70	-	" (with clevable olivine)
283	75	35	25	0.35	70	pf	"
284	55	35	25	0.25	45	pf	"
285	55	45	30	0.25	85	-	" (with clevable olivine)
286	55	40	30	0.7	70	pf	"
287	60	50	35	0.4	95	f	Dunite (with clevable olivine)
288	75	35	20	0.1	60	pf	Harzburgite
289	55	25	20	0.2	50	-	"
290	65	55	30	0.25	95	pf	"
291	50	35	30	0.1	60	-	"
292	50	50	30	0.15	55	-	"
293	55	45	21	0.2	55	pf	Dunite
294	65	55	30	0.3	95	pf	"
295	50	45	30	0.1	60	p1	Harzburgite
296	52	35	30	0.25	50	pf	"
297	60	30	25	0.1	50	-	"
298	45	35	30	0.4	50	-	"
299	70	40	20	0.1	80	p0.5	Dunite
300	60	45	25	0.1	65	p0.3	Harzburgite
301	52	32	17	0.2	45	pf	Dunite
302	50	40	30	0.1	50	pf	Harzburgite (with clevable olivine)
303	55	40	35	0.4	105	-	" "
304	53	33	15	0.15	40	-	"
305	60	40	40	0.15	75	-	" (with clevable olivine)
306	42	40	25	0.4	55	pf	"
307	50	25	30	0.25	70	pf	Dunite (with clevable olivine)
308	65	30	25	0.1	50	pf	"
309	50	40	30	0.3	60	-	Harzburgite (with clevable olivine)
310	40	30	30	0.6	40	-	" "
311	45	45	26	0.15	40	-	"
312	40	35	33	0.5	55	-	"
313	52	37	20	0.1	40	pf	"
314	40	32	25	0.15	55	pf	"
315	45	38	28	0.15	50	pf	"
316	52	34	30	0.3	70	pf	Harzburgite (with clevable olivine)
317	60	40	22	0.1	60	pf	Dunite
318	60	40	17	0.1	40	f	Harzburgite (with clevable olivine)
319	45	42	20	0.3	35	-	" "
320	55	40	25	0.1	60	p0.5	" "
321	43	35	30	0.4	50	pf	" "
322	45	40	25	0.1	35	p0.5	Dunite "
323	50	40	30	0.1	45	pf	Harzburgite "
324	40	25	23	0.35	30	p0.3	"

Sample No.	Diameter (mm) L	M	S	Round-ness	Wt. (g)	Mn-coating (mm)	Lithology & Remarks
D2-325	40	25	21	0.5	30	pf	Harzburgite
326	35	35	30	0.3	40	-	Dunite (with clevable olivine)
327	45	40	25	0.15	50	pf	" "
328	40	22	20	0.1	30	pf	" "
329	50	22	20	0.5	30	-	Harzburgite "
330	40	30	25	0.5	40	pf	"
331	40	35	25	0.5	45	f	" (with clevable olivine)
332	43	25	20	0.35	45	f	Dunite
333	45	27	25	0.1	40	pf	"
334	35	25	17	0.15	25	pf	"
335	35	30	17	0.25	25	-	Harzburgite (with clevable olivine)
336	40	35	20	0.35	35	-	Dunite
337	35	35	30	0.2	45	pf	Harzburgite (with clevable olivine)
338	50	45	30	0.1	45	pf	" "
339	35	30	20	0.15	25	-	" "
340	50	35	25	0.15	40	pf	" "
341	40	25	22	0.2	25	-	" "
342	40	33	20	0.2	30	-	Dunite
343	40	20	20	0.3	20	p0.5	Harzburgite
344	45	32	13	0.25	25	pf	"
345	40	20	20	0.25	25	-	" (with clevable olivine)
346	30	25	15	0.35	20	f	" "
347	45	30	15	0.1	20	-	Dunite "
348	37	22	22	0.35	20	-	"
349	40	32	20	0.35	30	-	" (with clevable olivine)
350	40	40	20	0.1	35	pf	"
351	46	30	25	0.3	45	-	" (with clevable olivine)
352	43	36	21	0.2	50	-	Pyroxenite
401	60	45	35	0.3	150	f	Harzburgite (with clevable olivine)
402	70	50	30	0.2	120	f	" "
403	70	55	23	0.1	100	f	" "
404	70	55	35	0.3	115	f	Greenrock
405	90	55	30	0.1	75	-	Harzburgite (with clevable olivine)
406	70	60	15	0.1	160	-	" "
407	65	55	30	0.4	200	f	Pyroxenite
408	70	40	30	0.1	185	-	Sandstone
409	60	45	35	0.5	165	-	Serpentinite
410	50	45	25	0.1	145	-	Harzburgite
411	45	35	35	0.3	145	p1	Pyroxenite
412	50	40	20	0.4	135	-	Harzburgite
421	78	50	23	0.1	55	p2	Pumice
422	37	30	12	0.3	15	-	Pumice
431	50	50	25	0.1	45	1	Serpentine sandstone

Sample No.	Diameter (mm) L	M	S	Round-ness	Wt. (g)	Mn-coating (mm)	Lithology & Remarks
D2-432	37	37	10	0.1	15	2	Serpentine sandstone
441	55	30	25	0.1	45	f1	Serpentine sandstone
442	80	40	20	0.2	50	-	"
451	60	50	35	0.2	58	-	Serpentine sandstone
452	55	30	15	0.1	22	-	"
453	33	22	30	0.3	20	-	"
501	120	100	65	0.4	905	0.5	Harzburgite (with clevable olivine)
502	70	70	45	0.35	300	pf	" "
503	95	70	40	0.1	395	pf	" "
504	90	75	65	0.1	495	-	"
505	80	65	40	0.4	240	pf	Dunite
506	75	55	45	0.5	180	pf	"
507	75	45	45	0.1	175	pf	Harzburgite (with clevable olivine)
508	75	65	45	0.1	300	-	Dunite
509	110	75	45	0.15	520	pf	"
510	100	90	60	0.1	570	pf	Harzburgite
511	85	70	45	0.2	370	pf	Dunite
512	105	80	60	0.3	525	pf	"
513	74	52	50	0.25	190	pf	"
514	90	80	45	0.15	375	-	" (with clevable olivine)
515	70	50	50	0.1	160	pf	"
516	75	50	35	0.4	185	pf	" (with clevable olivine)
517	72	60	40	0.1	200	pf	"
518	65	55	50	0.2	175	-	"
519	80	45	30	0.15	185	pf	"
520	130	75	30	0.1	320	pf	"
521	80	65	50	0.3	250	pf	Dunite (with clevable olivine)
522	155	70	30	0.1	265	0.3	Harzburgite "
523	90	60	30	0.1	235	pf	"
524	100	95	45	0.15	440	pf	Dunite
525	105	70	40	0.3	360	0.5	" (with clevable olivine)
526	80	50	47	0.1	240	-	" "
527	100	85	50	0.3	590	pf	Harzburgite "
528	105	65	50	0.25	290	pf	Dunite
529	90	75	50	0.1	340	pf	Harzburgite
530	125	80	40	0.1	395	pf	Dunite
531	80	70	60	0.25	370	pf	" (with clevable olivine)
532	70	50	40	0.4	250	pf	Harzburgite "
533	90	80	45	0.3	375	-	Dunite
534	90	70	35	0.3	295	pf	" (with clevable olivine)
535	85	65	35	0.1	160	pf	" "
536	80	50	40	0.1	210	pf	"
537	80	55	40	0.4	270	-	Harzburgite (with clevable olivine)
538	80	60	45	0.3	200	pf	Dunite "

Sample No.	Diameter (mm) L	M	S	Round-ness	Wt. (g)	Mn-coating (mm)	Lithology & Remarks
D2-539	95	70	35	0.3	230	-	Dunite (with clevable olivine)
540	85	55	45	0.3	280	pf	"
541	60	40	40	0.4	130	pf	"
542	70	45	45	0.4	190	pf	"
543	60	50	40	0.3	150	pf	Dunite (with clevable olivine)
544	73	55	45	0.2	150	f	Harzburgite "
545	95	55	40	0.5	240	pf	Dunite
546	80	60	35	0.5	225	pf	"
547	85	60	50	0.3	255	pf	" (with clevable olivine)
548	65	35	25	0.4	165	p1	"
549	105	40	25	0.1	185	pf	Harzburgite (with clevable olivine)
550	70	60	40	0.3	235	pf	Dunite
551	75	55	47	0.5	235	pf	"
552	85	50	25	0.1	125	-	Harzburgite (with clevable olivine)
553	75	65	40	0.6	200	pf	Dunite
554	70	58	50	0.4	185	-	"
555	75	50	35	0.3	190	pf	" (with clevable olivine)
556	85	60	34	0.4	170	pf	"
557	90	60	45	0.4	210	-	"
558	80	50	45	0.2	190	pf	" (with clevable olivine)
559	80	50	45	0.3	180	pf	" "
560	90	50	45	0.2	190	pf	" "
561	70	60	35	0.2	165	pf	"
562	60	40	33	0.1	110	pf	"
563	65	60	35	0.6	125	-	Harzburgite
564	70	65	40	0.3	140	-	Dunite (with clevable olivine)
565	60	55	35	0.4	105	pf	Harzburgite "
566	60	40	30	0.6	175	pf	Dunite
567	65	55	35	0.5	130	-	" (with clevable olivine)
568	80	70	45	0.6	150	-	"
569	65	50	35	0.4	180	pf	" (with clevable olivine)
570	80	53	35	0.4	170	pf	"
571	75	50	45	0.25	230	pf	Harzburgite (with clevable olivine)
572	60	60	35	0.25	110	pf	Dunite
573	80	52	30	0.6	160	p0.5	Harzburgite
574	75	50	30	0.3	110	p1	Dunite
575	60	60	60	0.1	185	p1	" (with clevable olivine)
576	75	40	30	0.3	125	-	Harzburgite "
577	80	55	25	0.3	130	pf	Dunite
578	80	35	30	0.35	115	pf	Harzburgite
579	65	55	35	0.2	120	0.5	" (with clevable olivine)
580	50	43	32	0.6	85	p0.7	Dunite
581	60	40	30	0.4	70	pf	"
582	55	50	40	0.3	105	p0.5	" (with clevable olivine)
583	65	45	25	0.3	110	pf	Harzburgite "
584	65	40	40	0.6	115	-	Dunite "

Sample No.	Diameter (mm) L	M	S	Round-ness	Wt. (g)	Mn-coating (mm)	Lithology & Remarks
D2-585	70	53	30	0.3	105	pf	Dunite
586	60	45	40	0.35	170	pf	"
587	65	50	28	0.4	115	p0.3	"
588	75	55	20	0.1	95	pf	"
589	55	45	30	0.7	95	p0.5	Harzburgite
590	55	35	35	0.6	100	pf	Dunite
591	60	40	40	0.2	145	p0.5	"
592	90	45	25	0.1	140	-	Harzburgite (with clevable olivine)
593	60	50	32	0.6	115	pf	" "
594	90	45	30	0.1	160	-	Dunite
595	65	45	34	0.4	120	pf	Harzburgite (with clevable olivine)
596	60	50	35	0.4	125	0.5	Dunite
597	55	35	33	0.3	120	pf	Harzburgite (with clevable olivine)
598	60	40	30	0.3	110	pf	Dunite
599	65	37	30	0.4	140	-	Harzburgite
600	83	50	20	0.1	95	pf	Dunite
601	72	60	30	0.3	95	pf	"
602	60	45	30	0.4	100	f	"
603	80	40	26	0.15	125	pf	" (with clevable olivine)
604	60	40	35	0.3	105	pf	Harzburgite
605	80	50	30	0.2	150	pf	Dunite
606	60	40	35	0.35	95	pf	"
607	60	50	30	0.1	135	0.5	" (with clevable olivine)
608	55	36	25	0.15	95	pf	"
609	50	40	35	0.35	85	pf	"
610	50	30	30	0.1	80	0.3	Harzburgite
611	60	45	30	0.35	95	0.5	" (with clevable olivine)
612	55	45	27	0.3	80	-	Dunite
613	60	30	25	0.15	50	pf	"
614	50	45	30	0.6	55	pf	"
615	60	40	20	0.1	60	pf	"
616	50	40	25	0.3	75	pf	Harzburgite (with clevable olivine)
617	65	45	25	0.1	75	-	" "
618	55	40	25	0.3	75	pf	" "
619	60	45	20	0.3	50	0.5	Dunite
620	55	40	33	0.5	75	pf	"
621	60	28	25	0.1	45	-	"
622	70	40	30	0.1	45	p0.5	"
623	45	32	30	0.2	130	pf	Harzburgite
624	55	45	30	0.4	45	p0.5	Dunite
625	45	30	22	0.4	55	pf	"
626	58	30	25	0.1	50	pf	"
627	43	40	30	0.3	65	1	"
628	50	35	23	0.1	45	pf	"
629	65	30	30	0.1	45	f	"
630	55	35	25	0.1	85	f	Harzburgite

Sample No.	Diameter (mm) L	M	S	Round-ness	Wt. (g)	Mn-coating (mm)	Lithology & Remarks
D2-631	60	40	15	0.1	40	-	Dunite (with clevable olivine)
632	65	36	20	0.1	60	pf	"
633	50	45	15	0.1	35	-	"
634	52	40	30	0.3	60	pf	"
635	53	45	20	0.2	45	pf	Dunite
636	45	37	20	0.4	55	pf	"
637	55	43	25	0.3	65	-	"
638	50	40	25	0.4	65	-	"
639	65	40	25	0.2	75	-	" (with clevable olivine)
640	55	33	22	0.15	40	p0.5	"
641	60	30	22	0.1	65	pf	"
642	50	33	20	0.3	40	-	"
643	63	30	20	0.1	55	pf	"
644	46	26	25	0.3	45	-	Harzburgite
645	50	25	25	0.35	35	-	"
646	55	45	30	0.1	50	0.5	Dunite
647	45	25	20	0.3	35	pf	Harzburgite (with clevable olivine)
648	50	35	13	0.2	35	-	Dunite "
649	50	40	10	0.2	35	pf	"
650	55	37	17	0.1	40	-	"
901	100	75	40	0.2	510	-	Harzburgite (with clevable olivine)
902	90	60	60	0.3	360	pf	" "
903	90	60	40	0.5	220	pf	" "
904	65	60	35	0.3	170	pf	" "
905	100	45	45	0.6	345	pf	Pyroxenite
906	95	60	45	0.3	355	-	Dunite (with clevable olivine)
907	95	60	45	0.3	400	f	Pyroxenite
908	80	50	50	0.3	225	f	Dunite
909	100	50	45	0.3	410	-	Harzburgite (with clevable olivine)
910	80	45	40	0.3	225	0.4	"
911	75	70	45	0.4	250	-	Dunite (with clevable olivine)
912	80	50	45	0.3	215	pf	Harzburgite "
913	90	65	30	0.2	280	pf	" "
914	70	60	50	0.3	230	-	" "
915	110	60	25	0.1	230	f	" "
916	70	60	50	0.15	255	f	" "
917	70	65	60	0.2	285	1	Dunite "
918	85	50	30	0.3	250	pf	" "
919	90	65	35	0.1	245	p1	Harzburgite "
920	60	52	35	0.1	165	1	" "
921	70	50	50	0.3	260	0.5	" "
922	80	60	30	0.3	185	pf	"
923	75	55	35	0.2	205	pf	Dunite (with clevable olivine)
924	70	65	40	0.35	235	0.5	Harzburgite "
925	70	55	45	0.3	195	p0.5	" "

Sample No.	Diameter (mm) L	M	S	Round-ness	Wt. (g)	Mn-coating (mm)	Lithology & Remarks
D2-926	85	45	23	0.1	185	0.5	Harzburgite (with clevable olivine)
927	73	55	32	0.3	190	p0.5	Dunite "
928	100	50	22	0.1	125	1	Harzburgite "
929	85	60	30	0.3	215	1	" "
930	60	50	40	0.4	190	-	Harzburgite "
931	70	60	30	0.4	175	pf	Dunite "
932	60	35	35	0.25	170	pf	" "
933	60	40	35	0.2	160	-	Harzburgite "
934	70	50	35	0.2	215	pf	" "
935	80	40	40	0.1	160	f	Dunite "
936	70	50	40	0.2	137	pf	Harzburgite "
937	55	40	30	0.35	95	-	" "
938	70	33	30	0.15	90	-	" "
939	50	45	30	0.3	115	1	"
940	55	50	35	0.4	100	0.5	" (with clevable olivine)
941	55	45	35	0.1	85	-	" "
942	50	30	30	0.1	70	0.5	Dunite
943	65	40	30	0.25	120	pf	Harzburgite (with clevable olivine)
944	60	35	32	0.25	100	pf	Dunite "
945	75	45	20	0.1	70	-	"
946	65	60	20	0.1	110	3	Harzburgite (with clevable olivine)
947	40	35	30	0.2	70	2	" "
948	45	45	30	0.4	75	-	Dunite "
949	50	40	30	0.3	80	pf	Harzburgite "
950	50	35	35	0.4	60	-	Dunite
951	70	45	25	0.1	90	-	Harzburgite (with clevable olivine)
952	70	40	15	0.1	55	pf	" "
953	60	30	20	0.1	60	f	"
954	60	30	25	0.1	45	pf	"
955	52	40	30	0.2	90	pf	Dunite (with clevable olivine)
956	55	45	25	0.15	50	-	"
957	45	30	25	0.35	50	-	Harzburgite
958	45	27	22	0.2	50	1	" (with clevable olivine)
959	40	30	27	0.3	50	f	" "
960	60	27	25	0.1	65	f	Dunite "
961	45	25	18	0.1	35	-	" "
962	30	28	20	0.15	25	-	"
963	36	30	10	0.3	18	-	" (with clevable olivine)
964	40	23	20	0.4	30	-	"
965	30	23	13	0.1	20	pf	Harzburgite (with clevable olivine)
966	35	30	20	0.35	20	pf	Dunite

Notes
p:partly
f:filmy

13.3 Amphibolites and Metabates Recovered from the Lower Part of the Southern Mariana Trench Inner Slope during KH92-1 Cruise

O. Takemura, T. Ishii and H. Maekawa

1. Introduction

Amphibolite to greenschist facies rocks have been reported from several places in the Mariana forearc region (Bloomer, 1983; Ishii, 1985; Maekawa et al., 1989; Maekawa et al., 1992). These metamorphic rocks are considered to provide important information on physicochemical conditions beneath the forearc region.

Together with abundant serpentinized peridotites, several metamorphic rock clasts have been recovered in the forearc area during the KH92-1 cruise (Ishii et al., this volume). We will briefly describe petrographic characteristics of these metamorphic rocks in this report.

2. Metamorphic Protoliths and Metamorphic Minerals

Metamorphic protoliths are variable. They are basalt, dolerite, gabbro, and pyroxenite. Relict clinopyroxene is commonly preserved. Samples KH92-1-D2-61, -404, -442B, and -905 (see Table 13-2-1, in Ishii et al., this volume) consist mainly of green to pale green hornblende, plagioclase, and sphene. In addition to these metamorphic minerals, sample D2-404 contains Fe^{3+}-poor epidote. On the basis of mineral assemblages, these rocks are considered to belong to amphibolite to epidote-amphibolite facies.

Sample D2-002, -019 and -408 is composed of colorless and acicular actinolite, chlorite, and albite. Sample D2-408 also contains epidote. Textural relations indicate that these metamorphic minerals occur in equilibrium with each other. Veins of fine-grained garnet are developed in Sample D2-019. These samples are thought to have been metamorphosed under greenschist facies conditions.

3. Deformation Fabrics

Some specimens show intense deformation fabrics. Sample D2-002 contains abundant anhedral plagioclase (relict?), which are deformed to show conspicuous wavy extinction. Colorless to pale green hornblende of sample D2-019 occurs as an aggregate of acicular crystals. The arrangements of hornblende define weak schistosity, and often exhibits micro-folds.

Sample D2-442 is a highly sheared rock. Two types of plagioclase are recognized. One occurs as coarse-grained porphyroclast. The other is fine-grained neoblast. Intense wavy extinction is frequent in porphyroclast plagioclase and hornblende crystals. Deformation lamella is also well developed in porphyroclast plagioclase. These fabrics suggest the initiation of mylonitization.

4. Discussion

Because of the deficiency of our present knowledge, we cannot address the precise tectonic setting where these metamorphic rocks have been formed. These metamorphic rocks, however, underwent greenschist to amphibolite facies metamorphism that was associated with shearing.

As the deformation fabrics observed in sample D2-442 suggest the initiation of mylonitization, synmetamorphic shearing may have occurred along the preexisting fracture zone, which was superseded by the subduction of the Pacific plate beneath the Philippine Sea plate at about 42 Ma.

References

Bloomer, S. H.:Distribution and origin of igneous rocks from the landward slopes of the Mariana trench: implications for its structure and evolution. J. Geophys. Res., 88, 7411-7428, 1983.

Ishii, T.: Dredged samples from the Ogasawara fore-arc seamount or "Ogasawara Paleoland" - "fore-arc ophiolite." In Formation of Active Ocean Margins (eds. Nasu, N. et al.), Terra Scientific Publishing Company, Tokyo, 307-342, 1985.

Maekawa, H., Shozui, M., and Ishii, T.: Fore-Arc Ophiolite. J. Geography, v. 98, 55-65. (in Japanese with English abstract), 1989.

Maekawa, H., Shozui, M., Ishii, T., Saboda, K., and Ogawa, Y.: Metamorphic rocks from the serpentinite seamounts in the Mariana and Izu-Ogasawara forearcs. Proc. of the Ocean Drilling Program, Scientific Results, v. 125, p. 415-430, 1992.

13.4 Description of Dredged Samples from the Ayu Trough during the Second Leg (Guam to Cebu) of KH92-1 Cruise

T. Ishii, O. Takemura, C. Igarashi, K. Tamaki and K. Kobayashi

More than two hundred rocks (about 20 kg weight in total) were dredged during the second leg (Guam to Cebu) of KH92-1 cruise. Four sites (Stations KH92-1-D3 to D6) were selected to investigate the origin and evolution of the Ayu Trough, which is assumed as the Philippine-Caroline plate boundary (Fornari et al.,1979). Precise position, depth of each station and relevant information are given at the operation logs (Chapter 13.1) of dredge hauls, and position of each station is shown in Fig. 13.4.1.

Detailed explanations of dredge method and sample processing are the same as mentioned in the previous Chapter 13.2 in this volume. Preliminary sample descriptions are shown in Table 13-4-1.

Remnant Island-Arc (?) in the Ayu Trough

The axial rift zone of the Ayu Trough is elongated from north to south as shown in Fig. 13.4.1. The detailed geological and geophygical investigations have been done along latitude 3° 30.0' N (Tamaki et al., Igarashi et al., Kinoshita et al., and Toho et al., in this volume).

Three dredge sites (Station KH92-1-D3, D4 and D5) were also selected along this line, that is , Station D3 for eastern slope of axial rift valley (5300 m deep) toward crest, Station D4 for eastern slope of fault escarpment locating about 40 km from the rift axis, and Station D5 for eastern slope of fault escarpment locating about 60 km from the rift axis.

The three stations were selected for the following purposes; 1) the petrological characterization of effusive rocks within the Ayu trough, 2) the investigation of current igneous activity (active or non-active ?) in the trough axis, and 3) the estimation of spreading rate of the trough on the basis of the K-Ar and/or Ar-Ar age determinations of basalt.

The dredge hauls of the stations D3 and D4 were not successful. Igneous rocks were not collected from both sites and only soft sediments and semiconsolid ated siltstones were recovered. About one hundred rocks (with about 5 kg in total weight) including igneous rocks and sedimentary rocks as well as metamorphic rocks were collected at station KH92-1-D5, which is located at the eastern end of the trough. Igneous rocks consist of very-angular to angular compact lavas with filmy Mn-coating. Chilled glass zones and/or

pillow textures were not observed among them. The lavas contain phenocrysts of augite, orthopyroxine, Fe-Ti oxide and plagioclase scattered among the groundmass of augite, Fe-Ti oxide, plagioclase and altered glass. Their major elements analyses for bulk chemistry estimated by XRF (Rigaku Model 3080, Ocean Research Institute) and their CIPW norms are shown in Table 11-4-2.

They differ from typical MORB (mid-oceanic ridge basalt) and/or BABB (back-arc basin basalt), on the other hand, their chemical and petrographical characteristics are similar to two-pyroxine andesite which occurs commonly in the island-arc environment. Finely laminated consolid ated siltstones (Fig. 13.4.2) and tuffacious sandstones are also recovered.

It is difficult to assume that these rocks were formed in the spreading axis environment like a mid-oceanic ridge and/or back-arc basin. Dredge site KH92-1-D5 might be situated in the remnant island-arc. It may be very interesting to compare these rocks with the rocks from the Kyusyu-Palau Ridge, which is located at the northern extention of the Ayu trough.

Abyssal Basalts from the Rift Valley in the Ayu Trough

Another dredge site (Station KH92-1-D6) was selected in the eastern slope of axial rift valley (4700 m deep) locating about 70 km north from the station D5. About 200 rock samples (12 kg in total weight) including compact fresh basalts with and without Mn-coating, pumices and Mn-crusts were dredged from the station D6 (Table 13-4-1). Pillow textures with and without fresh glass zone are commonly observed among dredged basalts.(Fig. 13.4.3A) The basalts lavas contain phenocrysts of olivine, augite, and plagioclase scatterd among the groundmass of olivine, plagioclase and devitrified glass.(Fig.13.4.3B) These bulk rock analyses estimated by EPMA are shown in Table 13-4-2. Their geochemical and petrographical characteristics are similar to typical MORB and/or BABB. It is assumed that these rocks were formed in the spreading axis environment.

There are many topographic highs as well as topographic depletions within so-called "the Ayu Trough" (Fig. 13.4.1), so it is very important to get constituting rock samples from each high (and depletion) by dredge hauls for petrological investigations and to discriminate the boundary between the Ayu Trough itself and the surrounding remnant island-arcs. Based on these geological and petrological data together with geophysical data, the origin and evolution of the Ayu Trough will be clarified.

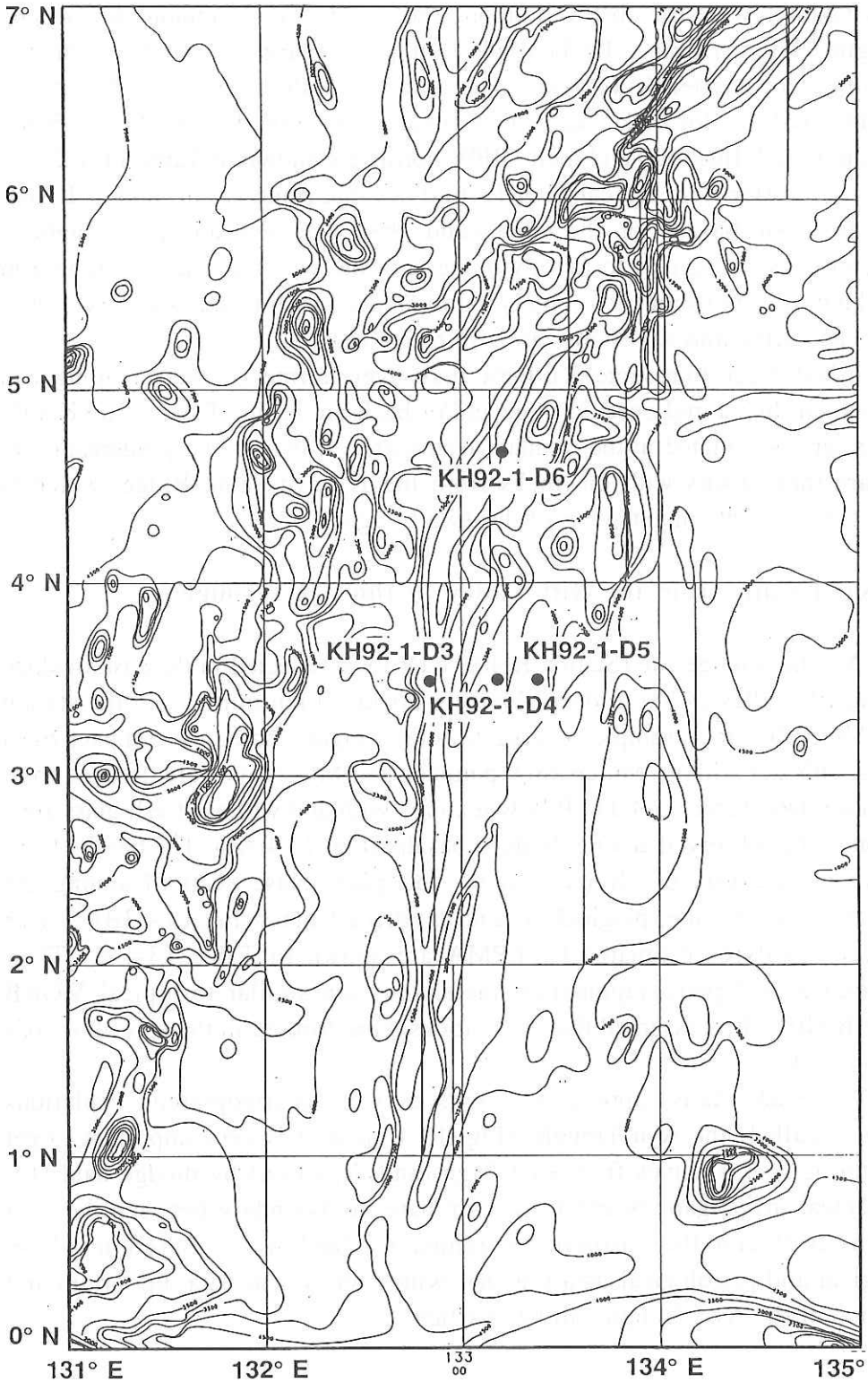

Fig. 13-4-1 Location of dredge hauls (Stations KH92-1-D3 to D6) in the Ayu Trough during the second leg (Guam-Cebu) of KH92-1 cruise.

References

Fonari, J. D., Weissel, K. J., Perfit, R. M., Anderson,N.R.: Petrochemistry of the Sorol and Ayu Trough : Implications for crustal accretion at the northern and western boundaries of the Caroline plate. Earth Planet. Sci. Lett., 45, 1-15, 1979.

Ishii, T., Robinson, P.T., Maekawa,H., and Fiske R.: Petrological studies of peridotites from diapiric serpentinite seamounts in the Izu-Ogasawara-Mariana forearc, Leg 125. Proceedings of the Ocean Drilling Program,Scientific Results, 125; Ocean Drilling Progrm, College Staion, TX, 445-485,1992.

Fig. 13.4.2 Photographs of a finely laminated consolid siltstones (KH92-1-D5-53)dredged in the AyuTrough.

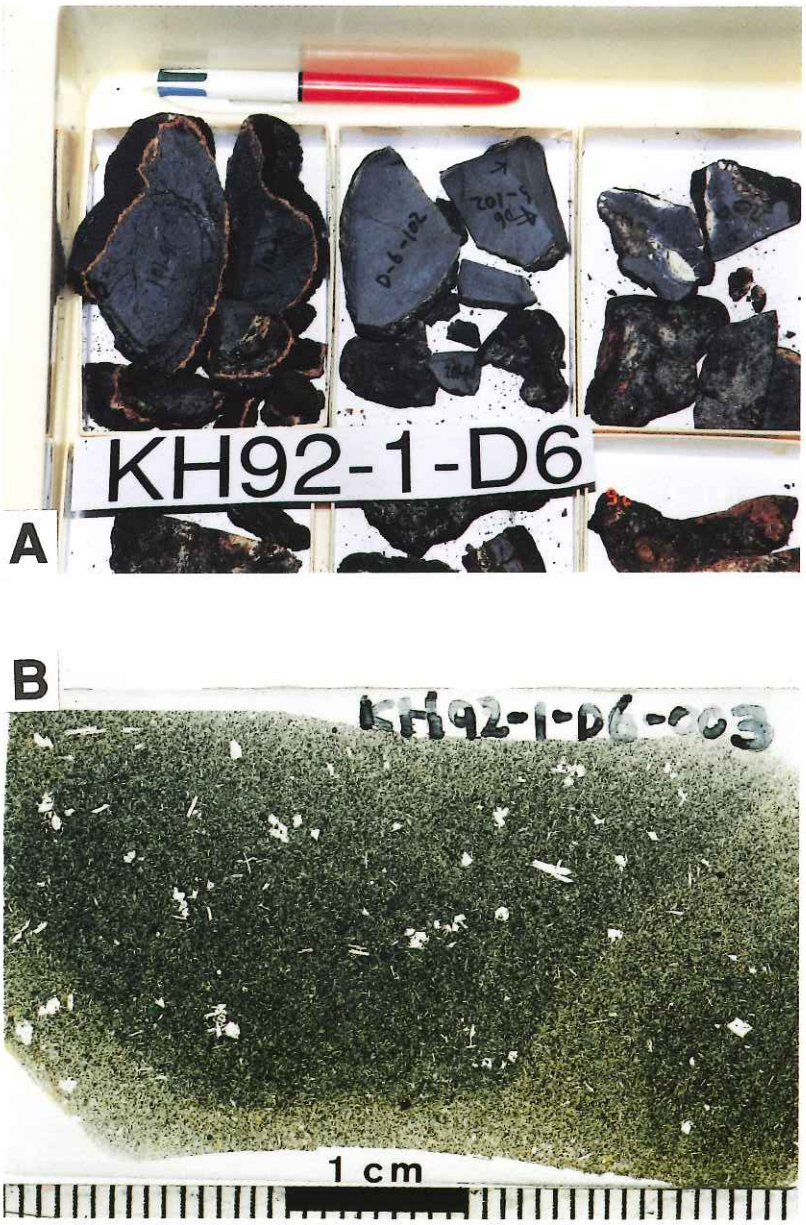

Fig. 13.4.3 Photographs of dredged rocks from the axial rift valley of the Ayu Trough (Station KH92-1-D6). (A) Cobbles of fresh basalt coated by Mnoxides with 2-8 mm thick. (B) Typical example of rock thin section of dredged basalts containing phenocrysts of olivine,augite,and plagioclase (KH92-1-D6-003).

Table 13-4-1 List of materials dredged during the second leg (Guam-Cebu) of KH92-1 cruise.

Sample No.	Diameter (mm) L	M	S	Round-ness	Wt. (g)	Mn-coating (mm)	Lithology & Remarks
D5-001	90	65	35	0.1	300	f	basalt
002	83	55	25	0.1	130	f	"
003	110	46	35	0.1	260	f	"
004	50	47	27	0.1	135	-	"
005	112	56	18	0.1	145	f	"
006	85	52	28	0.1	145	f	"
007	90	70	27	0.1	56	f	"
008	85	52	30	0.1	150	f	"
009	120	48	28	0.1	100	f	"
010	57	45	24	0.25	85	f	"
011	80	38	30	0.1	75	f	"
012	65	35	17	0.1	51	f	"
013	70	44	25	0.1	75	pf	"
014	97	27	19	0.1	55	f	"
015	50	45	18	0.15	47	f	"
016	39	36	17	0.2	33	f	"
017	45	34	20	0.2	37	f	"
018	52	33	31	0.1	44	pf	"
019	55	47	16	0.15	55	pf	"
020	45	36	20	0.1	32	f	"
021	55	43	12	0.1	39	f	"
022	56	35	20	0.15	54	0.3	"
023							
024	47	35	16	0.1	33	pf	basalt
025	40	23	16	0.2	17	pf	"
026	47	38	34	0.15	65	f	"
027	45	30	20	0.2	50	f	"
028	44	35	27	0.25	45	0-6.0	"
029	50	30	25	0.3	65	pf	"
030	40	35	13	0.1	30	0.5	"
031	30	24	10	0.1	10	f	"
032	67	18	12	0.1	10	f	"
033	40	12	10	0.1	10	pf	"
034	40	20	12	0.1	13	pf	"
035	24	16	12	0.1	10	f	"
036	30	20	9	0.1	10	pf	"
037	30	24	5	0.1	5	f	"
038	32	17	10	0.1	8	f	"
039	32	20	11	0.1	8	f	"
040	30	22	12	0.1	8	f	"
041	22	7	12	0.1	8	pf	"
042	25	15	7	0.1	4	pf	"
043	30	12	12	0.1	5	pf	"
044	27	17	7	0.1	5	f	"
045	23	18	5	0.1	3	f	"
046	25	14	10	0.1	4	f	"

Sample No.	Diameter (mm) L	M	S	Round-ness	Wt. (g)	Mn-coating (mm)	Lithology & Remarks
D5-047	40	20	7	0.1	4	-	green rock
048	37	22	13	0.1	14	pf	basalt
049	36	12	10	0.1	4	pf	"
051	147	42	37	0.1	235	f	conglomerate
052	110	75	35	0.1	300	f	green rock
053	70	40	40	0.1	175	f	shale
054	51	44	23	0.1	65	0-3.0	shale
055	52	35	32	0.15	59	f	green rock
056	55	40	30	0.35	66	0.4	pillow lava
057	55	20	17	0.2	26	1	altered lava
058	35	25	15	0.1	16	pf	"
059	45	30	6	0.1	8	f	"
060	30	23	15	0.15	11	pf	"
061	35	22	8	0.1	7	pf	"
062	30	38	15	0.1	7	f	"
063	30	19	12	0.1	7	0-2.0	"
064	20	15	10	0.1	5	pf	"
065	23	17	7	0.1	9	f	"
066	35	17	1	0.1	5	pf	"
067	17	14	9	0.1	3	pf	"
068	27	21	4	0.1	4	pf	"
069	18	17	8	0.1	4	-	"
070	25	15	9	0.1	2	f	"
071	20	17	5	0.1	30	f	"
072	26	25	5	0.1	4	f	"
073							
074	17	8	5	0.1	2	pf	altered lava
075	29	8	1	0.1	3	f	"
076	40	31	17	0.4	20	2	basalt
077	40	26	8	0.1	7	4	Mn-crust
078	30	25	19	0.2	23	9	"
079	28	26	6	0.3	4	4	"
080	50	47	7	0.2	22	6	"
081	38	30	18	0.3	16	8	"
082	40	25	10	0.1	5	4	"
083	24	23	18	0.1	8	9	"
084	100	57	19	0.1	90	8	"
085	73	33	17	0.1	42	8	"
086	54	35	20	0.1	31	11	"
087	40	29	19	0.4	9	-	pumice
088	13	12	6	0.5	1	-	"

Sample No.	Diameter (mm) L	M	S	Round-ness	Wt. (g)	Mn-coating (mm)	Lithology & Remarks
D6-001	90	65	35	0.1	300	f	basalt
002	93	55	25	0.1	130	f	"
003	110	46	35	0.1	260	f	"
004	50	47	27	0.1	135	-	"
005	90	65	60	0.1	300	0-1.0	"
006	100	65	40	0.2	340	0.2	"
007	85	65	50	0.2	290	pf	"
008	72	62	45	0.2	260	pf	"
009	80	70	45	0.15	255	-	"
010	80	45	45	0.2	210	pf	"
011	75	50	45	0.1	210	f	"
012	60	43	40	0.3	120	pf	"
013	88	52	32	0.2	190	pf	"
014	63	40	38	0.3	140	f	"
015	60	50	45	0.3	160	pf	"
016	65	60	45	0.2	185	f	"
017	66	46	37	0.15	170	f	"
018	57	45	35	0.15	135	0.5	"
019	60	40	35	0.3	130	0-1.0	"
020	80	35	20	0.1	90	pf	"
021	67	40	25	0.2	105	f	"
022	60	37	23	0.2	110	pf	"
023	55	20	20	0.1	65	f	"
024	45	34	20	0.2	45	f	"
025	87	28	13	0.1	50	f	"
101	100	60	60	0.6	400	10	basalt
102	75	60	50	0.35	220	8	"
103	55	40	20	0.4	70	2	"
104	70	45	40	0.4	160	2	"
105	60	68	12	0.5	80	10	"
106	67	50	30	0.35	120	1	"
107	70	50	20	0.1	70	6	"
108	60	50	35	0.4	125	1	"
109	75	40	27	0.5	100	10	"
110	65	55	13	0.1	65	0-1.0	"
111	76	30	20	0.3	100	0-1.0	"
112	83	35	20	0.3	100	10	"
113	57	40	30	0.25	60	2	"
114	57	28	10	0.1	35	0.5	"
115	45	30	27	0.4	45	0-1.0	"
116	55	33	12	0.1	30	6	"
117	40	26	20	0.1	20	0.5	"
118	55	38	13	0.1	40	0.5	"
119	72	42	12	0.5	45	1	"
120	50	35	14	0.3	45	0.5	"

Sample No.	Diameter (mm) L	M	S	Round-ness	Wt. (g)	Mn-coating (mm)	Lithology & Remarks
D6-121	53	25	25	0.3	40	7	basalt
122	37	22	15	0.1	12	f	phosphorite
201	110	55	37	0.1	225	23	Mn-crust
202	85	55	45	0.3	150	27	"
203	92	60	35	0.2	205	18	"
204	60	46	10	0.1	55	7	"
205	65	53	15	0.1	67	7	"
206	70	43	17	0.1	70	10	"
207	50	47	20	0.3	35	8	"
208	50	35	14	0.1	35	8	"
209	45	45	20	0.3	34	9	"
210	63	50	14	0.2	47	9	"
211	63	50	17	0.2	56	10	"
212	70	40	22	0.2	48	12	"
213	55	37	13	0.2	29	7	"
214	43	38	14	0.3	35	7	"
215	68	55	12	0.1	50	7	"
216	43	33	18	0.6	26	8	"
217	50	30	23	0.3	26	11	"
218	31	27	22	0.8	13	14	"
219	44	37	17	0.3	29	14	"
220	45	35	13	0.3	17	11	"
221	50	33	10	0.3	17	6	"
222							
223	56	53	12	0.3	37	7	Mn-crust
224	35	27	14	0.3	12	7	"
225	55	40	18	0.1	27	9	"
226	47	40	12	0.1	21	7	"
227	64	35	6	0.1	22	4	"
228	50	47	12	0.1	28	6	"
229	48	42	10	0.2	20	5	"
230	38	29	10	0.2	9	6	"
231	35	28	22	0.6	18	10	"
232	56	40	10	0.1	34	7	"
233	67	36	15	0.1	20	7	"
234	27	22	17	0.8	9	8	"
235	22	19	18	0.9	8	10	"
236	34	25	24	0.7	11	8	"
237	24	20	18	0.9	8	8	"
238	32	21	10	0.2	8	6	"
239	37	22	20	0.1	22	11	"
240	19	16	9	0.6	3	5	"
241	48	40	13	0.5	22	6	"
242	43	30	13	0.6	19	6	"
243	45	31	20	0.1	20	12	"

Sample No.	Diameter (mm) L	M	S	Round-ness	Wt. (g)	Mn-coating (mm)	Lithology & Remarks
D6-244	30	21	16	0.7	9	7	Mn-crust
245	42	30	9	0.2	16	6	"
246	25	17	12	0.5	4	7	"
247	25	20	15	0.3	6	7	"
248	33	23	9	0.3	6	3	"
249	33	20	12	0.3	1	7	"
250	20	20	15	0.9	6	8	"
251	32	21	14	0.3	51	7	"
252	23	14	11	0.4	4	6	"
253	35	24	12	0.4	12	7	"
254	28	18	17	0.3	10	9	"
255	30	25	7	0.3	6	5	"
256	30	18	17	0.6	7	9	"
257	23	20	14	0.5	5	6	"
258	22	18	12	0.5	5	5	"
259	48	36	6	0.1	11	8	"
260	30	18	15	0.3	11	8	"
261	30	25	18	0.4	10	6	"
262	17	17	12	0.9	3	7	"
263					8		"
264					9		"
265					203		"
266					17		"
267					18		"
268					2		"
269					4		"
270					4		"
271					5		"
272					2		"
273					7		Mn-nodule
274					7		Mn-crust
275					12		"
276					8		"
277					24		"
278					3		"
279					3		"
280					3		"
281					3		"
282					2		"
283					2		"
284					10		"
285					9		"
286					3		"
287					5		"
288					6		"
289					2		"

Sample No.	Diameter (mm) L	M	S	Round-ness	Wt. (g)	Mn-coating (mm)	Lithology & Remarks
D6-290					3		Mn-crust
291					4		"
292					10		"
293					3		"
294					6		"
295					7		"
296					5		"
297					5		"
298					3		"
299					6		"
300					3		"
401					3		Mn-crust
402					4		"
403					2		"
404					4		"
301	70	40	33	0.2	51	f	pumice
302	50	26	25	0.7	21	f	"
303	60	40	30	0.2	34	pf	"
304	50	25	23	0.4	23	-	"
305	40	30	30	0.1	25	pf	"
306	45	35	19	0.5	8	-	"
307	35	30	20	0.6	12	pf	"
308	40	24	22	0.6	10	pf	"
309	45	34	20	0.3	7	-	"
310	47	32	28	0.2	13	pf	"
311	30	23	20	0.8	7	pf	"
312	33	32	17	0.4	8	pf	"
313	40	22	22	0.1	11	pf	"
314	40	22	21	0.1	12	pf	"
315	37	31	16	0.3	10	pf	"
316	32	20	18	0.5	9	pf	"
317	40	26	15	0.5	12	0-0.5	"
318	36	20	17	0.3	7	pf	"
319	25	24	20	0.2	7	pf	"
320	32	32	20	0.6	8	pf	"
321	27	20	19	0.3	8	pf	"
322	34	25	17	0.4	7	-	"
323	22	22	13	0.3	2	-	"
324	34	27	19	0.5	10	pf	"
325	32	27	12	0.2	5	-	"
326	16	14	12	0.35	2	pf	"
327	25	20	15	0.5	4	pf	"
328	36	19	18	0.2	7	pf	"
329					4	pf	"

Sample No.	Diameter (mm) L	M	S	Round-ness	Wt. (g)	Mn-coating (mm)	Lithology & Remarks
D6-333					5	pf	pumice
331					7	pf	"
332					5	pf	"
333					4	pf	"
					170	pf	"

Notes
p:partly
f:filmy

Table 13-4-2 The major-element analyses by EPMA for dredged rocks from the Ayu Trough during the second leg (Guam-Cebu) of KH92-1 cruise. The analytic method is the same as that described by Ishii et al. (1992).

	KH92-1-D5		KH92-1-D6				
Rock No.	D5-01	D5-03	D6-001	D6-007	D6-101	D6-102	JB-1
SiO2	53.70	55.10	49.96	49.80	48.70	48.77	53.63
TiO2	1.18	0.99	1.92	1.93	1.91	1.91	1.38
Al2O3	17.81	17.29	15.93	15.94	15.28	15.72	14.67
FeO	8.83	7.73	9.27	9.31	9.71	9.87	7.81
MnO	0.19	0.17	0.18	0.18	0.18	0.22	0.16
MgO	5.38	5.14	5.71	6.04	7.69	6.26	7.55
CaO	5.05	3.92	10.80	10.57	10.27	10.67	9.38
Na2O	5.22	5.08	3.47	3.46	3.88	3.72	2.21
K2O	0.76	2.93	0.61	0.57	0.26	0.36	1.44
P2O5	0.24	0.17	0.10	0.10	0.13	0.12	0.15
Total	98.40	98.57	98.03	97.96	98.07	97.69	98.52
Fe/Fe+Mg	0.480	0.457	0.477	0.464	0.415	0.469	0.367

14. Sediment Sampling in the Western Equatorial Pacific

T. Oba, M. Murayama, H. Matsuoka, T. Okamoto, S. Morita, T. Suzuki
and
S. Tsukawaki

14.1 Introduction

Ocean floor sediments were collected at five stations using a piston corer (with 10 m length of Al pipe, I.D.=65 mm, wall thickness=7.5 mm, and weight=900kg) and a box corer with the size of 50 x 50 x 50 cm^3. General information on these core stations are listed on Table 14.1.

The failure of the piston coring at station 1 was probably because the weight of the pilot corer was too light compared with the main corer. The location of station 2 was selected as the best place for tephrochronological, micropaleontological, and stable isotopic studies. A duplicate piston coring was carried out at stations 3 and 5, because these cores are used for an inter-disciplinary study under the project "International Geosphere-Biosphere Program". About 20 scientists listed on Table 14.2 are planned to join the inter-disciplinary investigation of these cores. Station 4 was cancelled. The sediment cores at station 6 were taken as a reference sample for the study of the station 5.

Since surface sediments are frequently disturbed during piston coring, associated box coring were also carried out (T. Oba).

14.2 On-Board Treatment

The on-board routine work of bottom sediments obtained by a piston core sampler is as follows.

At first, magnetic susceptibility was measured for each whole core sample, then the sample was cut vertically into halves; an archive and a working sample. Both of them were immediately marked with white and blue pins at 10 and 50 cm intervals, respectively.

Before storage, the archive core was used for taking a photograph, visual description, and then sliced for soft X-ray observation.

As for the working core, quantitative sampling was conducted continuously along a double line with cubic samplers (2.2 x 2.2 x 2.2 cm^3) and the rest sample was cut into 2.2 cm thick segments.

For each box core sample, several 8 cm across vertical samples were collected from the whole sample. Then, the same operation core sample was done for a piston. (M. Murayama)

14.3 Core Log (See attached core log tables.)

14.4 Core Description

For visual and soft X-ray observations, a cutting surface of the archive core sample was first shaved by a stainless-steel ointment spatula, then well brushed by a water atomizer for detailed visual observation. 8 mm thick and 200 mm long vertically sliced sediments were cased in plastic boxes from the cutting surface of each archive core sample for soft X-ray observation. For soft X-raying ,the sliced samples were placed at a time on Fuji no.100 film. Source-to-sample distance on a Softex type CSM-2 X-ray unit was 70 cm.Voltage,amperage and exposure time were held constant at about 50kV, 4mA and 50 seconds, respectively.

Site 1

1BX(Fig.14.1): Box core 1BX, 25 cm long, is composed mainly of yellowish brown coloured muddy calcareous ooze. Scoriaceous sand is dominant in the lowest 6 cm. Dark grey rounded pumice grains,up to 4 mm in diameter are scattered 15 cm beneath bottom surface. Biogenic disturbance is weakly developed particularly in the lower part (Plate 14.1a).

Site 2

2PC (Fig. 14.2a - 2j): Piston core 2PC, 933 cm long, is composed chiefly of dull yellowish brown coloured muddy fine- to medium-grained calcareous ooze. Four dark brown coloured scoriaceous sand layers, 10 to 20 cm in thickness, are intercalated in the lower half of the core (Plate 14.2c). Biogenic disturbance is developed in whole (Plate 14.2a, 14.2b), particularly the boundaries between overlying calcareous ooze and underlying scoriaceous sand (Plate 14.2d).

Site 3

3aPC(Fig. 14.3a -3j) and 3bPC: Piston cores 3aPC and 3bPC, 915 cm and 984 cm long respectively, are composed mainly of light yellow orange coloured medium-grained calcareous ooze in the upper and ligh gray coloured fine- to medium-grained calcareous ooze in the lower.Trace fossils, such as Zoophycos sp., are developed in whole (Plate 14.3a, 3b, 3c). Two intercalations of

calcareous turbidite, composed of medium- to coarse-grain foraminiferal tests,are identified in the lower part. The contacts between overlying turbidite and underlain calcareous ooze are erosional. Parallel laminations are developed in the turbidites (Plate 14.3d).

3cBX(Fig. 14.4): Box core 3cBX, 31 cm long, is composed mainly of light yellow orange coloured, medium-grained calcareous ooze. Biogenic disturbance is weakly developed in whole (Plate 14.1b).

Site 5

5aPC(Fig. 14.5a-5j) and 5bPC: Piston cores 5aPC, 987 cm long, and 5bPC, 1006 cm long, are composed mainly of yellowish light gray coloured medium-grained massive calcareous ooze in the upper and bluish light grey coloured fine- to medium-grained massive calcareous ooze in the lower. Bright green coloured thin grauconitic sand layers, 5 to 20 mm in thickness, are intercalated particularly in the middle and lower parts (Plate 14.4c). Biogenic disturbance is generally weakly developed (Plate 14.4a, 14.4d), however, strongly identified in some parts (Plate 14.4b). A fragment of molluscan shell (?Dentalium sp.) is found 516 cm below the bottom surface.

5cBX(Fig. 14.6): Box core 5cBX, 31 cm long, is composed mainly of brownish light yellow coloured, medium-grained calcareous ooze. Biogenic disturbance is weakly developed entirely (Plate 14.1c).

Site 6

6PC (Fig. 14.7a-14.7j): Piston core 6PC, 985 cm long, consists of various coloured, mainly light gray, pale yellow and olive yellow, medium-grained massive calcareous ooze and thirteen thick intercalations of gray coloured calcareous turbidite. Several sorts of biogenic structures are identified in the part of calcareous ooze (Plate 14.5a, 14.5b). The calcareous turbidites, 15 to 100 cm thick, are composed mainly of medium- to coarse-grained foraminiferal tests and a small amount of pale yellow coloured pumice, and they commonly have erosional bases and bioturbated tops. Internally, the turbidite show parallel laminations with a normal grading in the upper part (Plate 14.5c). Obliquely developed purple coloured strips, presumably water escape structures,are identified between 170 and 200 cm from the top of the core. A contorted layer, occurred probably by syn- depositional surface sliding, is observed 820 cm beneath the bottom surface (Plate 14.5d). Bright green coloured grauconitic sand layers, 5 to 10 mm in thickness, are intercalated particularly in the upper part of the core.

6BX (Fig. 14.8): Box core 6BX, 31 cm long, is composed mainly of bright yellowish brown coloured, medium-grained calcareous ooze. A pumice

grain, 8 mm long, is identified 26 cm beneath bottom surface. Biogenic disturbance, such as vertical burrows, is developed in whole (Plate 14.1d).

14.5 Magnetic Susceptibility

Magnetic susceptibility of each whole core sample was measured at 5 cm intervals by using Bartington pass through type magnetic susceptibility system. It is valid for comparison of piston cores in the same site as shown in Figures 14.9 and 14.10 (S. Morita).

14.6 Sample Distribution

The sediment samples of these piston and box cores were distributed to the scientists who analyze the samples for their own research theme as shown on Table 14.2 (T. Oba).

Table 14.1 List of core samples

Station No.	Latitude (N)	Longitude (E)	Depth (m)	Length (cm)	Remarks
1BX	20°23.78'	142°33.62'	1656	25	Dull brown calcareous ooze with ash
2PC	16°45.15'	143°03.25'	2683	933	Dull brown calcareous ooze with ash
3aPC	8°00.94'	139°38.41'	2830	915	Light grey calcareous ooze
3bPC	8°01.07'	139°38.53'	2831	984	Light grey calcareous ooze
3cBX	8°01.18'	139°38.43'	2829	31	Light grey calcareous ooze
5aPC	3°31.91'	141°51.70'	2283	987	Yellowish light grey calcareous ooze
5bPC	3°32.10'	141°51.67'	2279	1006	Yellowish light grey calcareous ooze
5cBX	3°32.01'	141°51.58'	2282	31	Yellowish light grey calcareous ooze
6PC	4°42.03'	133°42.17'	2980	985	Bright yellowish brown calcareous ooze
6BX	4°41.95'	133°42.09'	2975	31	Bright yellowish brown calcareous ooze

Table 14.2 Sample distribution of piston cores

University	Scientists	St. 2	St. 3	St. 5	St. 6
Hokkaido	I. Koizumi, H. Fukuzawa		1/8	1/8	
Tohoku	S. Tsukawaki	1/16	1/16	1/16	1/16
Tokyo	R. Tada		1/8	1/8	
Tokyo (O.R.I.)	M. Murayama, S. Morita M. Okada, N. Ohkouchi,	1/2 cube	1/2 cube	1/2 cube	1/2 cube
Tokyo Metropolitan	R. Ishiwatari T. Suzuki		1/4	1/4	
Toyo	S. Aoki	1/8	1/8	1/8	
Nagoya	N. Handa, T. Nakazuka, N. Harada		1/4	1/4	
Kanazawa	T. Oba		1/2cube	1/2cube	
Kochi	H. Matsuoka, T. Okamoto H. Yasuda	1/8	1/8	1/8	
Kumamoto	M. Oda		1/4cube	1/4cube	

Research subjects

Diatom, Organic carbon content, C/N
Semiar slide, Mineral composition
Chemical and mineral composition, Grain size
Magnetic suseptibility, Paleomagnetism,
18O-13C(Foram.), 37Uk, Cd/Ca, Ba/Ca
Hydrocarbon composition, 13C (Neutral, Lipid),
Tephra
Clay mineral
Organic material composition, 37Uk, 15N-
13C (organic carbon and Foram.), D/L, Racemization
18O-13C (Foram.)
Grain size, Eorian dust, Coccolith, Benthic Foram.,
CaCO3 dissolution
Planktonic Foram.

Piston Core Log

Cruise KH92-1 **Station** 1BX **Date** 1/24/1992

Location West Mariana Rise

Weather clear **Wind** 7.5 m/sec **SeaSwell** large

Type of PC Box Core (L)

Main wire ____ m **Pilot wire** ____ m **Free fall** ____ m

Time Start 7:02

		Latitude	*Longitude*	*Depth*
Time Lowered	7:05	20 ° 23.50 ' N	142 ° 33.67 ' E	1656 m

Wire Speed *Winch Down* ____ m/sec

Winch Up ____ m/sec

		Depth	*Wire out*
Time Stop	7:33	1656 m	1550 m

Restart *Wire Speed* 0.5 m/sec *Tension* 1.85 ton

		Latitude	*Longitude*	*Depth*	*Wire out*
Time Hit	7:38	20 ° 23.78 ' N	142 ° 33.62 ' E	1656 m	1657 m

Tension Min 1.21 ton *Max* 2.32 ton

Time Surfaced 8:04

Time End 8:10 **Total** 1:10

Remarks

Pilot Length ____ cm **Core Length** 25 cm **No. of Section** ____

Length of Section

Main Lithology yellowish brown coloured muddy calcareous ooze

Piston Core Log

Cruise KH92-1 **Station** 1PC **Date** 1/24/1992

Location West Mariana Rise

Weather clear **Wind** 6.6 m/sec **SeaSwell** large

Type of PC POtype (900Kg) 10 m Al (5 m x2)

Main wire 13.26 m **Pilot wire** 13.49+0.30 m **Free fall** 1 m

Time Start 8:10

		Latitude	*Longitude*	*Depth*	
Time Lowered	8:45	20 ° 23.87 ' N	142 ° 33.12 ' E	1666	m

Wire Speed *Winch Down* ____ m/sec

Winch Up ____ m/sec

		Depth		*Wire out*	
Time Stop	9:13	1662	m	1550	m

Restart *Wire Speed* 0.3 m/sec *Tension* 2.50 ton

		Latitude	*Longitude*	*Depth*		*Wire out*	
Time Hit	9:22	20 ° 24.02 ' N	142 ° 33.01 ' E	1665	m	1634	m

Tension Min 1.92 ton *Max* 2.82 ton

Time Surfaced 9:55

Time End 10:10 **Total** 2:00

Remarks

Pilot Length 0 cm **Core Length** 0 cm **No. of Section** ____

Length of Section

Main Lithology

Piston Core Log

Cruise KH92-1 **Station** 2PC **Date** 1/31/1992

Location West Mariana Rise

Weather clear **Wind** 5.3 m/sec **SeaSwell** small

Type of PC POtype (900Kg) 10 m Al (5 m x2)

Main wire 13.26 m **Pilot wire** 13.49+0.60 m **Free fall** 1 m

Time Start 13:37

		Latitude	*Longitude*	*Depth*	
Time Lowered	14:55	16 ° 45.28 ' N	143 ° 03.41 ' E	2683	m

Wire Speed *Winch Down* ____ m/sec

Winch Up ____ m/sec

		Depth		*Wire out*	
Time Stop	15:42	2701	m	2590	m

Restart *Wire Speed* 0.3 m/sec *Tension* 3.35 ton

		Latitude	*Longitude*	*Depth*		*Wire out*	
Time Hit	15:49	16 ° 45.15 ' N	143 ° 03.25 ' E	2683	m	2665	m

Tension Min 2.98 ton *Max* 4.18 ton

Time Surfaced 16:22

Time End 16:45 **Total** 3:10

Remarks

Pilot Length 0 cm **Core Length** 933 cm **No. of Section** 10

Length of Section 38, 138, 237, 335, 435, 534, 634, 733, 833, 933

Main Lithology dull yellowish brown coloured muddy calcareous ooze

Piston Core Log

Cruise KH92-1 **Station** 3aPC **Date** 2/2/1992

Location West Caroline Basin

Weather Clear **Wind** 8.6 m/sec **SeaSwell** small

Type of PC POtype (900Kg) 10 m Al (5 m x2)

Main wire 13.26 m **Pilot wire** 13.49+0.50 m **Free fall** 1 m

Time Start 14:10

		Latitude	*Longitude*	*Depth*
Time Lowered	14:20	08 ° 00.92 ' N	139 ° 38.55 ' E	2830 m

Wire Speed *Winch Down* 1.5 m/sec
Winch Up 1.5 m/sec

		Depth	*Wire out*
Time Stop	14:57	2830 m	2760 m

Restart *Wire Speed* 0.3 m/sec *Tension* 3.5 ton

		Latitude	*Longitude*	*Depth*	*Wire out*
Time Hit	15:03	08 ° 00.94 ' N	139 ° 38.41 ' E	2830 m	2802 m

Tension Min 2.12 ton *Max* 4.58 ton

Time Surfaced 15:37

Time End 15:52 **Total** 1:45

Remarks

Pilot Length 0 cm **Core Length** 915 cm **No. of Section** 10

Length of Section 11, 114, 215, 314, 412, 518, 617, 716, 815, 915

Main Lithology light yellow orange coloured calcareous ooze

Piston Core Log

Cruise KH92-1 **Station** 3bPC **Date** 2/2/1992

Location West Caroline Basin

Weather clear **Wind** 9.1 m/sec **SeaSwell** small

Type of PC POtype (900Kg) 10 m Al (5 m x2)

Main wire 13.26 m **Pilot wire** 13.49+0.50 m **Free fall** 1 m

Time Start 15:52

		Latitude	*Longitude*	*Depth*
Time Lowered	16:12	08 ° 01.10 ' N	139 ° 38.46 ' E	2831 m

Wire Speed *Winch Down* 1.5 m/sec

Winch Up 1.5 m/sec

		Depth	*Wire out*
Time Stop	16:54	2830 m	2760 m

Restart *Wire Speed* 0.3 m/sec *Tension* 3.5 ton

		Latitude	*Longitude*	*Depth*	*Wire out*
Time Hit	17:00	08 ° 01.07 ' N	139 ° 38.53 ' E	2831 m	2805 m

Tension Min 1.92 ton *Max* 4.74 ton

Time Surfaced 17:35

Time End 17:50 **Total** 2:00

Remarks

Pilot Length 0 cm **Core Length** 984 cm **No. of Section** 10

Length of Section 67, 167, 267, 371, 472, 576, 677, 779, 882, 984

Main Lithology light yellow orange coloured calcareous ooze

Piston Core Log

Cruise KH92-1 **Station** 3cBX **Date** 2/2/1992

Location West Caroline Basin

Weather clear **Wind** 10.6 m/sec **SeaSwell** small

Type of PC Box Core (L)

Main wire ____ m **Pilot wire** ____ m **Free fall** ____ m

Time Start 17:50

		Latitude	*Longitude*	*Depth*
Time Lowered	18:00	08 ° 01.15 ' N	139 ° 38.33 ' E	2831 m

Wire Speed *Winch Down* 1.0 m/sec
Winch Up 1.5 m/sec

		Depth	*Wire out*
Time Stop	18:47	2830 m	2760 m

Restart *Wire Speed* 0.5 m/sec *Tension* 2.86 ton

		Latitude	*Longitude*	*Depth*	*Wire out*
Time Hit	18:52	08 ° 01.18 ' N	139 ° 38.43 ' E	2829 m	2824 m

Tension Min 2.12 ton *Max* 3.24 ton

Time Surfaced 19:28

Time End 19:45 **Total** 2:00

Remarks

Pilot Length ____ cm **Core Length** 31 cm **No. of Section** ____

Length of Section ____

Main Lithology light yellow orange coloured calcareous ooze

Piston Core Log

Cruise KH92-1 **Station** 5aPC **Date** 2/13/1992

Location Eauripik-New Guinea Rise

Weather clear **Wind** 8.6 m/sec **SeaSwell** small

Type of PC POtype (900Kg) 10 m Al (5 m x2)

Main wire 13.26 m **Pilot wire** 13.49+0.50 m **Free fall** 1 m

Time Start 10:45

		Latitude	*Longitude*	*Depth*	
Time Lowered	10:55	03 ° 31.88 ' N	141 ° 51.32 ' E	2275	m

Wire Speed *Winch Down* 1.1 m/sec

Winch Up 1.5 m/sec

		Depth		*Wire out*	
Time Stop	11:33	2283	m	2150	m

Restart *Wire Speed* 0.3 m/sec *Tension* 3.0 ton

		Latitude	*Longitude*	*Depth*		*Wire out*	
Time Hit	11:42	03 ° 31.91 ' N	141 ° 51.70 ' E	2283	m	2260	m

Tension Min 2.10 ton *Max* 3.52 ton

Time Surfaced 12:13

Time End 12:28 **Total** 1:45

Remarks

Pilot Length 0 cm **Core Length** 987 cm **No. of Section** 10

Length of Section 97, 195, 298, 395, 487, 586, 685, 781, 879, 987

Main Lithology yellowish light gray coloured calcareous ooze

Piston Core Log

Cruise KH92-1 **Station** 5bPC **Date** 2/13/1992

Location Eauripik-New Guinea Rise

Weather clear **Wind** 7.4 m/sec **SeaSwell** small

Type of PC POtype (900Kg) 10 m Al (5 m x2)

Main wire 13.26 m **Pilot wire** 13.49+0.50 m **Free fall** 1 m

Time Start 12:28

		Latitude	*Longitude*	*Depth*	
Time Lowered	12:59	03 ° 31.94 ' N	141 ° 51.40 ' E	2284	m

Wire Speed *Winch Down* 1.2 m/sec
Winch Up 1.5 m/sec

		Depth	*Wire out*	
Time Stop	13:34	2279	2200	m

Restart *Wire Speed* 0.3 m/sec *Tension* 3.10 ton

		Latitude	*Longitude*	*Depth*	*Wire out*	
Time Hit	13:41	03 ° 32.10 ' N	141 ° 51.67 ' E	2279	2258	m

Tension Min 2.10 ton *Max* 3.77 ton

Time Surfaced 14:12

Time End 14:20 **Total** 2:00

Remarks

Pilot Length 0 cm **Core Length** 1006 cm **No. of Section** 11

Length of Section 105, 210, 310, 408, 495, 592, 690, 787, 882, 982, 1006

Main Lithology yellowish light gray coloured calcareous ooze

Piston Core Log

Cruise KH92-1 **Station** 5cBX **Date** 2/13/1992

Location Eauripik-New Guinea Rise

Weather cloudy **Wind** 8.5 m/sec **SeaSwell** moderate

Type of PC Box Core (L)

Main wire ____ m **Pilot wire** ____ m **Free fall** ____ m

Time Start 14:55

	Latitude	*Longitude*	*Depth*
Time Lowered 14:59	03 ° 31.87 ' N	141 ° 51.35 ' E	2285 m

Wire Speed *Winch Down* 1.0 m/sec

Winch Up 1.5 m/sec

	Depth	*Wire out*
Time Stop 15:29	2282 m	2200 m

Restart *Wire Speed* 0.5 m/sec *Tension* 2.40 ton

	Latitude	*Longitude*	*Depth*	*Wire out*
Time Hit 15:35	03 ° 32.01 ' N	141 ° 51.58 ' E	2282 m	2272 m

Tension Min 1.68 ton *Max* 3.34 ton

Time Surfaced 16:00

Time End 16:15 **Total** 1:20

Remarks

Pilot Length ____ cm **Core Length** 31 cm **No. of Section** ____

Length of Section

Main Lithology yellowish light gray coloured calcareous ooze

Piston Core Log

Cruise KH92-1 **Station** 6PC **Date** 2/19/1992

Location Ayu Trough

Weather clear **Wind** 7.2 m/sec **SeaSwell** moderate

Type of PC POtype (900Kg) 10 m Al (5 m x2)

Main wire 13.26 m **Pilot wire** 13.49+0.50 m **Free fall** 1 m

Time Start 12:35

		Latitude	*Longitude*	*Depth*	
Time Lowered	12:47	04 ° 41.86 ' N	133 ° 41.94 ' E	2974	m

Wire Speed *Winch Down* 1.2 m/sec

Winch Up 1.5 m/sec

		Depth	*Wire out*	
Time Stop	13:30	2982	2900	m

Restart *Wire Speed* 0.3 m/sec *Tension* 3.60 ton

		Latitude	*Longitude*	*Depth*	*Wire out*	
Time Hit	13:38	04 ° 42.03 ' N	133 ° 42.17 ' E	2980	2952	m

Tension Min 2.24 ton *Max* 5.92 ton

Time Surfaced 14:15

Time End 14:25 **Total** 1:50

Remarks

Pilot Length 0 cm **Core Length** 985 cm **No. of Section** 11

Length of Section 98, 195, 292, 394, 478, 578, 677, 777, 874, 974, 985

Main Lithology light gray coloured calcareous ooze with calcareous turbidite

Piston Core Log

Cruise KH92-1 **Station** 6BX **Date** 2/19/1992

Location Ayu Trough

Weather clear **Wind** 5.1 m/sec **SeaSwell** moderate

Type of PC Box Core (L)

Main wire _____ m **Pilot wire** _____ m **Free fall** _____ m

Time Start 14:34

		Latitude	*Longitude*	*Depth*
Time Lowered	14:38	04 ° 42.21 ' N	133 ° 41.80 ' E	2948 m

Wire Speed *Winch Down* 1.0 m/sec

Winch Up 1.5 m/sec

		Depth	*Wire out*
Time Stop	15:34	2976 m	2800 m

Restart *Wire Speed* 0.5 m/sec *Tension* 3.10 ton

		Latitude	*Longitude*	*Depth*	*Wire out*
Time Hit	15:40	04 ° 41.95 ' N	133 ° 42.09 ' E	2975 m	2964 m

Tension Min 2.26 ton *Max* 3.74 ton

Time Surfaced 16:20

Time End 16:30 **Total** 2:00

Remarks

Pilot Length _____ cm **Core Length** 31 cm **No. of Section** ____

Length of Section _____

Main Lithology bright yellowish coloured calcareous ooze

CORE: KH92-1 1BX

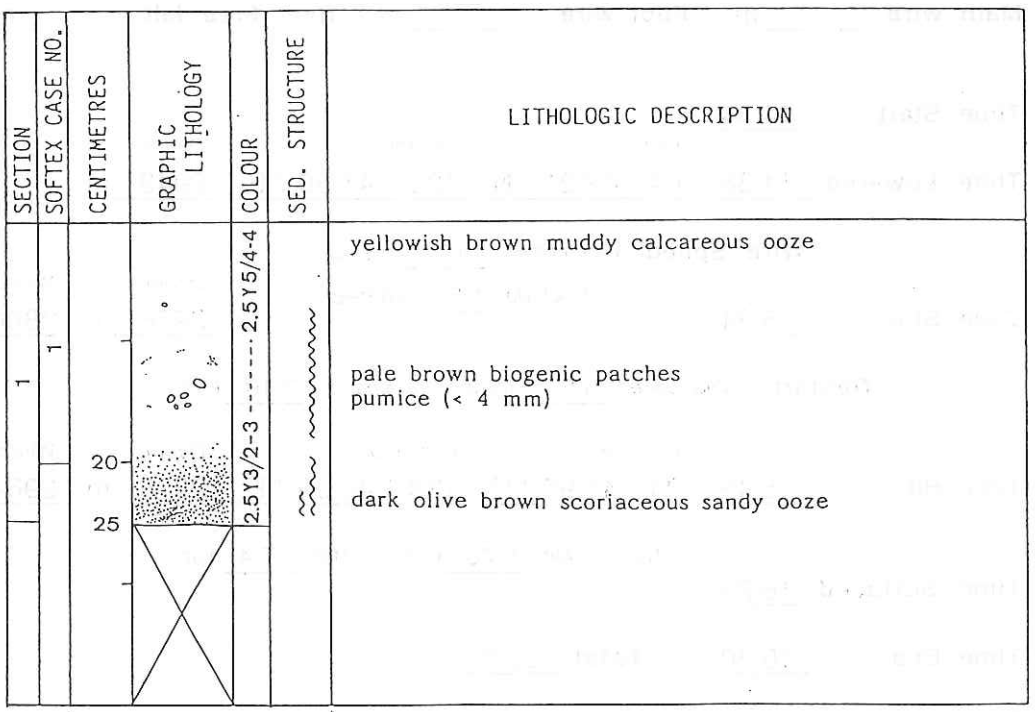

Fig. 14.1 Visual description of box core KH92-1 1BX.

CORE: KH92-1 2PC (0-100)

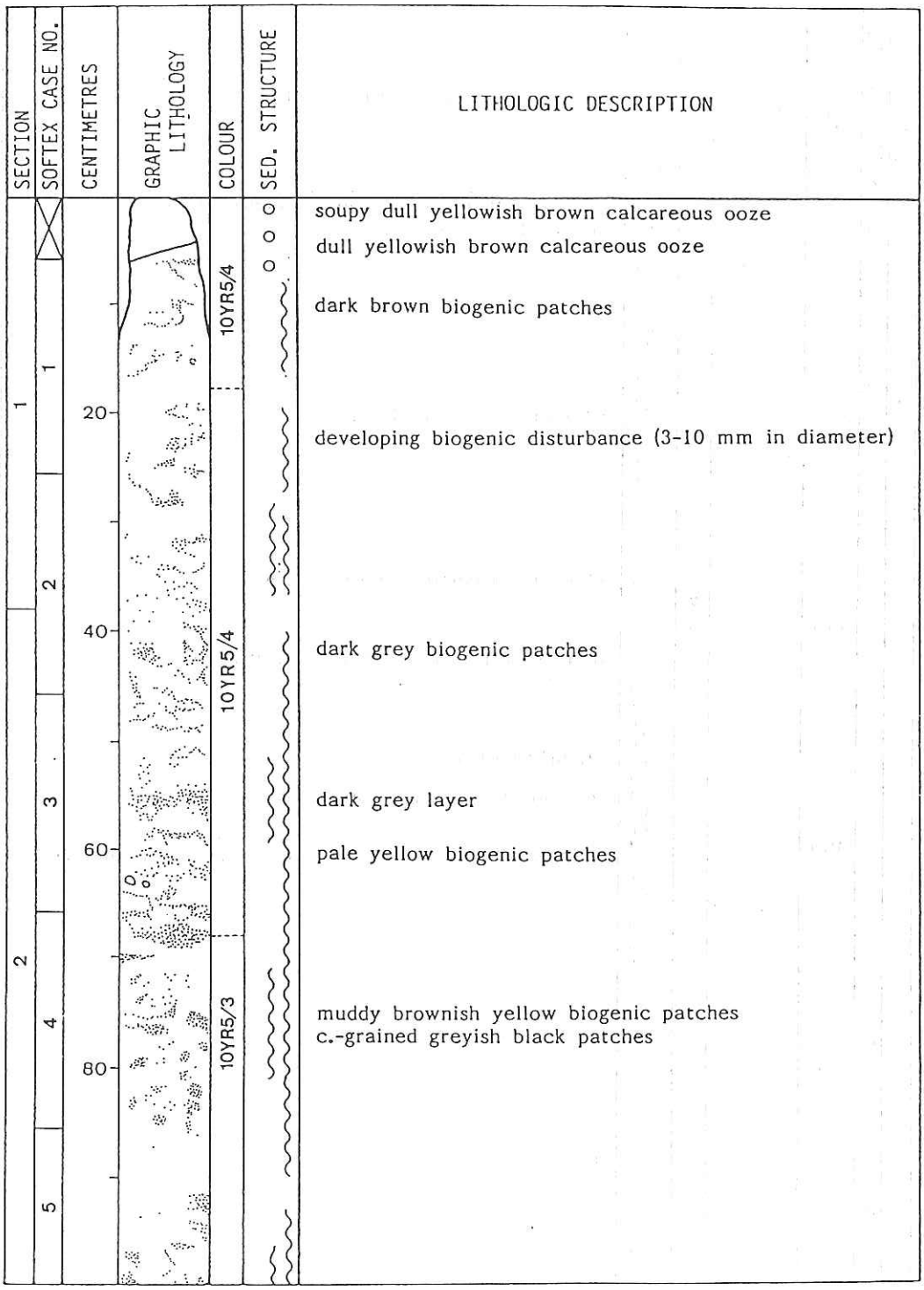

Fig. 14.2a Visual description of piston core KH92-1 2PC (0 - 100 cm).

CORE: KH92-1 2PC (100-200)

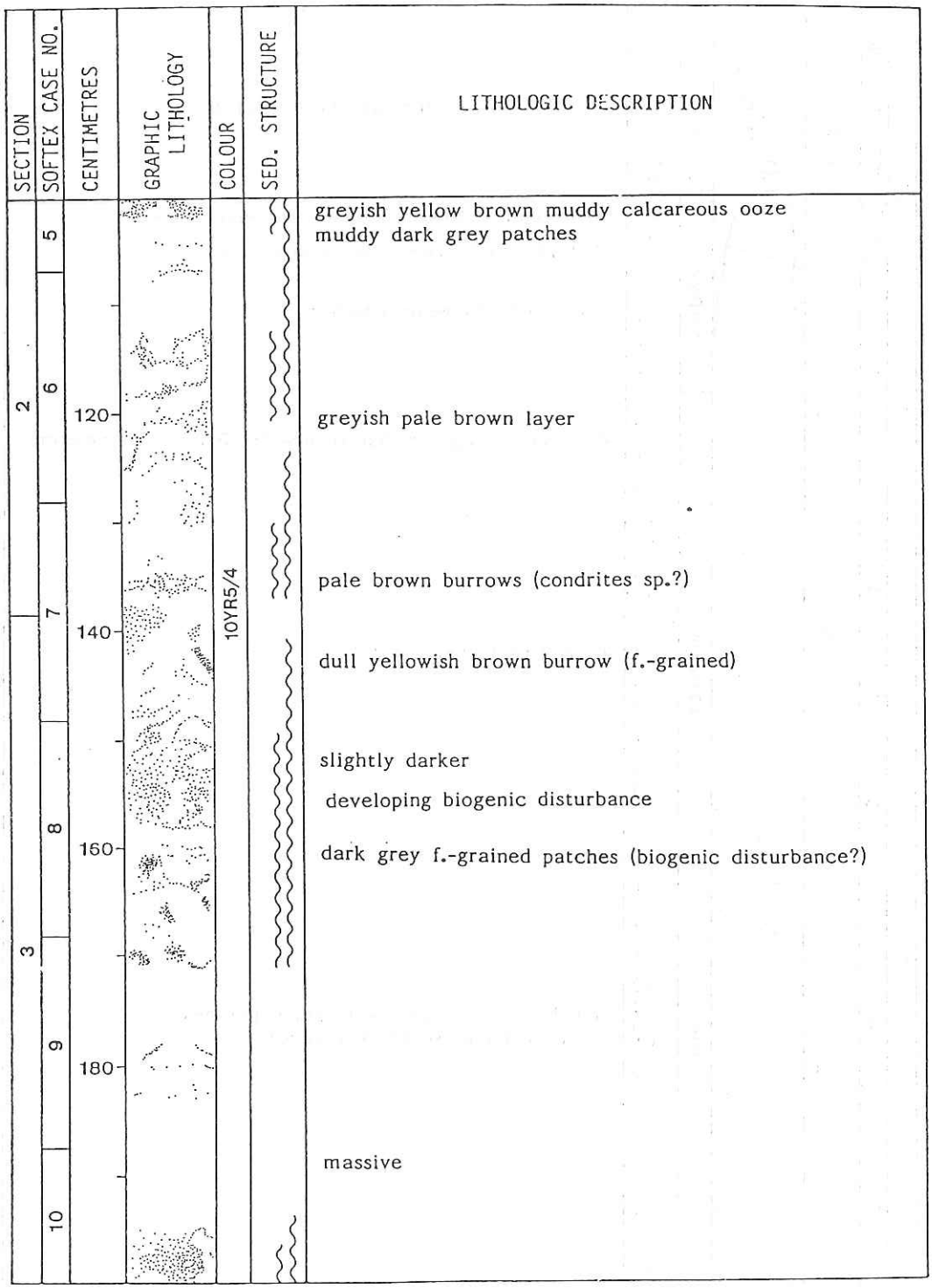

Fig. 14.2b Visual description of piston core KH92-1 2PC (100 - 200 cm).

CORE: KH92-1 2PC (200-300)

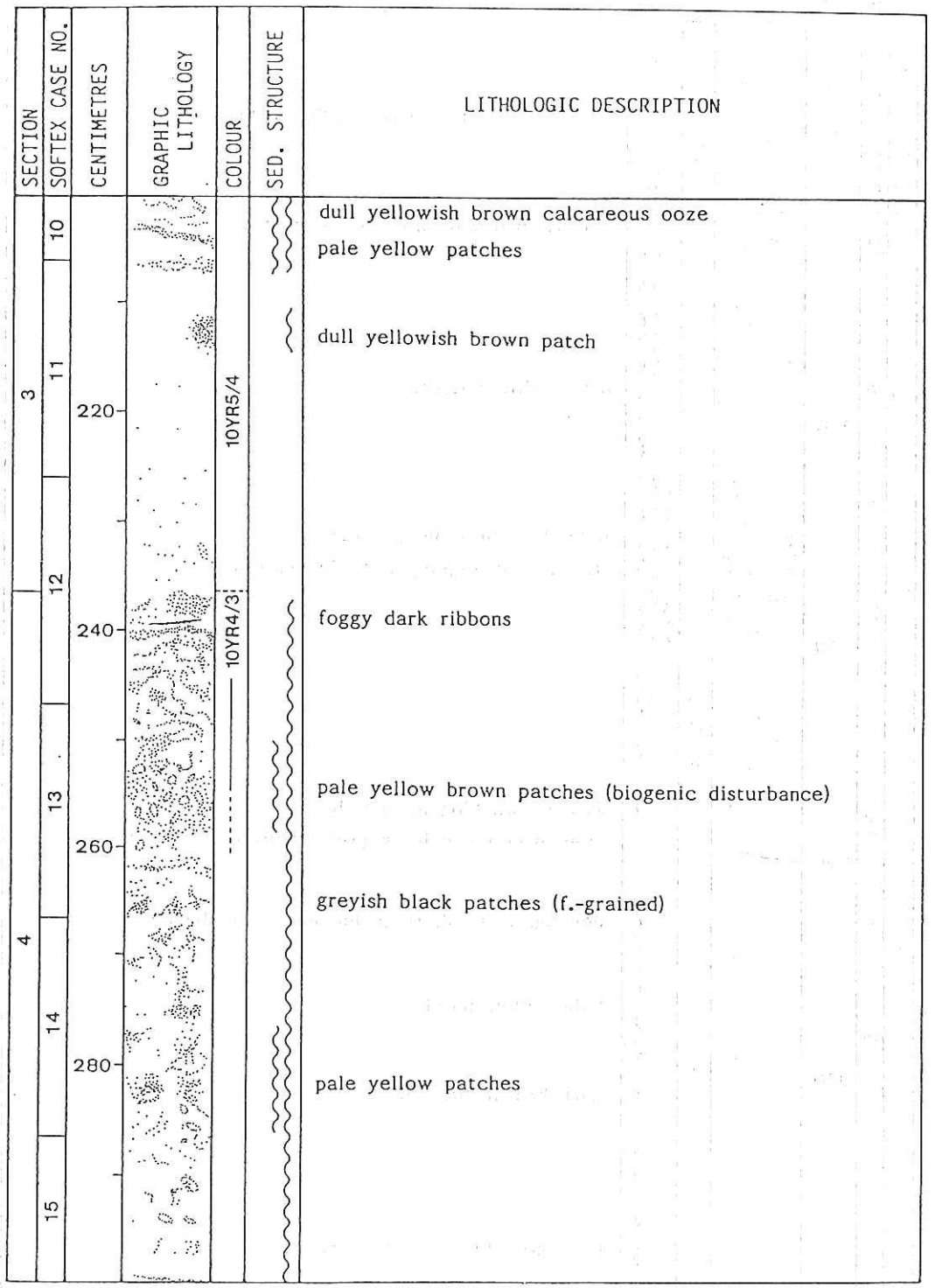

Fig. 14.2c Visual description of piston core KH92-1 2PC (200 - 300 cm).

CORE: KH92-1 2PC (300-400)

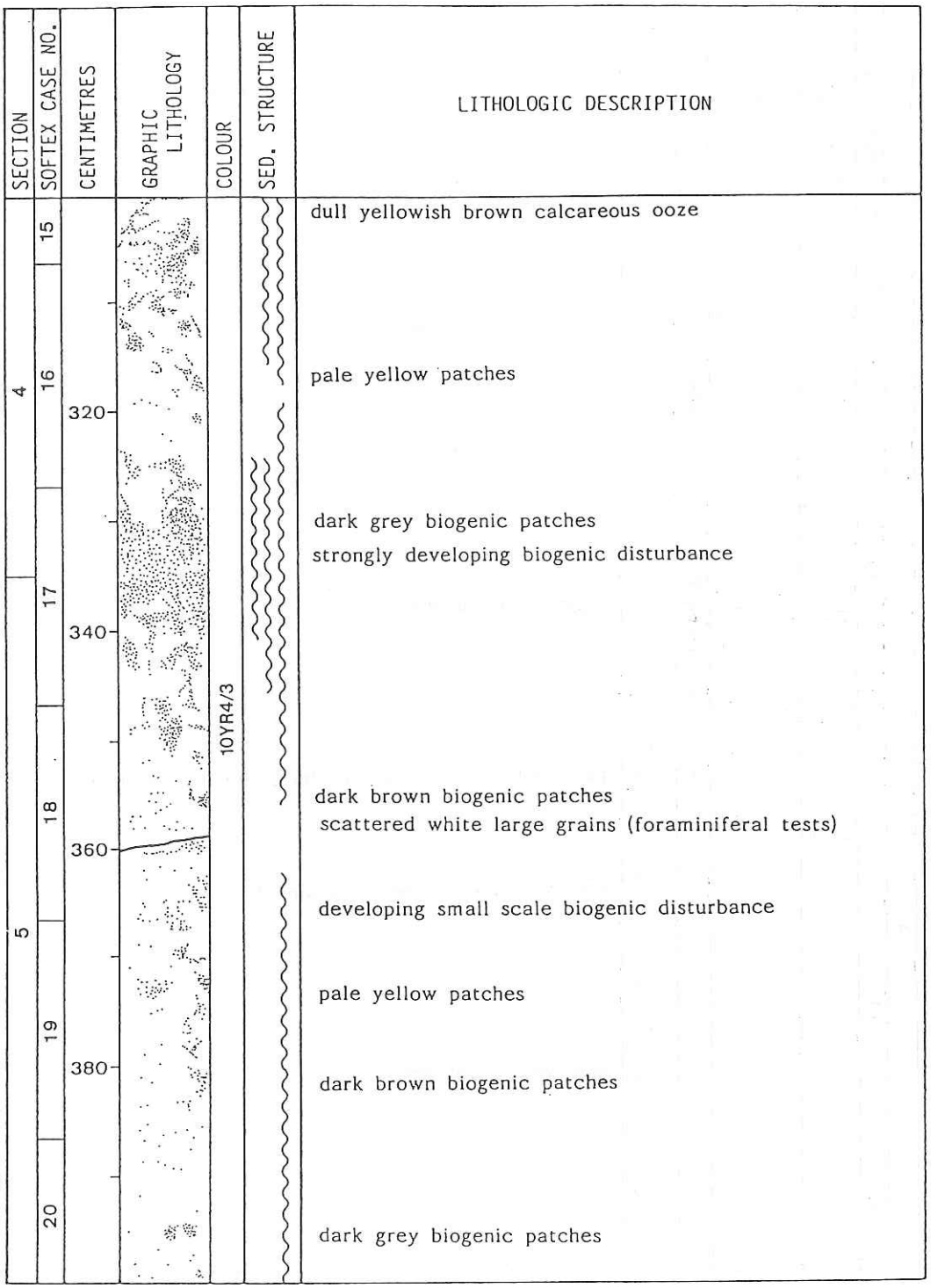

Fig. 14.2d Visual description of piston core KH92-1 2PC (300 - 400 cm).

CORE: KH92-1 2PC (400-500)

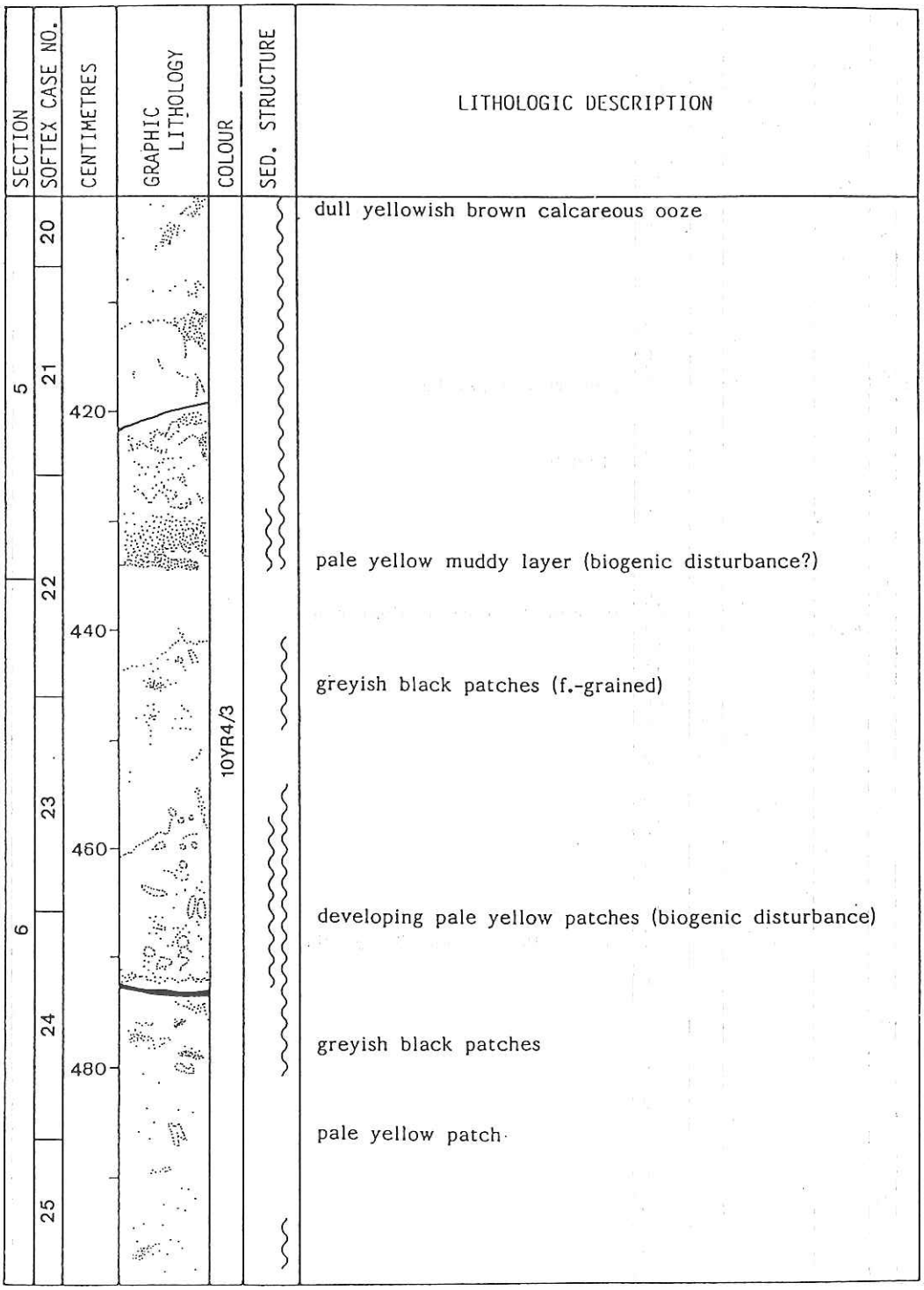

Fig. 14.2e Visual description of piston core KH92-1 2PC (400 - 500 cm).

CORE: KH92-1 2PC (500-600)

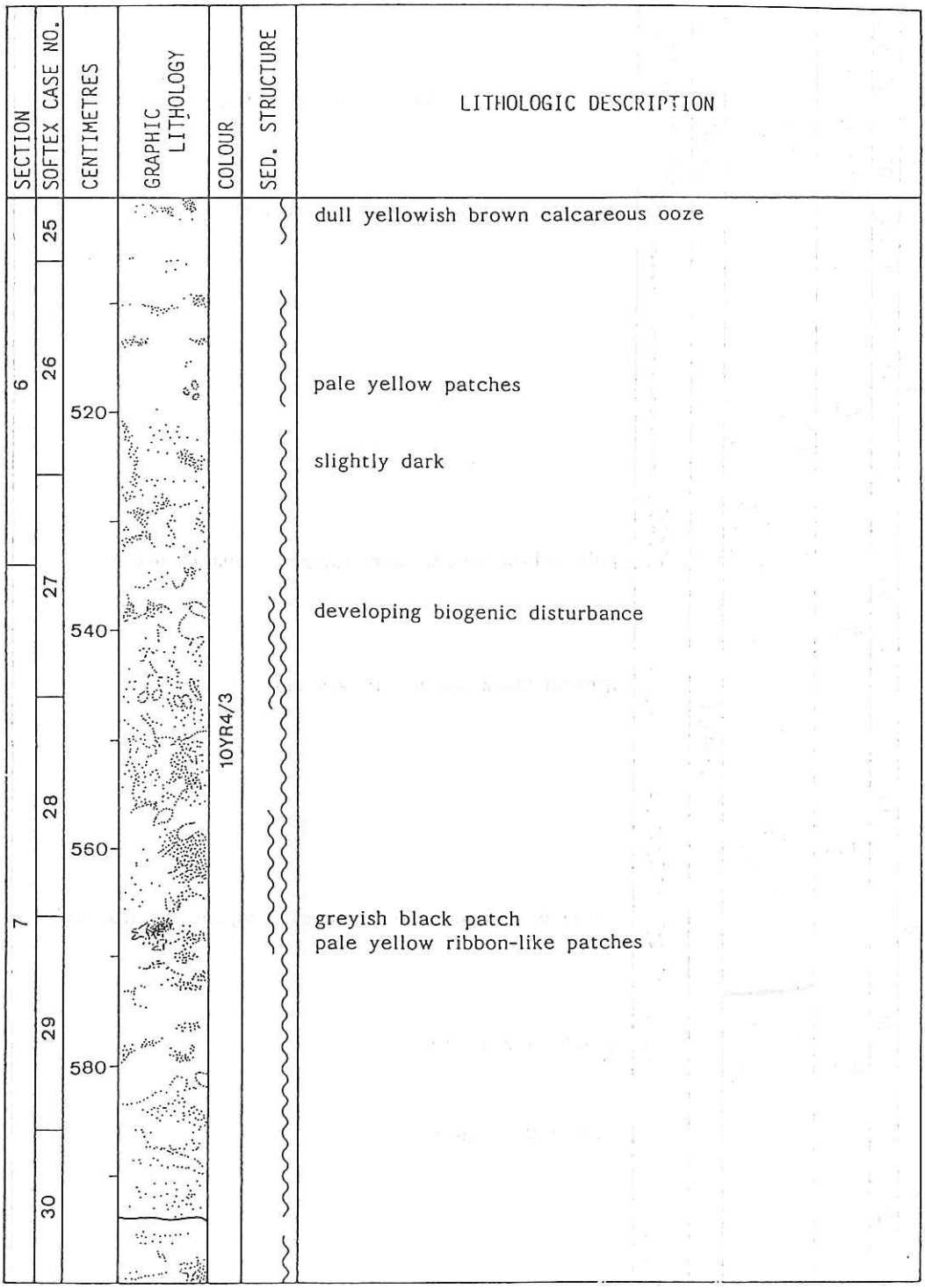

Fig. 14.2f Visual description of piston core KH92-1 2PC (500 - 600 cm).

CORE: KH92-1 2PC (600-700)

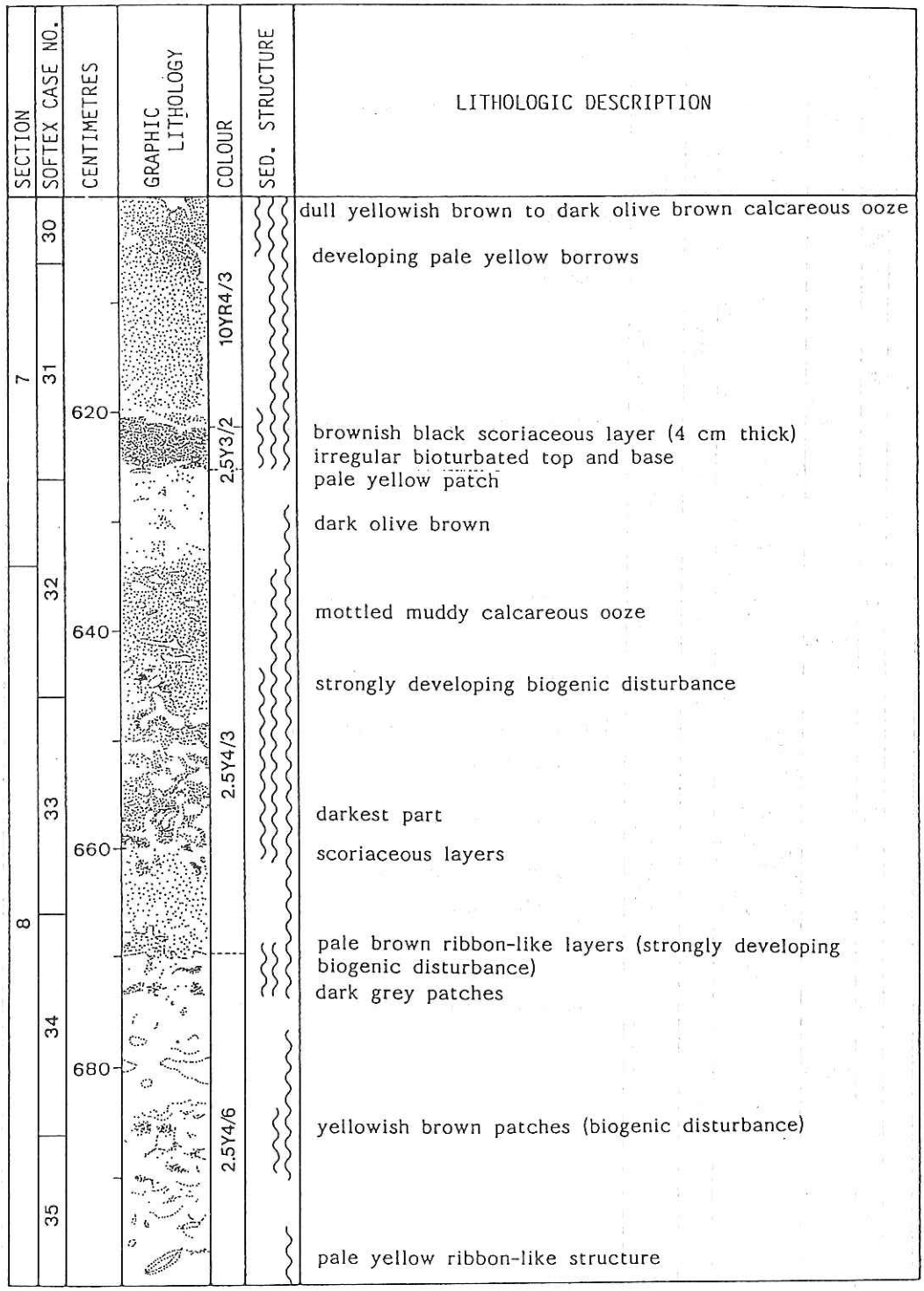

Fig. 14.2g Visual description of piston core KH92-1 2PC (600 - 700 cm).

CORE: KH92-1 2PC (700-800)

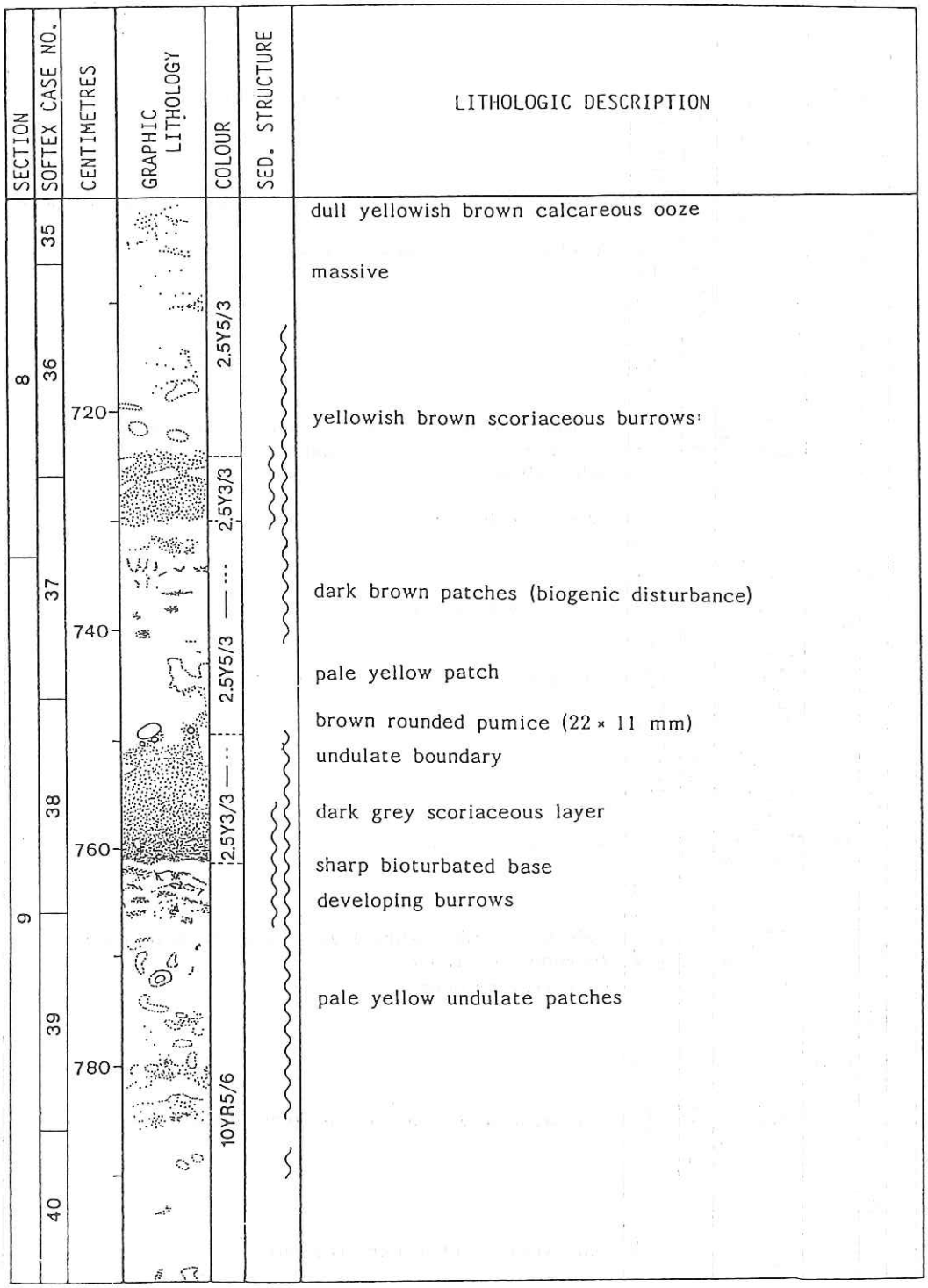

Fig. 14.2h Visual description of piston core KH92-1 2PC (700 - 800 cm).

CORE: KH92-1 2PC (800-900)

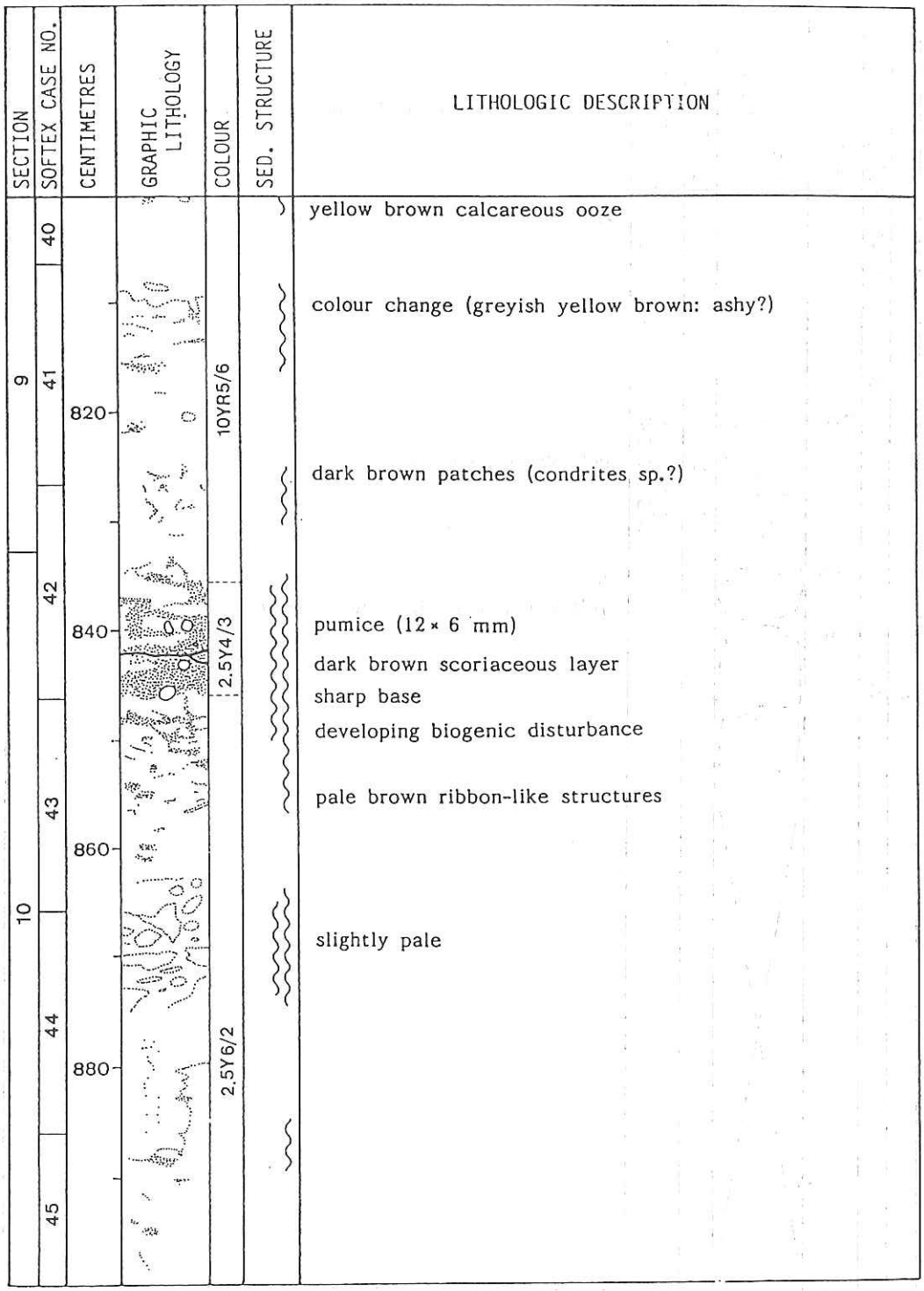

Fig. 14.2i Visual description of piston core KH92-1 2PC (800 - 900 cm).

CORE: KH92-1 2PC (900-933)

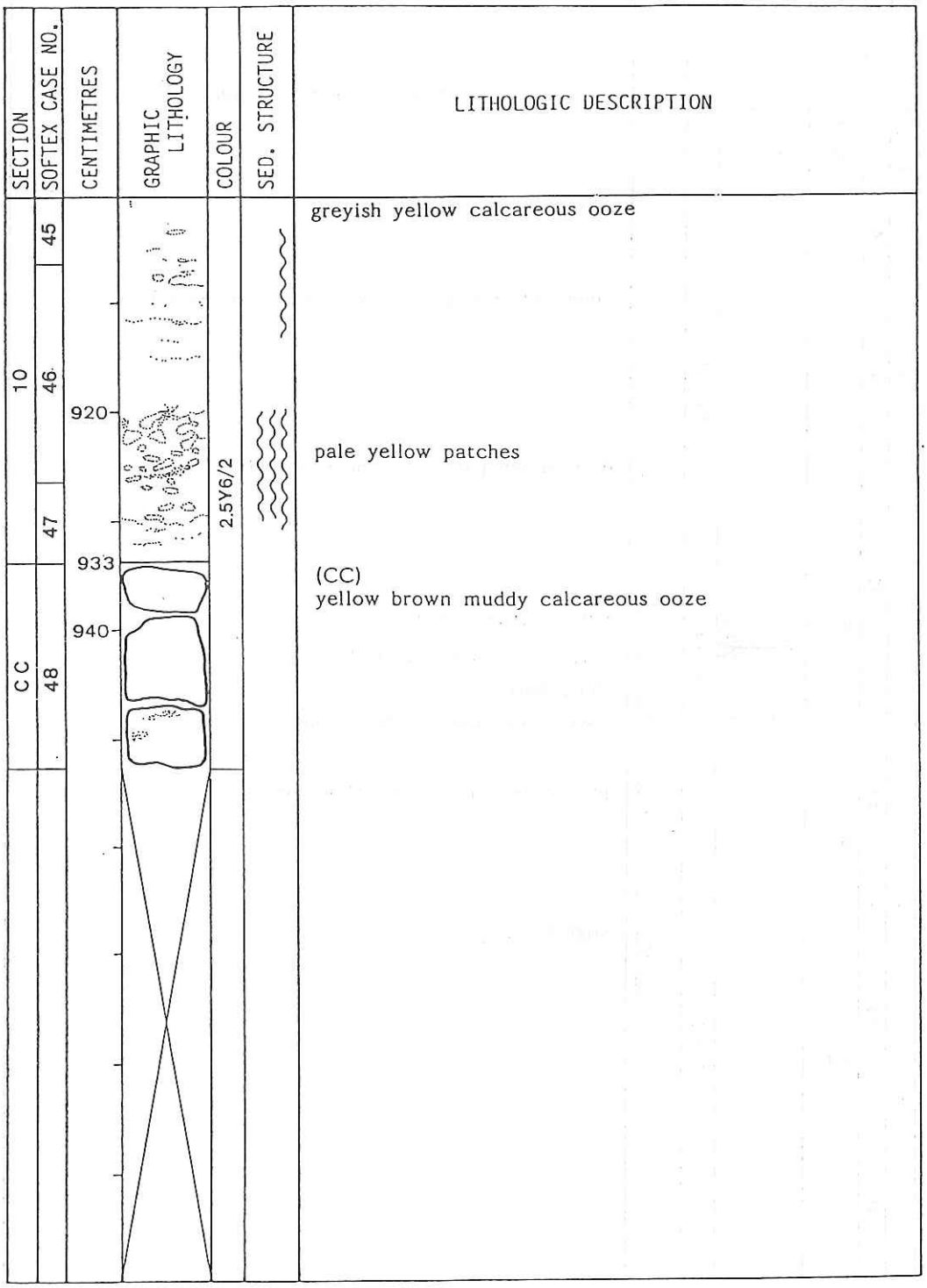

Fig. 14.2j Visual description of piston core KH92-1 2PC (900 - 933cm and core catcher sampre).

CORE: KH92-1 3aPC (0-100)

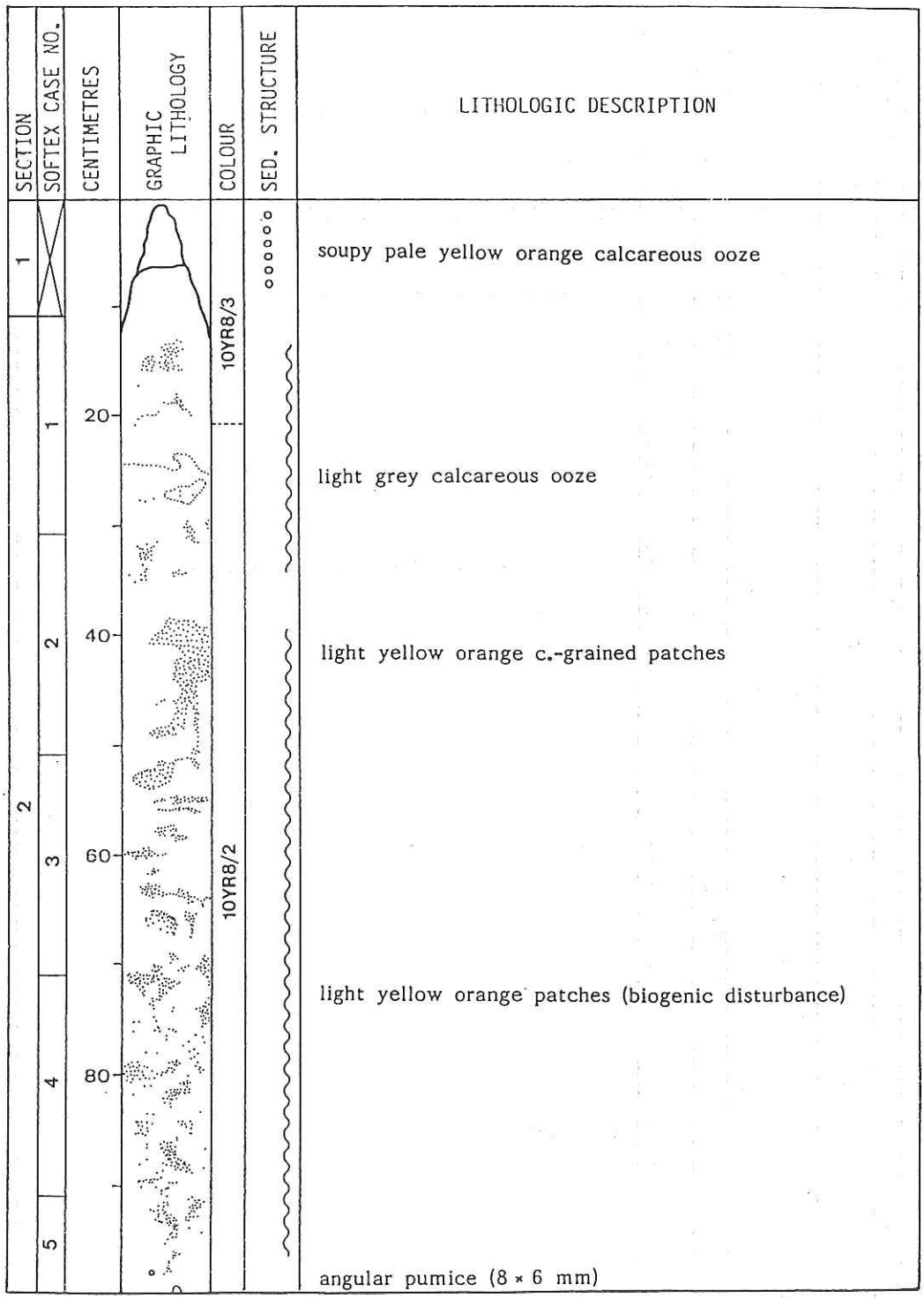

Fig. 14.3a Visual description of piston core KH92-1 3aPC (0 - 100 cm).

CORE: KH92-1 3aPC (100-200)

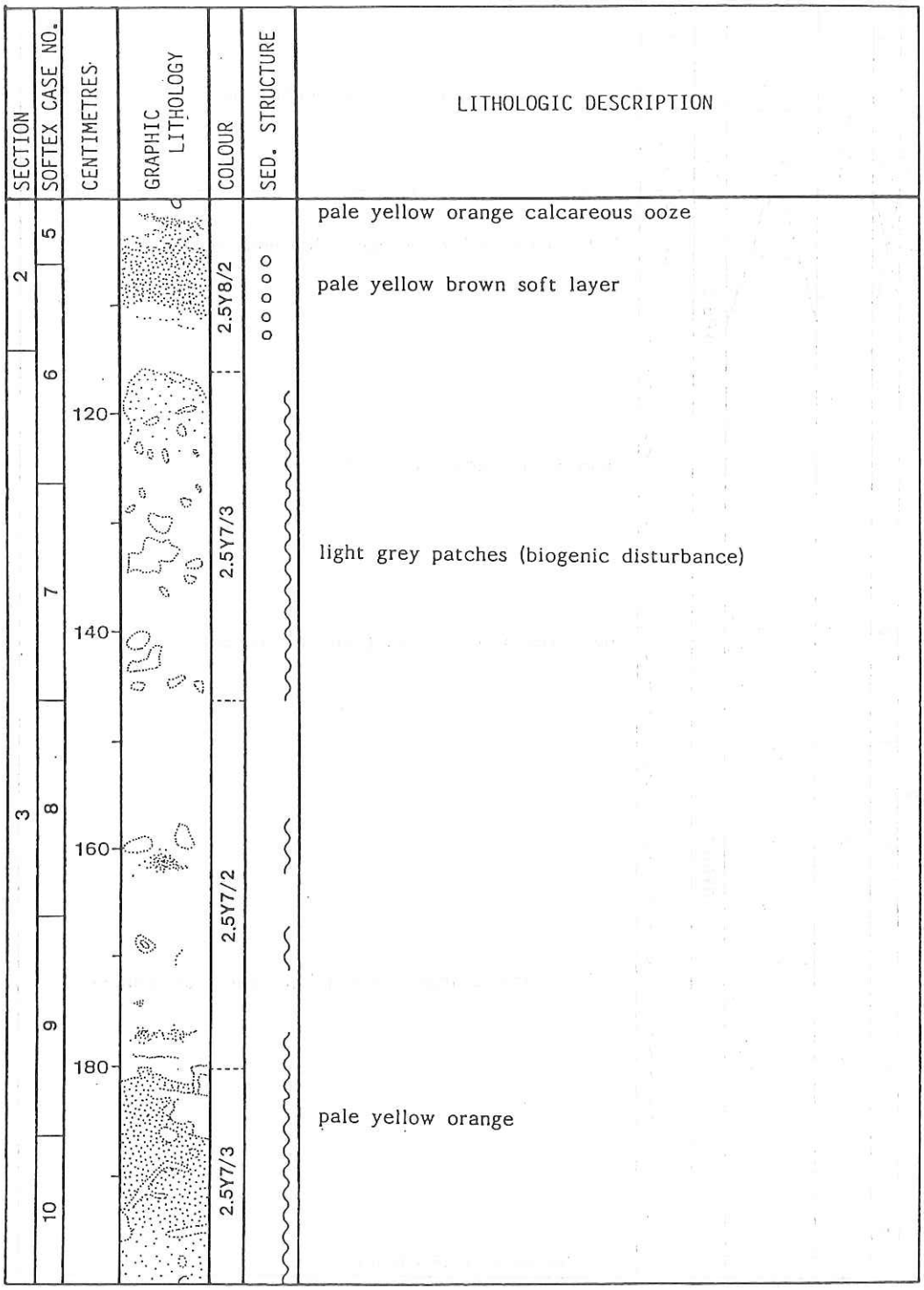

Fig. 14.3b Visual description of piston core KH92-1 3aPC (100 - 200 cm).

CORE: KH92-1 3aPC (200-300)

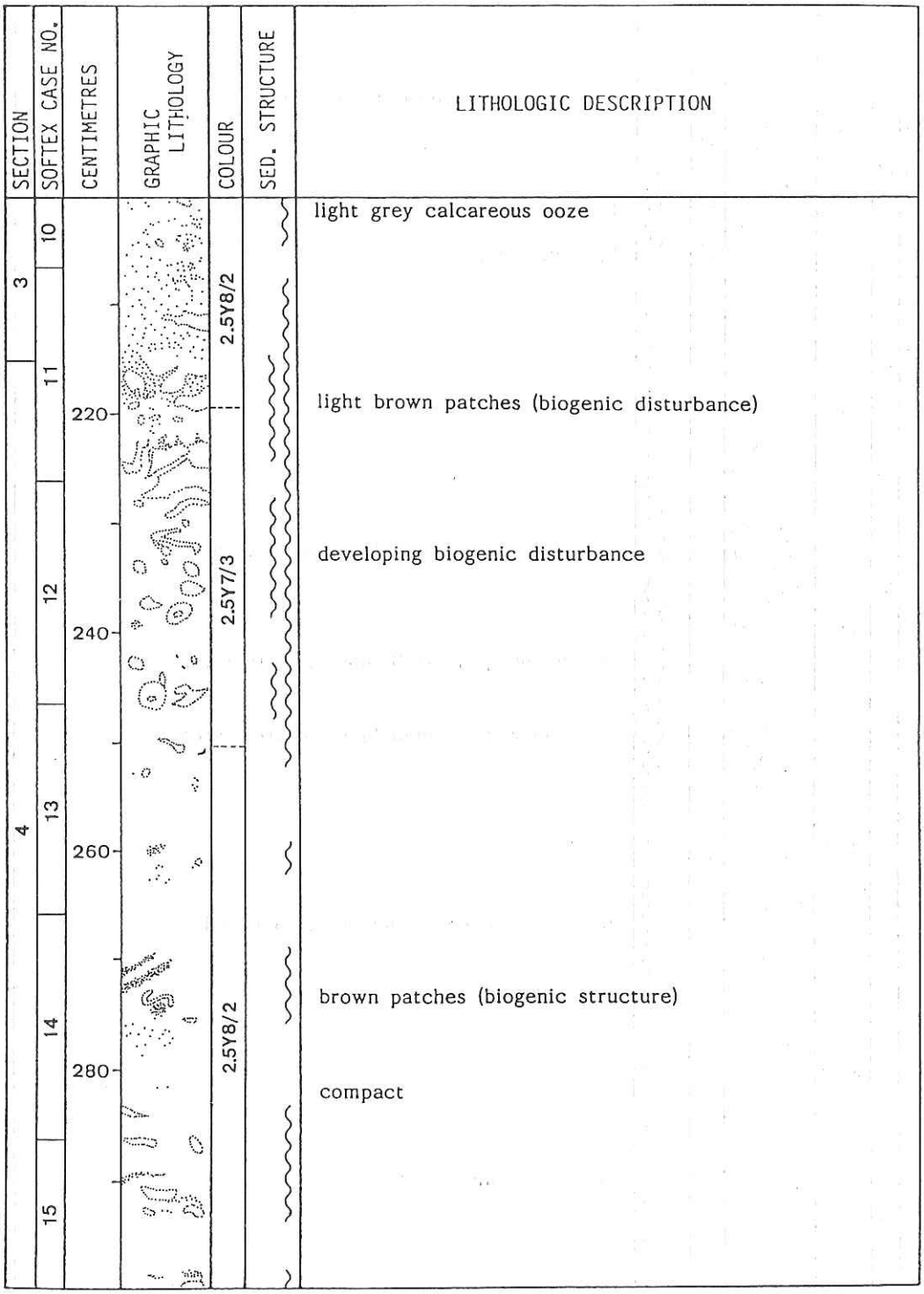

Fig. 14.3c Visual description of piston core KH92-1 3aPC (200 - 300 cm).

CORE: KH92-1 3aPC (300-400)

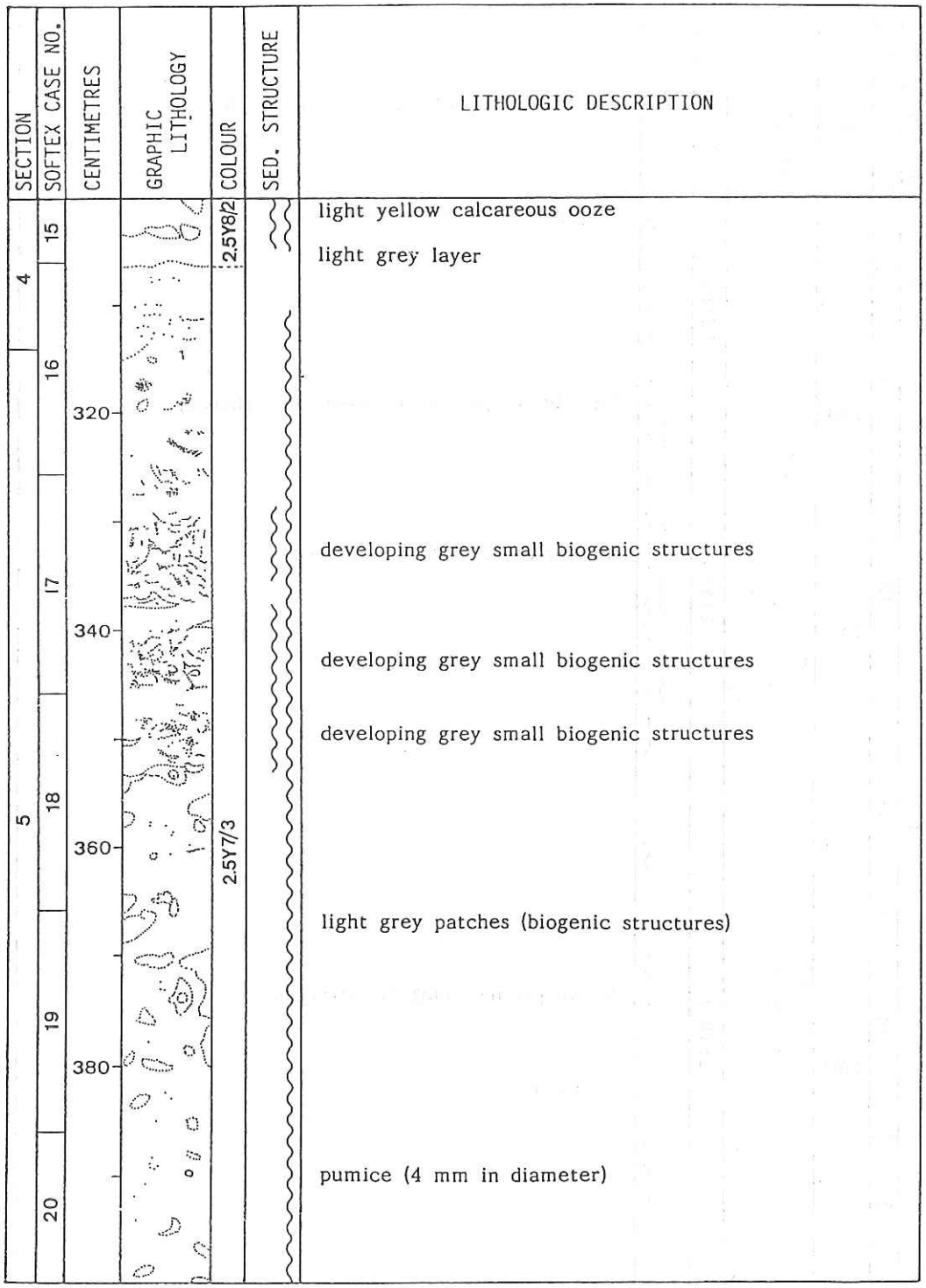

Fig. 14.3d Visual description of piston core KH92-1 3aPC (300 - 400 cm).

CORE: KH92-1 3aPC (400-500)

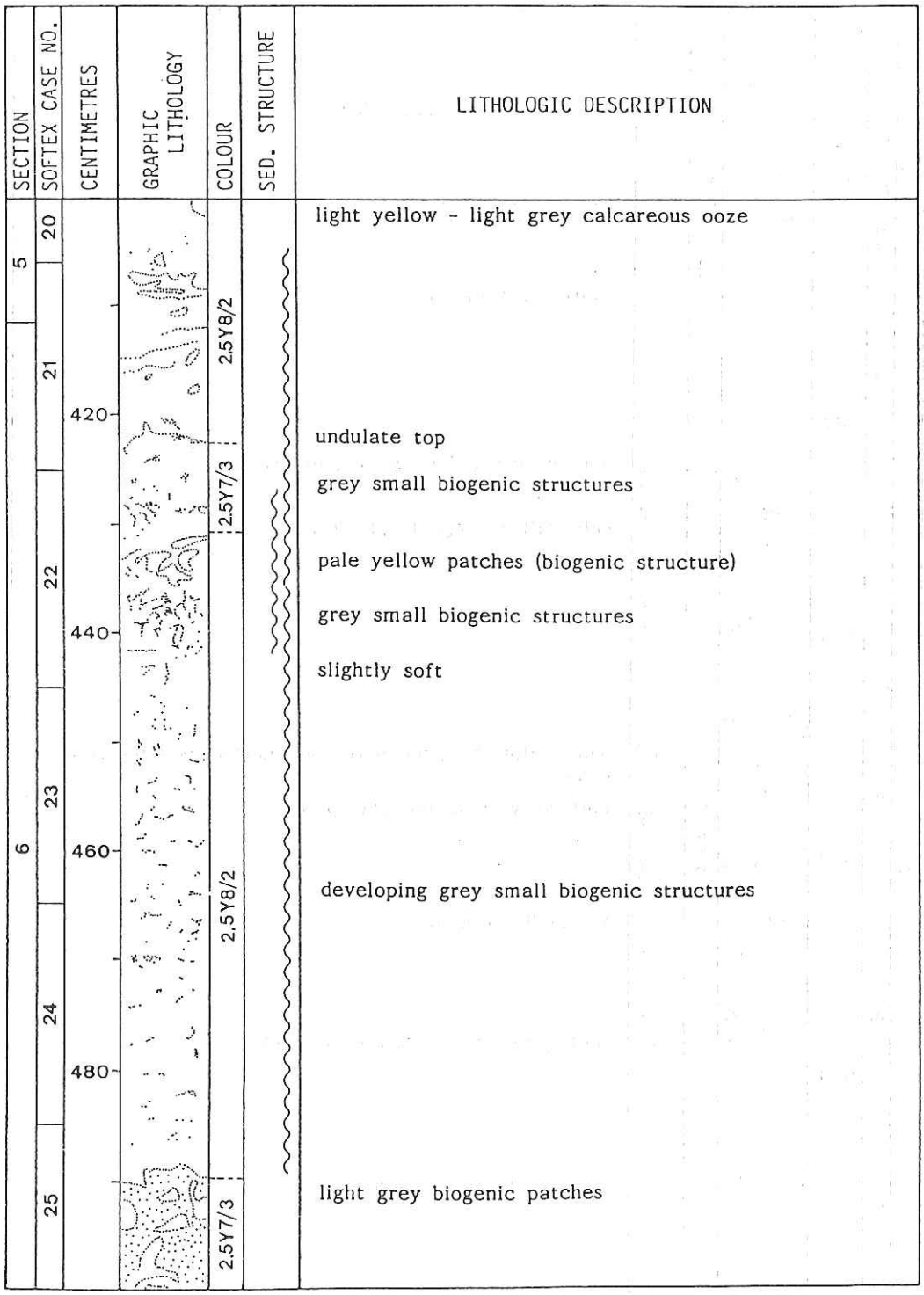

Fig. 14.3e Visual description of piston core KH92-1 3aPC (400 - 500 cm).

CORE: KH92-1 3aPC (500-600)

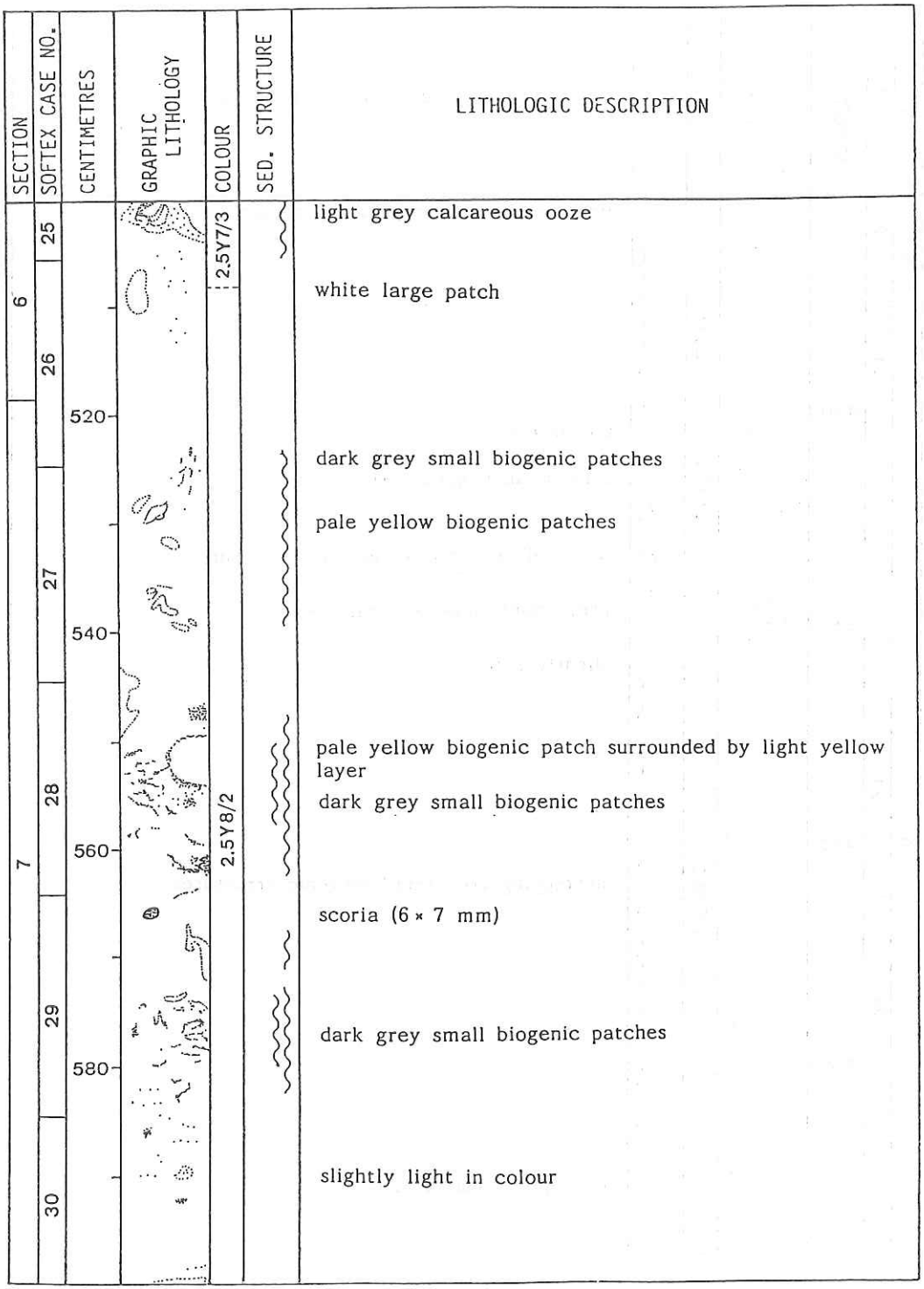

Fig. 14.3f Visual description of piston core KH92-1 3aPC (500 - 600 cm).

CORE: KH92-1 3aPC (600-700)

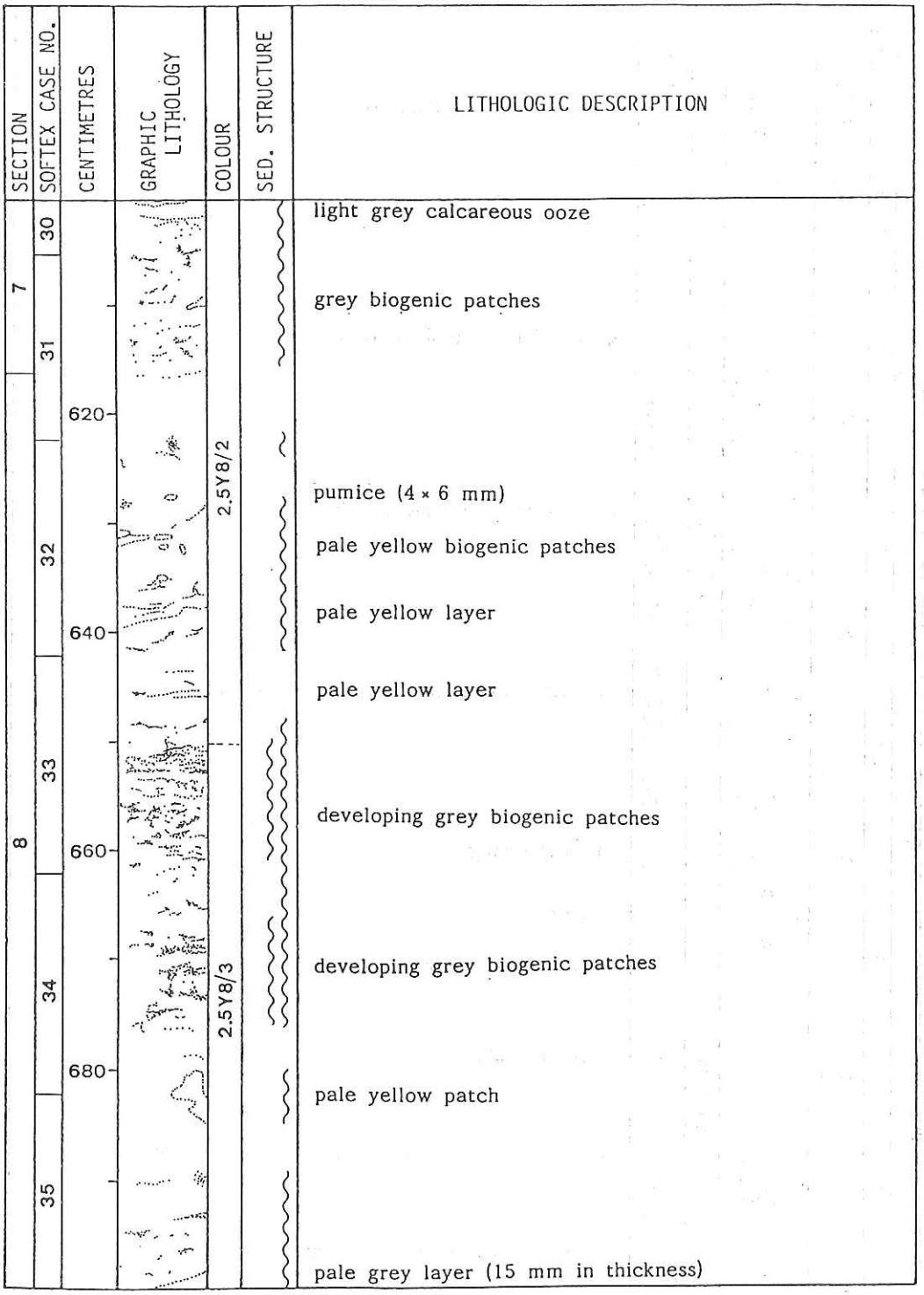

Fig. 14.3g Visual description of piston core KH92-13aPC (600 - 700 cm).

CORE: KH92-1 3aPC (700-800)

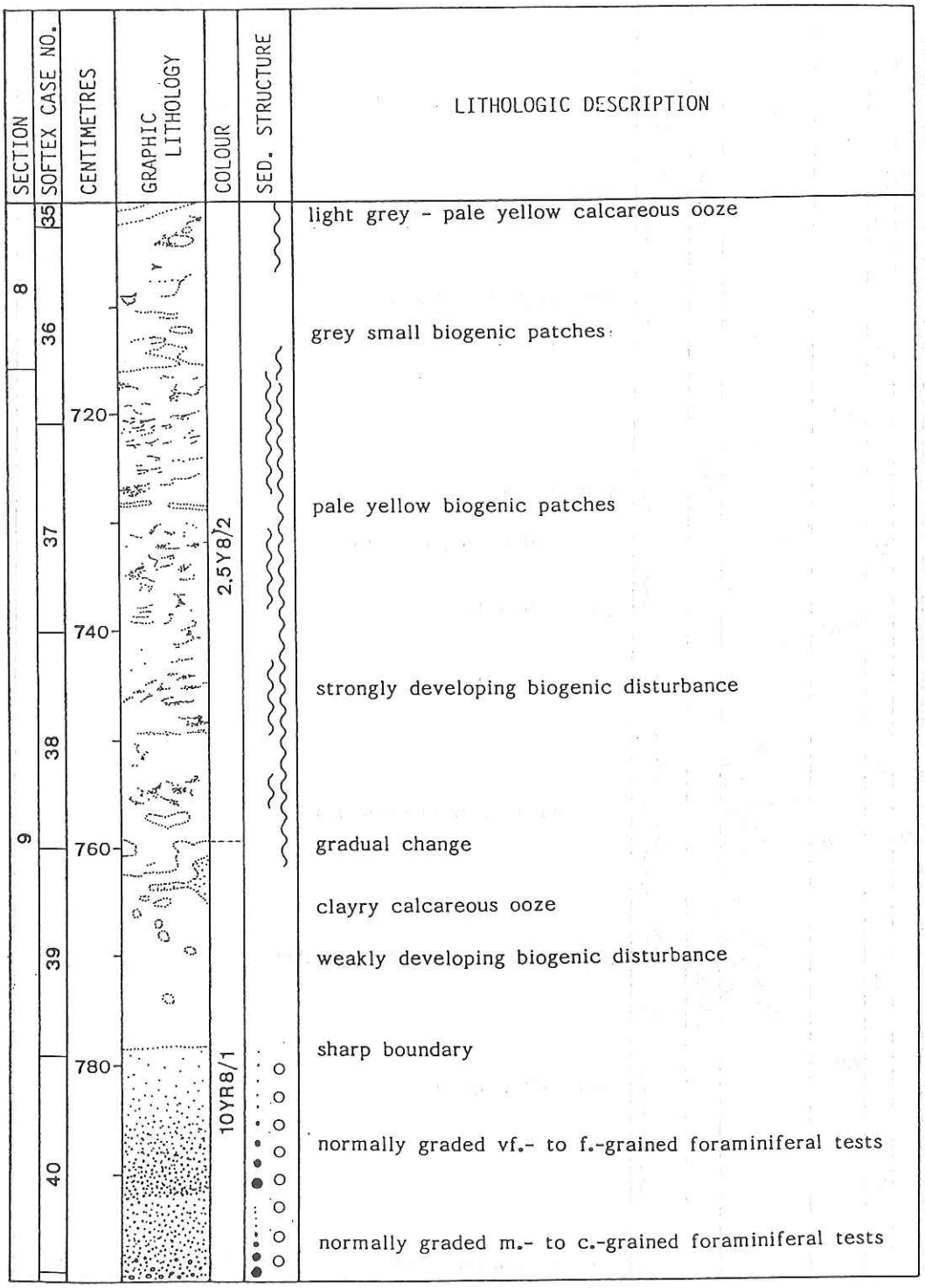

Fig. 14.3h Visual description of piston core KH92-13aPC (700 - 800 cm).

CORE: KH92-1 3aPC (800-900)

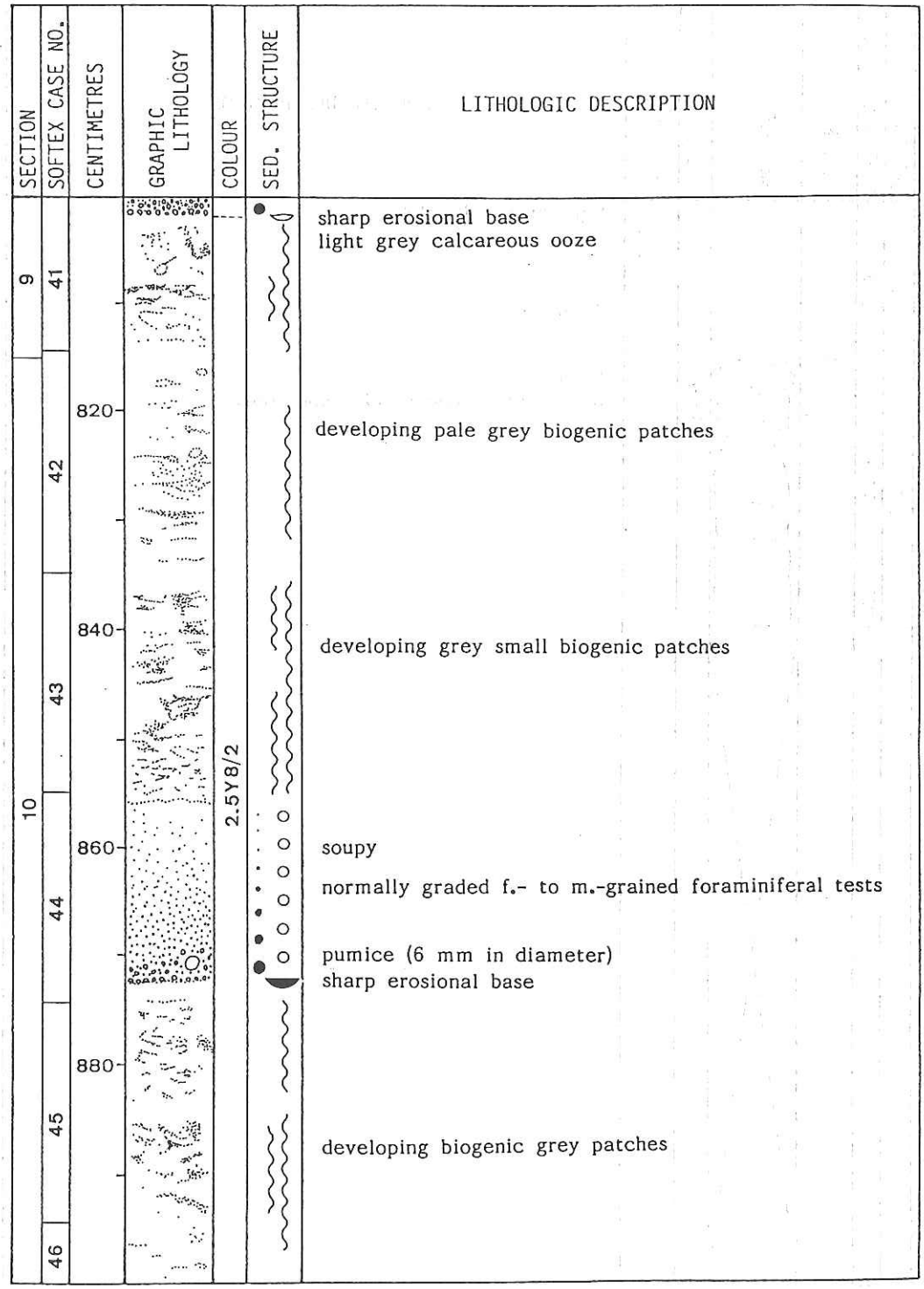

Fig. 14.3i Visual description of piston core KH92-1 3aPC (800 - 900 cm).

CORE: KH92-1 3aPC (900-915)

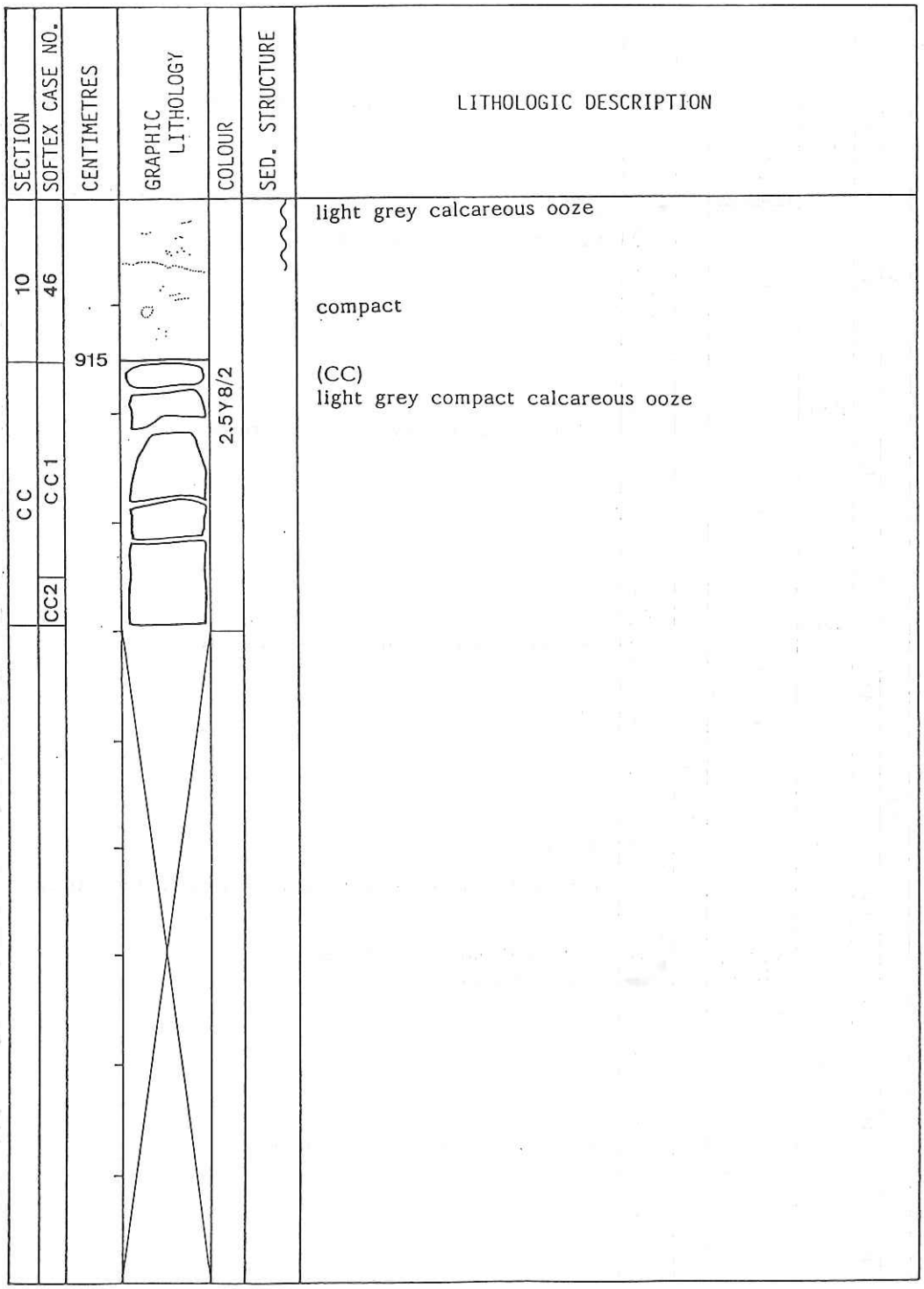

Fig. 14.3j Visual description of piston core KH92-1 3aPC (900 - 915 cm and core catch sample).

CORE: KH92-1 3cBX

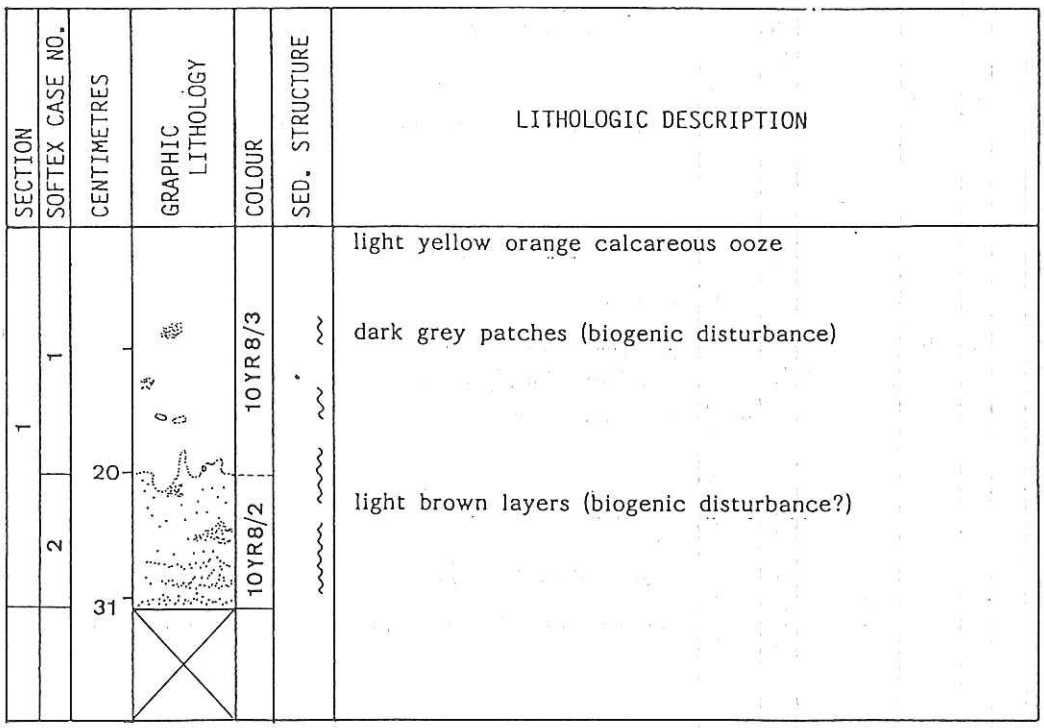

Fig. 14.4 Visual description of box core KH92-1 3cBX.

CORE: KH92-1 5aPC (0-100)

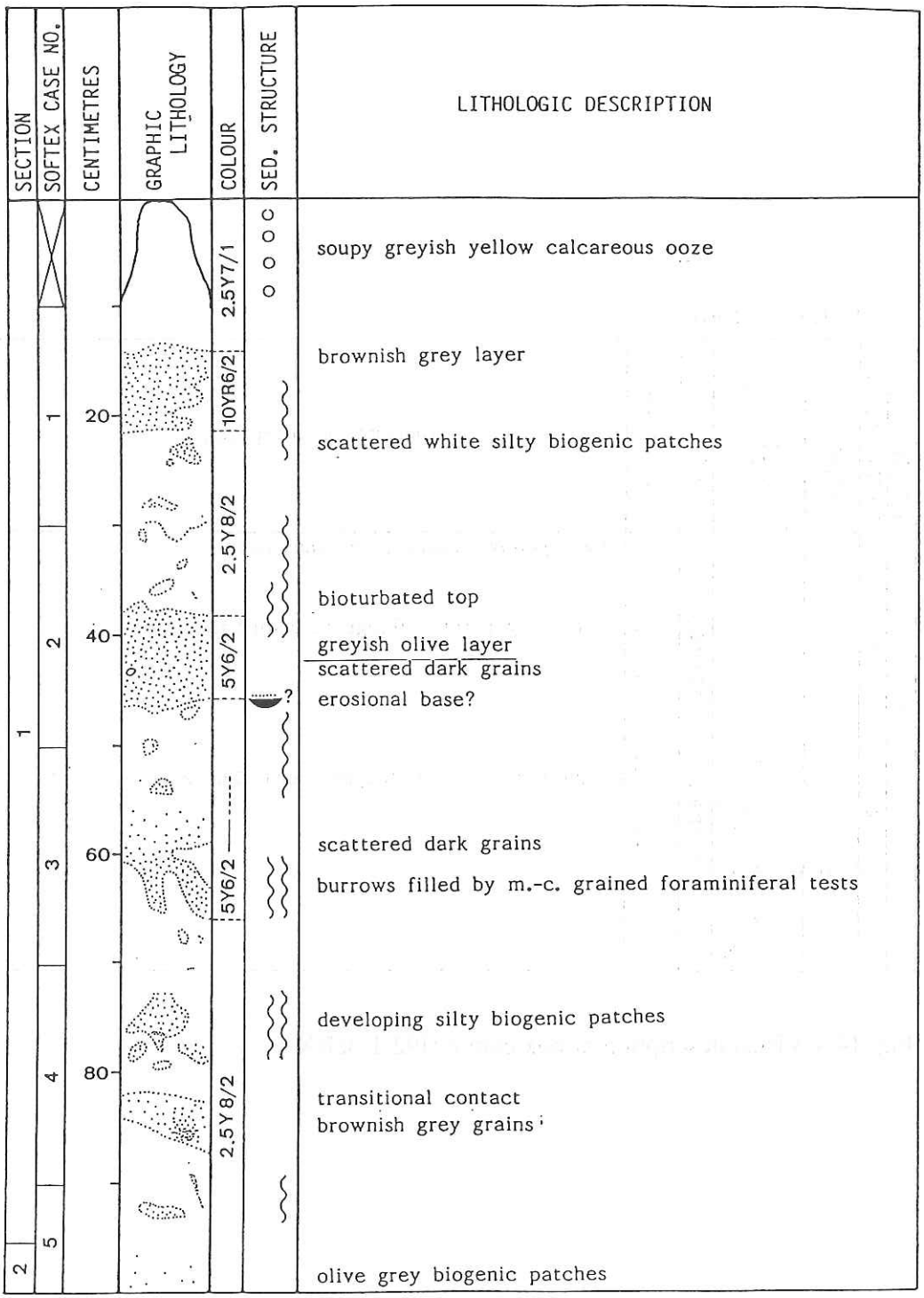

Fig. 14.5a Visual description of piston core KH92-1 5aPC (0 -100 cm).

CORE: KH92-1 5aPC (100-200)

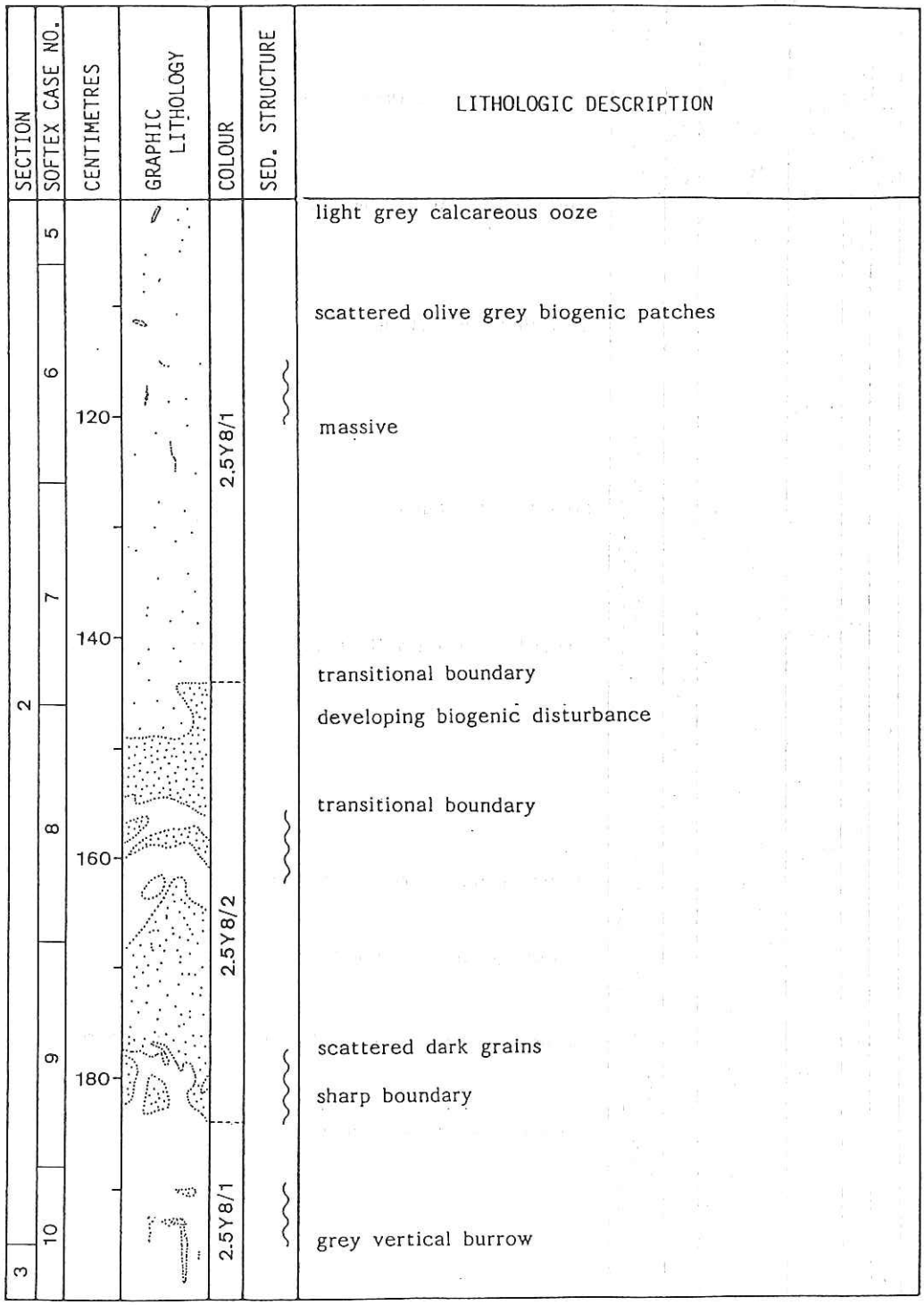

Fig. 14.5b Visual description of piston core KH92-1 5aPC (100 - 200 cm).

CORE: KH92-1 5aPC (200-300)

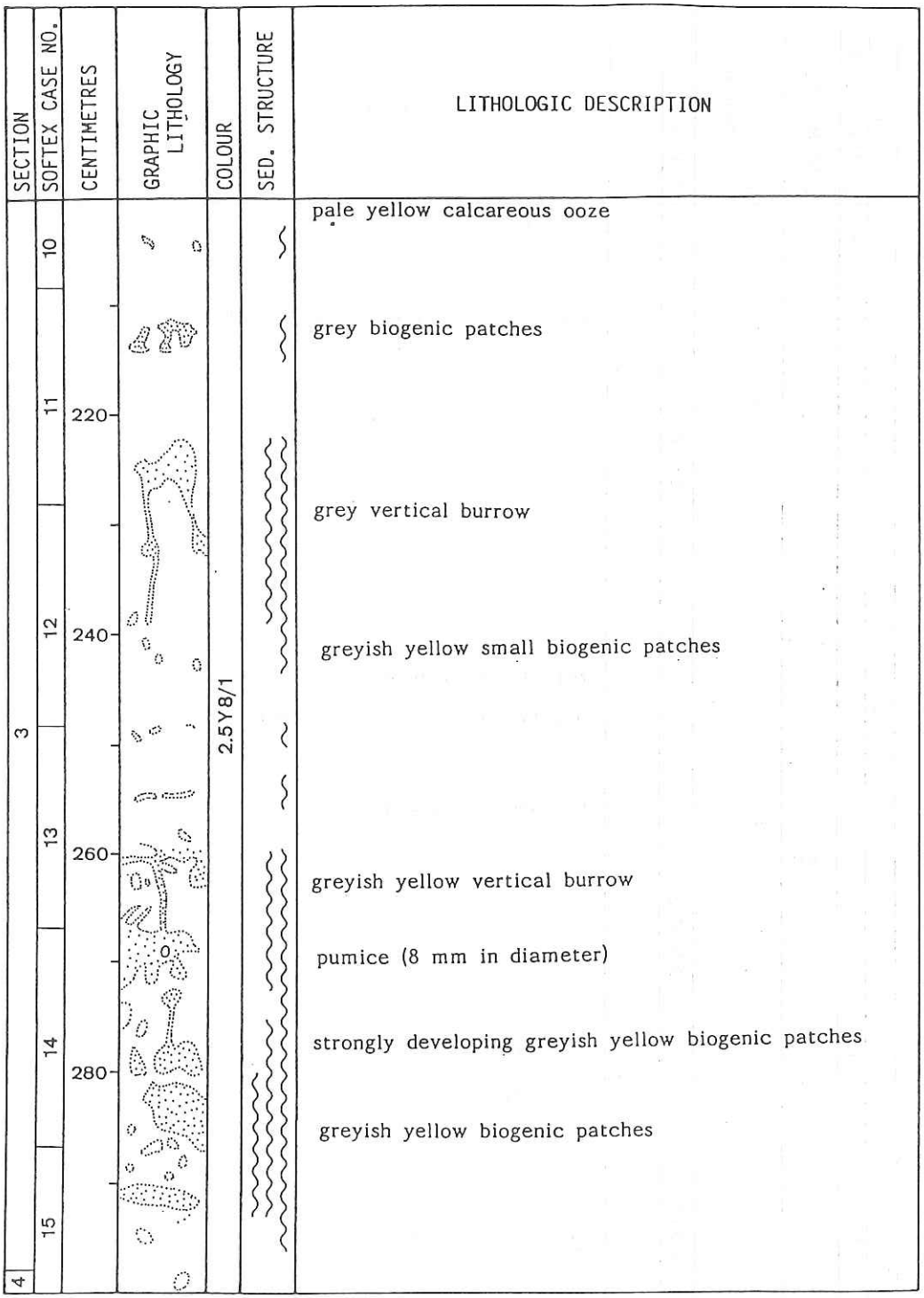

Fig. 14.5c Visual description of piston core KH92-1 5aPC (200 - 300 cm).

CORE: KH92-1 5aPC (300-400)

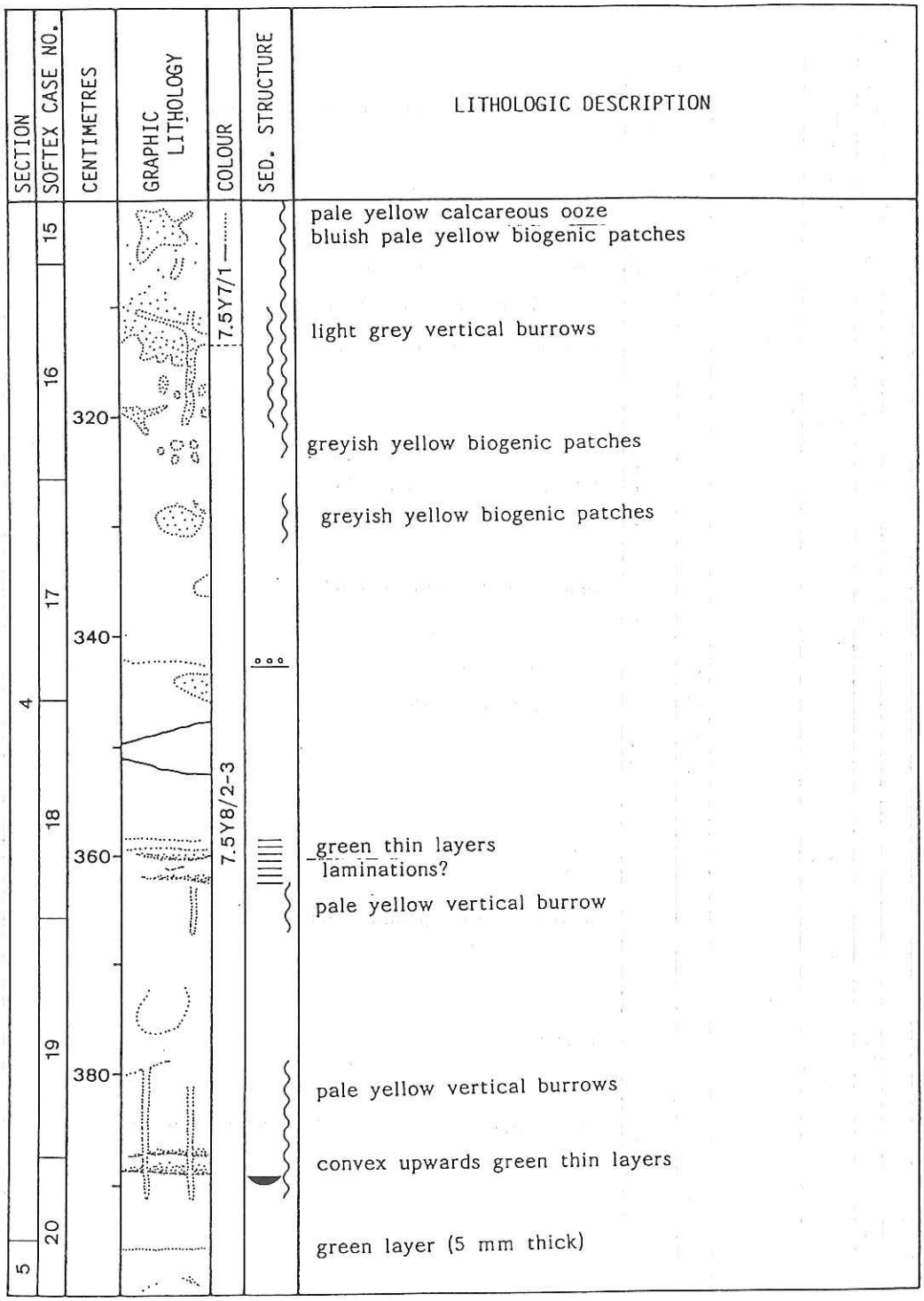

Fig. 14.5d Visual description of piston core KH92-1 5aPC (300 - 400 cm).

CORE: KH92-1 5aPC (400-500)

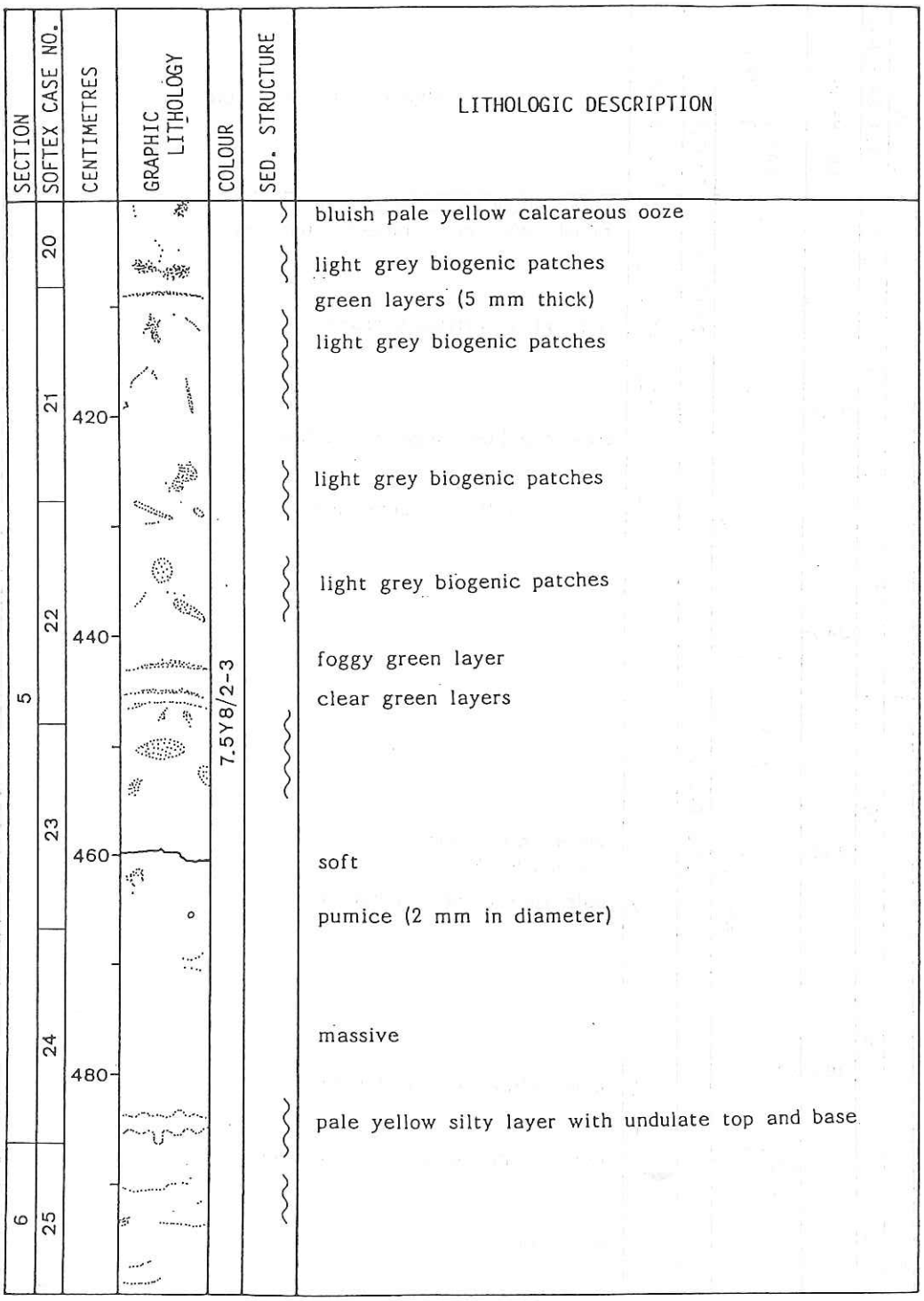

Fig. 14.5e Visual description of piston core KH92-1 5aPC (400 - 500 cm).

CORE: KH92-1 5aPC (500-600)

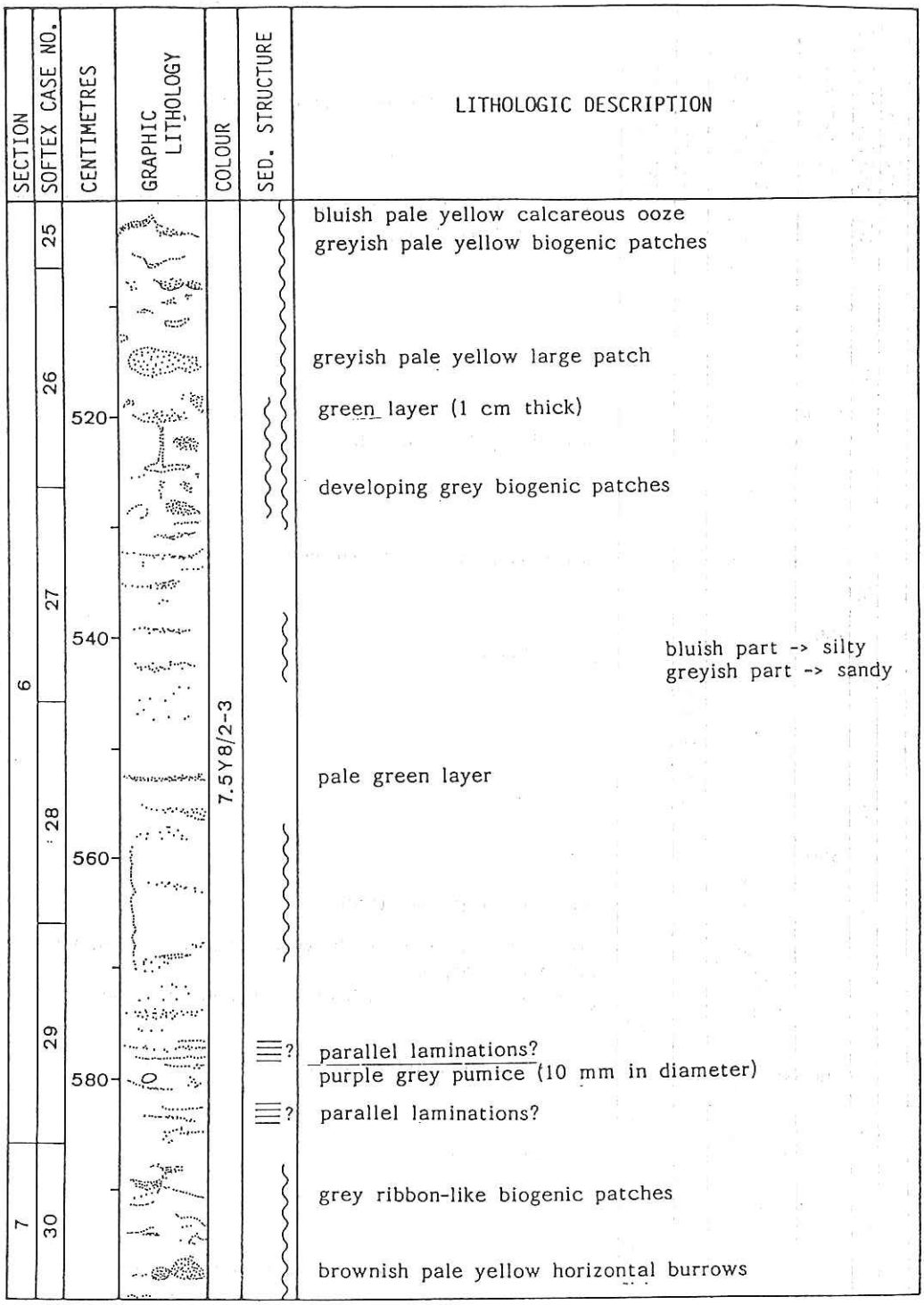

Fig. 14.5f Visual description 0f piston core KH92-1 5aPC (500 - 600 cm).

CORE: KH92-1 5aPC (600-700)

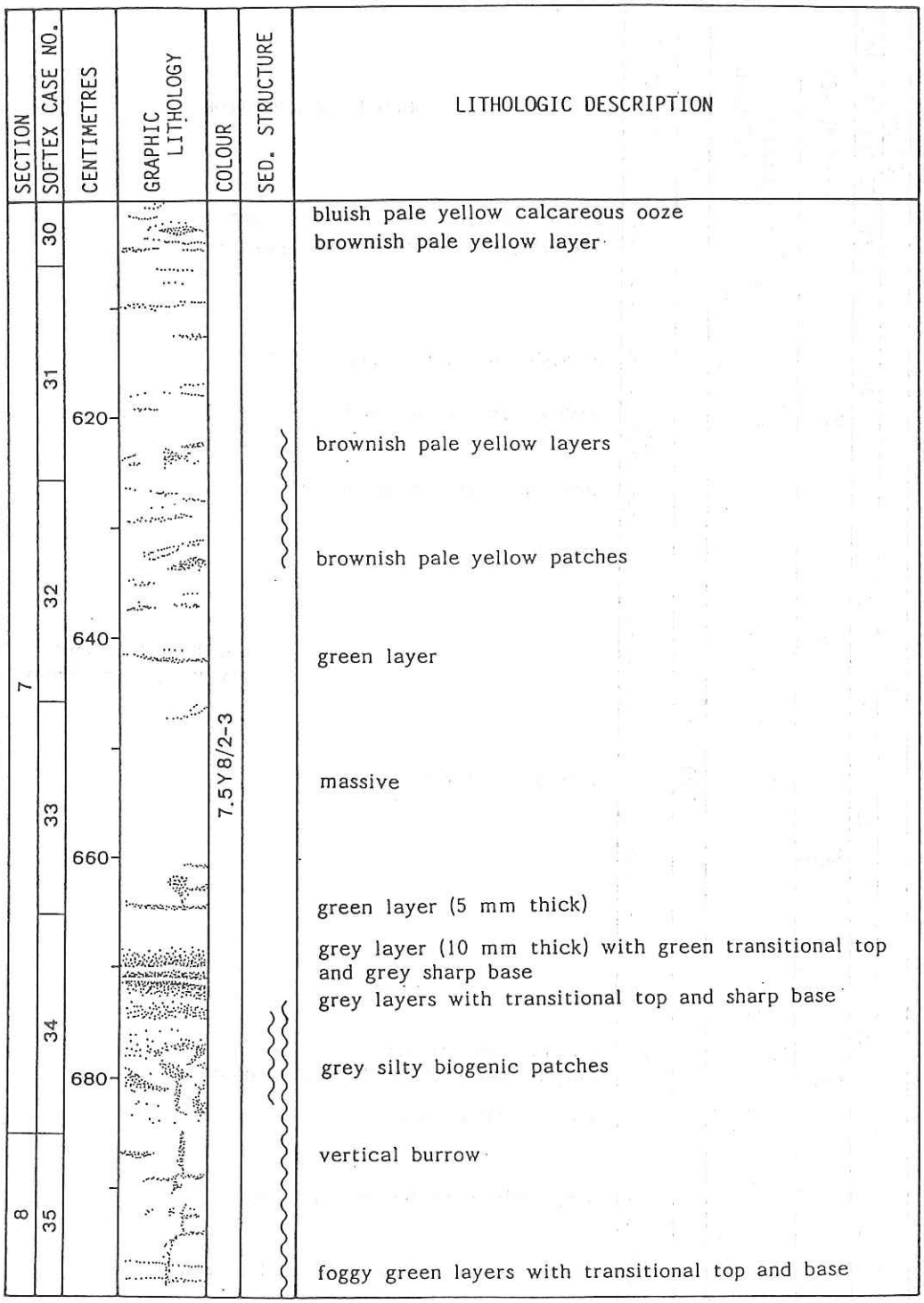

Fig. 14.5g Visual description of piston core KH92-1 5aPC (600 - 700 cm).

CORE: KH92-1 5aPC (700-800)

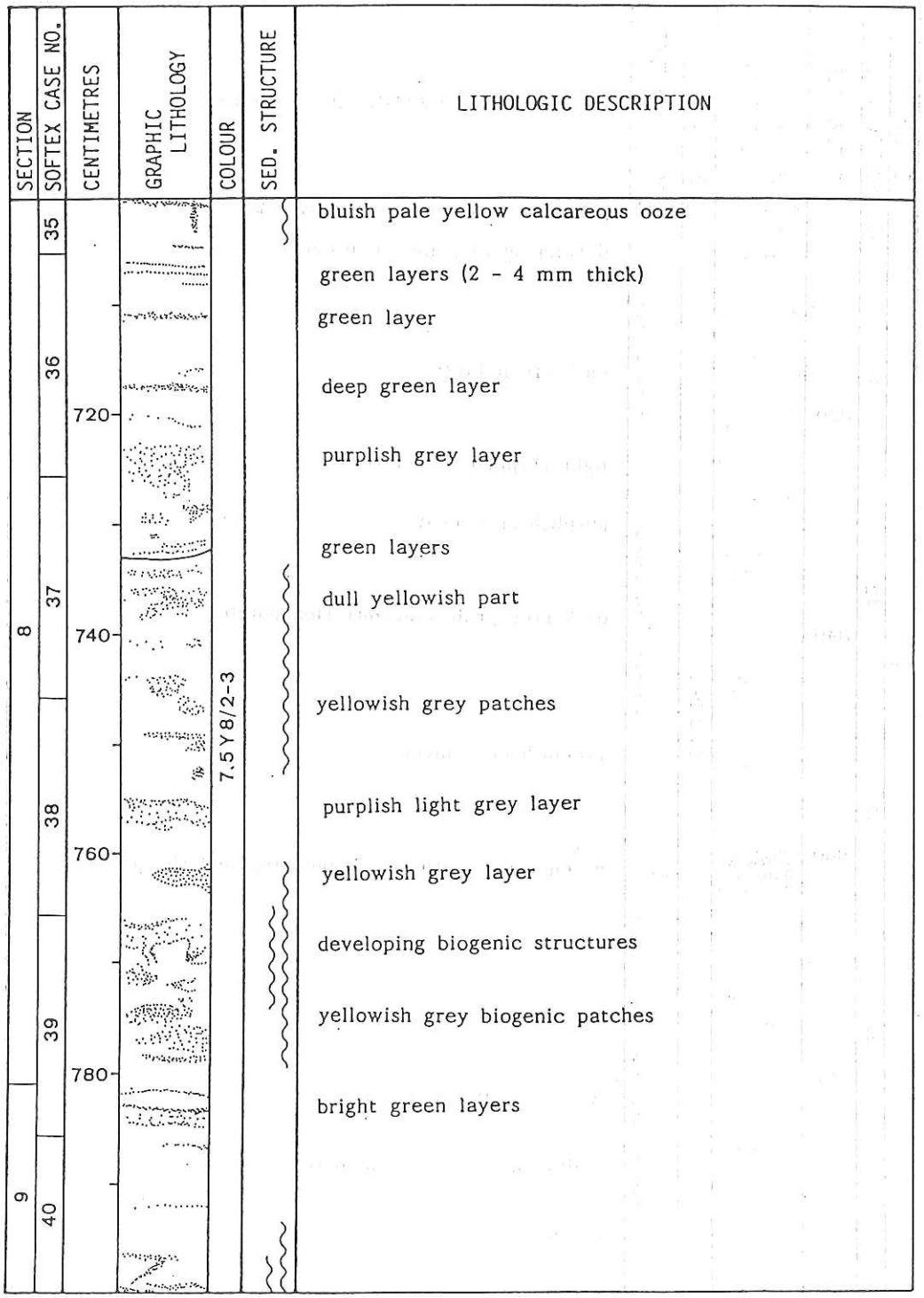

Fig. 14.5h Visual description of piston core KH92-1 5aPC (700 - 800 cm).

CORE: KH92-1 5aPC (800-900)

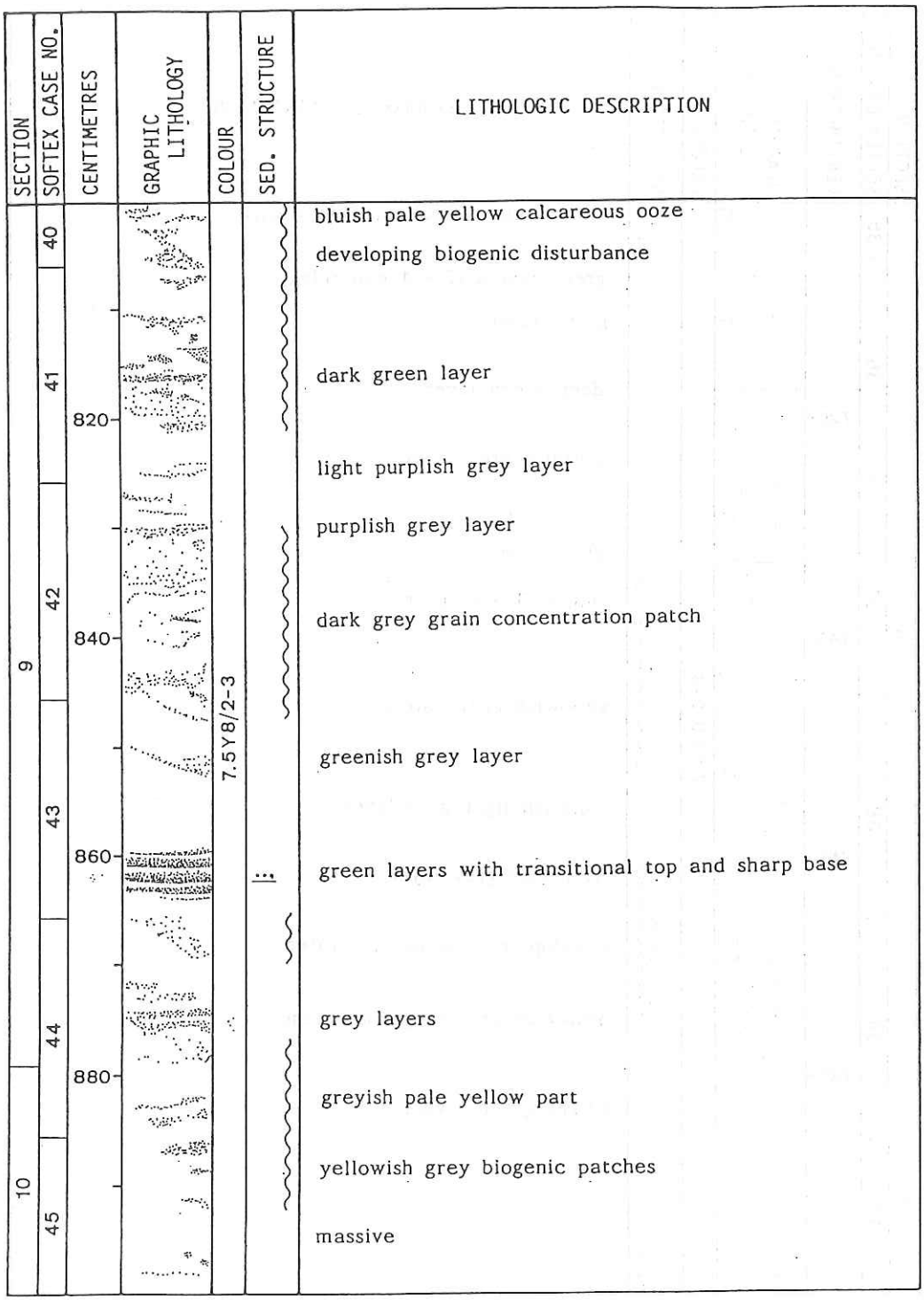

Fig. 14.5i Visual description of piston core KH92-1 5aPC (800 - 900 cm).

CORE: KH92-1 5aPC (900-987)

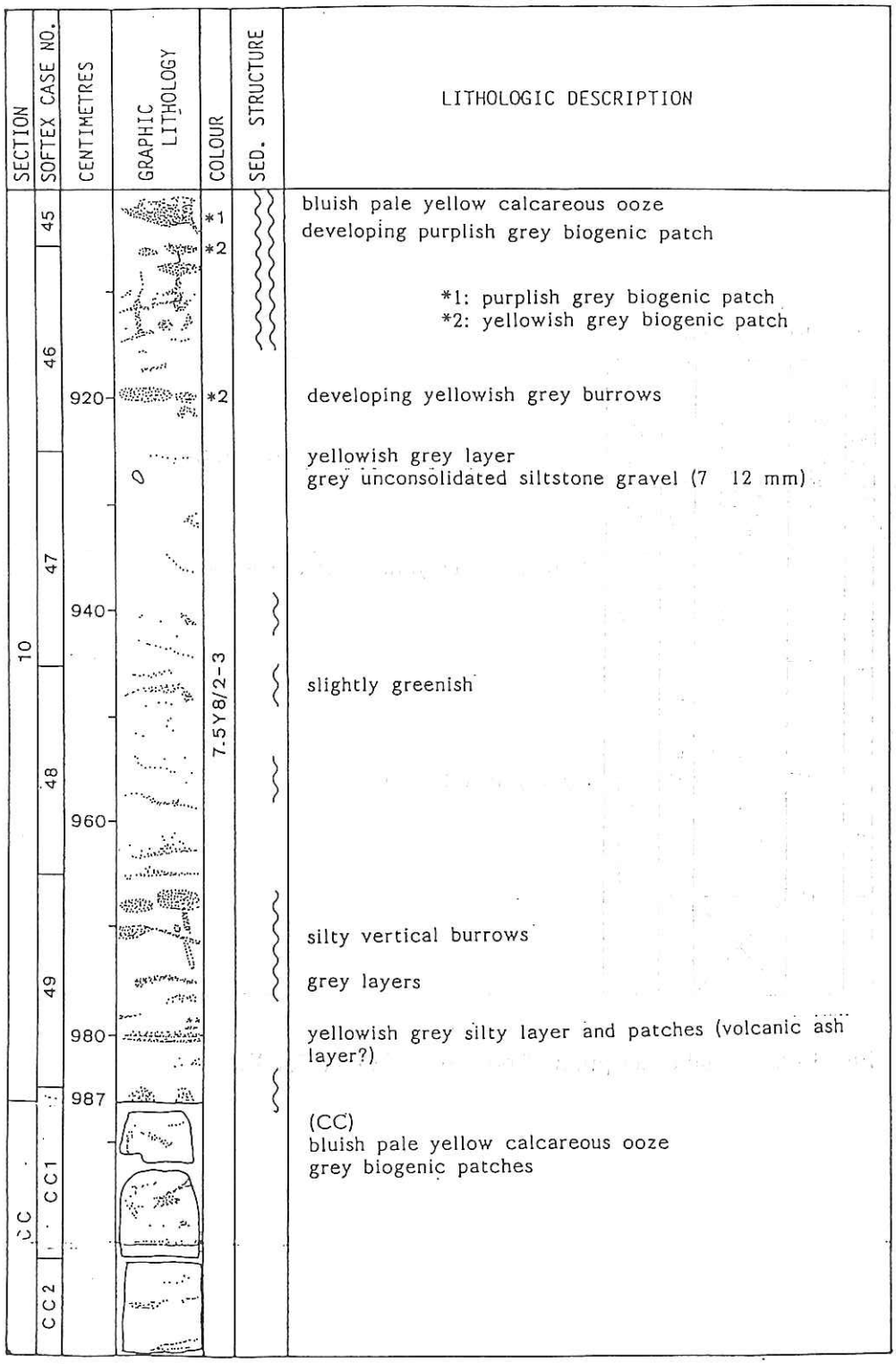

Fig. 14.5j Visual description of piston core KH92-1 5aPC (900 -987 cm and core catcher sample).

CORE: KH92-1 5cBX

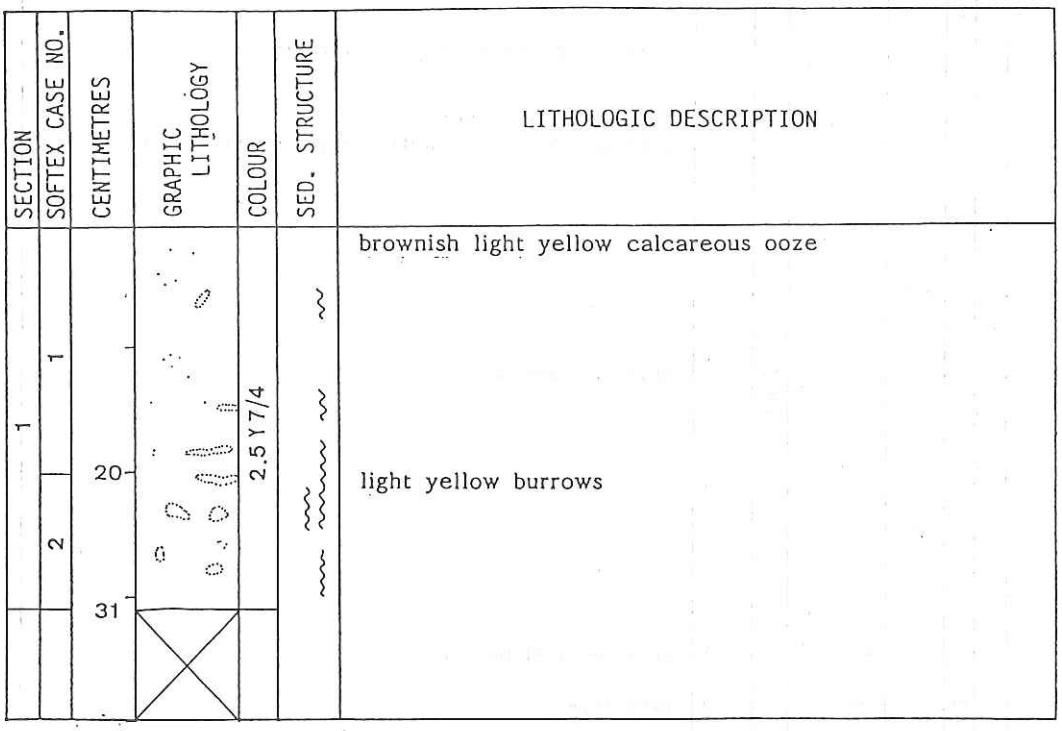

Fig. 14.6. Visual description of box core KH92-1 5cBX.

CORE: KH92-1 6PC (0-100)

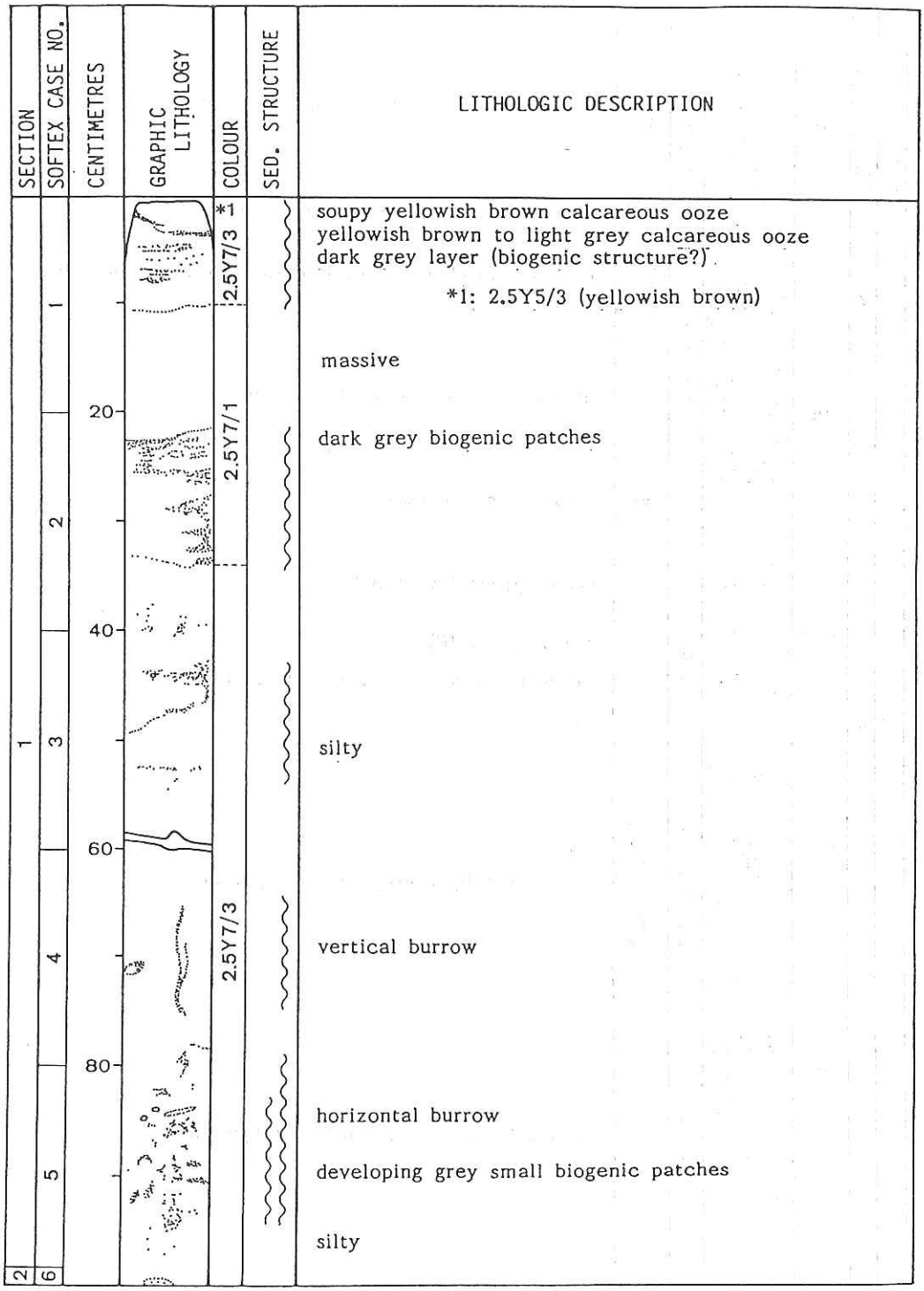

Fig. 14.7a Visual description of piston core KH92-1 2PC (0 - 100 cm).

CORE: KH92-1 6PC (100-200)

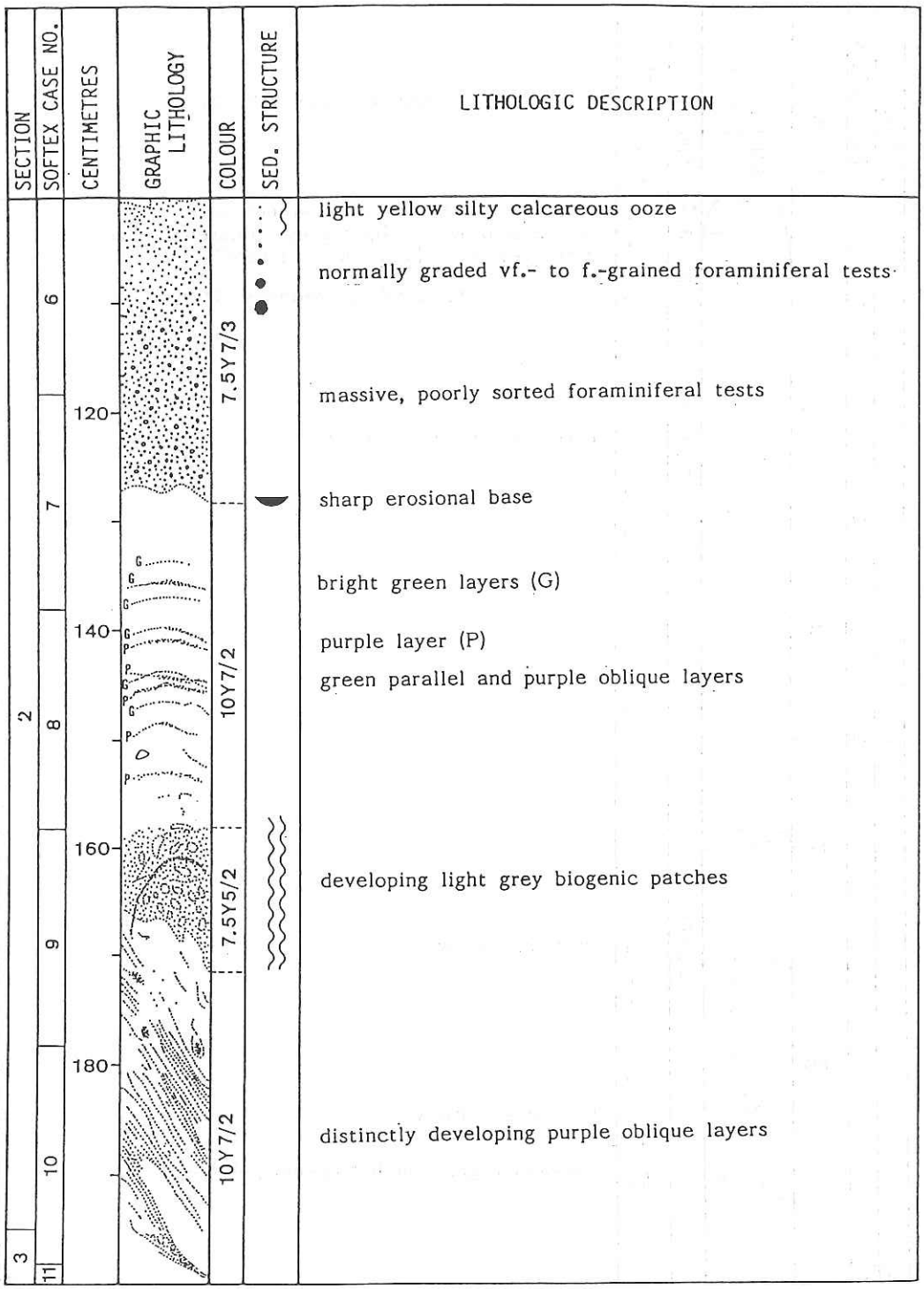

Fig. 14.7b Visual description of piston core KH92-1 2PC (100 - 200 cm).

CORE: KH92-1 6PC (200-300)

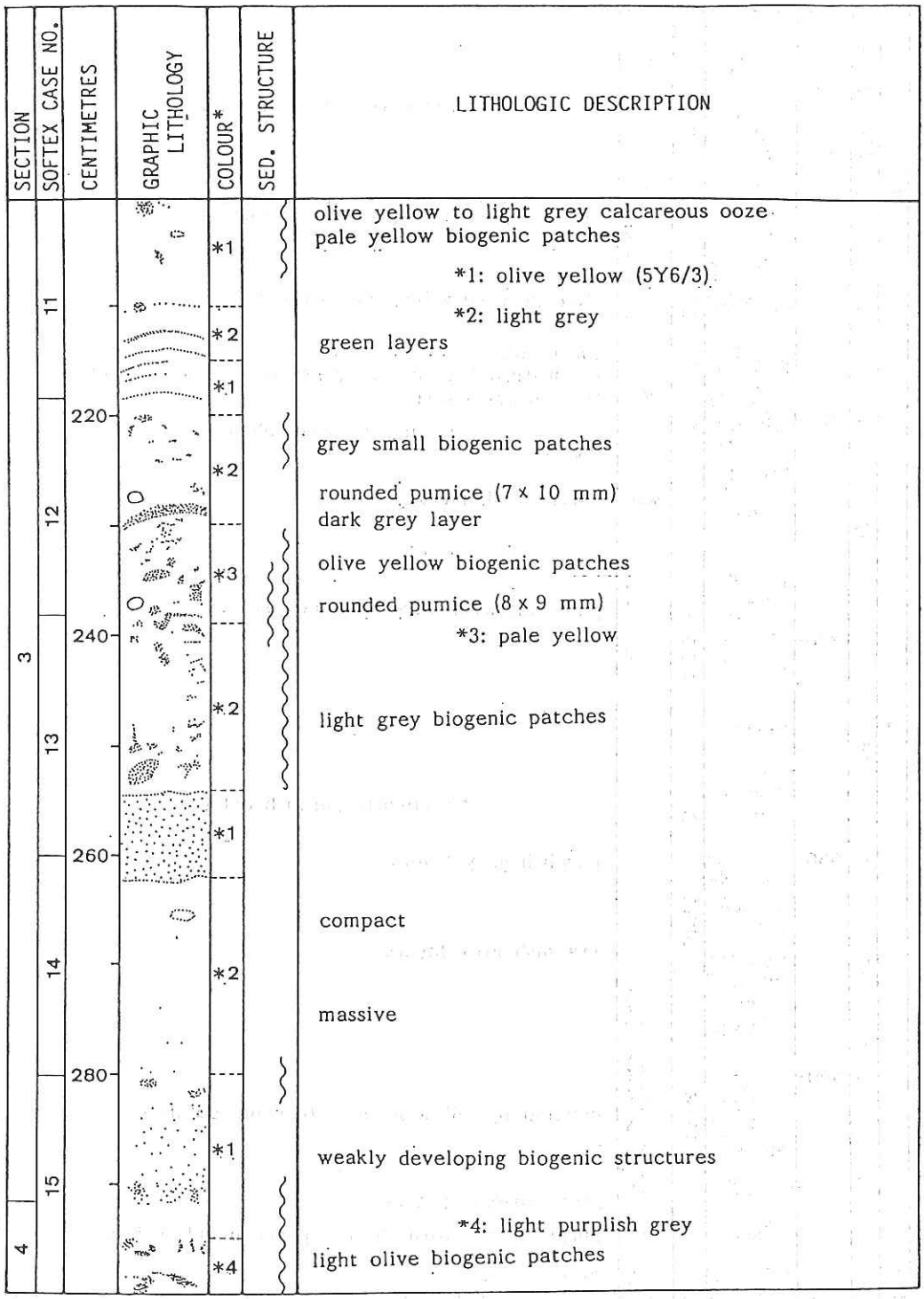

Fig. 14.7c Visual description of piston core KH92-1 2PC (200 - 300 cm).

CORE: KH92-1 6PC (300-400)

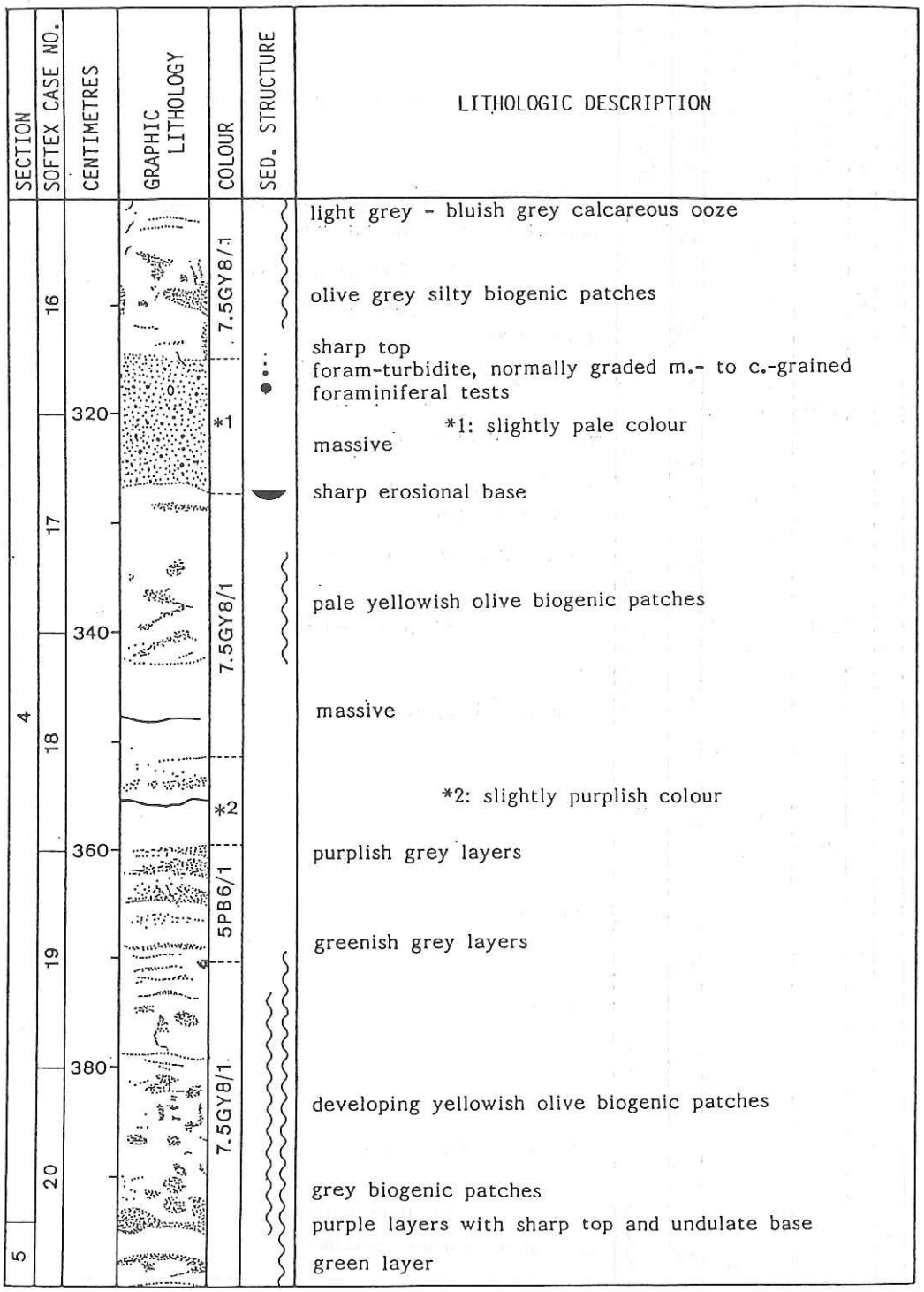

Fig. 14.7d Visual description of piston core KH92-1 2PC (300 - 400 cm).

CORE: KH92-1 6PC (400-500)

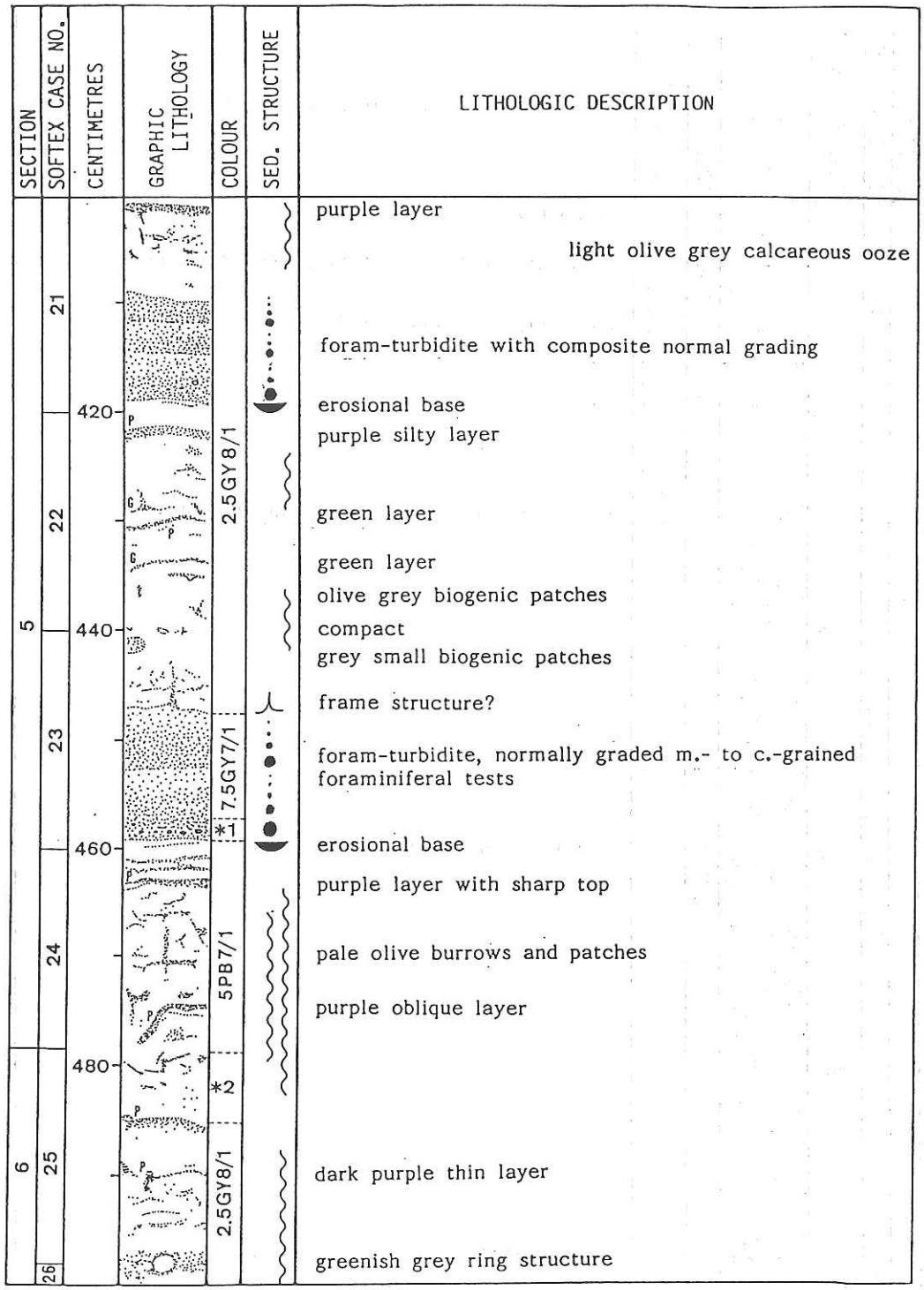

Fig. 14.7e Visual description of piston core KH92-1 2PC (400 - 500 cm).

CORE: KH92-1 6PC (500-600)

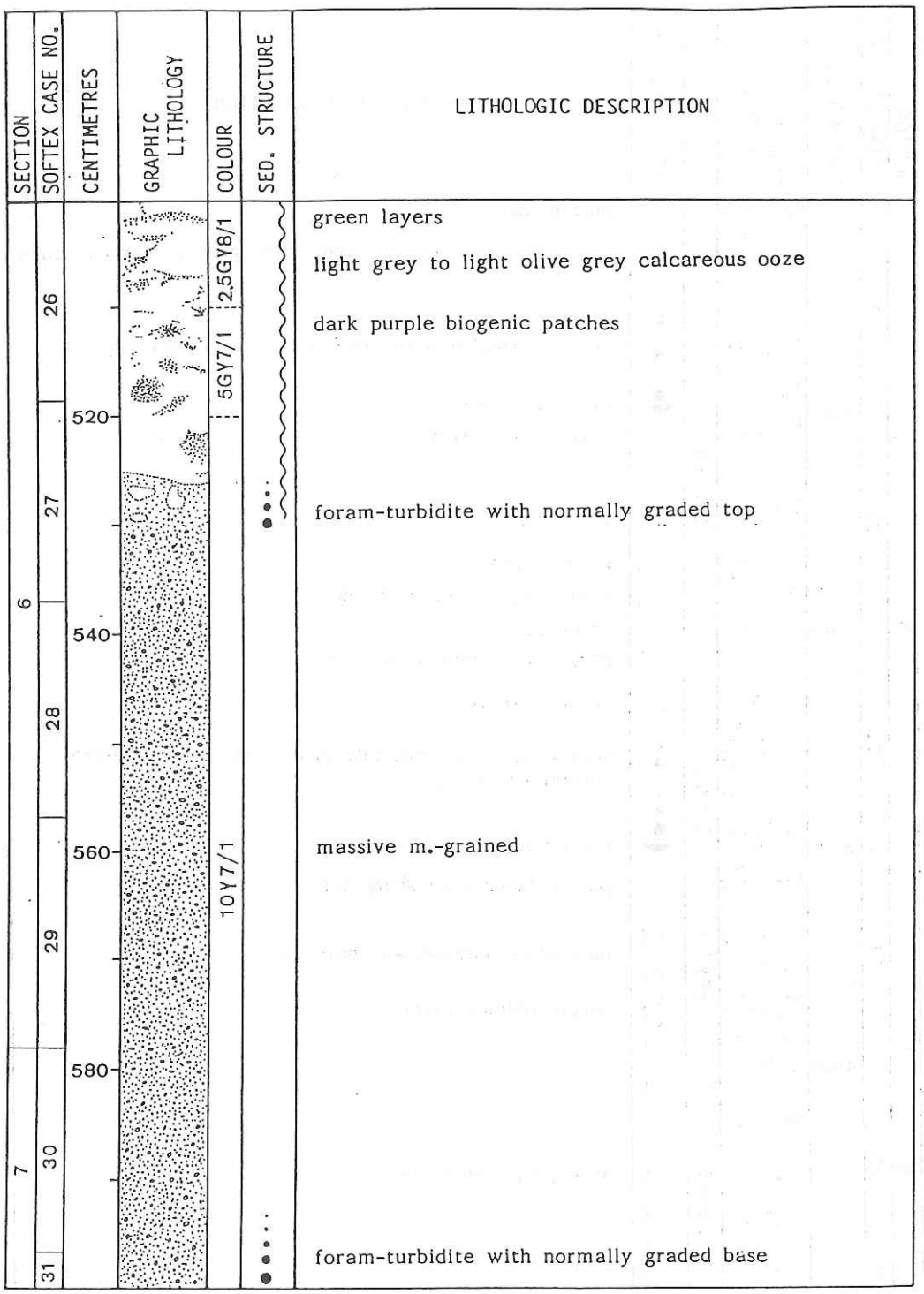

Fig. 14.7f Visual description of piston core KH92-1 2PC (500 - 600 cm).

CORE: KH92-1 6PC (600-700)

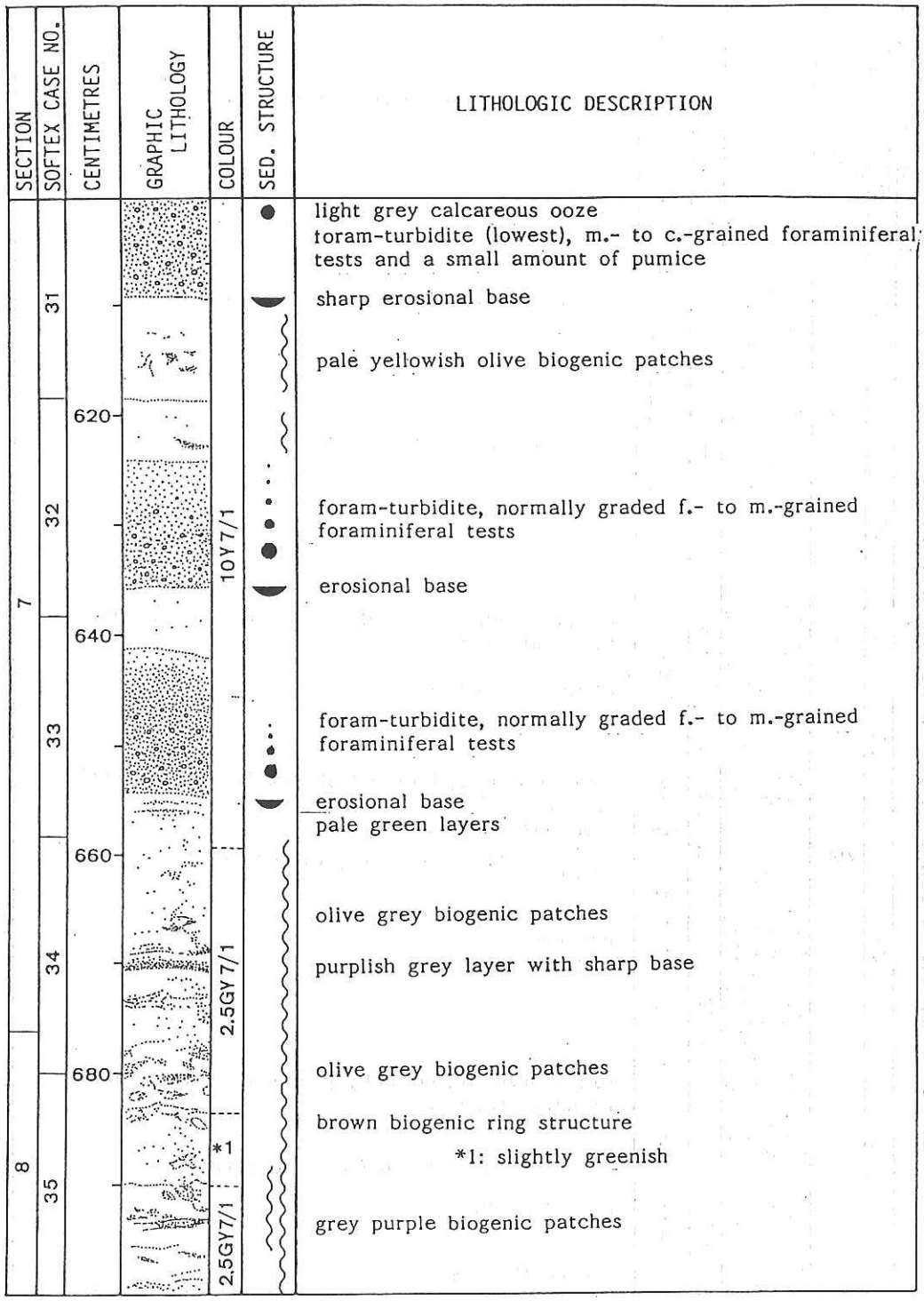

Fig. 14.7g Visual description of piston core KH92-1 2PC (600 - 700 cm).

CORE: KH92-1 6PC (700-800)

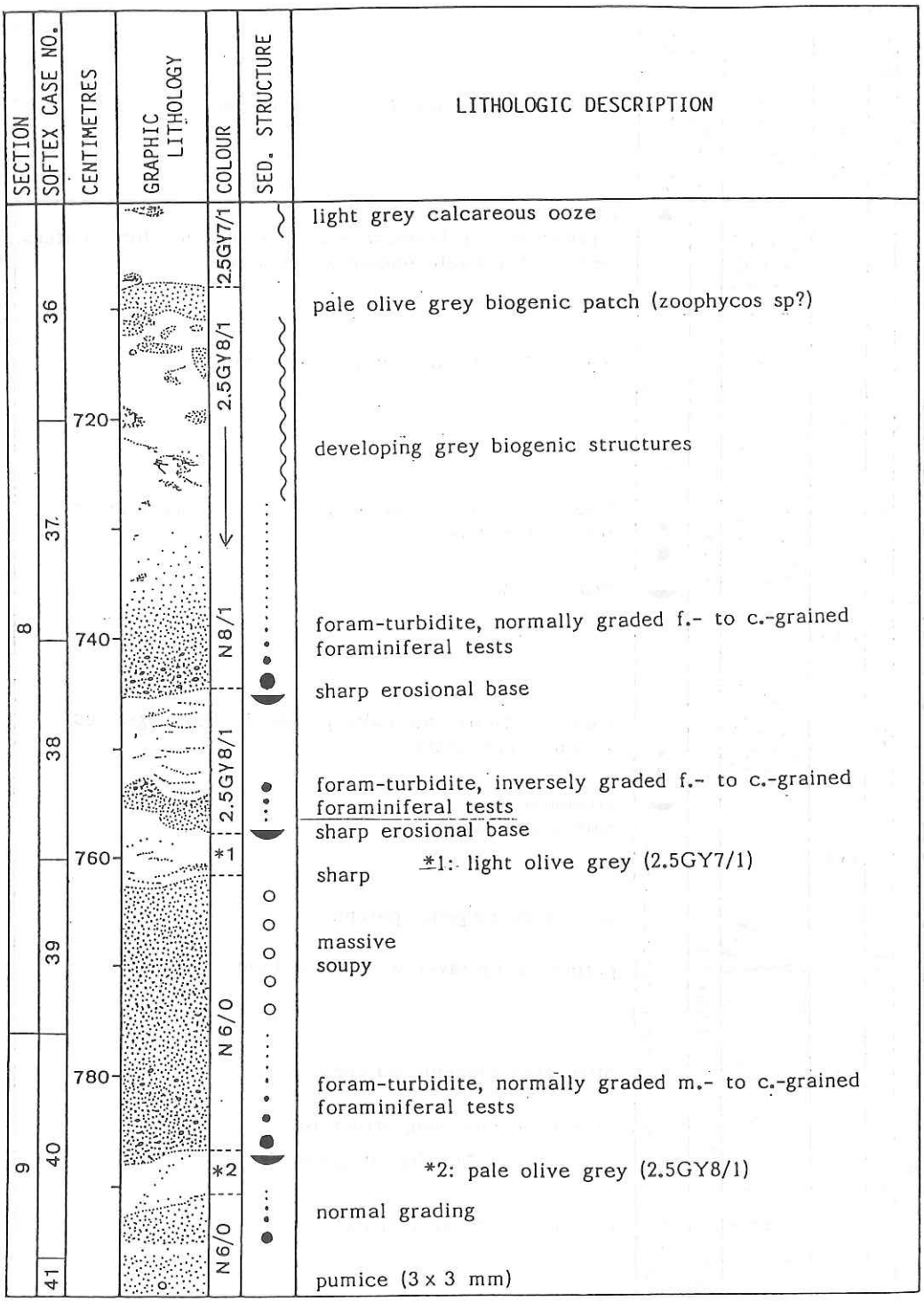

Fig. 14.7h Visual description of piston core KH92-1 2PC (700 - 800 cm).

CORE: KH92-1 6PC (800-900)

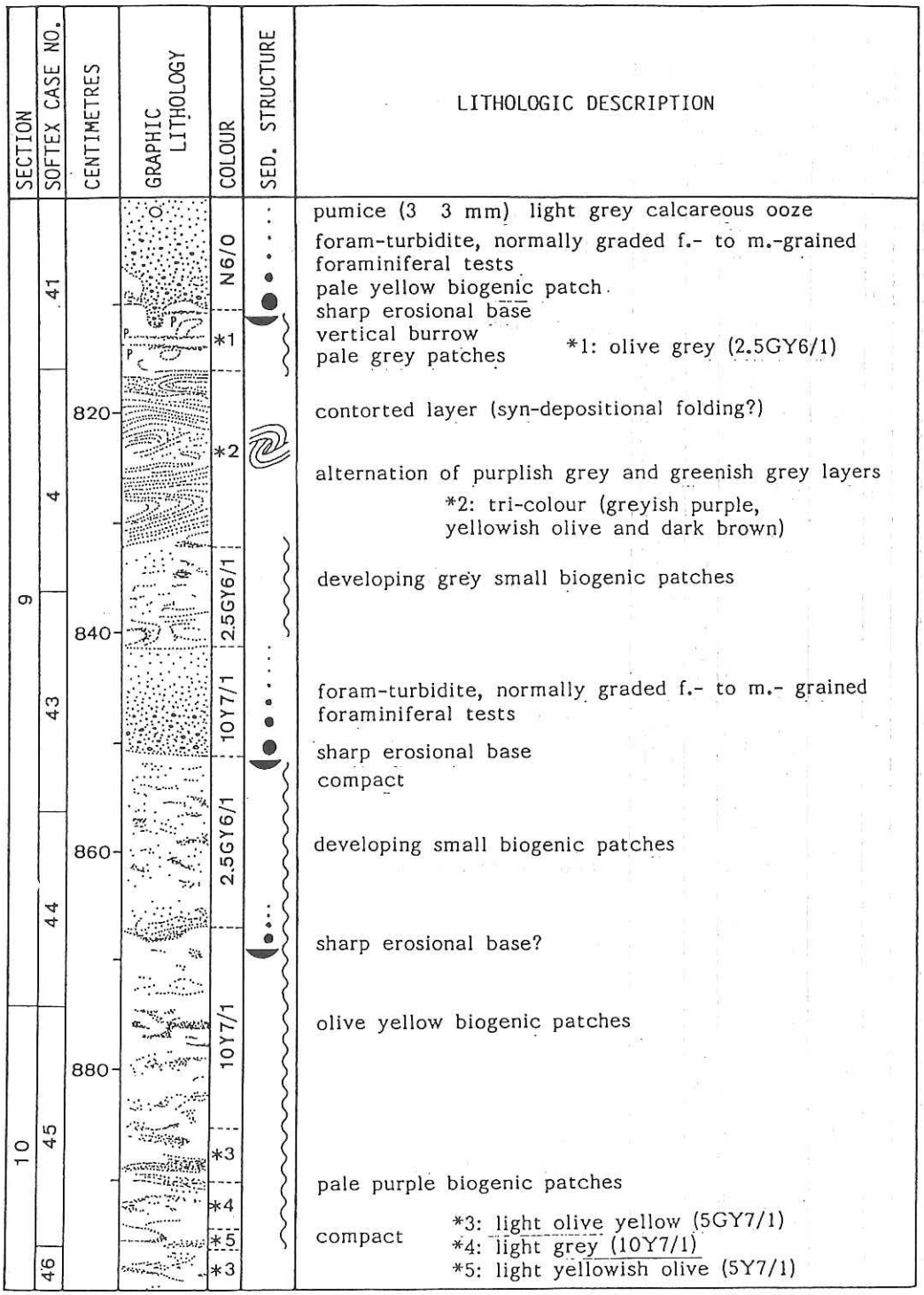

Fig. 14.7i Visual description of piston core KH92-1 2PC (800 - 900 cm).

CORE: KH92-1 6PC (900-985)

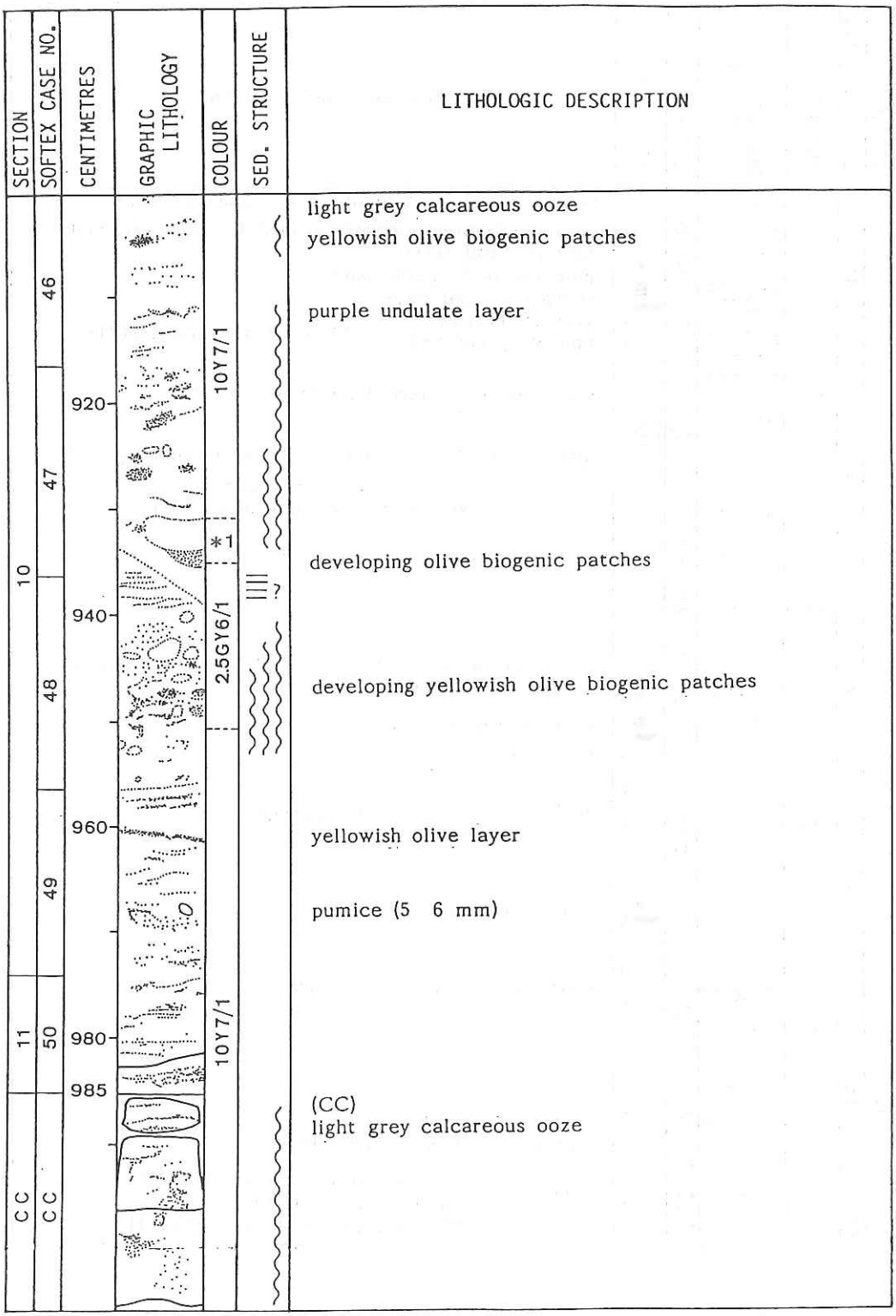

Fig. 14.7j Visual description of piston core KH92-1 2PC (900 - 985 cm and core catcher sample).

CORE: KH92-1 6BX

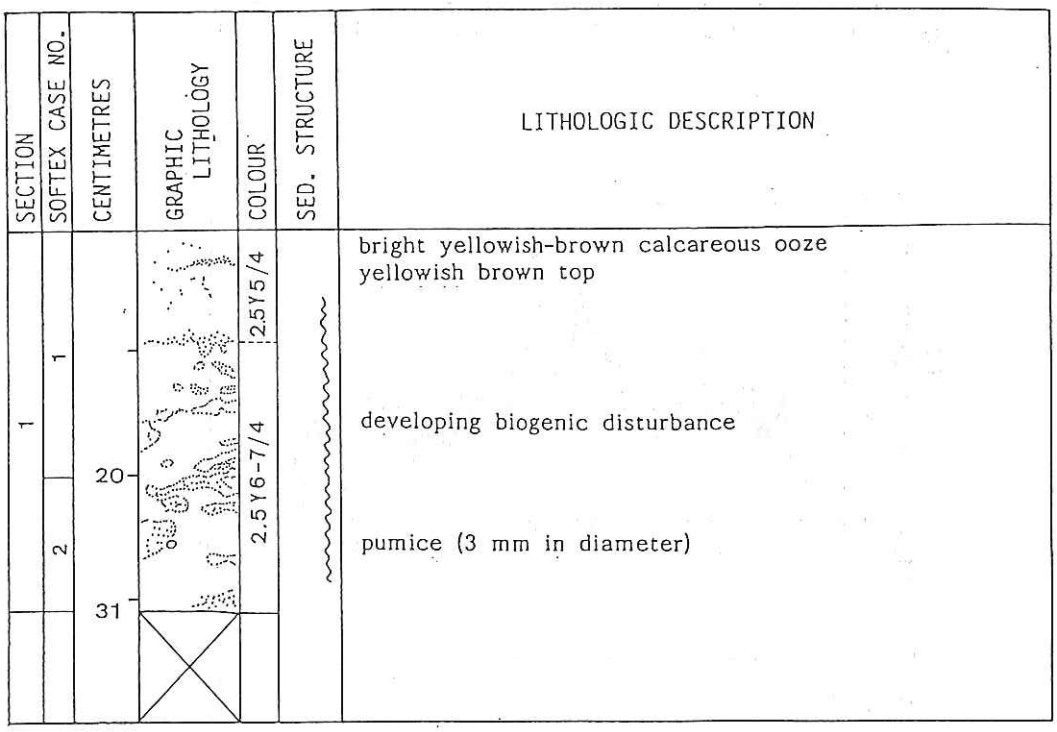

Fig. 14.8 Visual description of box core KH92-1 6BX.

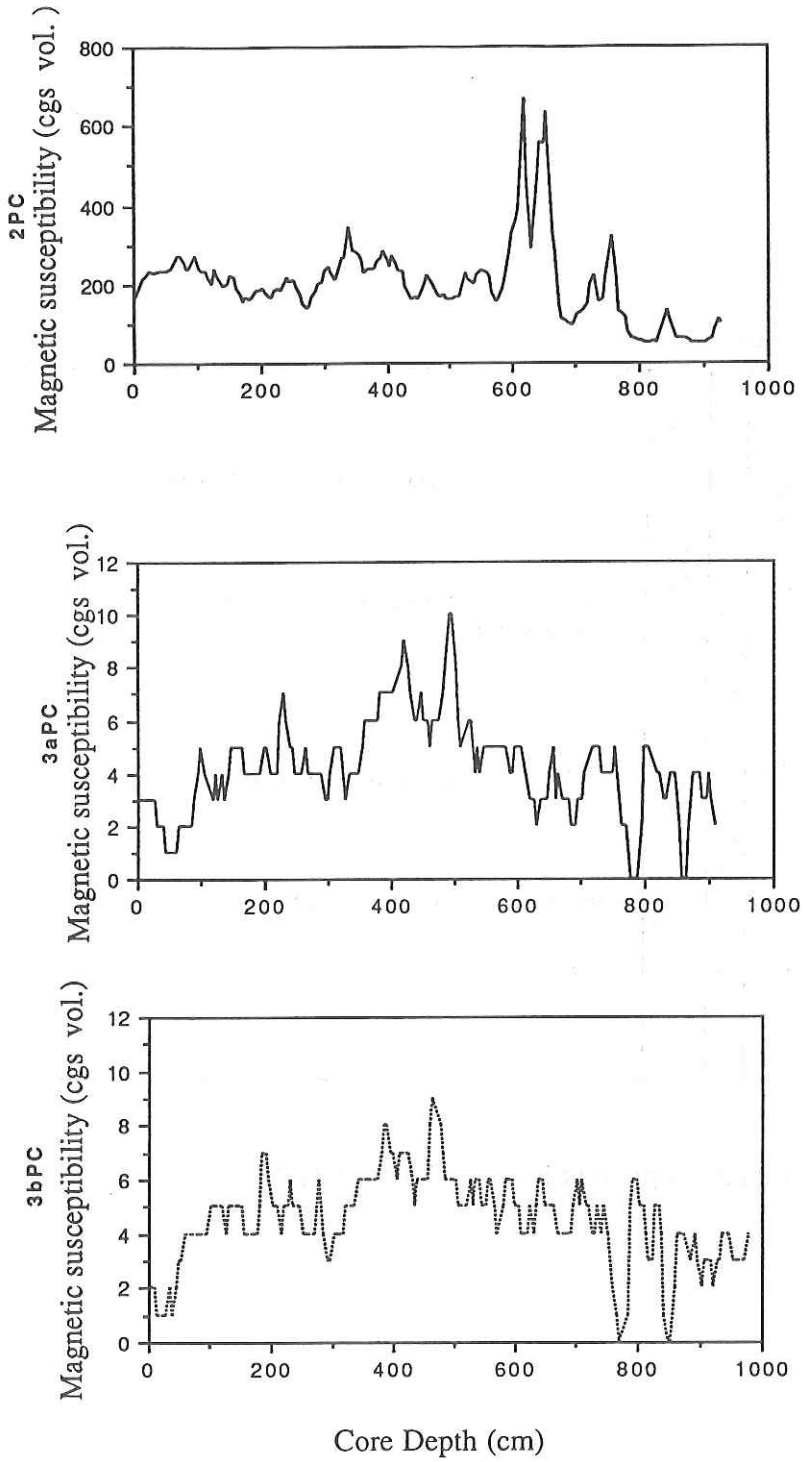

Fig. 14.9 Magnetic suscepibility of piston cores stations 2PC, 3aPC and 3bPC.

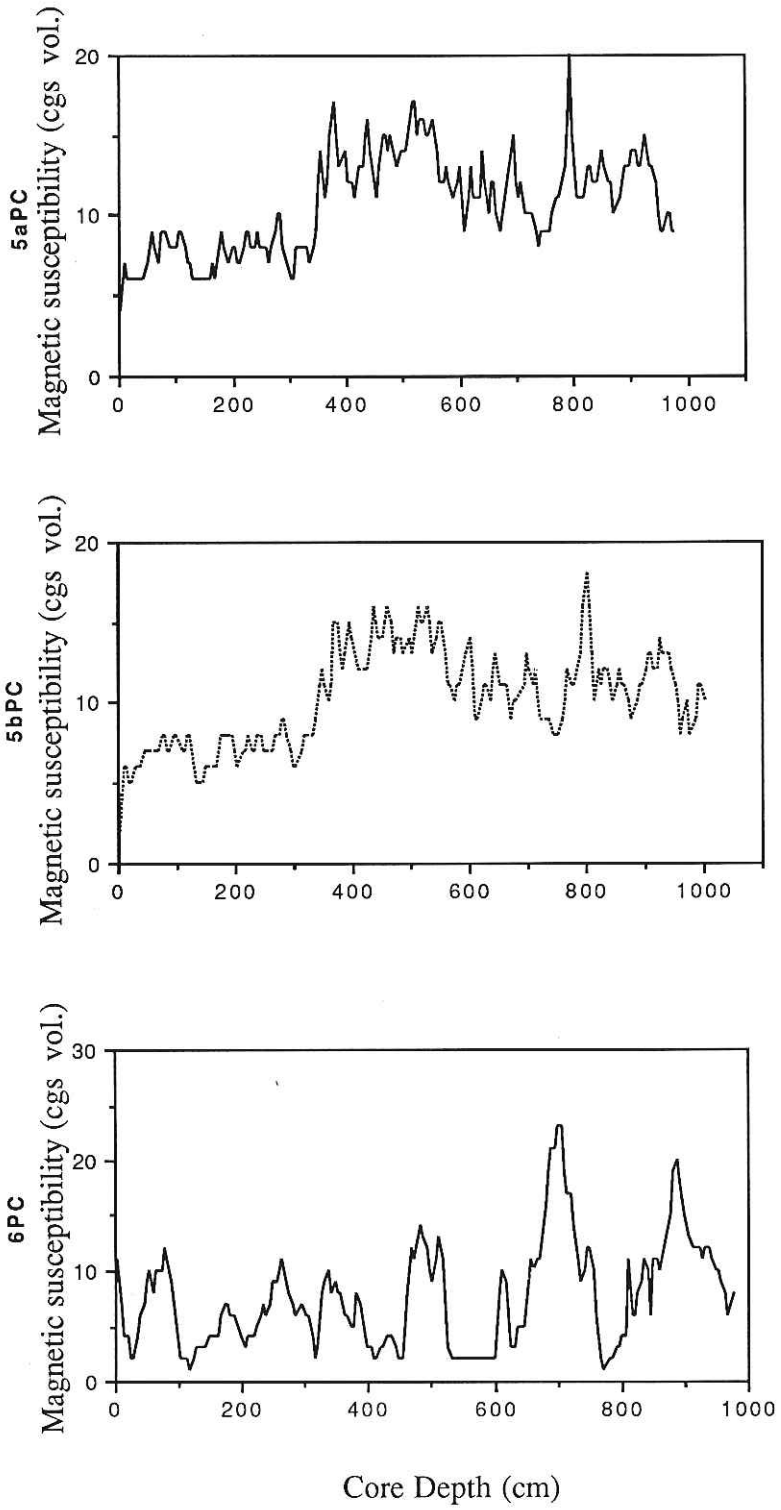

Fig. 14.10 Magnetic susceptibility of piston cores staions 5aPC, 5bPC and 6PC.

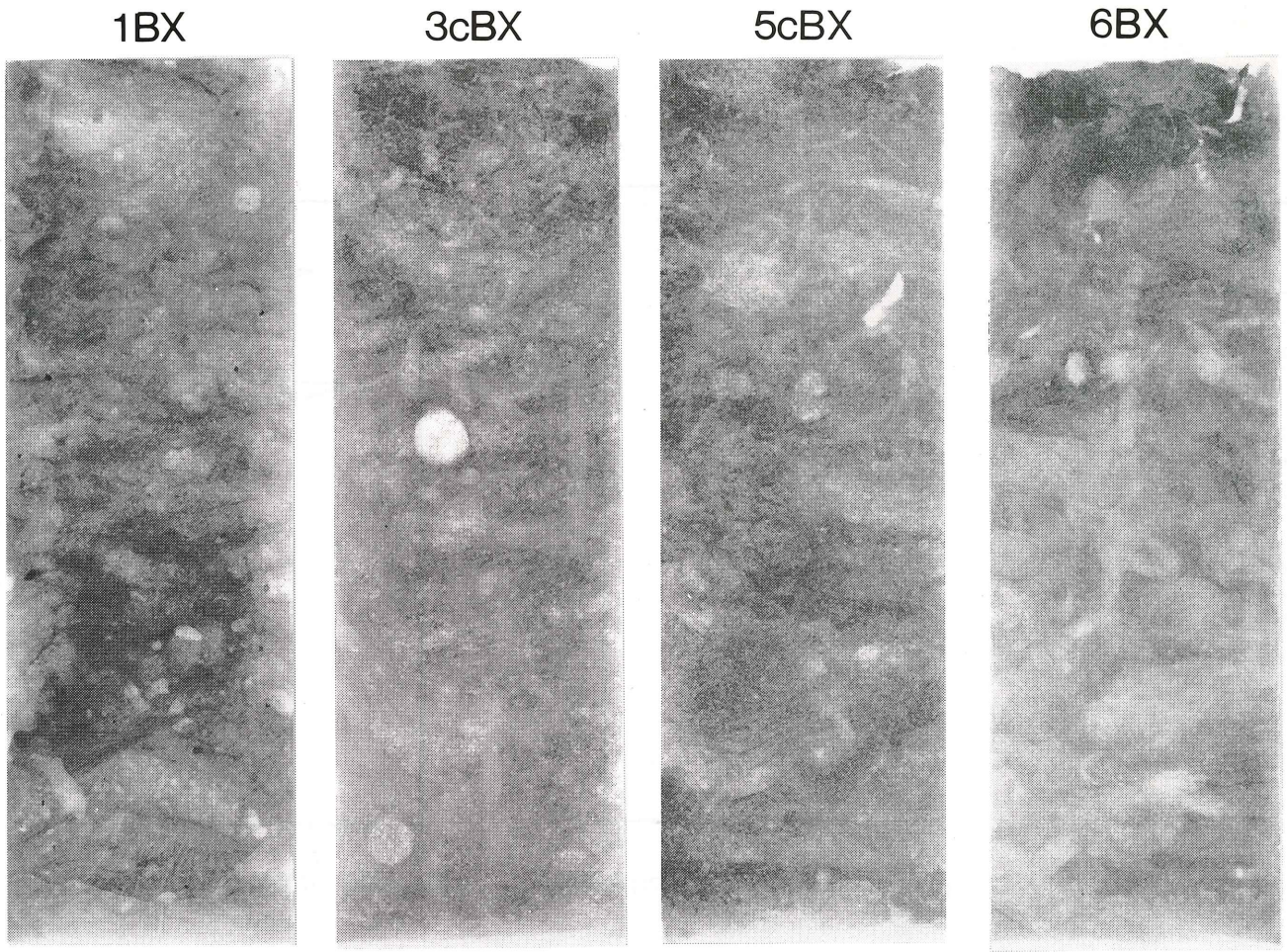

Plate 14.1 Selected soft X-ray radiographs of box cores KH92-1 1BX (a: 0 - 20 cm), 3cBX (b: 0 - 20 cm), 5cBX (c: 0 - 20cm) and 6BX (d: 0 - 20 cm).

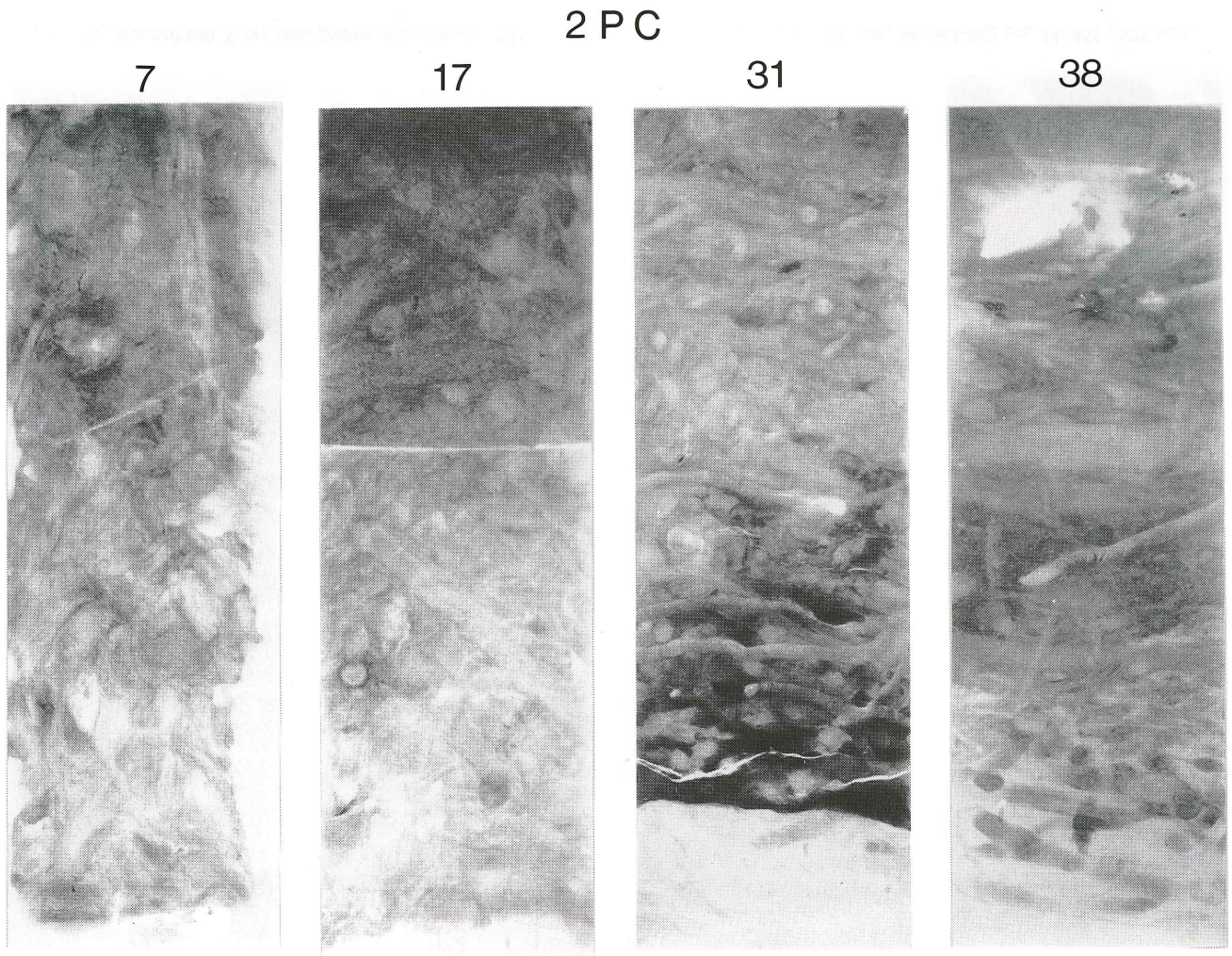

Plate 14.2 Selected soft X-ray radiographs of piston core KH92-1 2PC (7: 107 - 128 cm, 17: 327 - 347 cm, 31: 607 - 627 cm, 38: 747 - 767 cm).

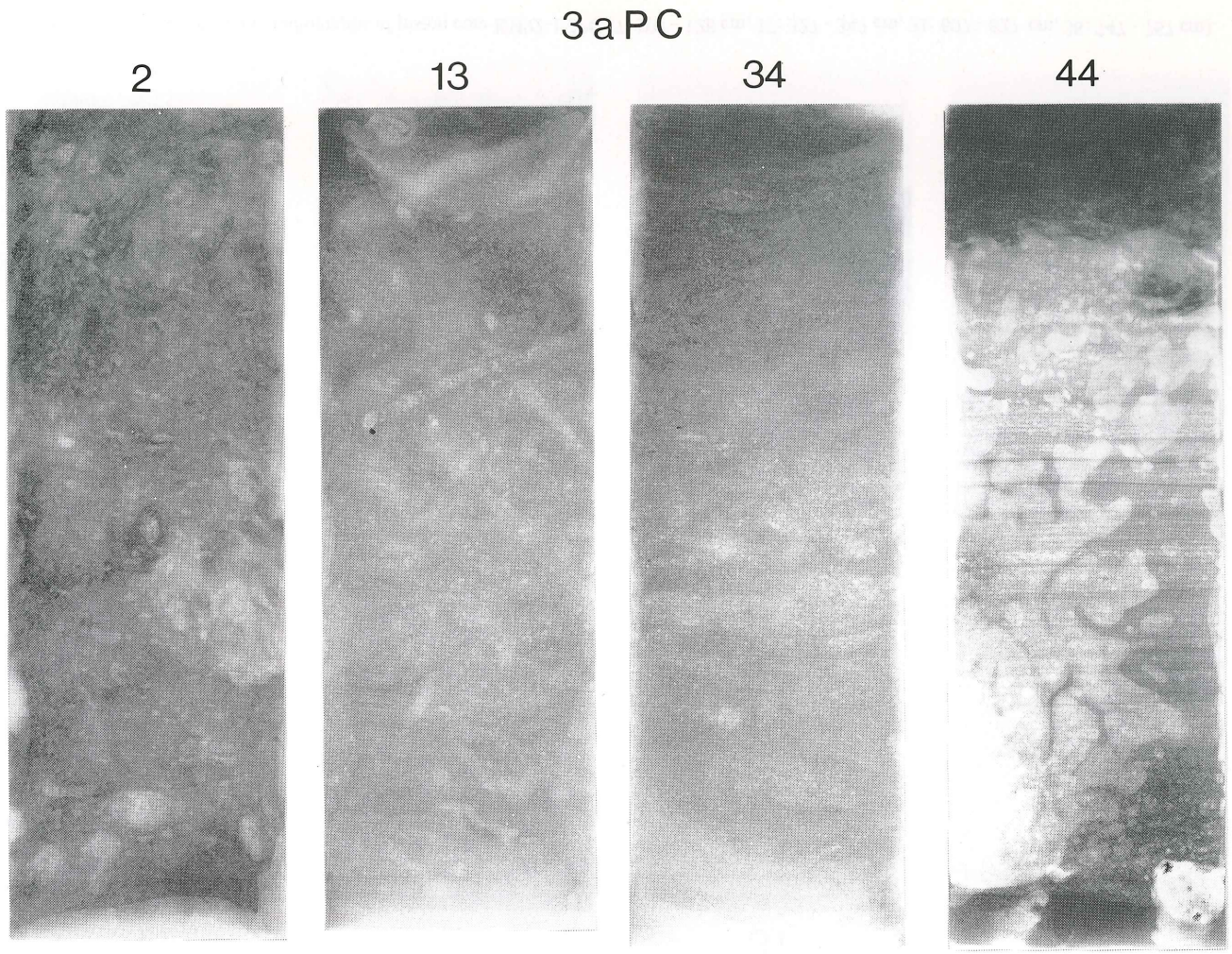

Plate 14.3 Selected soft X-ray radiographs of piston core KH92-1 3aPC (2: 31 - 51 cm, 13: 247 - 267 cm, 34: 662-682 cm, 44: 855 - 875 cm).

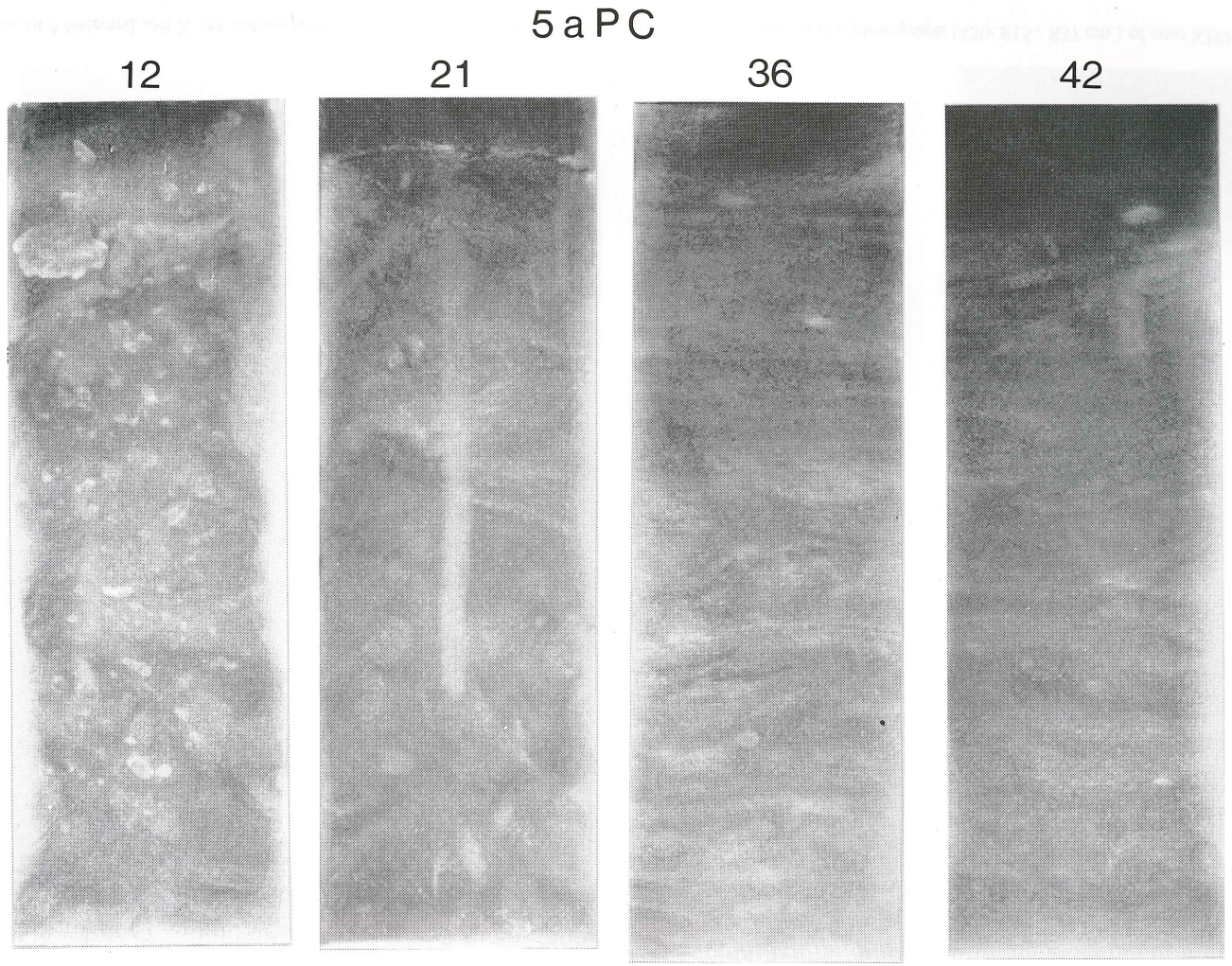

Plate 14.4 Selected soft X-ray radiographs of piston core KH92-1 5aPC (12: 228 - 248 cm, 21: 408 - 428 cm, 36: 705 - 726 cm, 42: 826-846cm).

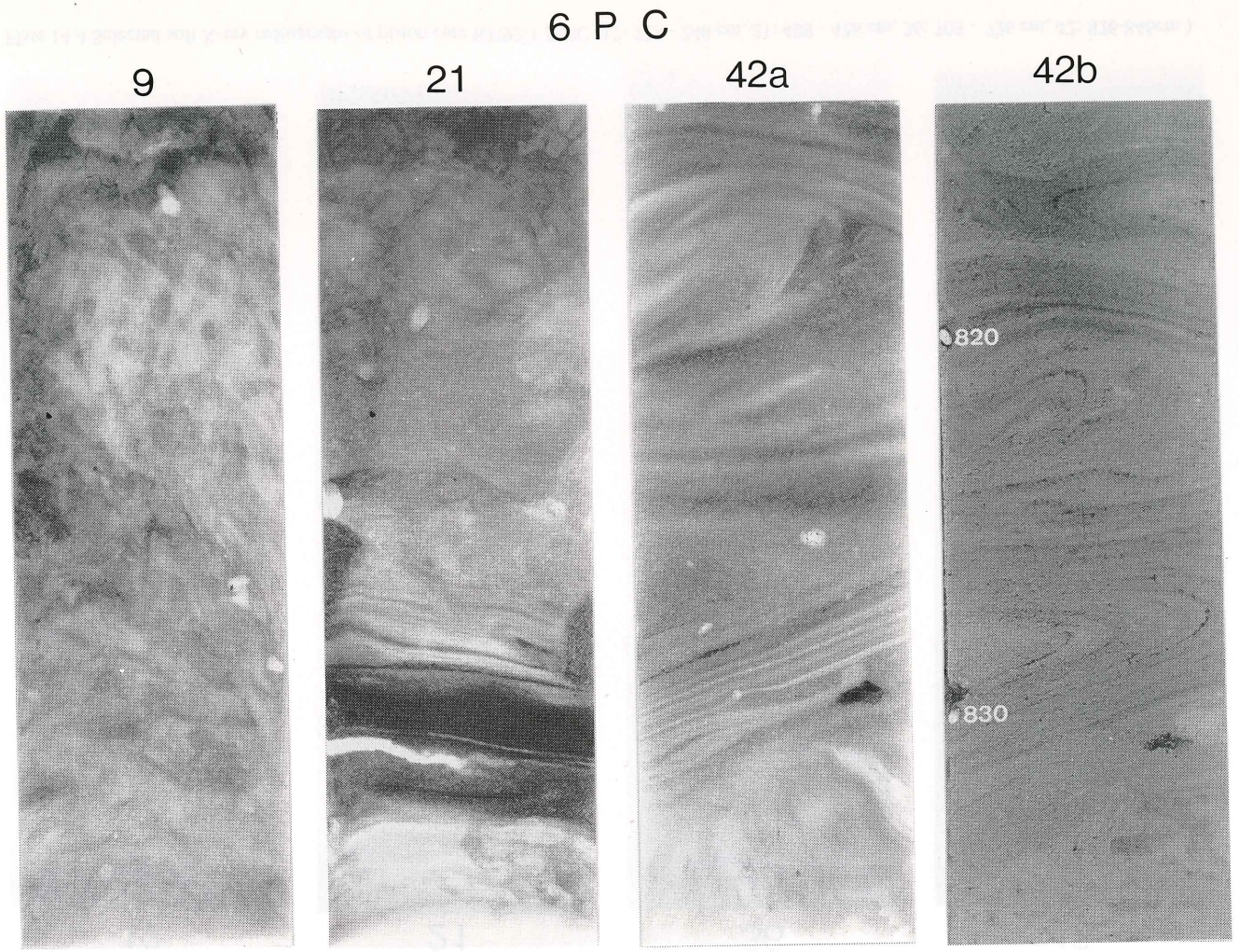

Plate 14.5 Selected soft X-ray radiographs (9: 159 - 179 cm, 21: 400 - 420 cm, 42a: 817 - 837 cm) and a photograph (42b: 815 - 837 cm) of core KH92-1 6PC.

15. Net Sampling

M. Murayama

In order to investigate species composition and vertical distribution patterns of living planktonic foraminifera and to measure the $^{14}C/^{12}C$ radioisotope ratios of its tests in comparison with that of sea water in the western equatorial Pacific, net sampling was conducted at two stations during this cruise. (Fig. 15.1). The sampling was done using MTD net (Motoda's Multiple Horizontal Tow Net) in the leg. 1, and using ORI-33 plankton net in the leg. 2.

The MTD horizontal towing nets (50, 100, 200, 300, 500m) were conducted at 8°01.10'N, 139°38.57'E to 8°01.57'N, 139°39.12'E. The nets were horizontally towed in the depth range of 0 - 500m for about half an hour at 1.0-1.5 knots, when the towing wire made an angle of about 45° with the attaining depth. The net-out time was at 20:25-21:17(JST) at the nightime.

During the leg.2 cruise, ORI net sampling was made twice at the same site; 4°41.990'N, 133°42.230'E (0-300m); 4°42.570'N, 133°42.240'E (0-100m). ORI Net was towed obliquely at two layers (0-100, 0-300m) for about half an hour at 1.0-1.5 knots. The net-out time was at 16:46-17:00 (JST: 0-300m depth) and at 17:39-18:00 (JST: 0-100m depth).

Net sampling data are shown Table 15.1.

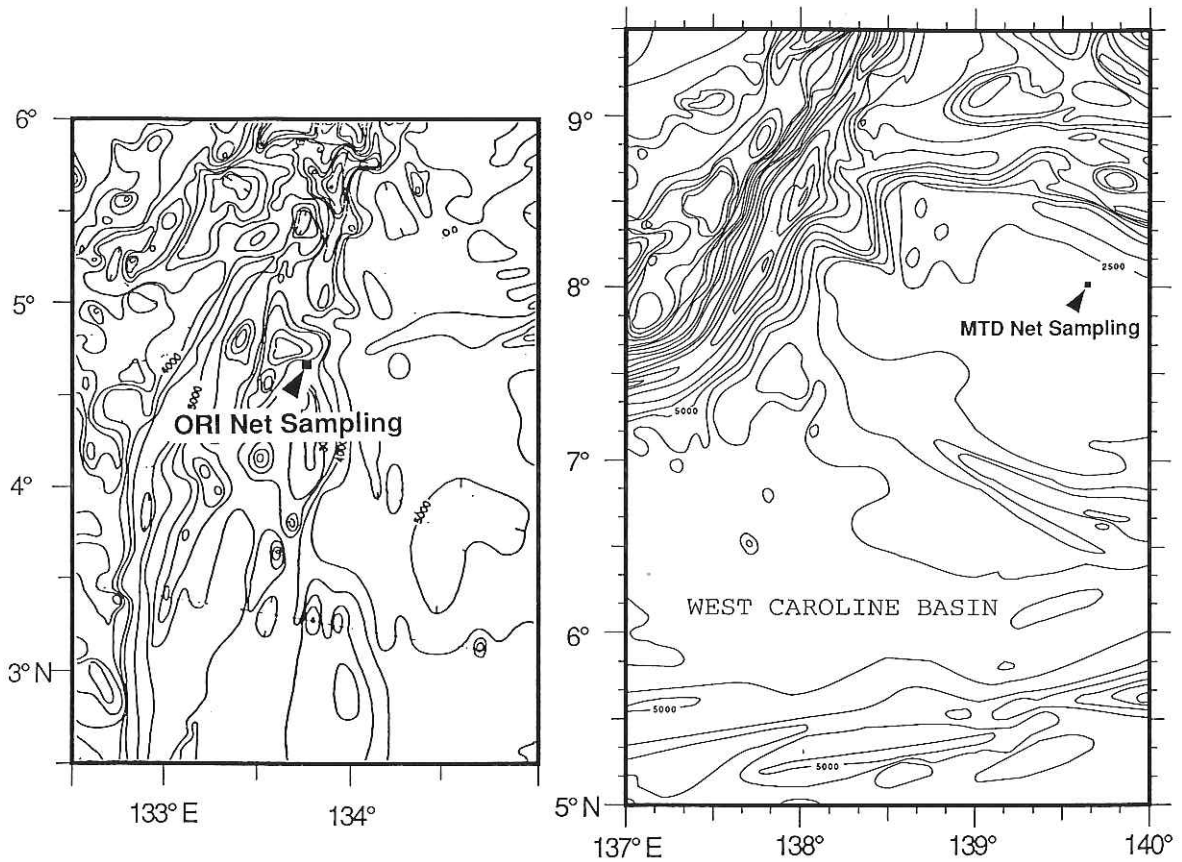

Fig. 15.1 Net sampling locations during the KH92-1 cruise.

Table.1 Net sampling data during KH92-1 cruise.

Leg.1. **MTD Net** Feb. 2,1992

	Time	Lat.	Long.
Start	20:17		
w/o 700	20:23	8°01.10'	139°38.57'
Mesenger	20:53	8°01.57'	139°39.12'
End			

Leg.2 **ORI Net** Feb. 19,1992

D:300m

	Time	Lat.	Long.
Start	16:34	04°41.94'	133°42.15'
w/o 420	16:46	04°41.99'	133°42.22'
w/o 420	17:16	04°42.42'	133°42,22'
End	17:27	04°42.46'	133°42,23'

D:100m

	Time	Lat.	Long.
Start	17:34	04°42.45'	133°42.29'
w/o 140	17:39	04°42.89'	133°42.23'
w/o 140	18:09	04°42.57'	133°42.16'
End	18:13	04°42.92'	133°42.16'

16. Geophysical Measurements of the Sorol Trough and the Caroline Basin

T. Seno, T. Fujiwara, H. Toh, K. Tamaki and K. Kobayashi

After the departure from Guam on Feb. 11, on the way to Site P5 on the Euaripik Rise, we crossed the Sorol Trough in the NNE-SS direction. We made the Seabeam survey on the topography of this trough along three crossing lines, together with the other conventional geophysical measurements such as gravity, magnetism (total force and three components), and 3.5 kHz sub bottom profiler. After the piston coring at Site P5, we turned to the west towards the eastern margin of the Ayu Trough, and crossed the west Caroline Basin. The ship's track is shown in Fig. 16.1; the ship's speed was 16 knot. Here we describe the surveys in these areas and present preliminary results.

16.1 Sorol Trough

The free-air gravity anomaly, magnetic anomaly, and seafloor topography along these three lines are shown in Fig. 16.2. The survey area is the place where the northern end of the Euaripik Rise meets the Sorol Trough. The northernmost flank of the Sorol Trough has 2200-2000 m depth (Fig. 16.2a), and the southern flank of the trough merges with the Euaripik Rise at 2200 m depth (Fig. 16.2c), and further to the south the rise deepens to 2500 m, which is the average depth of the rise. The trough in this area shows asymmetry. The axial ridge has a 400 m depth, with no appreciable sediment cover. Fifteen km to the north and to the south from the axial ridge, there are the 1st flank ridges; the northern one (2760 m deep) is much larger than the southern one (3260 m deep). The axial valleys between the axial and the 1st ridges are 4400-4500 m deep., and has no or very small amount of sediments. Further to the outside from the 1st ridges, there are basins, 3500-3600 m deep, filled with stratified sediments. The southern basin is wider than the northen one. Outside of these basins, there are 2nd flank ridges, which are 1950 m and 1500 m deep in the north and in the south, respectively

Magnetic anomalies associated with the Sorol Trough has a total amplitude of 100 nT, and are roughly symmetric about the trough axis. Free-air gravity anomalies of the order of 100 mgal correlate with the topography. However, it requires further analysis, e.g., using addmittance technique to see whether local or regional isostasy holds in this trough.

These ridges and basins probably represent the horsts (abbysal hills) and grabens, which were formed during the spreading in the Sorol Trough; the non-

existence of appreciable sediments in the axial area of the trough suggests that the spreading is still active.

16.2 West Caroline Basin

The topography and gravity profiles along the line from the Euaripik Rise to the West Caroline Basin are shown in Fig. 16.3. The Euaripik Rise deepens gradually from 2500 m to 4000-4500 m to the West Caroline Basin. The magnetic anomalies show a total amplitude amounting to 350 nT, with a wavelength of 120 km. These anomalies would be those associated with the opening of the West Caroline Basin during Oligocene in the NNW-SSE direction. The free-air gravity anomaly is almost flat from the center of the Euaripik Rise to the west Caroline Basin, except some undulations associated with the short wavelength topographic undulations in the center of the basin. This indicates the Euaripik Rise is isostatically compensated. The basin and the rise are covered by thick opaque-layered and transparent sediments, respectively. The seafloor topography revealed by the Seabeam shows some E-W lineations, which might be a remnant fabric of the NNW-SSE spreading.

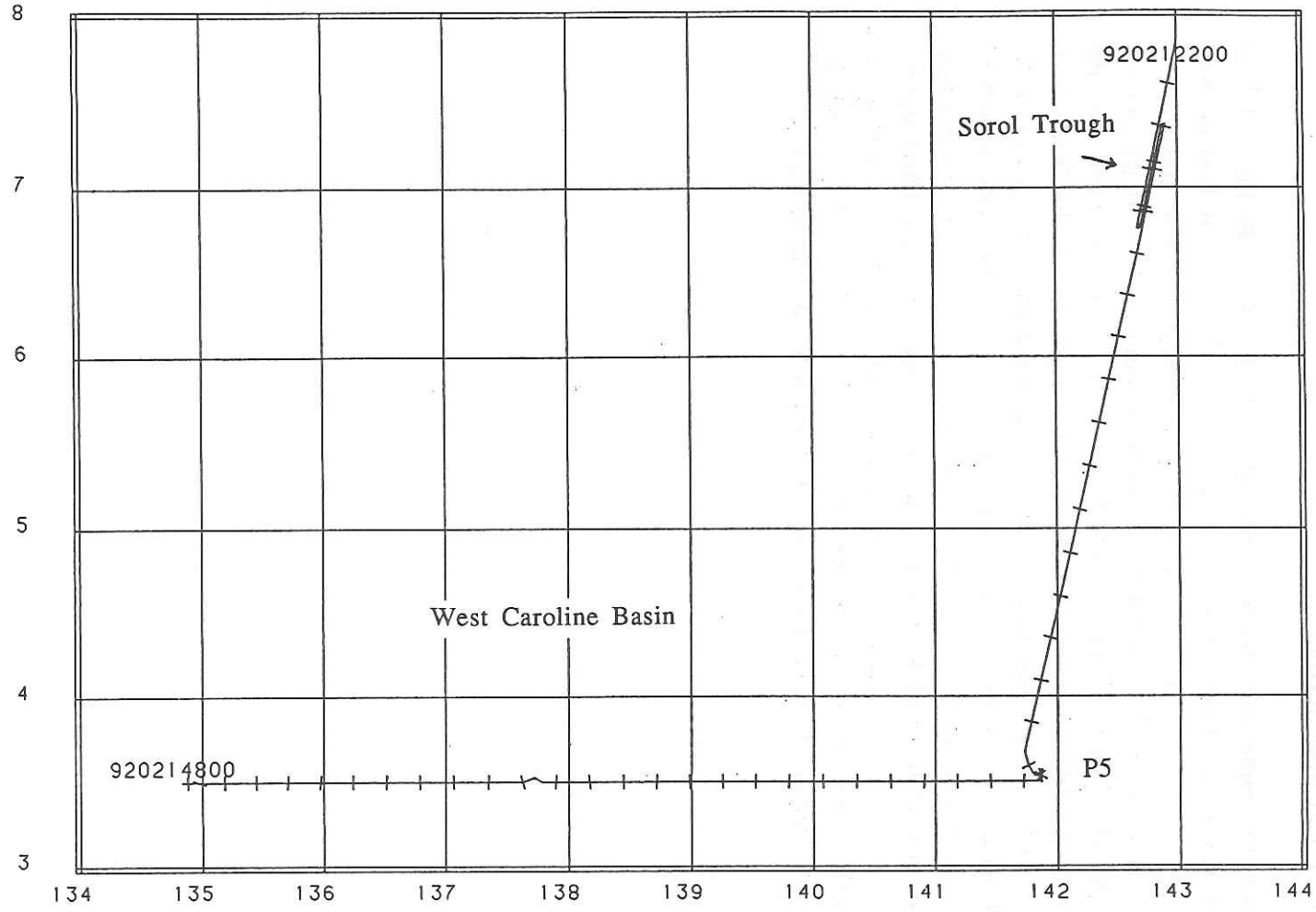

Fig. 16.1 Ship's track from north of the Sorol Trough to the eastern margin of the Ayu Trough. The track started at 02:00 GMT on Feb. 12, 1992 and ended at 08:00 Feb. 14, 1992. The tick mark shows hours.

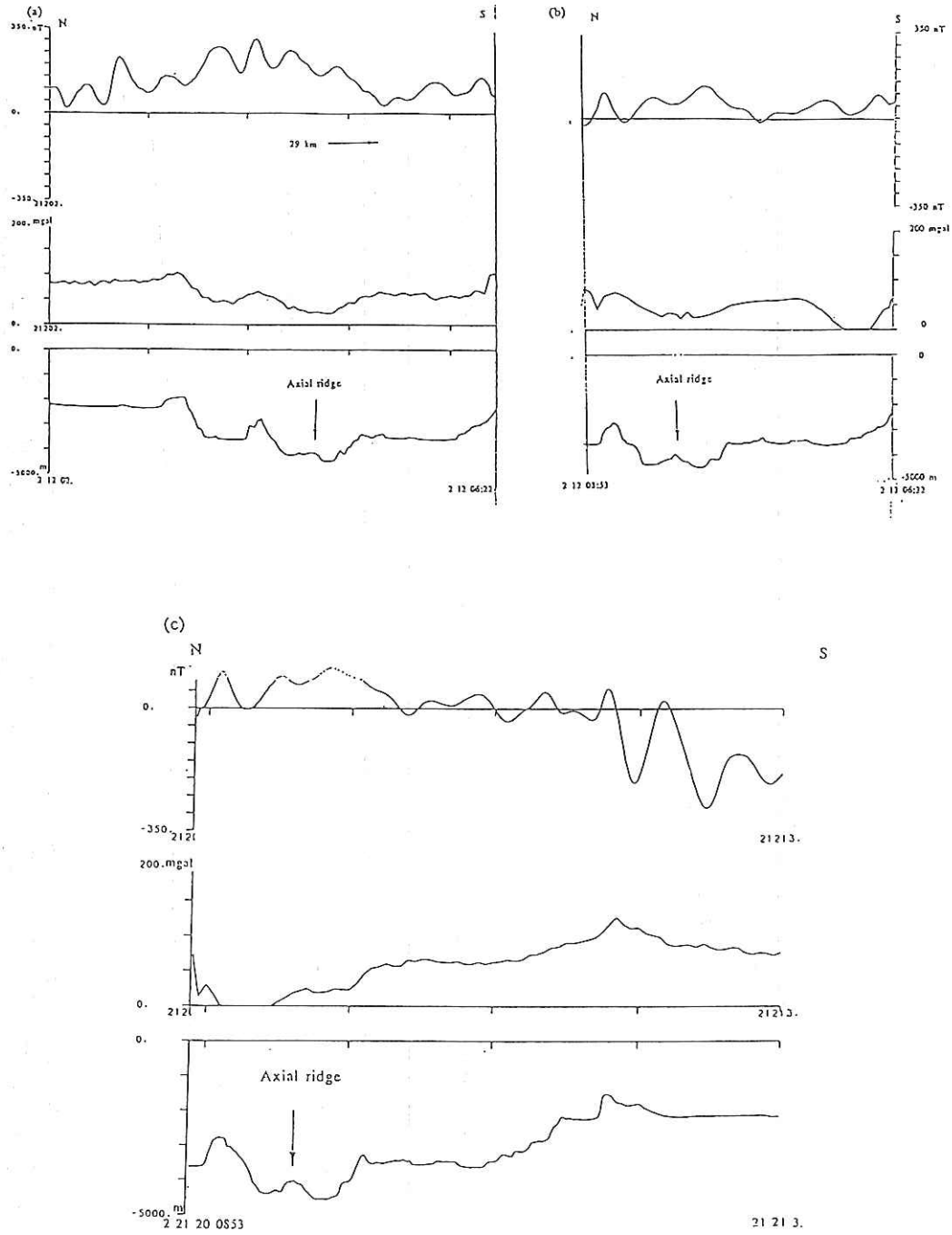

Fig. 16.2 Magnetic anomaly (upper),free-air gravity anomaly (middle), and topography (bottom) along the three lines crossing the Sorol Trough. The abscissa is time; a tick mark indicates hours, and the ordinates are in mgal, nT, and km, from the upper to the bottom. (a) from 02:00 Feb. 12 to 06:22 Feb. 12, (b) from 06:00 Feb. 12 to 08:53 Feb. 12, (in the plot, time is reversed to conform with other profiles from N to S), and (c) from 08:53 Feb. 12 to 13:00 Feb. 12. In profiles (b) and (c), the axial ridge is cearly seen, but in profile (a), it is not obvious.

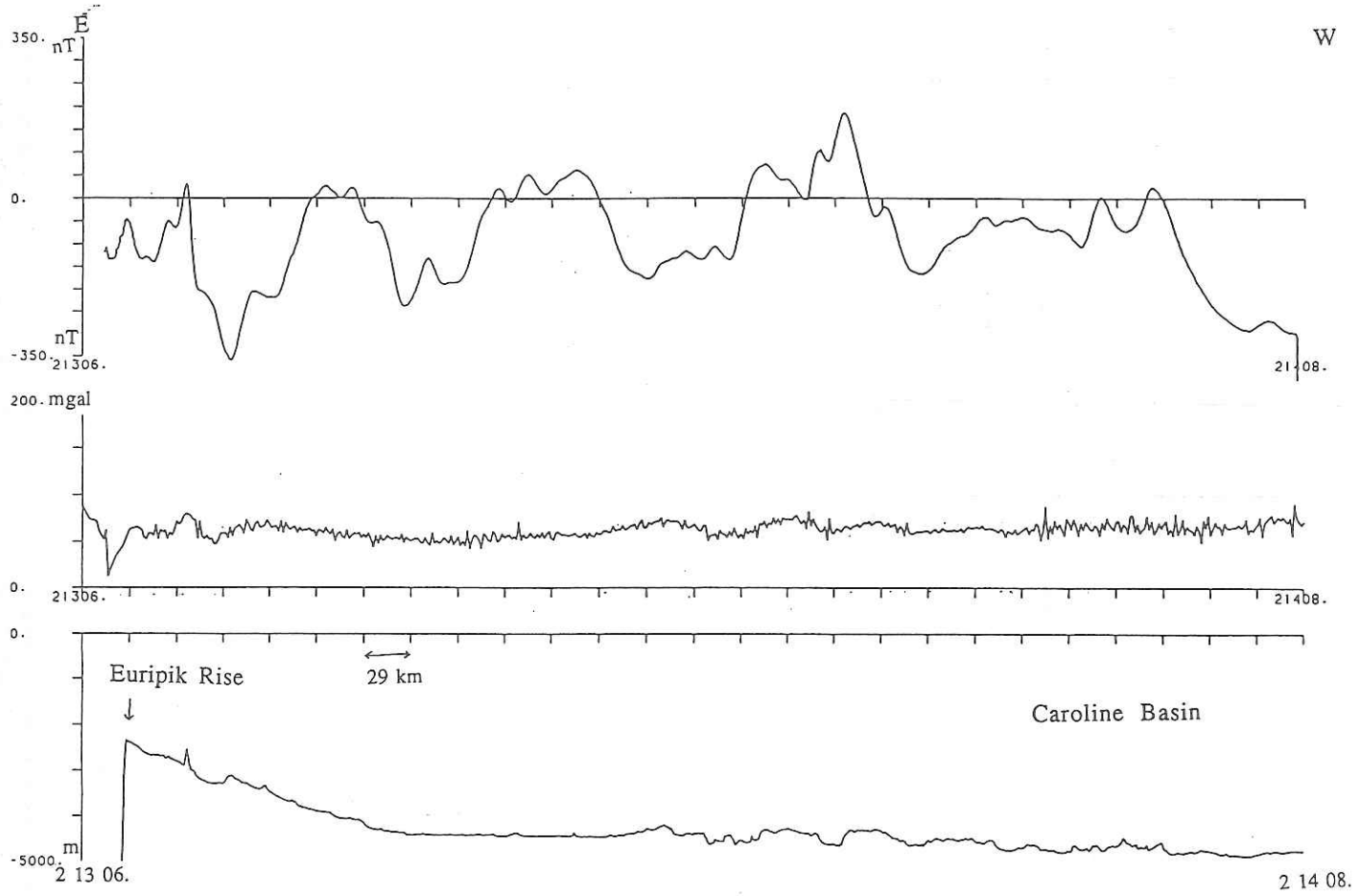

Fig. 16.3 Magnetic anomaly (upper),free-air gravity anomaly (middle), and topography (bottom) along the line crossing the West Caroline Basin. The abscissa is time; a tick mark indicates each hour, and the ordinates are in mgal, nT, and km, from the upper to the bottom. The profile starts at 06:00 Feb. 13 and ends at 08:00 Feb. 14. On the gravity profile, short-wavelength Etvos effects are seen, but the anomaly is almost flat. The large mangetic anomalies would be associated with the spreading of the Caroline Basin.

17. Geophysical Measurements of the West Philippine Basin and the Philippine Trench

H. Toh, T. Fujiwara, T. Seno, K. Tamaki and K. Kobayashi

17.1 Outline of the Measurements

In Leg 1, after the survey around the Ayu trough region terminated at (4°50'N, 132°50'E) on 20/FEB/'92 00:00 UT, the vessel went toward our next port of call, Cebu, (10°12'N, 123°53'E), on which way the West Philippine Basin and the Philippine Trench were crossed and the following geophysical measurements were conducted; SeaBeam mapping, 3.5 kHz subbottom profiler, geomagnetic total force and three-component measurement and sea surface gravity measurement. Thanks to the calm weather, the ship's speed was kept at about 16 knots and fortunately these measurements ended at 21/FEB/'92 08:30 UT without any fatal troubles. In Leg 2, these measurements were restarted at (13°00'N, 124°23'E) on 27/FEB/'92 14:00 UT and continued at (27°50'N, 137°20'E) on 1/MAR/'92 12:30 UT when a grid survey of the Hakuho Seamount, which is described in section 19, was onset. The ship's track is shown in Fig. 17.1.

We hope that these measurements provide an additional geophysical dataset of the West Philippine Basin including the deepest part of the Philippine Trench where conspicuous plate convergence occurs.

As for the 3.5 kHz subbottom profiler, refer to the respective section in this issue (section 18). In this section, a brief examination of the data derived from the SeaBeam mapping, total force and three-component geomagnetic measurement and sea surface gravity measurement will be made in the following.

17.2 Data

17.2.1 Gravity and Magnetics

Figure 17.2 shows the observed free-air gravity anomaly, magnetic anomalies and bathymetry along the ship's track during the latter half of Leg 2. Free-air anomaly coincides well with the topographic changes (A very steep drop at the leftmost part of the bathymetric profile might be a fail in echo-sounding.) showing an entire gravity profile from an oceanic basin to a deep trench though it is superimposed by strong Eotvos effect of short-wave lengths. The large Eotvos effects are to some extent inevitable because 1 knot change in

east-west velocity amounts to as much as 7.5 mgal change in gravity values at these low latitudes. Magnetic anomalies were also observed fairly well with an exception of some noisy part at the western edge of the West Philippine Basin. In contrast to the flatness of both gravity and topography profiles on the basin, the magnetic profiles show sinusoidal changes associated with magnetic lineations. Step-like changes of geomagnetic three-component profiles at the Philippine Trench are due to course changes of the ship accompanied by the SeaBeam survey of the trench. Topography of the Philippine Trench was observed successfully as well, indicating the depth of this part of the trench is as deep as 9500 m.

Figure 17.3 shows the observed free-air gravity anomaly, magnetic anomalies and bathymetry along the ship's track during the first half of Leg 3. Free-air anomaly coincides well with the topographic changes as in the case of Leg 2 showing a profile of the Philippine Trench, the West Philippine Basin and the Kyushu-Palau Ridge. Eotvos effects are reduced gradually as the ship went into higher latitudes. The ship's track was in the north-east direction and the large northward velocities resulted in significant reduction of the Eotvos effects. The basic level of the free-air anomalies on the West Philippine Basin shows a positive value as much as 100 mgal indicating that there is a systematic bias of the new gravity sensor as described in section 9. The anomalies next to the Kyushu-Palau Ridge are those associated with the Oki-Daito Ridge and the Minami-Daito Island. A relatively small anomaly at the left middle of the profile is the north-west extension of the Central Basin Fault discovered by Ben-Avraham and others (Ben-Avraham et al., 1972). The anomalies around the Philippine Trench are a little too small compared with those observed in Leg 2. The reason for this discrepancy is not clear at present and it needs further examination of the two gravity profiles. Magnetic anomalies were also observed fairly well except for a noisy part in the middle of geomagnetic total force profile and for a distinct drift of the sea surface geomagnetic Z-component which can be regarded as the increase of the ship's magnetization associated with the increase of the Z-component of the geomagnetic main field.

17.2.2 SeaBeam Mapping

Although all the SeaBeam data were successfully collected both in the latter half of Leg 2 and throughout Leg 3, most of the SeaBeam maps might become mere straight lines in deep oceans without detailed grid surveys. Here, we simply show the axis of the Philippine Trench surveyed during Leg 2 (Fig. 17.4), in which one of the deepest part of the trench is clearly observed.

In conclusion, the dataset obtained by these measurements is ready for further analyses. Specifically, the three-component geomagnetic measurement seems more successful than the total force measurement in this case and the vector geomagnetic data are suitable for analyses using a novel technique to determine precise magnetic boundaries of the oceanic crust because of their better sensitivity (Seama et al., 1992). Also, gravity anomalies are waiting for more appropriate analysis procedures such as an Eotvos correction method using a Bayesian approach (Fukuda, 1989).

References

Ben-Avraham, Z., C. Bowin and J. Segawa, An extinct spreading centre in the Philippine Sea, *Nature*, **240**, 453-455, 1972

Fukuda, Y., Eotvos correction of surface ship gravimeter using the Bayes type discrete spline function, *J. Geod. Soc. Jpn*, **35**, 299-305, 1989

Seama, N., Y. Nogi and N. Isezaki, A new method for precise determination of the position and strike of magnetic boundaries using vector data of the geomagnetic anomaly field, *Geophys. J. Int.*, 1992 (in press)

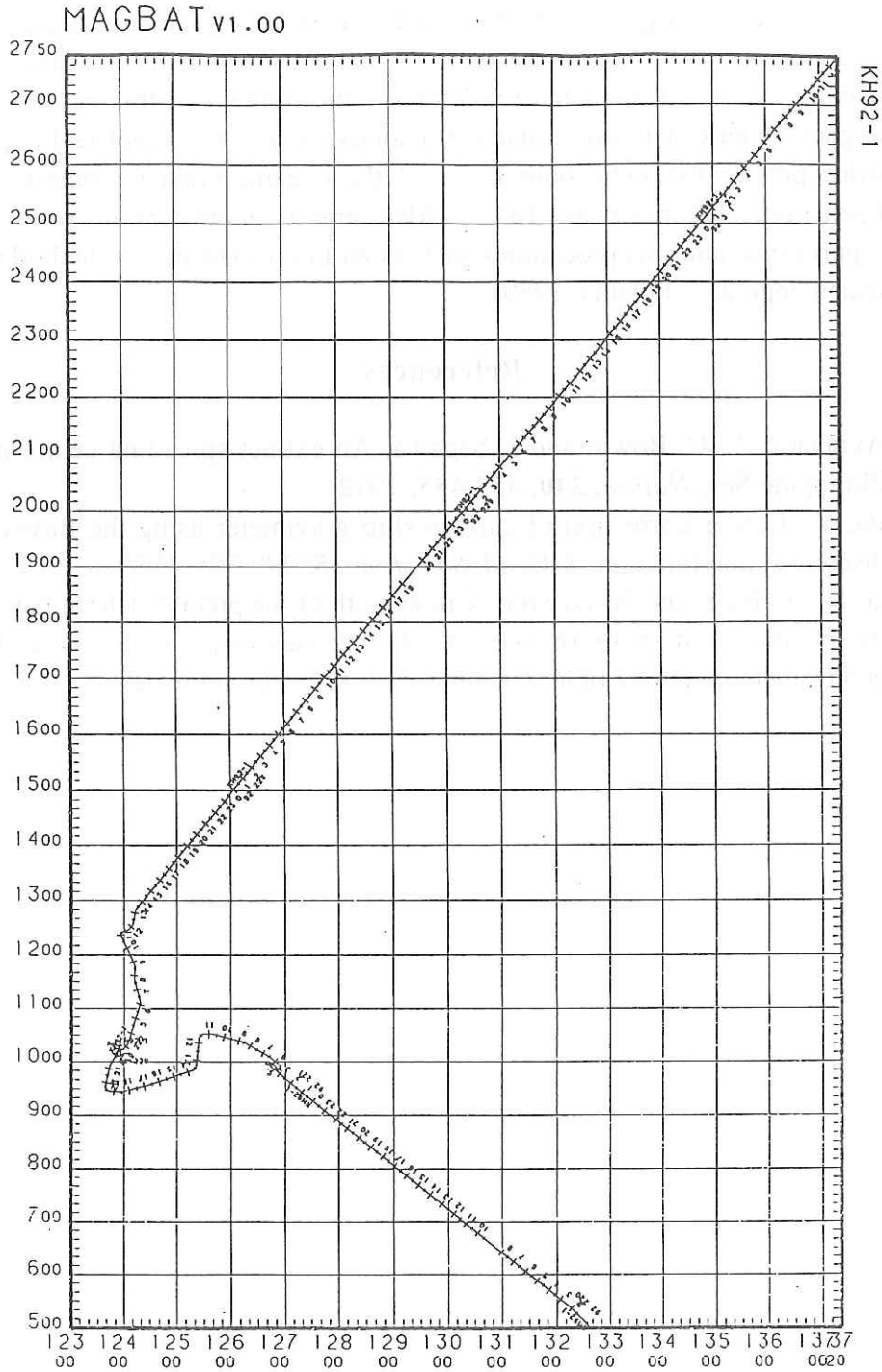

Fig. 17.1 The ship's track from the Ayu Trough to the Hakuho Seamount via Cebu crossing the southern and the central part of the West Philippine Basin. The track started at 00:00 UT on 20/FEB/'92 and ended at 12:30 UT on 1/MAR/'92.

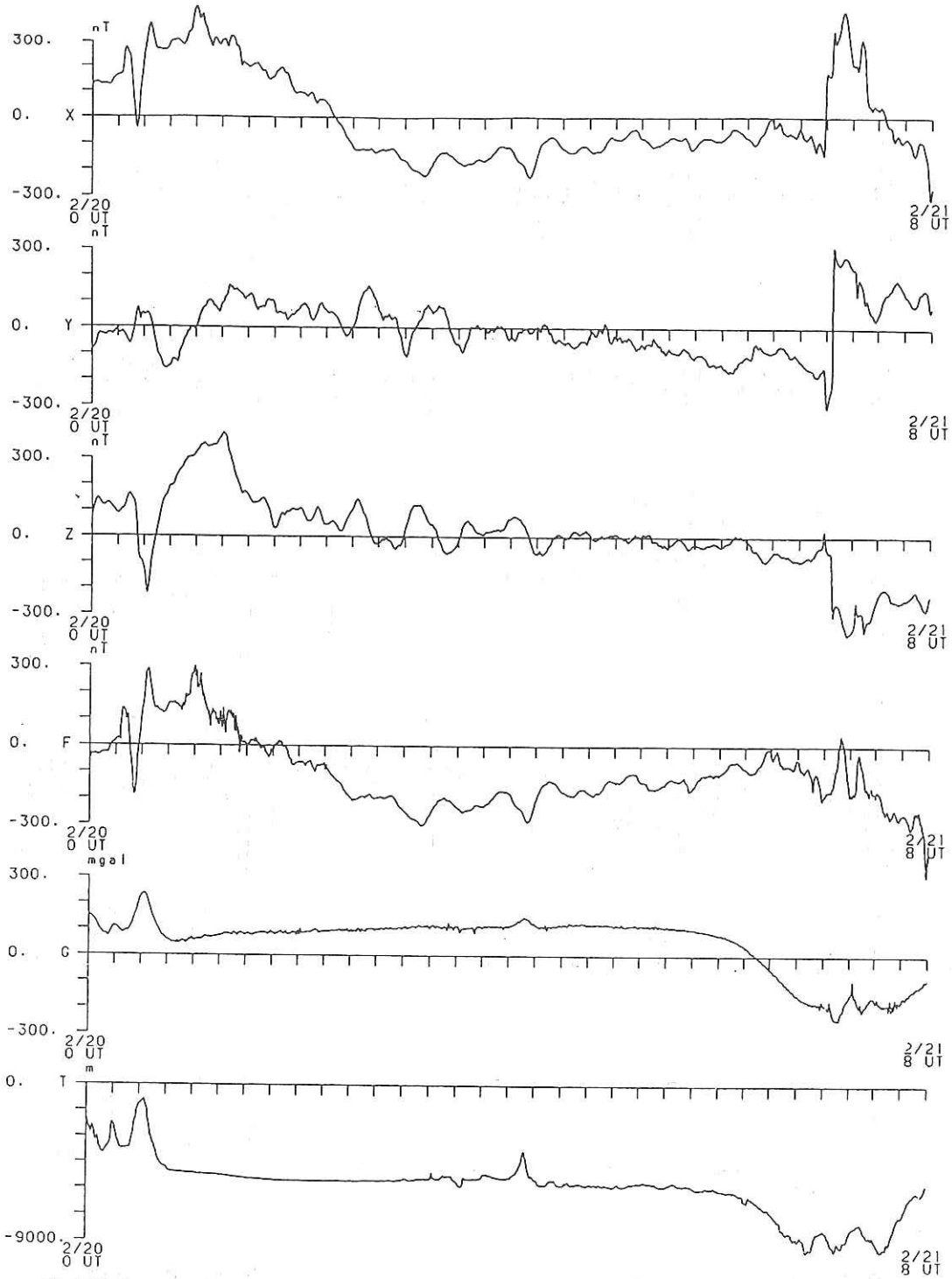

Fig. 17.2 Geomagnetic three-component and total force anomalies, free-air gravity anomaly and topography along the ship's track in Leg 2 from top to bottom. The abscissae are time in hour started at 00:00 UT on 20/FEB/'92 and ended at 08:00 UT on 21/FEB/'92. As the ship's speed was kept at about 16 knots at that time, one division of them corresponds to 30 km approximately. The ordinates are gravity in mgal, magnetic anomalies in nT and topography in m, respectively.

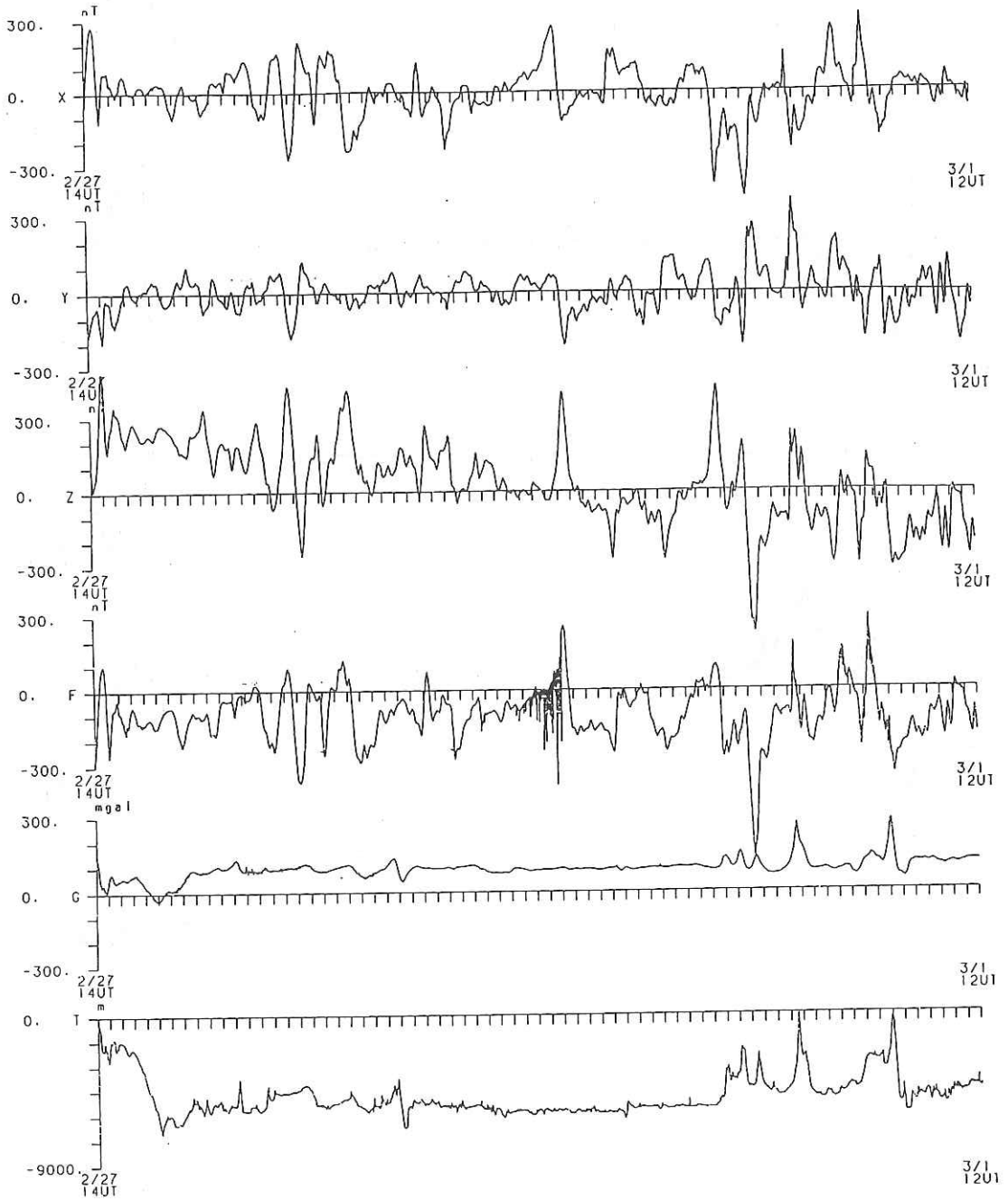

Fig. 17.3 Geomagnetic three-component and total force anomalies, free-air gravity anomaly and topography along the ship's track in Leg 3 from top to bottom. The abscissae are time in hour started at 14:00 UT on 27/FEB/'92 and ended at 12:00 UT on 1/MAR/'92. Legends for the ordinates are same as in Fig. 2.

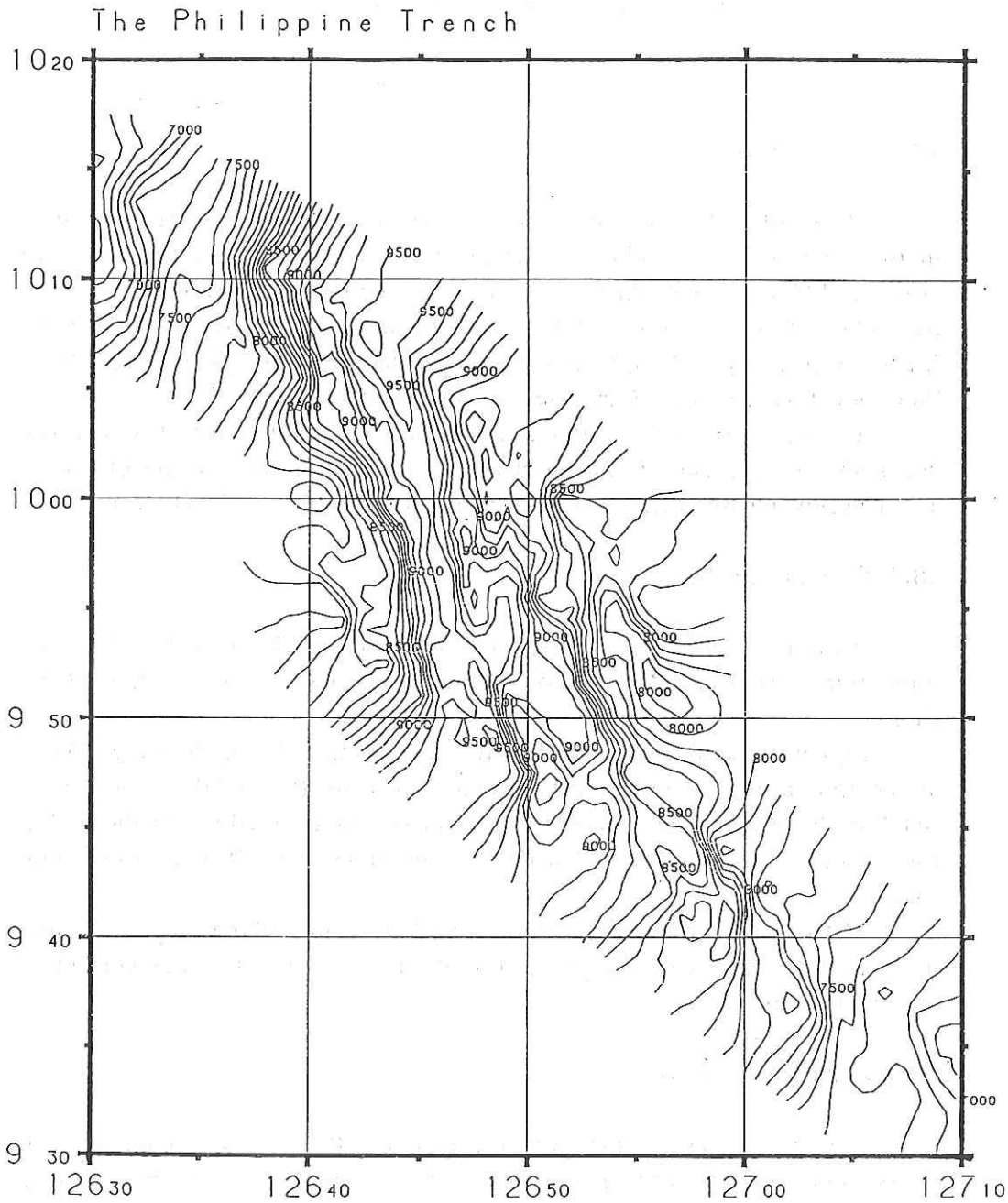

Fig. 17.4 A SeaBeam map of the axis of the Philippine Trench. The depth of this part of the trench is as deep as 9500 m.

18. 3.5 kHz Subbottom Profiling of the Caroline Basin and the West Philippine Basin

C. Igarashi and K. Kobayashi

18.1 Introduction

Mode of sediment cover and superficial sedimentary structure were investigated by 3.5 kHz subbottom profiling in Legs 2 & 3 of the Hakuho Maru cruise KH92-1. Survey tracks cover wide areas in the western central Pacific from Guam to West Caroline Ridge, Sorol Trough, Euripik Rise, West Caroline Basin, Ayu Trough, Philippine Trench to Cebu and from Cebu to the West Philippine Basin, Shikoku Basin via Hakuho Seamount to Tokyo.

The records obtained through this survey clearly indicates acoustic characteristics of surface sediment layers at each district. Sites of piston coring and heat flow measurement were selected according to these 3.5 kHz records.

18.2 System for Survey

Instruments used here consists of 12 acoustic transducer (3*4 TR109) and transceiver system installed in the sonar dome of the bow bottom hull of the ship.

Signal processor and recorder are equipped in Laboratory No. 3. They are composed of a correlation echo sounder processor (CESP III), a transceiver (PTR 105B) and a graphic recorder (LSR 1807) manufactured by Raytheon Co., Ltd. Ship's cruise data were fed through the onboard LAN using fibre-optic cables.

The present survey is set with a record width of 1,000m range, scanning interval of 1.33 sec/scan, a paper feed of 200 lines/ inch and transceiver output power of -6 db.

18.3 Results of Survey

The present cruise has demonstrated that this system in the present adjustment condition can provide good data of structures of bottom surface sediment layer as thick as 100 m at a cruising speed of 16 knots. Some examples of particularly notable results are represented below.

18.3.1 Caroline Basin

After crossing the Sorol Trough the ship approached the crest of the Eauripik Rise at 3°30'N at which piston coring of sedimentary bottom shallower than 3,500m was scheduled. Before reaching the crestal area the 3.5 kHz records show accumulation of sediments on the slope at depths ranging from 4,432m to 4,374m. It is remarkable that layering of sediments are observed even on midslope bottom (Fig. 18.1). At one spot relatively thick sediment accumulated in a deep valley appears to be vertically offset, implying that the active faulting motion is now going there (Fig. 18.2).

In the west Caroline Basin on the way from the Eauripik Rise to the Ayu Trough one area was found in which sedimentary features are quite contrasted by a barrier. In the east of the barrier wall sediment is uniformly stratified, whereas subbottom structure is more irregular and 100m deeper on its west than its east (Fig. 18.3).

18.3.2 Southern portion of the West Philippine Basin

From the Ayu Trough to Cebu port the ship passed through the southern portion of the West Philippine Basin. It is a zone whose ages and origin are not well understood yet. In a gentle northwestward slope (Fig. 18.4) and nearly flat plain (Fig. 18.5) the 3.5 kHz record beautifully reveal features of sedimentary layers. It should be noted that lower reflectors are not parallel to the overlying strata. It seems to indicate that sediments were deposited on a rugged bottom and further modified by later tectonic movement or bottom erosion repeatedly. Elucidation of such sedimentary processes may help us solve geological history of this region.

On the way to Cebu port the reported deepest part of the Philippine Trench was surveyed by Seabeam and 3.5 kHz profiler on a zigzag track. The largest water depth, 9,700m was recognized in the northern end of our track irrespective of previous data (Fig. 18.6a and b). Fig. 18.7 represents 3.5 kHz profile of sedimentary pockets in the seaward midslope terrace of the Philippine Trench.

18.3.3 Cebu port to the Central Basin Fault (West Philippine Basin south)

The ship took a heading of N38.7°E after leaving the San Bernardino Strait. In the southern portion of the West Philippine Basin a great number of small conical domes or knolls with average relative height of 200m were recognized in the Seabeam records. One knoll with crest of 5,440m depth (21°47.9'N, 131°54.0'E) shows clear morphology of caldera (Fig. 18.8). Basin

has topographic linearity composed of small ridge and trough of about 500m amplitude. Their trend is nearly normal to the ship's track N130°E in an area south of 22°N, whereas region close to the Central Basin Fault shows topographic lineation trending roughly NS. Local topography of the Central Basin Fault appears to be also composed of echelon aligned NS trending ridge.

18.3.4 Axial rift of the Central Basin Fault

The ship crossed the axial rift valley of the Central Basin Fault (CBF) of the West Philippine Basin at 17°50'N, 128°30'E. The maximum depth of the fault valley is 6,700m on this profile (Fig. 18.9). Topography of the axial zone is asymmetric relative to the trend of the axis with double ridge on the south and a deep trough on its north. Sediment layers recognized by the 3.5 kHz are rather thin in this rugged zone, whereas strata are clearly seen in a flat basin in its north.

18.3.5 Central Basin Fault to the Oki-Daito Ridge (West Philippine Basin north)

This basin has features similar to that south of the CBF, comprising of small ridges and troughs trending NS in the axial zone but aligned in a direction N130°E roughly normal to the ship's track. A number of knolls were again encountered by the ship.

18.3.6 Kyushu-Palau Ridge to the Shikoku Basin

The ship entered the South Daito Basin after passing through the Oki-Daito Ridge. In the South Daito Basin the ship came over the crest of Beijyu Seamount with minimum observed depth of 100m. It passed through the eastern end of the Daito Ridge at which topography of ridge is obscure. Then it crossed the Kyushu-Palau Ridge at the crest of Minami-Koho Seamount nearly 350m deep (26°10'N, 135°45'E).

The western portion of the central Shikoku Basin is characterized by very rugged topography observed by Seabeam. Majority of the topographic lineations trends roughly N10°W which is subparallel to the trend of the Kyushu-Palau Ridge N30°W (Fig. 18.10). Linear small ridge and trough assemblies are offset and aligned an echelon to become as a whole parallel to the magnetic lineations and the Kyushu-Palau Ridge.

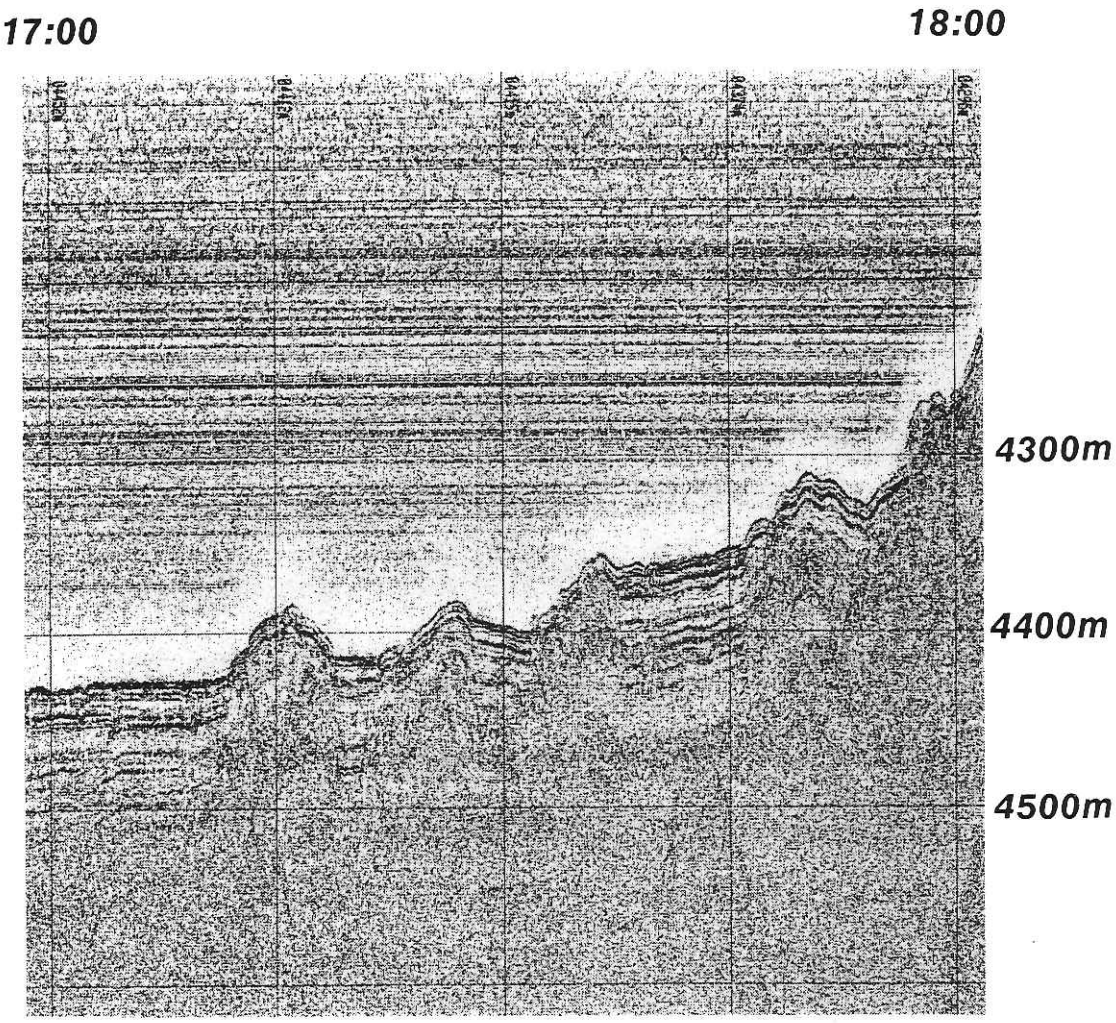

Fig. 18.1 3.5 kHz record showing layers of sediments in a slope of the Eauripik Rise. KH92-1 Leg 2, Feb.13, 17:00~17:45GMT.

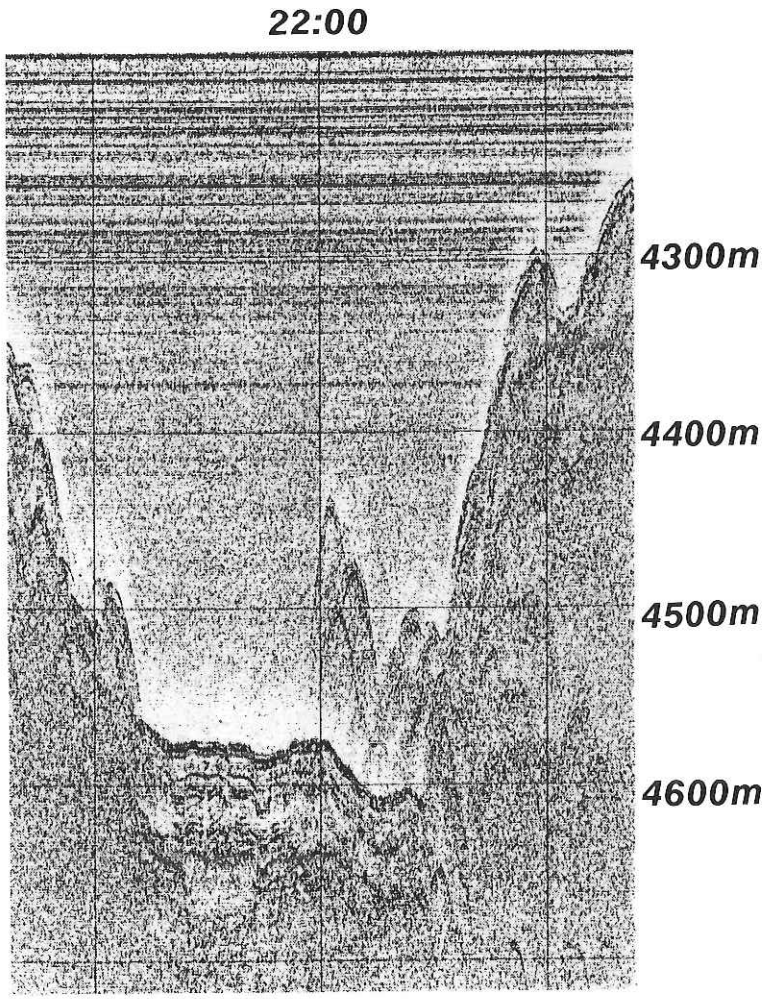

Fig. 18.2 3.5 kHz record providing evidence of faulted sediments in a valley i n the Caroline Basin. D=4,593m. Feb.13, 21:45~22:00GMT.

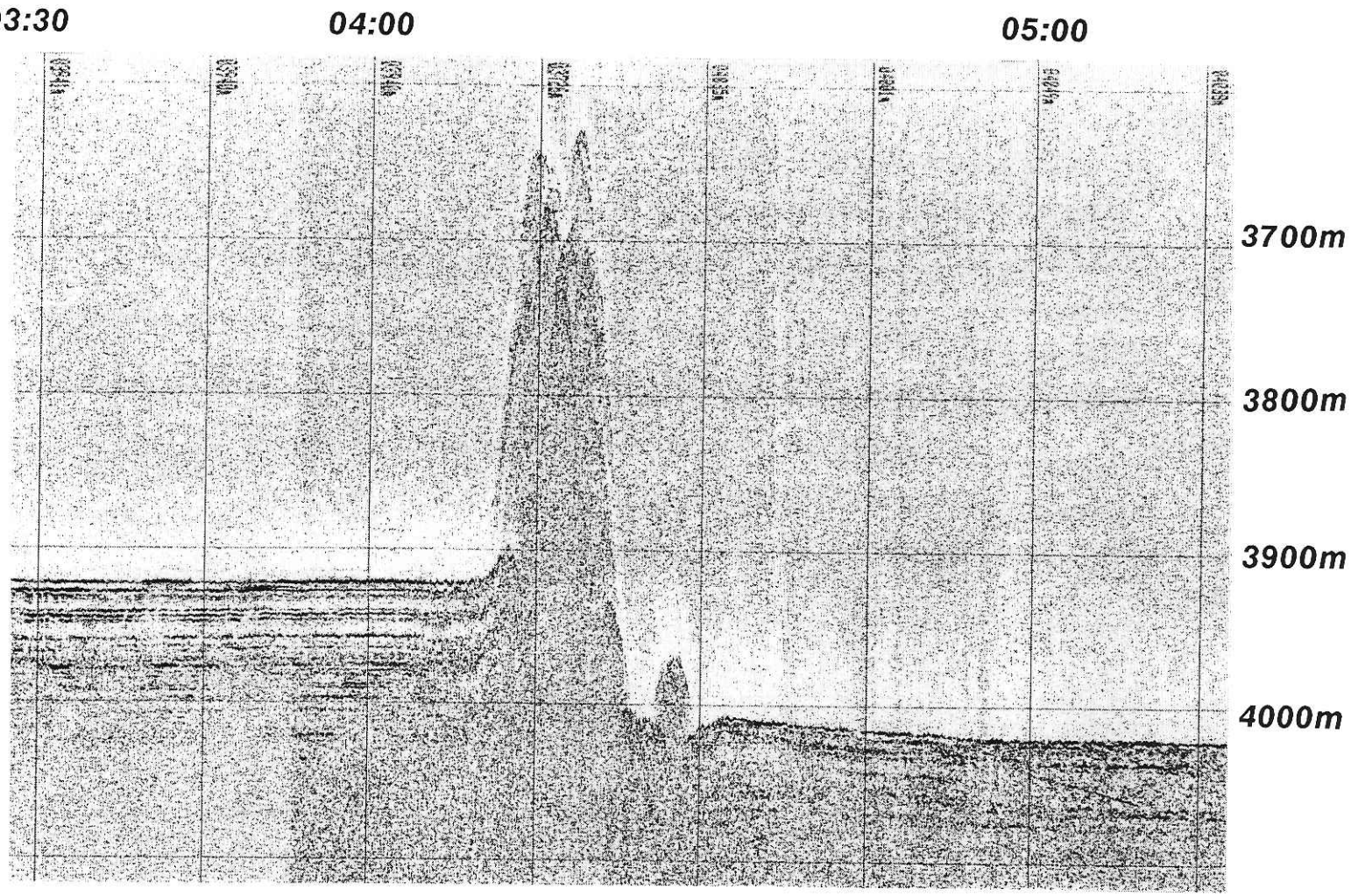

Fig. 18.3 3.5 kHz record indicating contrasts of two wings in water depths and sediment structure. D=3,941m (east), 4,049m (west). Feb. 16, 03:30~05:15GMT.

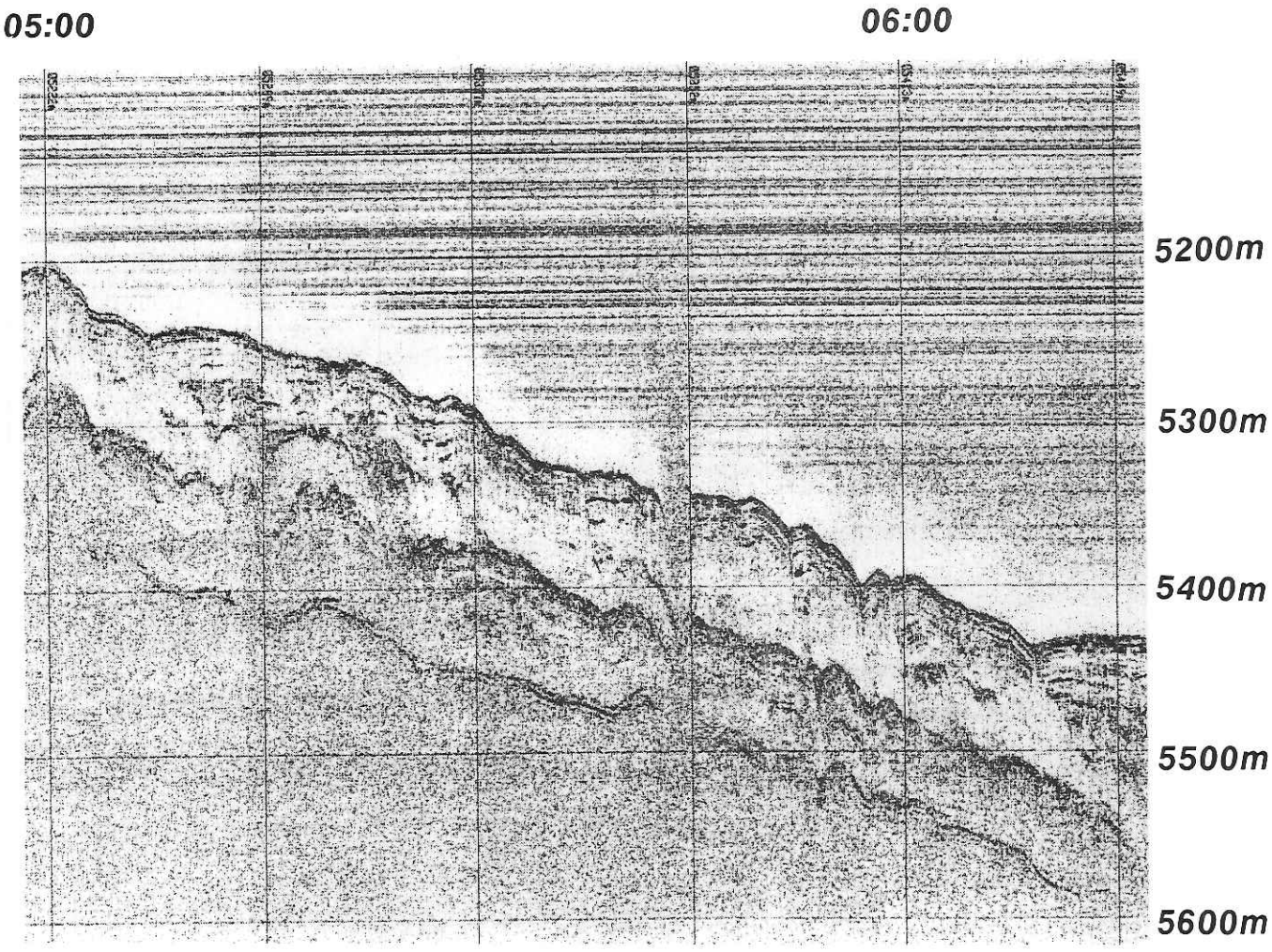

Fig. 18.4 3.5 kHz record demonstrating iregular overlapping of sediment layers in the southern West Philippine Basin. D=5,222m~5,449m. Feb. 20, 05:00~06:15GMT

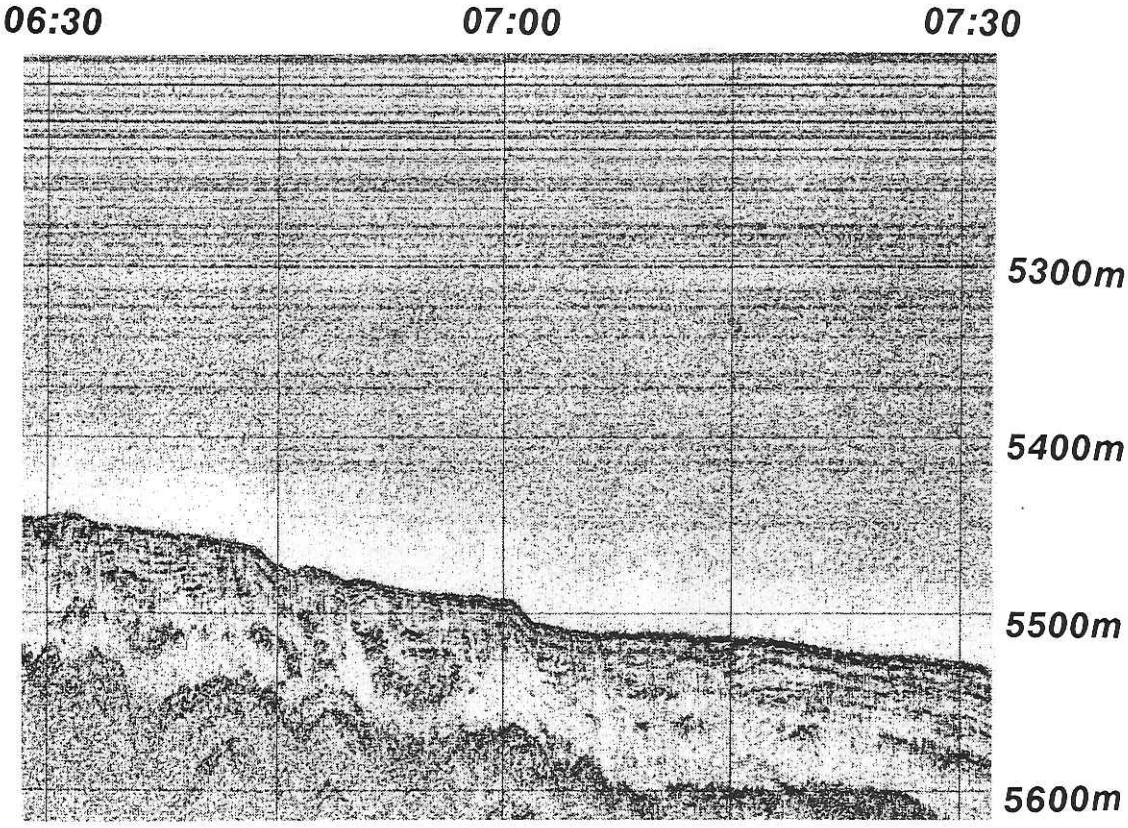

Fig. 18.5 3.5 kHz record showingirregular overlapping of sediment layers overlying rugged basement beneath flat sea bottom. D=5,445m~5,556m. Feb. 20, 06:30 07:30GMT

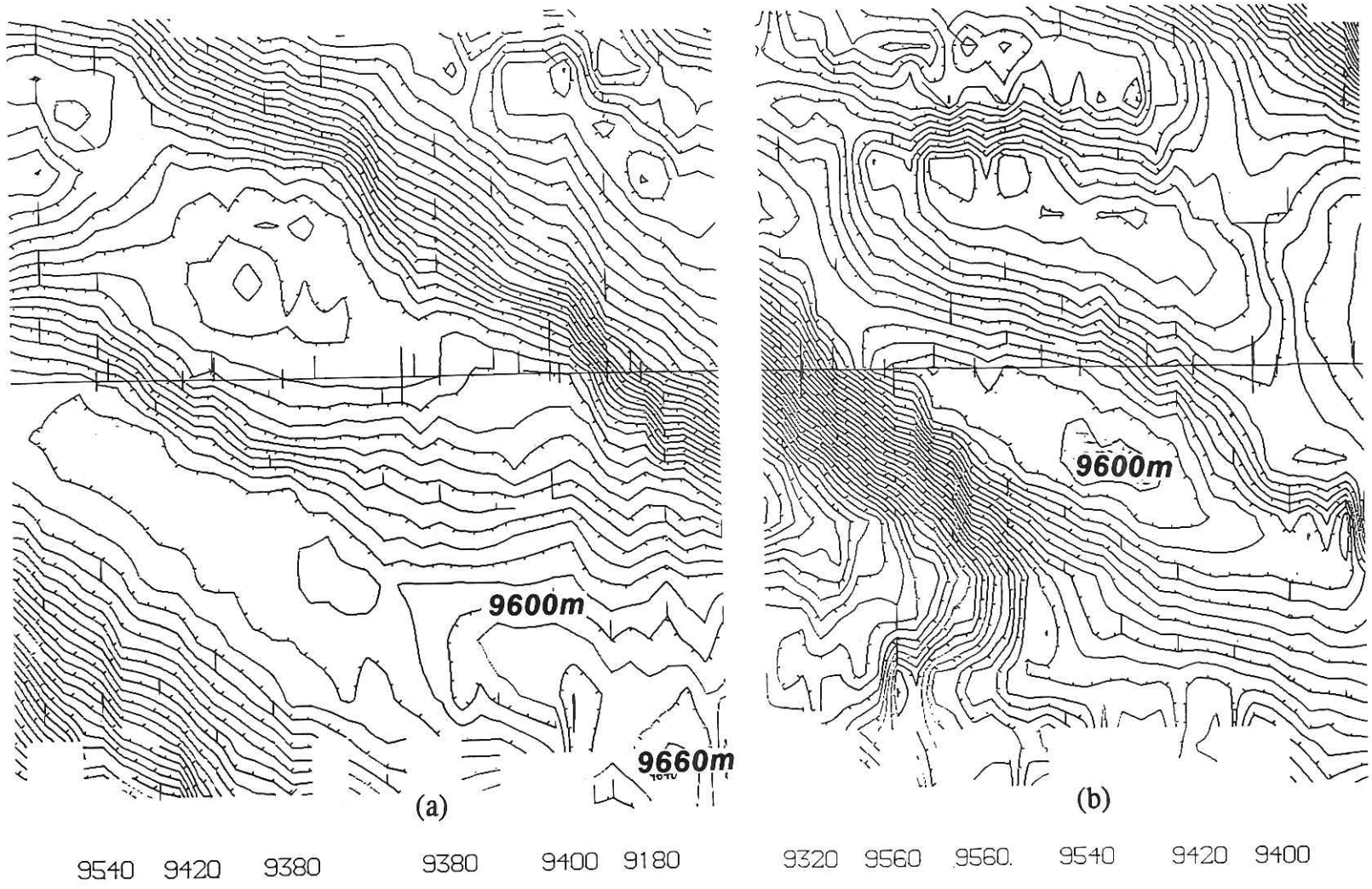

Fig. 18.6 Seabeam chart of axis of the Philippine Trench south. (a) southe6rn deep, D= 9,600m. (b) a deep in the northern extremity of our tracks, D= 9,660m.

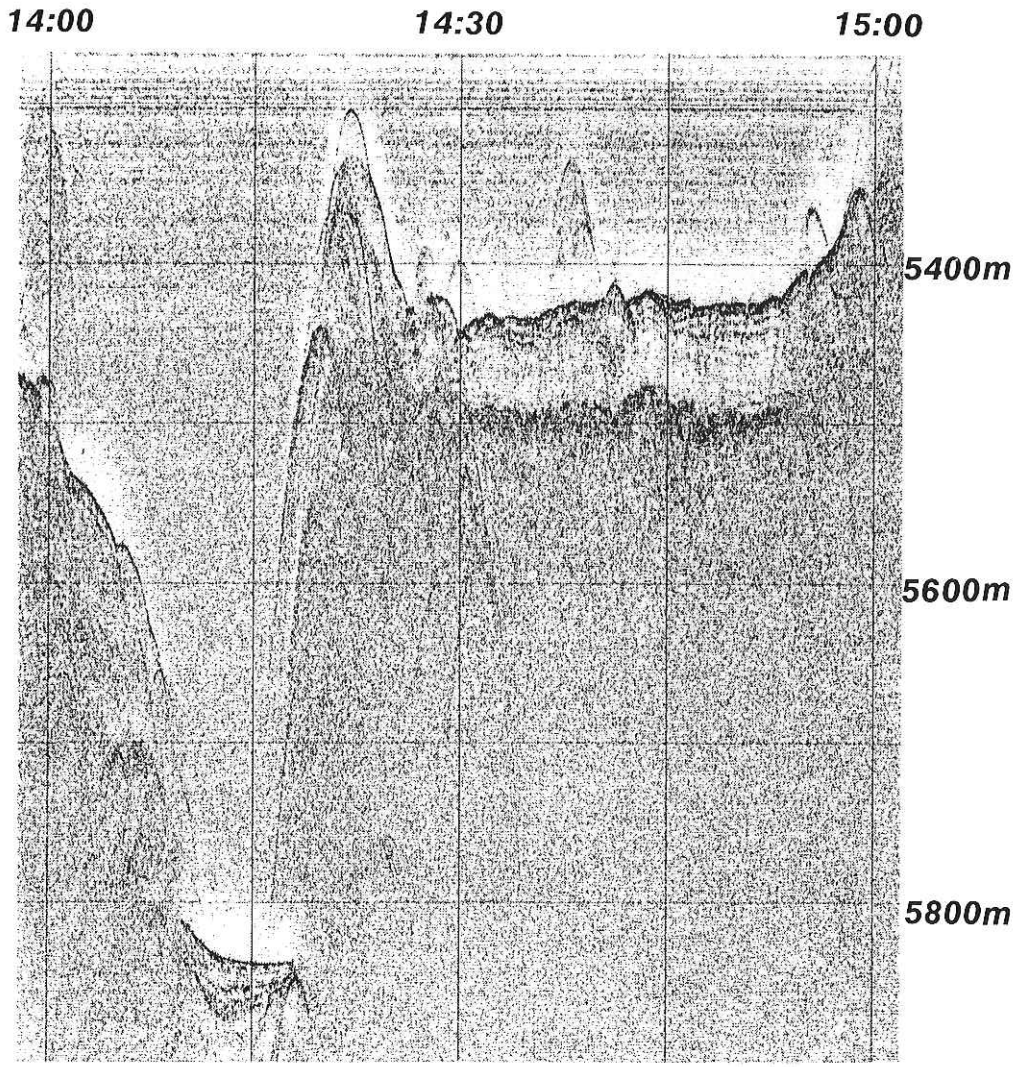

Fig. 18.7 3.5 kHz record of sediment pockets in the seaward terrace of the Philippine Trench south.

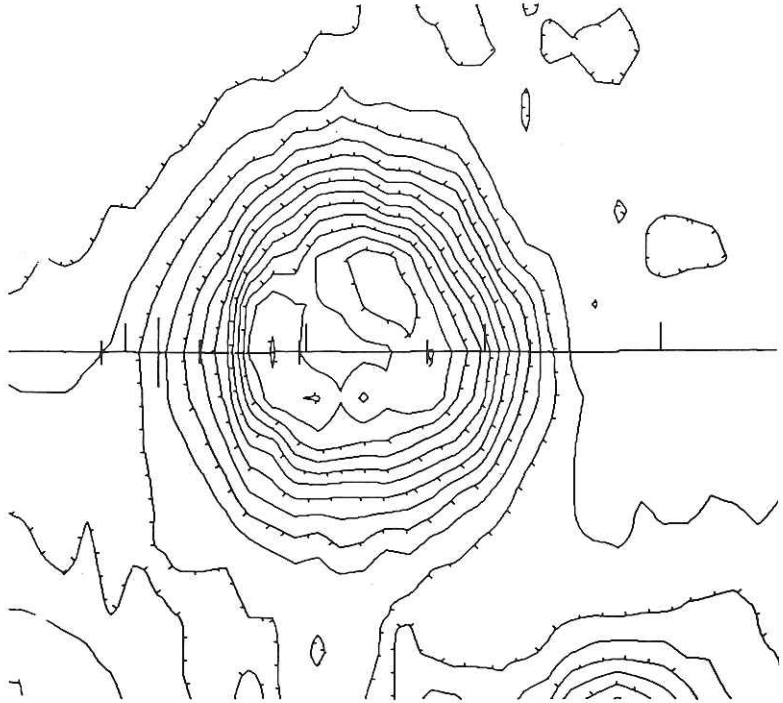

5660 5580 5460. 5440 . 5600

Fig. 18.8 Seabeam chart showing a knoll in the central portion of theWest philippine Basin. Remark the peculiar topography of the crest similar to a caldera. Feb. 28, 08:48GMT. Contour interval is 20 m.

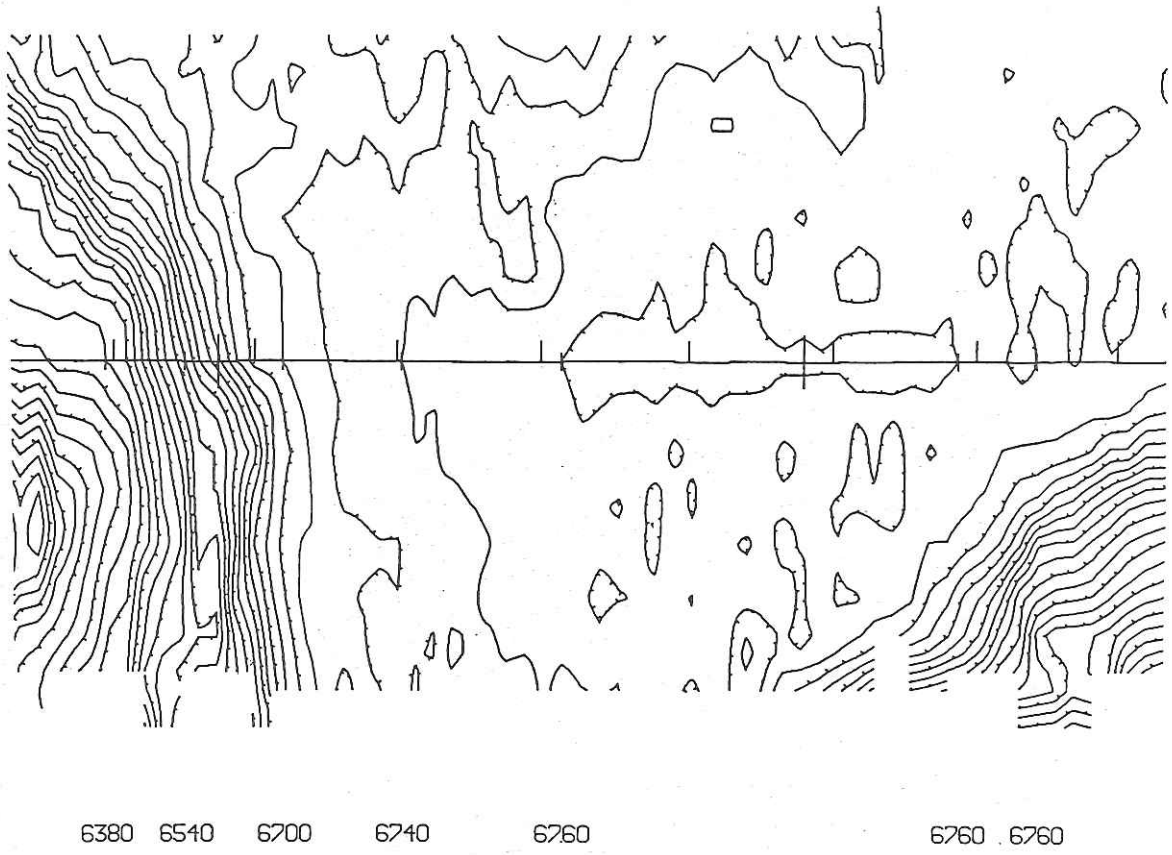

Fig. 18.9 Seabeam chart of the axial valley of the Central Basin Fault;

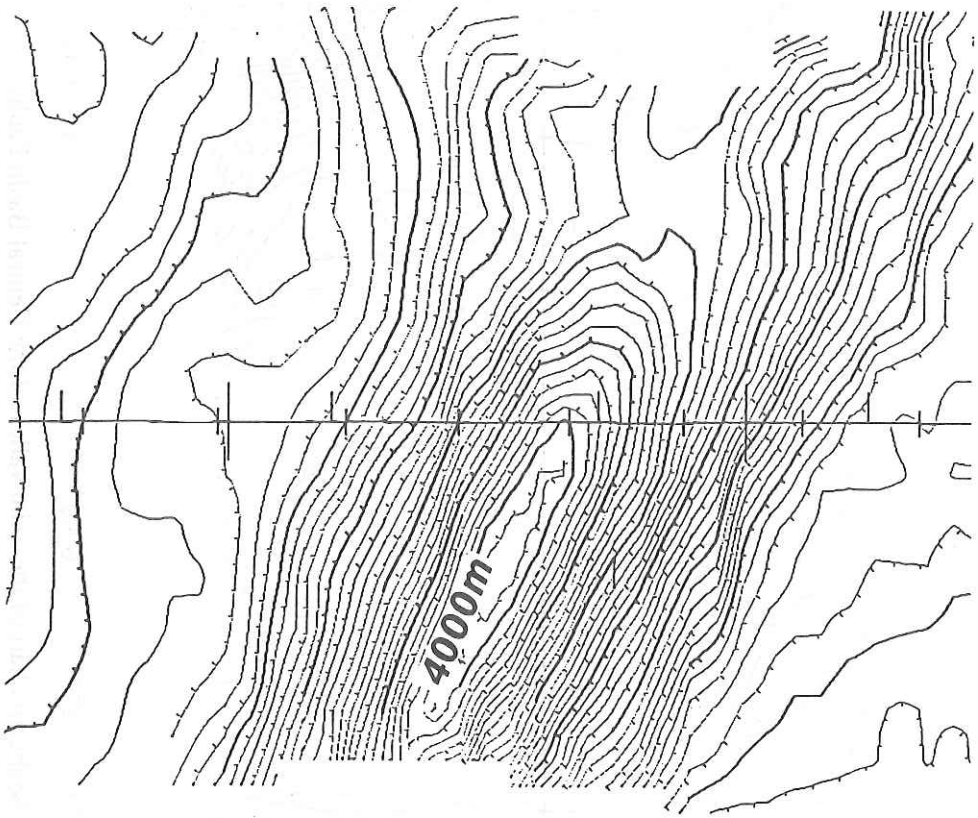

4400 . 4360 4300 4100 3900. 4120 4380. 4460

Fig. 18.10 Topographic trend of the Shikoku Basin west.

19. Survey of HAKUHO Seamount in the Shikoku Basin

K. Kobayashi and T. Fujiwara

19.1 Background Knowledge

The Hakuho Seamount exists at 28°N;137°30'E in the midst of the Shikoku Basin. It was recorded in hydrographic chart but its detailed topography and geophysical features were surveyed for the first time by the R.V.Hakuho Maru using a widebeam echo sounder in her cruise KH 74-4. A boulder of pillow basalt was collected by a dredge haul from the upper slope of the seamount (D=2,200-2,700m). Petrographic and magnetic properties of the rock were studied (Tokuyama and Fujioka, 1976; Furuta et al., 1980) The name Hakuho was officially approved by the Committee for Topographic Names of the Sea and listed in up-dated hydrographic charts.

This seamount is one of the Kinan Seamount Chain aligned in the central portion of the Shikoku Basin. The chain trends in a direction of N25°W,which is nearly parallel to overall trend of the magnetic lineaments in the Shikoku Basin (Tomoda et al , 1975; Watts and Weisel, 1975;Kobayashi and Nakada, 1977; Shi 1980; Chamot-Rooke et al., 1987).

Hydrographic Department, Maritime Safety Agency of Japan recently made comprehensive survey of the Shikoku Basin area as a part of their Continental Shelf Survey Program using Seabeam multi-narrow beam echo sounder equipped with S.V. Takuyo and measured bathymetry and other geophysical parameters of the ocean floor surrounding this seamount. However, since their survey tracks were mostly running EW spaced by 5-nautical miles, precise topography of the seamount was not fully revealed yet.

19.2 Bathymetric and Geophysical Survey in the Cruise KH 92-1

On the way back from Cebu, Philippine we took a survey track crossing the central portion of Oki-Daito and Daito Ridges, Kyushu-Palau Ridge and eastern half of the Shikoku Basin toward the Hakuho Seamount. Over the Hakuho Seamount the ship took survey tracks shown in Fig. 19.1. Water depths, 3.5kHz subbottom profiles, gravity, magnetic total force and magnetic three components were continuously measured along these track lines at a speed of 16 knots in average. All the measurements were completely done and recorded in the ship's data logger. In this section the bathymetric results are briefly presented, leaving other studies in other sections in this issue or elsewhere.

Fig. 19.2 represents topographic map with contour interval of 100 m. Depths have an accuracy better than 20 m. Topographic features are essentially the same as revealed by the old-fashioned echo sounder. Most remarkable is elongation of topography in a direction of N40-45°W, which is quite oblique to general trend of the basin structure (Kobayashi, 1984). Such an obliqueness seems to have been caused by a change in tectonic stress field in the final stage of basin opening.

SeaBeam data obtained by Hydrographic Department are not included in the present investigation. If both sets of data are combined, further complete analysis may be possible, as directions of tracks in two works are roughly perpendicular and mutually supplementary with each other.

References

Chamot-Rooke, N., R. Vincent and X. Le Pichon, Magnetic anomalies in the Shikoku Basin: a new interpretation. Earth Planet. Sci. Lett. 83, 214-228, 1987.

Furuta, T., S. Tonouchi and M. Nakada, Magnetic properties of pillow basalt from the Kinan Seamount Chain, the Shikiku Basin. J. Geomag. Geoelectr., 32, 567-573, 1980

Kobayashi, K., Subsidence of the Shikoku back-arc basin. Tectonophysics, 102, 105-117, 1984

Kobayashi, K. and M. Nakada, Magnetic anomalies and tectonic evolution of the Shikoku inter-arc basin. J. Phys. Earth, 26 (suppl.), 391-402, 1978

Shi, T. C., Magnetic lineations in the Shikoku Basin. In Klein, G. de V. and K. Kobayashi (eds.), Initial Reports DSDP, US Govern. Printing, 58, 783-788, 1980.

Tokuyama, H. and K. Fujioka, Petrologic study on basalt from Kinan Seamount and DSDP site 54 (in Japanese). Kaiyo Monthly, 8, 184-191, 1976.

Tomoda, Y., K. Kobayashi, J. Segawa, M. Nomura, K. Kimura and T. Saki, Linear magnetic anomalies in the Shikoku Basin, northeastern Philippine Sea. J. Geomag. Geoelectr., 28, 47-56, 1975.

Watts, A., B. and J. K. Weissel, Tectonic evolution of the Shikoku marginal basin, Earth Planet. Sci. Lett. 25, 39-250, 1975.

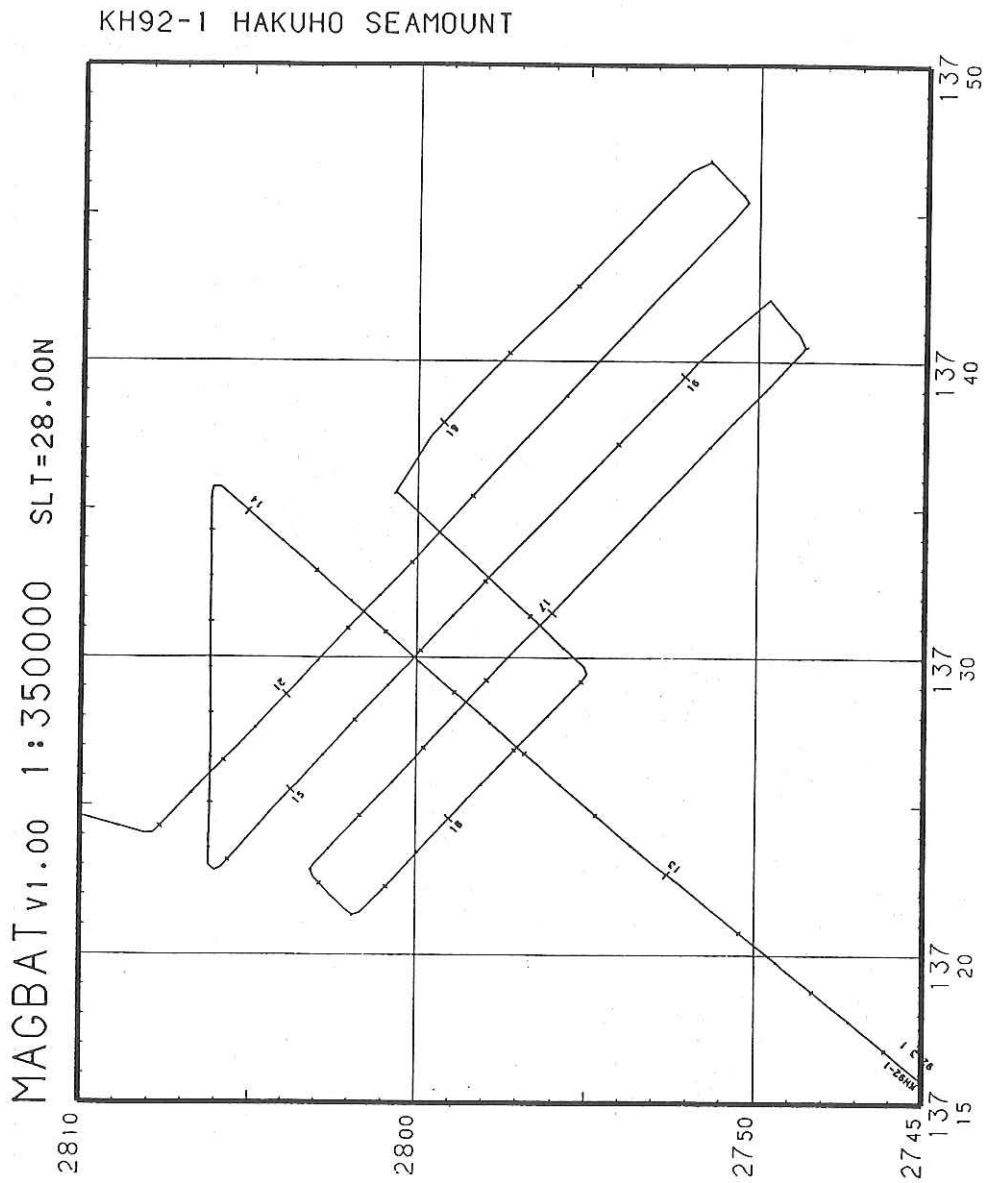

Fig. 19.1 Ship's tracks for bathymetric and geophysical survey of the Hakuho Seamount in the cruise KH 92-1.

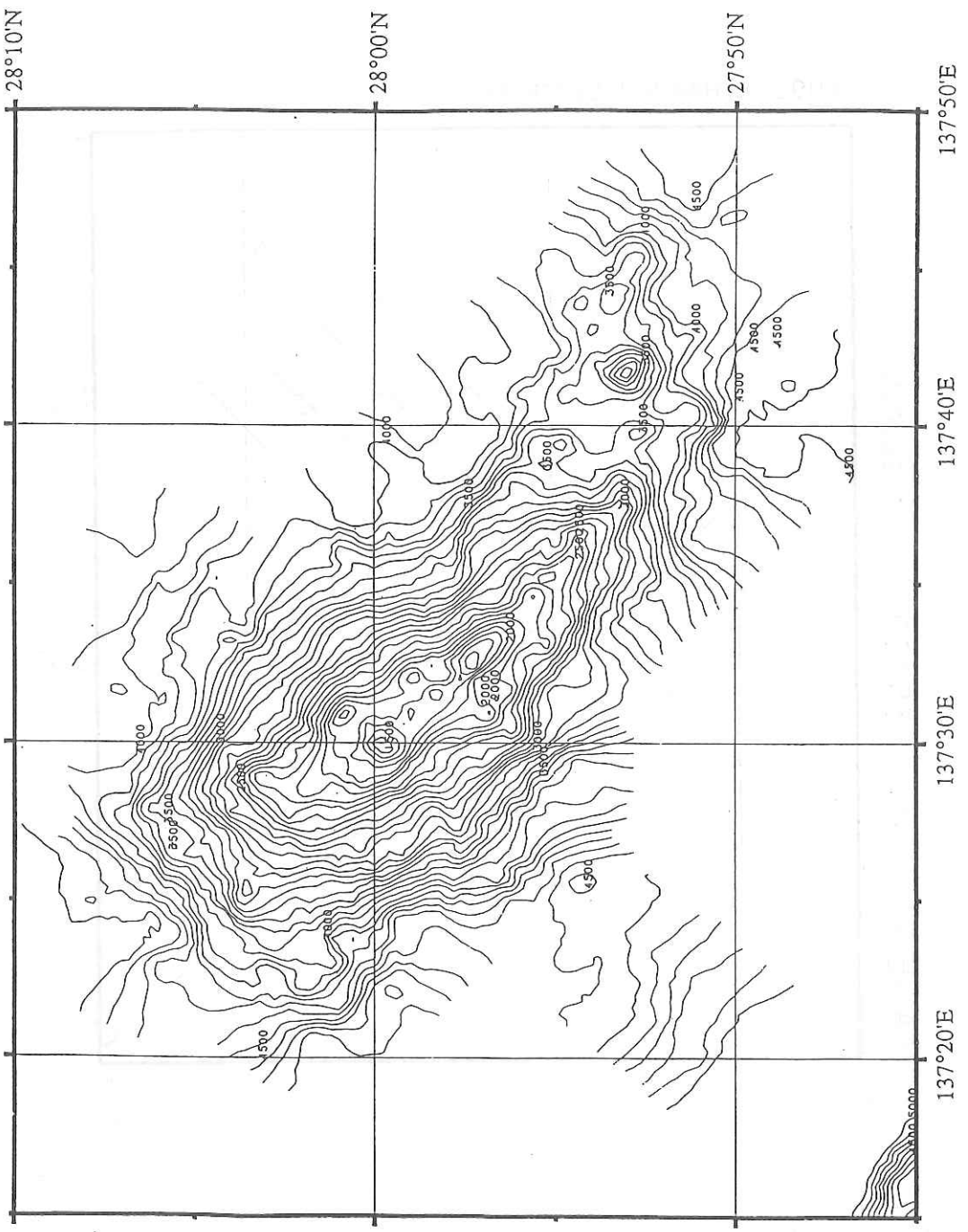

Fig. 19.2 Newly obtained SeaBeam map of HAKUHO Seamount in the KH92-1 cruise.

20. Measurements of Aerosols (RaA, RaC', Mie-Particles and Condensation Nuclei) and Electrical Conductivity in the Atmosphere near the Sea Surface

T. Tanji

20.1 Introduction

For ten years we have made measurements of RaA, RaC', Mie-particles, condensation nuclei and electric conductivity in the atmosphere near the sea-surface over the Pacific Ocean, to clarify the present condition of atmospheric environment. In this cruise we made measurements of the items mentioned above. Since the analysis of measuring results of Mie-particles and condensation nuclei is going on because of large numbers of data, we present measuring results of radon daughters in this report.

20.2 Measuring Methods and Instruments

To make these measurements we have adopted the same instrument and method for each measuring item.

For RaA and RaC' measurement we adopted a filter-pack method in which aerosols in sample air fed by suction pump are collected on a membrane filter and alpha events from radioactive aerosols on the filter are counted by a silicon semiconductor detector fitted with a mutichannel pulse-height analyzer. We operated the system every four hours during full period of the cruise. Each operation contained three counting phases, i.e.' growth, decay 1 and decay 2. At the growth phase the system counted alpha events during the period of aerosol sampling on a filter. We set this phase 10,000 seconds. In two decay phases followed the growth phase the system counted alpha events from aerosols on the filter after sampling. Each decay phase was set 1,000 seconds.

For Mie-particle measurement a light-scattering type particle counter was adopted. It works automatically and counts aerosol particles in five ranges, 0.3 - 0.5 μm, 0.5 - 1.0 μm, 1.0 - 2.0 μm, 2.0 - 5.0 μm and over 5.0 um in diameter. The system was set to count these particles every one liter of sample air and to calculate mean values of 10 counting results for each size range, generally over the open sea. The period of one counting cycle was 130 seconds.

For condensation nucleus measurement we adopted a Pollak type condensation nucleus counter. Bacically this instrument consists of a pipe-

shaped cloud chamber fitted with a lamp and a solar battery at one and the other ends of the chamber, respectively. It was operated automatically every 78 seconds during full period of the cruise.

For measurement of atmospheric electric conductivity a Gerdien type conductivity apparatus was adopted. Basically it consists of a cylindrical air condenser fitted with a vibrating reed electrometer. This apparatus should be operated automatically every 10 minutes during full period of the cruise but it did not work well.

20.3 Results and Discussions on RaA Concentration

Fig. 20.1 shows distribution of RaA concentration observed along the cruise route. In the figure notations A, B, C, ..., U on the abscissae denote ship positions corresponding to those on the cruise route. From Japanese Islands to point C or D, northern part of Mariana Islands, RaA concentration distributed 0.05 - 0.3 Bq/m^3. From Cebu (Philippine) to Tokyo (excepting areas among or close to Philippine Islands), we observed similar values of RaA concentration. Among the southern part of Mariana Islands and the western part of Caroline Islands it distributed 0.005 - 0.02 Bq/m^3, and these values seemed to be comparable to those obtained at some areas of ocean more than 1,000 or 1,500 km offing from large islands or continent during foregoing expedition cruises.

The Philippine Sea locates near continents (Eurasian and Australian) or large islands (e.g., Japanese Islands, Taiwan, Philippine Islands, Borneo and Surawesi) within 1,500 km roughly. Therefore the values of RaA concentration obtained during this cruise over the Philippine Sea seems to be somewhat lower than those forecast before the cruise comparing with the values obtained during foregoing cruises. We have not clarified yet why RaA concentration obtained during this cruise over the Philippine Sea distributed such values.

For more detailed discussion, much more observation data are required. We wish to make some more measurements in the near future.

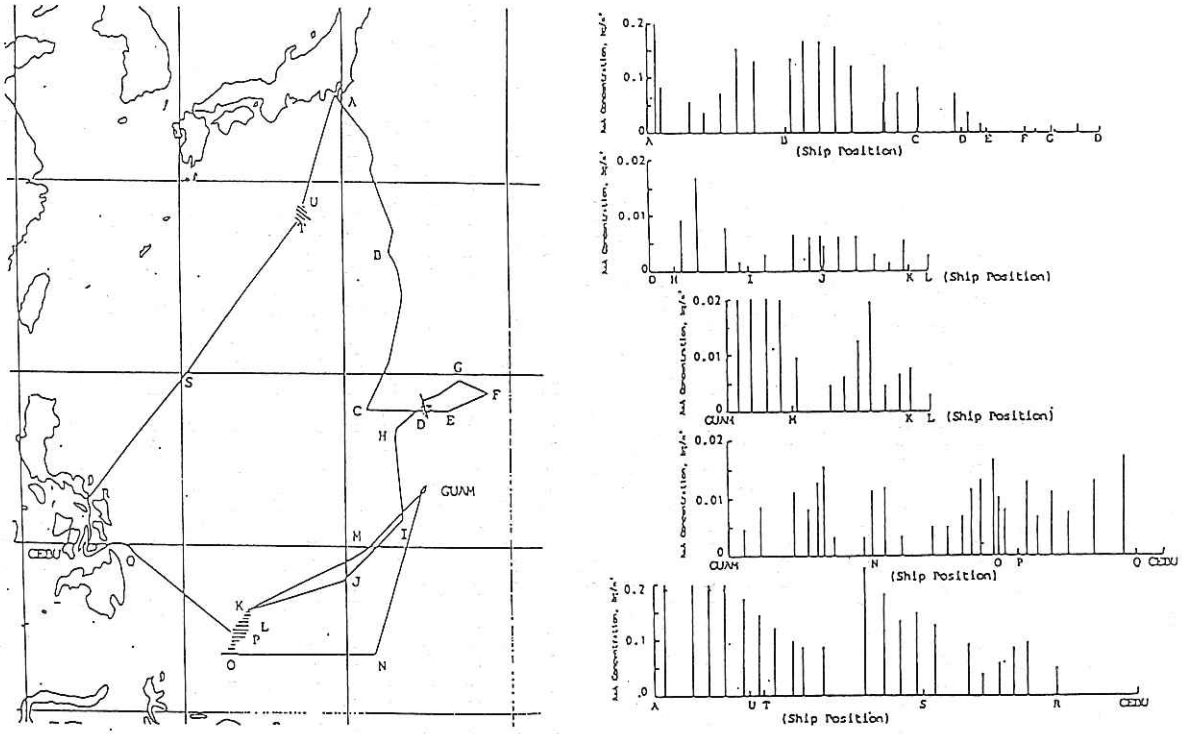

Fig. 20.1 Distributions of RaA concentration observed over the Philippine Sea.

21. Station Log of KH92-1 Cruise

Date/Time	Latitude	Longitude	Depth	Event

Leg 1 : Set Sail from Tokyo to Guam

9201210800+09C35 06.275N139 43.517E 0671
9201210851+09S34 53.860N139 42.050E 0476 a/co to 144°
9201211130+09S34 20.800N140 12.040E 2349 8-SHAPE ROTATION RIGHT TURNING
9201211139+09S34 20.870N140 11.890E 2355 8-SHAPE ROTATION LEFT TURNING
9201211150+09S34 20.930N140 12.030E 2355 8-SHAPE ROTATION FINISH
9201211159+09S34 20.300N140 12.700E 2334 PROTON SURVEY START
9201220013+09S31 45.100N142 00.010E 7369 a/co to 200°
9201220259+09S31 05.280N141 43.140E 5561 a/co to 161°
9201220400+09S30 49.660N141 49.130E 4969 PRACTICED BOAT DRILL
9201220436+09S30 40.150N141 52.940E 5437 a/co to 155°
9201221545+09S27 50.150N143 05.910E 6430 a/co to 200°
9201221949+09S26 49.820N142 40.980E 2885 a/co to 149°
9201222325+09S26 00.020N143 13.970E 4524 a/co to 172°
9201230400+09S24 46.490N143 25.810E 6674 PRACTED FIRE DRILL
9201230542+09S24 20.130N143 30.150E 7979 8-SHAPE ROTATION LEFT TURNING
9201230552+09S24 20.000N143 30.150E 7961 8-SHAPE ROTATION RIGHT TURNING
9201230602+09S24 19.940N143 30.240E 7973 8-SHAPE ROTATION FINISH & a/c 192°
9201230612+09S24 17.870N143 29.660E 7359 RUNG UP ENGINES
9201231239+09S22 36.550N143 07.390E 2487 a/co to 194°
9201231257+09S22 32.370N143 05.410E 1703 a/co to 191°
9201231954+09S20 41.960N142 41.980E 1976 a/co to 203°
9201232134+09S20 20.280N142 31.830E 1599 PROTON SURVEY FINISH
9201232158+09S20 23.580N142 33.780E 1657 STOP ENG
9201232203+09S20 23.490N142 33.710E 1657 CHANGED ENG TO ELECTRIC MOTION
9201232206+09S20 23.500N142 33.660E 1657 1BX BCL STARTED
9201232238+09S20 23.780N142 33.620E 1655 1BX BCL HIT BOTTOM
9201232307+09S20 23.900N142 33.490E 1664 1BX BCL ON DECK
9201232335+09S20 23.930N142 33.320E 1667 P1 PISTON CORING STARTED
9201240000+09S20 23.880N142 33.030E 1663 P1
9201240022+09S20 24.020N142 33.000E 1664 P1 PISTON CORER LANDED
9201240101+09S20 24.210N142 32.920E 1670 P1 PISTON CORING ENDED
9201240119+09S20 24.000N142 32.630E 1672 s/co on 206°
9201240121+09S20 23.790N142 32.510E 1613 PROTON SURVEY START
9201241206+09S17 55.620N141 15.300E 4635 8-SHAPE ROTATION RIGHT TURNING

9201241216+09S17 55.690N141 15.440E 4643 8-SHAPE ROTATION LEFT TURNING
9201241226+09S17 55.890N141 15.430E 4622 8-SHAPE ROTATION FINISH
9201241227+09S17 55.680N141 15.320E 4629 s/co on 200°
9201241230+09S17 55.140N141 15.100E 4644 a/co to 090°
9201241232+09S17 54.880N141 15.340E 4703 RUNG UP ENGINES
9201250703+09S17 55.020N145 59.800E 2705 a/co to 067°
9201251751+09S18 59.950N148 41.760E 5014 G1 a/co to 293°
9201260102+09S19 41.070N146 56.910E 5806 PROTON SURVEY FINISH
9201260116+09S19 40.500N146 57.560E 5876 D1 DREDGE START DOWN
9201260254+09S19 40.570N146 57.310E 5879 D1 DREDGE ON BOTTOM
9201260533+09S19 42.010N146 54.320E 5005 D1 DREDGE OFF BOTTOM
9201260646+09S19 42.920N146 54.030E 4785 D1 DREDGE ON DECK
9201260654+09S19 43.080N146 53.950E 4764 PROTON SURVEY START
9201260657+09S19 43.060N146 53.800E 4720 s/co on 237°
9201261322+09S18 54.090N145 37.160E 2229 a/co to 248°
9201261626+09S18 35.700N144 48.260E 4162 a/co to 250°
9201261809+09S18 26.360N144 21.480E 3851 a/co to 160°
9201261817+09S18 24.610N144 21.910E 3698 a/co to 070°
9201261958+09S18 33.360N144 48.240E 3771 a/co to 160°
9201262006+09S18 31.570N144 49.030E 3623 a/co to 250°
9201262143+09S18 22.330N144 23.140E 3412 a/co to 160°
9201262151+09S18 20.450N144 23.540E 3451 a/co to 070°
9201262333+09S18 29.350N144 49.980E 3719 a/co to 160°
9201262341+09S18 27.660N144 50.950E 3187 a/co to 250°
9201270121+09S18 18.220N144 24.610E 3381 a/co to 160°
9201270129+09S18 16.290N144 25.080E 3608 a/co to 070°
9201270312+09S18 25.330N144 51.680E 3468 a/co to 160°
9201270320+09S18 23.710N144 52.660E 3900 a/co to 250°
9201270502+09S18 14.120N144 26.090E 3795 a/co to 160°
9201270510+09S18 12.210N144 26.470E 3961 a/co to 070°
9201270654+09S18 21.270N144 53.290E 3573 a/co to 160°
9201270702+09S18 19.610N144 54.160E 3993 a/co to 250°
9201270840+09S18 10.030N144 27.740E 3952 a/co to 160°
9201270850+09S18 08.020N144 28.650E 3714 a/co to 070°
9201271030+09S18 17.130N144 54.610E 3467 a/co to 160°
9201271038+09S18 15.330N144 55.690E 3612 a/co to 250°
9201271218+09S18 06.010N144 29.340E 3577 a/co to 160°
9201271226+09S18 04.070N144 29.750E 3582 a/co to 070°
9201271408+09S18 13.060N144 56.260E 3513 a/co to 160°
9201271416+09S18 11.320N144 57.130E 3530 a/co to 250°

9201271556+09S18 01.970N144 30.780E 3807 a/co to 160°
9201271604+09S18 00.000N144 31.120E 3689 a/co to 070°
9201271748+09S18 09.040N144 57.840E 3626 a/co to 160°
9201271756+09S18 07.320N144 58.770E 3636 a/co to 250°
9201271935+09S17 57.850N144 32.390E 3770 a/co to 160°
9201271944+09S17 55.860N144 32.790E 3521 a/co to 070°
9201272129+09S18 04.960N144 59.460E 3850 a/co to 160°
9201272137+09S18 03.160N145 00.210E 3840 a/co to 250°
9201272313+09S17 53.750N144 33.970E 3598 a/co to 160°
9201272321+09S17 51.840N144 34.440E 3482 a/co to 070°
9201280107+09S18 00.860N145 00.940E 3732 a/co to 160°
9201280115+09S17 59.080N145 01.750E 3503 a/co to 250°
9201280250+09S17 49.740N144 35.600E 3243 a/co to 160°
9201280258+09S17 47.870N144 35.920E 3033 a/co to 070°
9201280447+09S17 56.820N145 02.570E 3321 a/co to 160°
9201280455+09S17 55.070N145 03.440E 3312 a/co to 250°
9201280632+09S17 45.570N144 37.570E 2846 a/co to 160°
9201280639+09S17 43.950N144 38.130E 3170 a/co to 070°
9201280820+09S17 52.440N145 03.160E 3378 a/co to 160°
9201280829+09S17 50.620N145 04.130E 3390 a/co to 250°
9201281002+09S17 41.840N144 39.400E 2968 a/co to 160°
9201281010+09S17 39.910N144 39.820E 2887 a/co to 070°
9201281151+09S17 48.350N145 04.710E 3534 a/co to 160°
9201281159+09S17 46.540N145 05.600E 3518 a/co to 250°
9201281332+09S17 37.720N144 40.910E 3576 a/co to 160°
9201281340+09S17 35.770N144 41.460E 4147 a/co to 070°
9201281520+09S17 47.160N144 54.930E 4064 PROTON SURVEY FINISH
9201281539+09S17 48.860N144 53.530E 4231 MT-1 LAUNCH OF OBS MT-1
9201281600+09S17 49.000N144 53.210E 4179 MT-1
9201281649+09S17 48.830N144 53.530E 4231 MT-1 MOORING ON BOTTOM OF OBS MT1
9201281730+09S17 56.560N144 49.070E 4792 MT-2 LAUNCH OF OBS MT-2
9201281735+09S17 56.590N144 48.970E 4795 CHIBA LAUNCH OF OBS CHIBA
9201281834+09S17 56.640N144 48.960E 4795 MT-2 MOORING ON BOTTOM OF OBS MT2
9201281931+09S18 07.530N144 45.170E 3847 MT-3 LAUNCH OF MT-3
9201282000+09S18 07.540N144 44.700E 3855 MT-3
9201282023+09S18 07.610N144 45.100E 3871 MT-3 MOORING ON BOTTOM OF MT-3
9201282023+09S18 07.610N144 45.100E 3850 MT-3 SLOW AHEAD ENG
9201282106+09S18 15.040N144 41.990E 3651 MT-4 LAUNCH OF MT-4
9201282140+09S18 14.910N144 41.420E 3798 MT-4 SLOW AHEAD ENG
9201282150+09S18 15.020N144 41.990E 3635 MT-4 STOP ENG

9201282158+09S18 15.010N144 41.920E 3659 MT-4 MOORING ON BOTTOM OF MT-4
9201282247+09S18 23.530N144 40.290E 4050 MT-5 LAUNCH OF MT-5
9201282300+09S18 23.520N144 40.190E 4048 MT-5
9201282305+09S18 23.530N144 40.210E 4053 MT-5
9201282349+09S18 23.480N144 40.250E 4048 MT-5 MOORING ON BOTTOM OF MT-5
9201290029+09S18 31.040N144 39.740E 4912 MT-6 LAUNCH OF MT-6
9201290259+09S19 01.580N144 31.020E 4234 AIR-GUN STARTED
9201290328+09S18 59.530N144 31.720E 4479 START OF SEISMIC SURVEY
9201290820+09S18 35.570N144 38.990E 5306 SUNSET & PUT ON REGULATION LIGHTS
9201290843+09S18 33.590N144 39.580E 5025 a/co to 185°
9201291024+09S18 25.005N144 38.948E 3768 a/co to 165°
9201291601+09S17 56.510N144 47.060E 4339 a/co to 106°
9201291701+09S17 55.480N144 51.450E 4505 a/co to 164°
9201291716+09S17 54.420N144 51.960E 4460 AIR-GUN STARTED AGAIN
9201291716+09S17 54.410N144 51.970E 4460 START OF SEISMIC SURVEY
9201292320+09S17 28.150N144 59.950E 3126 END OF SEISMIC SURVEY
9201292327+09S17 27.760N145 00.030E 3235 AIR-GUN ENDED
9201300147+09S17 48.970N144 53.260E 4190 MT-1 RELEASE FOR MT-1
9201300335+09S17 48.970N144 53.470E 4227 MT-1 POPPING UP OF MT-1
9201300337+09S17 48.960N144 53.420E 4235 MT-1 FINISH TO RETREIVE OF OBS MT-1
9201300348+09S17 48.940N144 53.160E 4192 MT-1 FINISH TO RETREIVE OF MT-1
9201300437+09S17 56.710N144 48.930E 4800 MT-2
9201300443+09S17 56.690N144 48.800E 4800 CHIBA RELEASE FOR OBS CHIBA
9201300503+09S17 56.680N144 48.370E 4679 MT-2 RELEASE FOR OBS MT-2
9201300610+09S17 56.650N144 48.740E 4792 POPPING UP OF OBS CHIBA
9201300625+09S17 56.500N144 48.750E 4769 CHIBA FINISH
9201300632+09S17 56.480N144 48.690E 4737 POPPING UP OF MT-2
9201300636+09S17 56.610N144 48.820E 4790 MT-2 FINISH TO RETREIVE OF OBS
9201300746+09S18 07.540N144 44.970E 3931 MT-3 RELEASE FOR MT-3 AT 1638
9201300800+09S18 07.520N144 44.760E 3868 MT-3
9201300910+09S18 07.500N144 44.080E 3744 MT-3 POPPING UP OF MT-3
9201300931+09S18 07.600N144 44.990E 3962 FINISH TO RETREIVE OF MT-3
9201301019+09S18 15.120N144 41.920E 3641 MT-4 RELEASE FOR MT-4
9201301213+09S18 23.510N144 40.300E 4047 RELEASE FOR MT-5
9201301320+09S18 23.510N144 40.300E 4047 POPPING UP OF MT-5
9201301336+09S18 23.500N144 40.340E 4047 FINISH TO RETREIVE OF MT-5
9201301447+09S18 31.020N144 39.780E 4913 MT-6 RELEASE FOR MT-6
9201301500+09S18 31.070N144 39.740E 4912 MT-6
9201301700+09S18 31.010N144 39.730E 4916 MT-6 POPPING UP OF MT-6
9201301719+09S18 30.930N144 39.740E 4918 FINISH TO RETREIVE OF MT-6

9201301901+09S18 15.040N144 41.930E 3648 OBS MT-4 WAS NOT RELEASED
9201301907+09S18 15.060N144 41.770E 3687 s/co on 228°
9201301907+09S18 15.060N144 41.760E 3689 PROTON SURVEY START
9201310310+09S16 46.740N143 01.210E 2743 PROTON SURVEY FINISH
9201310323+09S16 45.560N143 02.770E 2722 RUNG UP ENGINES
9201310440+09S16 45.220N143 03.310E 2688 P-2 PISTON CORING STARTED
9201310547+09S16 45.210N143 03.480E 2674 P-2 DROPPED P.C. & TRIED AGAIN
9201310649+09S16 45.150N143 03.250E 2700 P-2 PISTON CORER LANDED
9201310744+09S16 45.090N143 03.660E 2661 P-2 PISTON CORING ENDED
9201310749+09S16 45.110N143 03.660E 2662 PROTON SURVEY START
9201310752+09S16 45.010N143 03.710E 2659 s/co on 195°
9201310848+09S16 31.560N143 00.050E 2676 a/co to 174°
9202010329+09S11 43.050N143 29.730E 7051 8-SHAPE ROTATION RIGHT TURNING
9202010340+09S11 42.950N143 29.640E 7017 8-SHAPE ROTATION LEFT TURNING
9202010350+09S11 42.830N143 29.460E 7016 8-SHAPE ROTATION FINISH
9202010350+09S11 42.810N143 29.460E 7033 PROTON SURVEY FINISH
9202010411+09S11 40.450N143 29.950E 7502 D-2 DREDGE START DOWN
9202010600+09S11 41.160N143 29.620E 7431 D-2 DREDGE ON BOTTOM
9202010600+09S11 41.160N143 29.620E 7431 D-2 DREDGE ON BOTTOM
9202010800+09S11 42.650N143 28.010E 6726 D-2
9202010823+09S11 42.940N143 27.640E 6594 D-2 DREDGE OFF BOTTOM
9202011004+09S11 43.190N143 26.100E 6138 D-2 DREDGE ON DECK
9202011006+09S11 43.200N143 26.020E 6128 PROTON SURVEY START
9202011009+09S11 43.010N143 25.760E 6143 s/co on 225°
9202020511+09S08 01.050N139 38.780E 2829 P-3 PISTON CORING STARTED
9202020602+09S08 00.930N139 38.410E 2830 P-3 PISTON CORER LANDED
9202020649+09S08 01.120N139 38.170E 2828 P-3 PISTON CORING ENDED
9202020706+09S08 01.160N139 38.600E 2830 P-3 PISTON CORING STARTED 2ND TIME
9202020801+09S08 01.070N139 38.530E 2831 P-3 PISTON CORER LANDED
9202020845+09S08 01.230N139 38.470E 2830 P-3 PISTON CORING ENDED
9202020901+09S08 01.140N139 38.330E 2831 P-3 BCL STARTED
9202020952+09S08 01.180N139 38.430E 2829 P-3 BCL HIT BOTTOM
9202021032+09S08 01.130N139 38.680E 2830 P-3 BCL ON DECK
9202021048+09S08 01.000N139 38.570E 2831 MTD START
9202021125+09S08 01.130N139 38.590E 2829 MTD START TO TOWING
9202021153+09S08 01.520N139 39.080E 2827 MTD MESS CAST
9202021217+09S08 01.880N139 39.080E 2826 MTD FINISH
9202021229+09S08 01.730N139 38.630E 2826 PROTON SURVEY START
9202021239+09S08 01.220N139 36.810E 2823 RUNG UP ENGINES
9202030828+09S06 20.090N134 08.320E 5974 a/c 270° & STARTED SEA BEAM SURVEY

9202030937+09S06 19.970N133 48.160E 3409 a/co to 180°
9202030955+09S06 15.350N133 48.030E 4620 a/co to 090°
9202031119+09S06 15.000N134 07.820E 5564 a/co to 180°
9202031138+09S06 10.240N134 08.020E 4255 a/co to 270°
9202031340+09S06 10.000N133 33.280E 3265 a/co to 180°
9202031359+09S06 05.116N133 33.063E 4576 a/co to 090°
9202031630+09S06 05.000N134 07.830E 3875 a/co to 180°
9202031648+09S06 00.230N134 08.050E 4290 a/co to 270°
9202031911+09S05 59.960N133 27.250E 3019 a/co to 180°
9202031930+09S05 55.210N133 27.120E 3920 a/co to 090°
9202032219+09S05 54.960N134 07.940E 2605 a/co to 180°
9202032238+09S05 50.160N134 08.000E 3994 a/co to 270°
9202040130+09S05 49.960N133 20.220E 2387 a/co to 180°
9202040148+09S05 45.270N133 20.040E 3127 a/co to 090°
9202040409+09S05 45.040N133 54.720E 2898 a/co to 180°
9202040428+09S05 40.290N133 55.020E 2174 a/co to 270°
9202040711+09S05 39.960N133 10.230E 4213 a/co to 180°
9202040729+09S05 35.220N133 10.010E 3649 a/co to 091°
9202040958+09S05 35.010N133 46.840E 4744 a/co to 180°
9202041017+09S05 30.150N133 47.050E 5779 a/co to 270°
9202041258+09S05 30.000N133 05.180E 3761 a/co to 180°
9202041317+09S05 25.120N133 05.080E 4445 a/co to 090°
9202041625+09S05 25.020N133 54.700E 2988 a/co to 180°
9202041644+09S05 20.290N133 55.010E 2629 a/co to 270°
9202042019+09S05 19.990N133 00.160E 3279 a/co to 180°
9202042038+09S05 15.180N133 00.090E 3464 a/co to 090°
9202050017+09S05 15.010N133 59.760E 4547 a/co to 180°
9202050036+09S05 10.160N134 00.000E 4418 a/co to 270°
9202050534+09S05 10.010N132 45.340E 4661 a/co to 180°
9202050557+09S05 04.510N132 45.070E 3939 8-SHAPE ROTATION LEFT TURNING
9202050607+09S05 04.470N132 45.160E 3922 8-SHAPE ROTATION LEFT TURNING
9202050617+09S05 04.560N132 45.320E 3961 8-SHAPE ROTATION FINISH
9202050619+09S05 04.280N132 45.490E 3874 s/co on 090°
9202050901+09S05 05.050N133 30.040E 4728 a/co to 021°
9202050902+09S05 05.220N133 30.140E 4726 FINISHED SEA BEAM SURVEY
9202051425+10S06 24.855N133 59.902E 5050 a/co to 064°

Leg 2 : Set Sail from Guam to Cebu

9202110326+1013 25.110N144 39.930E 1400 TESTED STEERING GEARS AT 1220 & ALL WE

9202110335+1013 25.090N144 39.930E 1400 TESTED ENGINES
9202110336+1013 25.090N144 39.940E 1400 S/B ENG WITH SEPARATE MOTION & THRUSTE
9202110352+1013 25.160N144 39.970E 1400 PILOT & OBSERVER CAME ON BOARD
9202110355+1013 25.200N144 39.960E 1400 SINGLED UP LINES
9202110355+1013 25.200N144 39.960E 1400 LET GO SHORE LINES
9202110358+1013 25.200N144 40.000E 1400 ENG. USED VARLY
9202110400+1013 25.250N144 40.030E 1400 HALF AHEAD ENG
9202110400+1013 25.250N144 40.030E 1400 HALF AHEAD ENG
9202110412+1013 26.550N144 39.880E 1400 PASSED INNER HARBOUR
9202110432+1013 27.130N144 37.420E 1400 CLEARED BREAKWATER END
9202110432+1013 27.130N144 37.340E 1400 PILOT LEFT HER
9202110433+1013 27.130N144 37.260E 1400 PILOT LEFT HER
9202110437+1013 27.080N144 36.720E 1400 s/co on 265°
9202110440+1013 26.980N144 36.190E 1400 FULL AHEAD ENG
9202110444+1013 26.850N144 35.350E 0003 a/co to 197°
9202110447+1013 26.450N144 35.060E 0003 PROTON SURVEY START
9202110500+1013 24.370N144 34.360E 1946 RUNG UP ENGINES
9202110500+1013 24.370N144 34.360E 1946 RUNG UP ENGINES
9202110552+1013 10.270N144 29.990E 1777 a/co to 180°
9202110726+1012 44.990N144 29.940E 1731 a/co to 197°
9202110828+1012 28.230N144 24.770E 3119 SUNSET & PUT ON REGULATION LIGHTS
9202112046+1009 14.560N143 25.370E 4786 SUNRISE & PUT OFF REGULAION LIGHTS
9202120311+1007 33.450N142 54.620E 2064 STATIONED BOAT DRILL AT 1300
9202120331+1007 28.710N142 53.170E 3235 FINISED BOAT DRILL
9202120623+1006 45.270N142 39.960E 2765 a/co to 090°
9202120628+1006 45.070N142 41.190E 2330 a/co to 017°
9202120840+1007 19.390N142 51.790E 2774 SUNSET & PUT ON REGULATION LIGHTS
9202120849+1007 21.820N142 52.570E 3630 a/co to 090°
9202120855+1007 22.040N142 54.050E 3620 a/co to 197°
9202121125+1006 45.100N142 42.730E 2594 a/co to 198°
9202122047+1004 24.220N141 57.700E 1910 SUNRISE & PUT OFF REGULAION LIGHTS
9202122340+1003 40.410N141 43.730E 2384 a/co to 160°
9202130000+1003 35.470N141 45.540E 2370 a/co to 140°
9202130000+1003 35.470N141 45.540E 2370 a/co to 140°
9202130015+1003 32.380N141 48.130E 2336 HALF AHEAD ENG & USED COURSE VARIOUSLY
9202130020+1003 31.980N141 48.570E 2321 PROTON SURVEY FINISH
9202130037+1003 31.960N141 51.360E 2283 STOP ENG
9202130043+1003 31.920N141 51.360E 2283 CHANGED ENG TO ELECTRIC MOTION
9202130047+1003 31.890N141 51.330E 2283 P5 PISTON CORING STARTED
9202130100+1003 31.850N141 51.370E 2283 P5

9202130142+1003 31.910N141 51.700E 2282 P5 PISTON CORER LANDED
9202130200+1003 31.930N141 51.960E 2281 P5
9202130224+1003 31.980N141 52.180E 2281 P5 PISTON CORING ENDED
9202130255+1003 31.920N141 51.360E 2284 P5 PISTON CORING STARTED 2ND TIME
9202130300+1003 31.940N141 51.400E 2284 P5
9202130341+1003 32.100N141 51.680E 2279 P5 PISTON CORER LANDED
9202130400+1003 32.130N141 51.740E 2280 P5
9202130423+1003 32.360N141 51.820E 2277 P5 PISTON CORING ENDED
9202130447+1003 31.850N141 51.260E 2286 P5 BCL STARTED
9202130500+1003 31.980N141 51.490E 2284 P5
9202130535+1003 32.010N141 51.580E 2283 P5 BCL HIT BOTTOM
9202130600+1003 32.030N141 51.580E 2282 P5
9202130608+1003 32.030N141 51.610E 2281 P5 BCL ON DECK
9202130616+1003 32.060N141 51.630E 2282 CHANGED ENG TO DIESEL MOTION & SLOW AH
9202130620+1003 31.830N141 51.550E 2284 s/co on 197°
9202130627+1003 30.890N141 51.220E 2301 PROTON SURVEY START
9202130630+1003 30.120N141 51.000E 2312 a/co to 270°
9202130632+1003 30.000N141 50.710E 2312 RUNG UP ENGINES
9202130849+1003 30.060N141 13.670E 3281 SUNSET & PUT ON REGULATION LIGHTS
9202132102+1003 30.080N137 53.250E 4250 SUNRISE & PUT OFF REGULAION LIGHTS
9202132144+1003 31.280N137 41.970E 4515 BAD CURRENT DATA 2/13 22:00
9202132201+1003 29.970N137 37.240E 4603 s/co on 270°
9202140745+1003 30.010N134 59.360E 4733 HALF AHEAD ENG
9202140749+1003 30.010N134 58.800E 4734 PROTON SURVEY FINISH
9202140754+1003 30.030N134 58.600E 4740 STOP ENG
9202140758+1003 30.020N134 58.600E 4736 CHANGED ENG TO ELECTRIC MOTION
9202140758+1003 30.020N134 58.600E 4736 SLOW AHEAD ENG
9202140802+1003 30.050N134 58.580E 4734 PROTON SURVEY START
9202140812+1003 30.070N134 57.890E 4744 AIR-GUN STARTED
9202140915+1003 30.080N134 51.030E 4814 SUNSET & PUT ON REGULATION LIGHTS
9202140920+1003 30.090N134 50.210E 4816 SET SP'D 10KT
9202140921+1003 30.090N134 50.200E 4814 START OF SEISMIC SURVEY
9202141100+1003 30.120N134 35.370E 4844 PUT CLOCKS BACK 1 HOUR FOR JST
9202141100+1003 30.120N134 35.370E 4844 PUT CLOCKS BACK 1 HOUR FOR JST
9202141453+0903 30.030N134 00.680E 3402 SET SPEED 8KT
9202141659+0903 30.050N133 46.110E 3929 POSITION UNFAIR 2/14 1025-1048 GMT
9202141701+0903 30.040N133 45.890E 3927 CURRENT DATA UNUSABLE 2/14 1100
9202142122+0903 30.030N133 15.950E 3451 SUNRISE & PUT OFF REGULAION LIGHTS
9202150747+0903 30.010N131 59.710E 3277 END OF SEISMIC SURVEY
9202150751+0903 30.050N131 59.380E 3293 AIR-GUN ENDED

9202150805+0903 30.050N131 58.520E 3334 PROTON SURVEY FINISH
9202150807+0903 30.050N131 58.520E 3338 STOP ENG
9202150814+0903 30.070N131 58.510E 3337 CHANGED ENG TO DIESEL MOTION & SLOW AH
9202150816+0903 30.190N131 58.520E 3342 s/co on 360°
9202150816+0903 30.210N131 58.520E 3340 PROTON SURVEY START
9202150829+0903 32.500N131 58.440E 3505 RUNG UP ENGINES
9202150838+0903 34.790N131 58.440E 3784 a/co to 090°
9202150925+0903 34.990N132 11.810E 3064 SUNSET & PUT ON REGULATION LIGHTS
9202151113+0903 34.810N132 42.750E 4281 POSITION IS DR 2/15 1010-1040
9202151540+0903 34.960N133 59.830E 2260 FULL AHEAD ENG
9202151543+0903 35.400N134 00.290E 2675 8-SHAPE ROTATION RIGHT TURNING
9202151554+0903 35.600N134 00.410E 2828 8-SHAPE ROTATION LEFT TURNING
9202151604+0903 35.670N134 00.650E 2922 8-SHAPE ROTATION FINISH & a/co to 360°
9202151611+0903 37.240N134 00.440E 3047 RUNG UP ENGINES
9202151620+0903 39.740N134 00.080E 3603 a/co to 270°
9202152124+0903 40.050N132 44.800E 4637 SUNRISE & PUT OFF REGULAION LIGHTS
9202152240+0903 40.010N132 25.010E 1981 a/co to 231°
9202152334+0903 31.100N132 14.030E 3943 HALF AHEAD ENG
9202152338+0903 30.650N132 13.520E 3943 PROTON SURVEY FINISH
9202152350+0903 30.060N132 12.830E 0003 STOP ENG
9202152355+0903 30.050N132 12.820E 0003 CHANGED ENG TO ELECTRIC MOTION
9202160011+0903 29.970N132 12.810E 0003 HEAT FLOW STARTED
9202160133+0903 29.740N132 13.340E 3941 HF1 HEAT FLOW LANDING
9202160155+0903 29.610N132 13.480E 3943 HF1 HEAT FLOW PULLED OUT
9202160200+0903 29.700N132 13.590E 3943 HF1
9202160209+0903 29.440N132 13.520E 3942 HF1 POSITION IS DR 2/16 0155-0204
9202160216+0903 29.410N132 13.570E 3941 HF1 HEAT FLOW LANDING
9202160242+0903 29.450N132 13.780E 3941 HF1 HEAT FLOW PULLED OUT
9202160300+0903 29.500N132 13.910E 3941 HF1
9202160351+0903 29.060N132 14.120E 3944 HF1 HEAT FLOW ENDED & STOPPED ENG
9202160402+0903 28.960N132 14.110E 3939 CHANGED ENG TO DIESEL MOTION SLOW AHEAD
9202160406+0903 29.060N132 14.210E 3941 s/co on 085°
9202160415+0903 29.160N132 15.880E 3733 RUNG UP ENGINES
9202160428+0903 29.420N132 19.540E 3995 FULL AHEAD ENG
9202160432+0903 29.600N132 20.140E 4027 STOP ENG
9202160437+0903 29.570N132 20.060E 4030 HF2 CHANGED ENG TO ELECTRIC MOTION
9202160440+0903 29.530N132 20.050E 4033 HF2 HEAT FLOW STARTED
9202160500+0903 29.300N132 20.230E 4046 HF2
9202160600+0903 29.160N132 20.540E 4037 HF2
9202160606+0903 29.180N132 20.570E 4039 HF2 HEAT FLOW LANDING

9202160622+0903 29.200N132 20.610E 4033 HF2 HEAT FLOW PULLED OUT
9202160639+0903 29.210N132 20.620E 4034 HF2 HEAT FLOW PULLED OUT AGAIN
9202160700+0903 29.210N132 20.640E 4032 HF2
9202160752+0903 29.230N132 20.820E 4034 HF2 HEAT FLOW ENDED
9202160755+0903 29.060N132 20.780E 4034 CHANGED ENG TO DIESEL MOTION & SLOW AH
9202160759+0903 29.260N132 20.890E 4027 s/co on 360°
9202160804+0903 30.010N132 20.960E 3987 a/co to 090°
9202160808+0903 30.030N132 21.990E 3972 RUNG UP ENGINES
9202160828+0903 30.080N132 27.510E 3764 FULL AHEAD ENG
9202160832+0903 30.330N132 27.940E 3762 STOP ENG
9202160837+0903 30.290N132 28.000E 3765 CHANGED ENG TO ELECTRIC MOTION
9202160837+0903 30.290N132 28.000E 3767 HF3 HEAT FLOW STARTED
9202160900+0903 30.090N132 28.400E 3763 HF3
9202160928+0903 29.810N132 28.690E 3765 HF3 SUNSET & PUT ON REGULATION LIGHTS
9202161000+0903 29.790N132 28.770E 3764 HF3
9202161003+0903 29.770N132 28.790E 3763 HF3 HEAT FLOW LANDING
9202161030+0903 29.570N132 28.950E 3763 HF3 HEAT FLOW PULLED OUT
9202161039+0903 29.730N132 28.840E 3759 HF3 POSITION IS DR 2/16 10:07-10:38
9202161100+0903 29.740N132 28.880E 3759 HF3
9202161133+0903 29.550N132 28.980E 3745 HF3 HEAT FLOW ENDED
9202161133+0903 29.550N132 28.980E 3743 CHANGED ENG TO DIESEL MOTION
9202161134+0903 29.540N132 28.980E 3742 SLOW AHEAD ENG
9202161138+0903 29.530N132 29.180E 3728 s/co on 360°
9202161138+0903 29.560N132 29.200E 3728 USED ENGINES VARIOUSLY
9202161151+0903 32.270N132 29.470E 3666 a/co to 090°
9202161249+0903 32.460N132 45.845E 4959 a/co to 180°
9202161256+0903 30.720N132 46.140E 5152 SLOW AHEAD ENG
9202161300+0903 30.360N132 46.140E 5164 STOP ENG
9202161308+0903 30.220N132 46.340E 5170 CHANGED ENG TO ELECTRIC MOTION
9202161308+0903 30.220N132 46.340E 5170 HF4 HEAT FLOW STARTED
9202161400+0903 30.060N132 46.500E 5161 HF4
9202161441+0903 30.300N132 46.380E 5172 HF4 HEAT FLOW LANDING
9202161500+0903 30.300N132 46.390E 5168 HF4
9202161522+0903 30.200N132 46.410E 5172 HF4 HEAT FLOW PULLED OUT
9202161600+0903 30.110N132 46.480E 5148 HF4
9202161635+0903 29.950N132 46.740E 5148 HF4 HEAT FLOW ENDED
9202161636+0903 29.940N132 46.750E 5147 HF4 COMMENCED SHIFTING
9202161658+0903 28.860N132 48.660E 5195 D-3 FINISHED SHIFTING
9202161700+0903 28.860N132 48.690E 5198 D-3
9202161701+0903 28.850N132 48.710E 5203 D-3 DREDGE START DOWN

9202161800+0903 28.870N132 49.300E 5303 D-3
9202161832+0903 29.050N132 49.280E 5312 D-3 DREDGE ON BOTTOM
9202161900+0903 29.250N132 49.630E 5227 D-3
9202162000+0903 29.800N132 50.390E 5031 D-3
9202162031+0903 30.110N132 50.670E 5062 D-3 DREDGE OFF BOTTOM
9202162100+0903 30.300N132 51.060E 5104 D-3
9202162121+0903 30.530N132 51.360E 5115 D-3 SUNRISE & PUT OFF REGULAION LIGHTS
9202162141+0903 30.500N132 51.670E 5139 D-3 DREDGE ON DECK
9202162145+0903 30.460N132 51.700E 5142 CHANGED ENG TO DIESEL MOTION & SLOW AH
9202162149+0903 30.540N132 51.840E 5144 a/co to 360°
9202162159+0903 32.490N132 52.100E 5160 RUNG UP ENGINES
9202162159+0903 32.510N132 52.170E 5129 a/co to 090°
9202162300+0903 32.450N133 09.600E 2760 a/co to 180°
9202162308+0903 30.570N133 09.870E 3094 SLOW AHEAD ENG
9202162312+0903 30.110N133 09.920E 3249 STOP ENG
9202162317+0903 30.080N133 09.990E 3213 D4 CHANGED ENG TO ELECTRIC MOTION
9202162318+0903 30.070N133 10.010E 3211 D4 DREDGE START DOWN
9202170000+0903 30.070N133 10.250E 2963 D4
9202170026+0903 30.030N133 10.300E 2924 D4 DREDGE ON BOTTOM
9202170100+0903 30.260N133 10.880E 2800 D4
9202170133+0903 30.120N133 10.860E 2866 D4 DREDGE OFF BOTTOM
9202170200+0903 29.950N133 10.820E 2870 D4
9202170223+0903 29.880N133 11.220E 2939 D4 HEAT FLOW ENDED
9202170230+0903 29.840N133 11.310E 3011 CHANGED ENG TO DIESEL MOTION
9202170230+0903 29.840N133 11.310E 3011 SLOW AHEAD ENG
9202170244+0903 32.280N133 11.530E 2665 a/co to 090°
9202170245+0903 32.420N133 11.630E 2664 RUNG UP ENGINES
9202170326+0903 30.520N133 20.930E 4294 FULL AHEAD ENG
9202170331+0903 29.960N133 21.080E 4305 STOP ENG
9202170335+0903 29.950N133 21.120E 4304 CHANGED ENG TO ELECTRIC MOTION
9202170336+0903 29.960N133 21.110E 4305 D5 DREDGE START DOWN
9202170400+0903 30.050N133 21.500E 4070 D5
9202170446+0903 29.980N133 21.690E 4086 D5 DREDGE ON BOTTOM
9202170500+0903 30.100N133 21.940E 4020 D5
9202170600+0903 30.480N133 22.870E 3226 D5
9202170700+0903 30.470N133 23.060E 3285 D5
9202170749+0903 30.130N133 22.510E 3601 D5 DREDGE OFF BOTTOM WIRE OUT 3650M
9202170800+0903 30.050N133 22.450E 3671 D5
9202170839+0903 30.070N133 22.500E 3675 D5 DREDGE ON DECK
9202170842+0903 30.080N133 22.520E 3663 CHANGED ENG TO DIESEL MOTION & SLOW AH

9202170842+0903 30.080N133 22.520E 3663 PROTON SURVEY START
9202170843+0903 30.120N133 22.490E 3659 s/co on 320°
9202170855+0903 31.704N133 21.226E 4025 RUNG UP ENGINES
9202170922+0903 37.160N133 16.620E 3345 SUNSET & PUT ON REGULATION LIGHTS
9202171001+0903 44.900N133 10.110E 4100 a/co to 270°
9202171039+0903 45.090N133 00.500E 2513 POSITION IS DR 2/17 10:06-10:36
9202171159+0903 45.030N132 40.260E 4021 a/co to 360°
9202171217+0903 49.820N132 40.070E 4256 a/co to 090°
9202171358+0903 49.970N133 09.730E 4024 a/co to 360°
9202171417+0903 54.790N133 10.020E 4180 a/co to 270°
9202171618+0903 55.030N132 40.260E 3923 a/co to 360°
9202171636+0903 59.710N132 40.040E 3135 a/co to 090°
9202171815+0903 59.950N133 09.690E 3569 a/co to 360°
9202171833+0904 04.710N133 10.010E 3389 a/co to 270°
9202172017+0904 04.960N132 45.200E 2666 a/co to 360°
9202172036+0904 09.840N132 45.130E 3613 a/co to 090°
9202172123+0904 10.040N132 58.400E 5031 SUNRISE & PUT OFF REGULAION LIGHTS
9202172203+0904 10.090N133 09.980E 3527 a/co to 360°
9202172221+0904 14.830N133 10.060E 3446 a/co to 270°
9202172358+0904 15.020N132 45.260E 3118 a/co to 360°
9202180016+0904 19.740N132 45.070E 3741 a/co to 090°
9202180154+0904 20.000N133 14.770E 4022 a/co to 360°
9202180212+0904 24.790N133 14.980E 3925 a/co to 270°
9202180352+0904 25.020N132 50.220E 3784 a/co to 360°
9202180411+0904 29.760N132 50.040E 3714 a/co to 090°
9202180730+0904 30.030N133 50.000E 2657 a/co to 360°
9202180748+0904 34.870N133 50.020E 2357 a/co to 270°
9202180922+0904 35.050N133 26.700E 3490 SUNSET & PUT ON REGULATION LIGHTS
9202181147+0904 35.040N132 50.210E 4391 a/co to 360°
9202181205+0904 39.830N132 50.030E 4408 a/co to 090°
9202181558+0904 39.960N133 59.710E 4799 a/co to 360°
9202181616+0904 44.730N134 00.010E 4395 a/co to 270°
9202182000+0904 45.040N133 04.150E 4376 HALF AHEAD ENG
9202182005+0904 45.060N133 03.470E 4425 PROTON SURVEY FINISH
9202182021+0904 43.920N133 04.990E 4000 s/co on 120°FOR DREDGE POINT
9202182044+0904 40.380N133 10.980E 4882 HALF AHEAD ENG
9202182049+0904 40.420N133 11.450E 4960 STOP ENG
9202182053+0904 40.430N133 11.530E 4950 CHANGED ENG TO ELECTRIC MOTION
9202182053+0904 40.430N133 11.540E 4956 D-6 DREDGE START DOWN
9202182100+0904 40.350N133 11.640E 4931 D-6

9202182121+0904 40.160N133 11.910E 4752 D-6 SUNRISE & PUT OFF REGULAION LIGHTS
9202182200+0904 40.480N133 12.110E 4864 D-6
9202182208+0904 40.420N133 12.260E 4796 D-6 DREDGE ON BOTTOM
9202182249+0904 40.170N133 12.690E 4600 D-6 DREDGE ON BOTTOM
9202182300+0904 40.010N133 12.930E 4480 D-6
9202190000+0904 39.380N133 14.020E 3775 D-6
9202190003+0904 39.370N133 14.030E 3776 D-6 DREDGE OFF BOTTOM
9202190100+0904 38.940N133 14.830E 3407 D-6
9202190102+0904 38.930N133 14.800E 3385 D-6 CHANGED ENG TO DIESEL MOTION
9202190104+0904 38.940N133 14.860E 3368 D-6 DREDGE ON DECK
9202190105+0904 38.940N133 14.900E 3361 SLOW AHEAD ENG & a/co to 360°
9202190119+0904 40.800N133 15.190E 4139 RUNG UP ENGINES
9202190124+0904 42.270N133 15.350E 4503 a/co to 090°
9202190306+0904 42.490N133 45.700E 2065 USED COURSE VARIOUSLY
9202190324+0904 42.200N133 42.060E 2966 FULL AHEAD ENG
9202190328+0904 42.150N133 41.590E 2856 P-6 STOP ENG
9202190334+0904 42.100N133 41.610E 2882 P-6 CHANGED ENG TO ELECTRIC MOTION
9202190347+0904 41.910N133 41.860E 2974 P-6 PISTON CORING STARTED
9202190400+0904 41.740N133 42.070E 2983 P-6
9202190436+0904 42.040N133 42.200E 2980 P-6 PISTON CORER LANDED
9202190500+0904 42.080N133 42.050E 2972 P-6
9202190524+0904 41.870N133 42.240E 2987 P-6 PISTON CORING ENDED
9202190537+0904 42.210N133 41.780E 2934 P-6 BCL STARTED
9202190600+0904 41.950N133 41.930E 2974 P-6
9202190640+0904 41.950N133 42.090E 2978 P-6 BCL HIT BOTTOM
9202190700+0904 41.950N133 41.980E 2975 P-6
9202190722+0904 41.930N133 42.010E 2976 P-6 BCL ON DECK
9202190734+0904 41.940N133 42.150E 2980 P-6 ORI NET START
9202190746+0904 41.990N133 42.220E 2981 P-6 ORI NET DEEPEST WIRE OUT 420M
9202190800+0904 42.210N133 42.230E 2972 P-6
9202190828+0904 42.460N133 42.240E 2954 P-6 ORI NET FINISH 300 M
9202190834+0904 42.450N133 42.290E 2954 P-6 ORI NET START 100 M
9202190839+0904 42.570N133 42.240E 2951 P-6 ORI NET DEEPEST WIRE OUT 140M
9202190900+0904 42.780N133 42.180E 2931 P-6
9202190915+0904 42.980N133 42.150E 2916 P-6 ORI NET FINISH
9202190920+0904 42.970N133 42.190E 2916 P-6 CHANGED ENG TO DIESEL MOTION & SLOW AH
9202190925+0904 43.330N133 42.210E 2892 PROTON SURVEY START
9202190925+0904 43.350N133 42.210E 2888 s/co on 360°
9202190934+0904 45.080N133 42.150E 2789 RUNG UP ENGINES
9202190939+0904 46.330N133 42.130E 2684 SUNSET & PUT ON REGULATION LIGHTS

9202191011+0904 54.934N133 42.157E 2834 a/co to 270°
9202191338+0904 55.090N132 50.130E 2999 a/co to 360°
9202191356+0904 59.810N132 50.000E 3134 a/co to 090°
9202191735+0904 59.980N133 53.760E 3141 a/co to 360°
9202191753+0905 04.790N133 54.020E 3271 a/co to 270°
9202191928+0905 04.980N133 30.010E 4725 a/co to 180°
9202192023+0904 50.120N133 29.940E 4350 a/co to 270°
9202192123+0904 50.030N133 14.810E 5095 SUNRISE & PUT OFF REGULAION LIGHTS
9202192302+0904 50.050N132 50.070E 2926 a/co to 310°
9202200148+0905 19.380N132 17.680E 2249 a/co to 315°
9202200400+0905 42.320N131 50.900E 5138 STATIONED FIRE DRILL
9202200430+0905 47.620N131 44.500E 5189 DISMISSED STATION FIRE DRILL
9202200929+0906 41.350N130 39.220E 5571 SUNSET & PUT ON REGULATION LIGHTS
9202201600+0907 51.960N129 13.320E 5378 ADJUSTED CLOCKS 1HOUR BACK IN LON. 120
9202202204+0808 55.993N127 55.196E 5844 SUNSET & PUT ON REGULATION LIGHTS
9202210354+0809 55.630N126 42.190E 8490 a/co to 360°
9202210412+0810 00.290N126 42.010E 8525 a/co to 130°
9202210506+0809 50.530N126 53.630E 8386 STATIONED LEAK DRILL AT 1300
9202210508+0809 50.220N126 53.990E 8308 a/co to 360°
9202210528+0809 54.790N126 54.390E 8009 a/co to 310°
9202210530+0809 55.200N126 54.160E 7941 DISMISSED LEAK DRILL STATION
9202210630+0810 05.670N126 42.230E 9404 a/co to 300°
9202210830+0810 22.130N126 13.740E 5109 HALF AHEAD ENG
9202210837+0810 22.460N126 13.050E 5105 PROTON SURVEY FINISH
9202210848+0810 22.830N126 11.160E 4211 a/co to 285°
9202210848+0810 22.840N126 11.120E 4177 RUNG UP ENGINES
9202211015+0810 29.170N125 47.640E 0456 SUNSET & PUT ON REGULATION LIGHTS
9202211048+0810 31.540N125 38.130E 0117 a/co to 270°
9202211121+0810 31.520N125 28.010E 0109 a/co to 223°
9202211140+0810 27.170N125 23.920E 0178 a/co to 185°
9202211320+0809 55.640N125 20.960E 1248 a/co to 205°
9202211337+0809 50.870N125 18.620E 1194 a/co to 251°
9202211650+0809 33.370N124 25.890E 1802 a/co to 256°
9202211830+0809 26.240N123 56.380E 0835 a/co to 275°
9202211923+0809 27.500N123 40.850E 0789 BALICASAG I. ABEAM ON 005 3.4'
9202211939+0809 30.920N123 38.010E 0781 a/co to 012°
9202212107+0809 54.440N123 42.790E 0324 a/co to 028°
9202212200+0810 07.250N123 49.740E 0277 HALF AHEAD ENG
9202212205+0810 07.800N123 49.830E 0277 SUNRISE & PUT OFF REGULAION LIGHTS
9202212206+0810 07.800N123 49.830E 0277 STOP ENG

9202212207+0810 07.780N123 49.800E 0277 CHANGED ENG. TO SEPARATE MOTION
9202212352+0810 07.940N123 49.670E 0277 SLOW AHEAD ENG
9202220040+0810 12.800N123 52.850E 0277 TESTED CRASH ASTERN
9202220046+0810 13.290N123 52.880E 0277 S/B THRUSTRS
9202220057+0810 13.870N123 52.950E 0277 STATIONED TO ENTER PORT CEBU
9202220106+0810 14.440N123 53.040E 0277 S/B STARBO ANCHOR
9202220106+0810 14.450N123 53.040E 0277 PILOT CAME ON BOARD
9202220112+0810 15.060N123 53.140E 0277 S/B PORT ANCHOR
9202220112+0810 15.070N123 53.140E 0277 USED ENGINES VARIOUSLY
9202220112+0810 15.080N123 53.140E 0277 USED COURSE VARIOUSLY
9202220152+0810 17.480N123 54.290E 0277 SENT SHORE LINES
9202220158+0810 17.480N123 54.290E 0277 PILOT LEFT HER
9202220215+0810 17.480N123 54.290E 0277 F/W ENGINES
9202220216+0810 17.480N123 54.290E 0277 MADE FAST HER STARBO SIDE ALONG PIER 3

Leg 3 : Set Sail from Cebu to Tokyo

9202270118+08S10 17.480N123 54.290E 0277 TESTED CPP OF SCREW & THRUSTERS
9202270125+08S10 17.480N123 54.290E 0277 STATIONED TO LEAVE PORT CEBU
9202270125+08S10 17.480N123 54.290E 0277 PILOT CAME ON BOARD
9202270127+08S10 17.480N123 54.290E 0277 TESTED ENGINES
9202270127+08S10 17.480N123 54.290E 0277 PILOT CAME ON BOARD
9202270128+08S10 17.480N123 54.290E 0277 S/B ENG. WITH SEPARATE MOTION & THRUST
9202270132+08S10 17.470N123 54.270E 0277 SINGLED UP LINES
9202270132+08S10 17.470N123 54.270E 0277 LET GO SHORE LINES
9202270137+08S10 17.460N123 54.250E 0277 USED ENGINES VARIOUSLY USED COURSE VARIOUSLY
9202270205+08S10 14.970N123 53.280E 0277 PILOT LEFT HER
9202270206+08S10 14.950N123 53.260E 0277 SLOW AHEAD ENG
9202270208+08S10 14.800N123 53.240E 0277 S/B ENG TANDEM MOTION
9202270210+08S10 14.450N123 53.130E 0277 DISMISSED STATION AT 1007
9202270212+08S10 14.110N123 53.080E 0277 FULL AHEAD ENG
9202270217+08S10 13.195N123 52.939E 0277 a/co to 120°
9202270219+08S10 12.707N123 53.374E 0277 RUNG UP ENGINES
9202270224+08S10 12.220N123 54.600E 0277 a/co to 090°
9202270232+08S10 12.340N123 56.810E 0298 a/co to 042°
9202270306+08S10 18.804N124 03.303E 0392 a/co to 018°
9202270510+08G10 50.934N124 14.044E 0816 SNA90K SYSTEM PC BOARD TROUBLED
9202270511+08G10 51.264N124 14.164E 0825 TROUBLED FROM 1130 SMT 27TH FEB
9202270605+08G11 05.599N124 18.933E 0671 CALAMGAN I. AB'M ON 288
9202270751+08G11 33.970N124 11.618E 0235 GIGANTANGAN I. AB'M ON 76 3.7'

9202270838+08G11 46.629N124 12.685E 0310 a/co to 337°
9202270944+08S12 02.940N124 05.310E 0224 a/co to 333°
9202270952+08S12 04.950N124 04.130E 0209 PUT ON REGULATION LIGHTS
9202270953+08S12 05.280N124 03.960E 0208 SUNSET
9202271057+08S12 21.350N123 55.990E 0536 a/co to 360°
9202271109+08S12 24.810N123 55.980E 0294 a/co to 072°
9202271146+08S12 27.930N124 05.410E 0095 a/co to 040°
9202271210+08S12 33.110N124 09.980E 1150 a/co to 012°
9202271313+08S12 49.860N124 13.450E 0051a/co to 039°
9202271329+08S12 53.350N124 16.340E 0222 HALF AHEAD ENG & USED ENGINES VARIOUSLY
9202271335+08S12 53.920N124 16.790E 0223 PROTON SURVEY START
9202271345+08S12 55.600N124 18.170E 0252 RUNG UP ENGINES
9202272158+08S14 35.380N125 42.330E 5501 SUNRISE & PUT OFF REGULAION LIGHTS
9202280934+08S16 55.860N127 41.260E 5007 SUNSET & PUT ON REGULATION LIGHTS
9202281700+08S18 29.034N129 01.113E 5532 ADVANCED CLOCKS 1 HOUR FOR JST
9203010916+09S21 51.710N131 57.390E 5564 SUNSET & PUT ON REGULATION LIGHTS
9203012124+09S24 28.890N134 17.350E 2333 SUNRISE & PUT OFF REGULAION LIGHTS
9203012135+09S24 31.210N134 19.360E 0110 PASSED BEIJYU SEA MOUNT
9203020906+09S27 01.730N136 36.140E 5432 SUNSET & PUT ON REGULATION LIGHTS
9203021306+09S27 53.990N137 23.990E 4432 STARTED GRID SURVEY OF HAKUHO KAIZAN
9203021306+09S27 54.030N137 24.030E 4431 a/co to 041°
9203021404+09S28 05.910N137 35.720E 4241 a/co to 270°
9203021446+09S28 06.200N137 23.030E 4266 a/co to 133°
9203021611+09S27 50.060N137 42.080E 4373 a/co to 223°
9203021618+09S27 48.680N137 40.830E 4435 a/co to 313°
9203021737+09S28 03.040N137 23.010E 3931 a/co to 223°
9203021744+09S28 01.990N137 21.420E 4270 a/co to 133°
9203021820+09S27 55.100N137 29.240E 3518 a/co to 044°
9203021850+09S28 00.740N137 35.650E 3505 a/co to 133°
9203021938+09S27 51.660N137 46.830E 4366 a/co to 226°
9203021945+09S27 50.330N137 45.460E 4293 a/co to 313°
9203022115+09S28 06.780N137 25.330E 4325 SUNRISE & PUT OFF REGULAION LIGHTS
9203022121+09S28 07.960N137 24.020E 4525 FINISHED SEA BEAM SURVEY & a/co to 015°
9203030048+09S29 02.590N137 41.930E 4357 USED CO VAR'LY
9203030049+09S29 02.780N137 42.000E 4355 S/C ON 15°
9203030400+09S29 54.160N137 57.960E 3970 STATIONED BOAT DRILL
9203030428+09S30 01.890N138 00.390E 4049 PUT ON NAVIGATION LIGHTS UNDER SHORT V
9203030430+09S30 02.220N138 00.490E 4044 F/W BOAT DRILL & STATIONED FIRE DRILL
9203030500+09S30 10.150N138 03.050E 4112 F/W FIRE DRILL
9203030847+09S31 08.710N138 21.540E 3614 SUNSET & PUT ON REGULATION LIGHTS

9203031559+09S32 58.170N138 56.330E 1880 SYSTEM POSITION UNFAIR 3/2 1545-1600 G
9203031600+09S32 58.400N138 56.390E 1893 CURRENT DATA UNFAIR 3/2 1600 GMT
9203031852+09S33 40.640N139 10.210E 1822 INANBA SA. AB'M ON 105 6.6' OFF
9203032102+09S34 13.900N139 19.660E 0330 SUNRISE
9203032227+09S34 34.390N139 27.950E 0082 PUT OFF REGULATION LIGHTS
9203032257+09S34 41.830N139 30.820E 0980 a/co to 029°
9203032302+09S34 42.890N139 31.570E 1212 FULL AHEAD ENG
9203032315+09S34 45.270N139 33.290E 1774 a/co to 005°
9203032328+09S34 48.280N139 33.670E 1812 USED ENGINES VARIOUSLY
9203032331+09S34 48.570N139 33.710E 1818 PROTON SURVEY FINISH
9203032334+09S34 48.700N139 33.740E 1824 a/co to 035°
9203040014+09S34 56.470N139 40.520E 0254 a/co to 020°
9203040025+09S34 59.250N139 41.430E 0292 USED COURSE VARIOUSLY
9203040307+09C35 29.310N139 52.310E 0674 a/co to 328°
9203040343+09C35 33.574N139 49.886E 0829 STATIONED TOLED GO ANCHOR
9203040350+09C35 34.235N139 49.520E 0788 STAND BY ANCHOR
9203040354+09C35 34.410N139 49.500E 0788 LET GO ANCHOR
9203040359+09C35 34.320N139 49.450E 0788 BROUGHT UP ANCHOR & STOP ENG
9203040359+09C35 34.320N139 49.450E 0788 F/W ENGINES
9203040400+09C35 34.325N139 49.451E 0788

And we safely returned to Tokyo ! Don't you think that *"All's well that ends well."* ?